

**BORON- AND NITROGEN-DOPED CARBON NANOTUBES:  
SYNTHESIS, CHARACTERIZATION AND APPLICATION IN  
SOLAR CELLS**

by

GODFREY KAMITHA KERU

A thesis submitted to the School of Chemistry and Physics, College of Agriculture,  
Engineering and Science, University of KwaZulu-Natal, Westville campus, for the  
award of the degree of Doctor of Philosophy.

July 2015

Supervisor: Prof Vincent O. Nyamori

Co-supervisors: Prof Patrick G. Ndungu and Prof Genene T. Mola

## ABSTRACT

The investigations in this project focused on the synthesis and characterization of boron- and nitrogen-doped carbon nanotubes (B- and N-CNTs), and the subsequent application of the doped-CNTs in organic solar cells (OSCs). The CNTs (B-CNTs and N-CNTs) were synthesized by using a floating catalyst chemical vapour deposition method with either ferrocene or its derivatives as the catalysts. A novel ferrocenyl derivative, namely, (4-[[pyridin-4-yl)methylidene]amino}phenyl)-ferrocene, was synthesised by a mechanochemical solvent-free method and its crystal structure was also determined. The ferrocenyl derivative was obtained in high yields (94%) within a short reaction time (30 min). To synthesise N-CNTs, this ferrocenyl derivative was used as a catalyst, nitrogen source as well as an extra source of carbon. To synthesize B-CNTs, ferrocene was used as the catalyst, triphenylborane was the boron source as well as an extra source of carbon at 900 °C. The main carbon source was either toluene or acetonitrile, where applicable, in all CNT synthesis reactions.

The shaped carbon nanomaterials formed were characterized by means of transmission electron microscopy, scanning electron microscopy, high resolution transmission electron microscopy, electron dispersive X-ray spectroscopy, Raman spectroscopy, thermogravimetric analysis and X-ray photoelectron spectroscopy (XPS). In addition, a vibrating sample magnetometer, four probe conductivity measurement instrument, and an inverse gas chromatography surface energy analyser were used for B-CNT analysis. Formation of bamboo compartments in N-CNTs and cone structures in B-CNTs was a preliminary indication that boron and nitrogen were successfully doped in the hexagonal carbon network of carbon nanotubes (CNTs). XPS was used to ascertain the bonding environment of boron and nitrogen in the carbon network.

Boron in the B-CNTs was quantified with inductively coupled plasma-optical emission spectroscopy, while the nitrogen content in the N-CNTs was determined by elemental analysis. The amount of boron incorporated was found to be directly proportional to the percentage by weight of the boron-containing precursor used. At the same time, it was also observed that the amount of boron incorporated had an effect on the conductivities, dispersive surface energies and ferromagnetic properties, among other physicochemical

properties, of the B-CNTs. For N-CNTs, the amount of nitrogen incorporated was found to be dependent on synthesis temperature and the amount of nitrogen in the precursors. A temperature of 850 °C and acetonitrile as a carbon source, as well as an extra source of nitrogen, were found to be the best conditions in this study. This resulted in high nitrogen incorporation of about 17.57 at.% and high yield of  $\approx 85\%$  of carbon nanotubes in the total mass of the products obtained.

The B-CNTs or N-CNTs were then used to synthesize nanocomposites with poly(3-hexylthiophene) [P3HT] by either *in situ* polymerization or direct solution mixing. The nanocomposites were characterized with electron microscopy, UV-Vis spectrophotometry, and photoluminescence spectrophotometry. These nanocomposites were subsequently mixed with a fullerene derivate, [6,6]-phenyl C61 butyric acid methyl ester, to form donor-acceptor components in the photoactive layer in OSCs. Nanocomposites that were synthesized by *in situ* polymerization method performed better than those by direct solution mixing. Organic photovoltaic cell devices were fabricated on indium tin oxide coated glass substrates which were coated with a very thin layer of a hole transport layer, namely, 3,4-ethylenedioxythiophene:poly(styrenesulphonate). The nanocomposite photoactive layer of the devices was spin coated from a chloroform based solution. Finally, an ultra-thin layer of lithium fluoride and a 60 nm aluminium counter electrode were thermally evaporated in a vacuum.

The electrical properties of the fabricated solar cell devices were characterized by using a standard solar simulator operating at air mass (AM) of 1.5 at a light intensity of 100 mW cm<sup>-2</sup>. Important cell parameters, such as, fill factor (FF) and efficiency ( $\eta$ ) were determined from the current-voltage characteristics of the devices. The effects of B-CNTs or N-CNTs in the photoactive layer were studied and then compared with a standard device structure without doped-CNTs. Several techniques such as transient absorption spectroscopy (TAS) and atomic force microscopy (AFM) were used to understand the effects of B-CNTs or N-CNTs as part of the photoactive layer. The TAS technique was used to determine the yield and lifetime of the photo-generated charge carriers. This was compared with the power output (or  $\eta$ ) of the cell devices. AFM was

used to study the morphology of the photoactive layer with B-CNTs or N-CNTs films on the substrates.

Doped-CNTs were also tested as charge extracting layer under various device configurations. The position of B- or N-CNTs in the photoactive layer was altered whereby a thin film of B- or N-CNT/P3HT was spin coated next to the hole or electron collecting electrodes. B-CNTs had a positive Hall coefficient and their film was coated close to the ITO electrode, while N-CNTs had negative coefficient and the film was placed close to the Al counter electrode. The short circuit current density and  $\eta$  improved by 31% and 141%, respectively, for the devices with B-CNTs. While, in the case of N-CNTs, the respective values changed by 35% and 38%, respectively. B- or N-CNTs in the photoactive layer were found to improve the absorption of the polymer, the lifetime of the photo-generated free charge carriers and, also, the charge transport properties. The open circuit voltage was found to decrease in some devices which was attributed to recombination.

This work has shown that incorporation of doped-CNTs in the photoactive layer, markedly improves the photovoltaic properties of organic solar cells.

## **PREFACE**

The experimental work described in this thesis was carried out in the School of Chemistry and Physics, University of KwaZulu-Natal, Westville campus, from July 2012 to April 2015, under the supervision of Prof Vincent O. Nyamori, Prof Patrick G. Ndungu and Prof Genene T. Mola.

These studies represent original work by the author and have not otherwise been submitted in any form for any degree or diploma to any tertiary institution. Where use has been made of the work of others it is duly acknowledged in the text.

Signed:.....

## **DECLARATION 1–PLAGIARISM**

I, **Godfrey Kamitha Keru** declare that;

1. The research reported in this thesis, except where otherwise indicated, is my original research.
  
2. This thesis has not been submitted for any degree or examination at any other University.
  
3. This thesis does not contain other person's data, pictures, graphs or other information, unless specifically acknowledged as being sourced from other persons.
  
4. This thesis does not contain other persons' writing, unless specifically acknowledged as being sourced from other researchers. Where other written sources have been quoted, then:
  - a. Their words have been re-written but the general information attributed to them has been referenced
  - b. Where their exact words have been used, then their writing has been placed in italics and inside quotation marks, and referenced.
  
5. This thesis does not contain text, graphics or tables copied and pasted from the internet, unless specifically acknowledged, and the source being detailed in the thesis and in the references sections.

Signed:.....

## DECLARATION 2-PUBLICATIONS

Details of contribution to publications that form part and/or include research presented in this thesis (include publications in preparation, submitted, in press and published and give details of the contributions of each author to the experimental work and writing of each publication)

1. Godfrey Keru, Patrick G. Ndungu and Vincent O. Nyamori. A review on carbon nanotube/polymer composites for organic solar cells. *International Journal of Energy Research* 2014, 38 (13) 1635 – 1653.
2. Vincent O. Nyamori, Godfrey Keru and Bernard Omondi. (4-[(Pyridin-4-yl)methylidene] amino} phenyl) ferrocene *Acta Crystallographica Section E*: 2012, E68 (12) m 1535.
3. Godfrey Keru, Patrick G. Ndungu and Vincent O. Nyamori. Nitrogen-doped carbon nanotubes synthesised by pyrolysis of (4-[(pyridine-4-yl)methylidene] amino} phenyl) ferrocene. *Journal of Nanomaterials* 2013 (2013) Article identity 750318. 7 pages.
4. Godfrey Keru, Patrick G. Ndungu and Vincent O. Nyamori. Effect of boron concentration on physicochemical properties of boron-doped carbon nanotubes. *Materials Chemistry and Physics* 153 (2015) 323-332.
5. Godfrey Keru, Patrick G. Ndungu, Genene T. Mola and Vincent O. Nyamori. Bulk heterojunction solar cell with nitrogen-doped carbon nanotubes in the active layer: Effect of nanocomposite synthesis technique on photovoltaic properties. *Materials* 2015, 8, 2415-2432.
6. Godfrey Keru, Patrick G. Ndungu, Ana F. Nogueira, Genene T. Mola and Vincent O. Nyamori. Performance of organic solar cells P3HT:PCBM with B-CNTs or N-CNTs in the photoactive layer. Manuscript submitted to *Thin Solid Films Journal*.

7. Godfrey Keru, Patrick G. Ndungu, Vincent O. Nyamori and Genene T. Mola. Boron- or -Nitrogen doped CNT as charge extracting and transporting layer in bulk heterojunction organic solar cell. Manuscript submitted to Journal of Physics: Condensed Matter-IOPscience.

From all the above publications, my role included carrying out all the experimental work, and contributing to the writing of the manuscripts along with the guidance of my supervisors. My supervisors' roles were to edit, checking scientific content and my correct interpretation of data. Based on their expertise, they have added some parts to the manuscripts.

Signed:.....



## CONFERENCE CONTRIBUTIONS

1. IBSA workshop on Nanotechnology that was held at the Thaba Ya Batswana, south of Johannesburg. An oral presentation entitled “Doped carbon nanotubes functionalized with macrocyclic molecules for organic photovoltaic cells”. (October 2012)
2. IBSA workshop on Nanotechnology that was held at St. Georges Hotel. An oral presentation was given entitled “Bulk heterojunction solar cell with P3HT/MWCNTs active layer and Ni(II)Pc/N-CNTs hole transport layer”. (May 2013)
3. Inorg2013 SACI Inorganic Chemistry Conference, held in Durban South Africa. A poster was presented entitled “Nitrogen-doped carbon nanotubes synthesized by pyrolysis of (4-[(pyridin-4-yl)methylidene]amino]phenyl)-ferrocene”. (4 July 2013)
4. Eskom Exhibition. A poster presentation was presented entitled “Solar energy harvesting materials” (August 2013)
5. College of Agriculture, Engineering and Science Research Day. An oral presentation was given entitled “Bulk heterojunction solar cell with nitrogen-doped carbon nanotubes/polymer composites in the active layer”. (November 2013)
6. IBSA 10 year’s celebration held at Birchwood hotel & OR Tambo conference centre. An oral presentation was presented entitled “Bulk heterojunction solar cell with nitrogen-doped carbon nanotubes/polymer composites in the active layer”. (April 2014).
7. A three months visit to Nanotechnology and Solar Cells Laboratory (LNES), Chemistry Institute, University of Campinas, Brazil (9<sup>th</sup> August- 5<sup>th</sup> November 2014).

## **DEDICATION**

This work is dedicated to **Prof. Stephen K. Wambugu** for discovering a hidden potential in me and ensuring it was utilized to the fullest. Thank you for encouraging me to further my education.

## ACKNOWLEDGEMENTS

First and foremost I would like to thank God Almighty for this far I have come.

I wish to express sincere gratitude to my supervisors Prof. Vincent O. Nyamori, Prof. Patrick G. Ndungu and Prof. Genene T. Mola for their guidance and encouragement. Your Advice and input made this work enjoyable and possible. You were always there for me any time I required your help. Special thanks to Prof Nyamori for coming to my rescue when in Brazil and my bank could not let me access my account. I also wish to thank Prof. Bice Martincigh for proof reading my manuscripts, Dr Bernard Owaga for the crystal structure data and Dr Nolwazi Nombona for good advice, in the course of this work.

I would like to recognize University of KwaZulu-Natal for accepting me to study, College of Agriculture, Engineering and Science for post graduate bursary and School of Chemistry and Physics for the equipment that I used during the study.

I wish to extend special gratitude to India, Brazil and South Africa (IBSA) nanotechnology and energy initiative for the sponsorship. Every time we had a workshop the members always gave very good contribution to this work which was part of this initiative.

I wish to thank the late Prof. Naftali T. Muriithi *aromama kwega kuraga* (may his soul rest in peace) for his encouragement and believing in me. Every time I visited your office in Kenyatta University I left with renewed spirit.

I acknowledge the former and current nanochemistry research group students; Lucy, Tonderai, Njogu, Kudzai, Ntokozo, Nonjabulo, Zulu and Rachel. You guys made the life in the lab quite enjoyable. Special mention to Nonjabulo, for introducing me to the synthesis of organometallic compounds and taking me through NMR. Rachel for enlightening me on synthesis and characterisation of carbon nanotubes.

In the course of this work many technical staff in the School of Chemistry and Physics were a blessing to me and they deserve to be mentioned; Anita, Neal, Dilip, Gregory,

Miller, Shanon, Patience, Unathi among others. Additionally, Philip, Vishal and Nelisha of the Microscope Unit.

My acknowledgement would not be complete without thanking members of Nanotechnology and Solar Cell Lab in the University of Campinas, Brazil. Thank you, Prof. Dr Ana for accepting me in your group. Group members: Matheus, Nicolau, Mauricio, Douglas, Luiz, Rodrigo, Emre, Gabriela, Andreia, Joa Paulo, Paulo, Felipe and Ivo. Thank you for making my life comfortable the time I was in your lab and being there for me especially when I wanted to be assisted due to language barrier and also, when going to *Restaurante Universitario (Bandejao)*. To you all *obrigados*

Kenyan students in UKZN, Westville, you also deserve special mention for ensuring I felt at home all the time. Special thanks to Moses Ollengo for ensuring I settled well the first time I landed in South Africa and showing me around Durban City.

My deepest gratitude to my parents: Ephantus Keru and Grace Wangari for parental love and support. Also, my brothers: Alex, Steve, James and Peter for support and prayers. Thank you for being there for me always.

Finally I wish to extend heartfelt gratitude to my dear wife Martha, children Chris, Teddy and Debra for allowing me to leave them and study abroad. Thank you for your support, prayers and encouragement.

## TABLE OF CONTENTS

<i>Abstract</i>	ii
<i>Preface</i>	v
<i>Declaration 1–Plagiarism</i>	vi
<i>Declaration 2-Publications</i>	vii
<i>Conference Contributions</i>	ix
<i>Dedication</i>	x
<i>Acknowledgements</i>	xi
<i>Table of Contents</i>	xiii
<i>List of Abbreviations and Symbols</i>	xix
<b>Chapter One: Introduction</b>	<b>1</b>
1. History and discovery of carbon nanotubes	1
2. Structure of CNTs	2
2.1 Types of CNTs	5
3. Synthesis of CNTs	6
3.1 Arc discharge method	6
3.2 Laser ablation method	7
3.3 Chemical vapour deposition	9
4. Organometallic compounds as CVD catalyst for CNTs synthesis	10
5. Boron- and nitrogen-doping of CNTs	11
6. Application of CNTs	14
7. Organic solar cells	17
8. Aim and objectives of this research	20
9. Overview of this research	20
10. Conclusion	24
References	24
<b>Chapter Two: A review on carbon nanotube/polymer composites for organic solar cells</b>	<b>31</b>
Summary	32
1. Introduction	33

1.1.	Solar energy	35
1.2.	Inorganic versus organic solar cells (OSCs)	35
1.3.	Photo-excitation and carrier generation in OSCs	39
1.3.1.	Calculating efficiencies in OSCs	39
1.3.2.	Physicochemical factors that affect the efficiency of OSCs	41
2.	Incorporation of carbon nanotubes in organic solar cells	44
2.1.	Advantageous properties of carbon nanotubes for organic solar cell	47
2.2.	Physicochemical properties of CNTs	47
2.2.1.	Electronic properties of CNTs	48
2.2.2.	Mechanical properties of CNTs	49
2.2.3.	Thermal properties of CNTs	50
2.2.4.	Chemical properties of CNTs	51
2.3.	Functionalization of CNTs	51
2.3.1.	Non-covalent functionalization	52
2.3.2.	Covalent functionalization	53
3.	Assembling solar cells	53
3.1.	Processing conjugated polymer/CNT composites	53
3.1.1.	Solution processing	54
3.1.2.	Melt processing	54
3.1.3.	<i>In situ</i> processing	55
3.2.	Film deposition techniques	56
3.2.1.	Spin coating method	56
3.2.1.	Knife-coating and slot-die coating method	56
3.2.1.	Inject printing and spray coating method	57
3.2.1.	Dip coating	58
3.2.1.	Other printing techniques	58
4.	Case studies	58
4.1.	Single-walled carbon nanotubes	58
4.2.	Double-walled carbon nanotubes	58
4.3.	Multiwalled carbon nanotubes	59
5.	Conclusion	59
	Acknowledgements	64

References	64
<b>Chapter Three: (4-[(Pyridin-4-yl)methylidene]amino)phenylferrocene</b>	<b>80</b>
Abstract	81
1. Related literature	81
2. Comment	81
3. Experimental	83
4. Refinement	83
5. Computing details	83
6. Crystal data	84
7. Cell parameters from 36615 reflections	84
8. Data collection	84
9. Refinement	84
10. Special details	85
10.1 Geometry	85
10.2 Refinement	85
Acknowledgement	86
Supplementary data and figures	86
References	86
<b>Chapter Four: Nitrogen-doped carbon nanotubes synthesised by pyrolysis of 4-[(pyridin-4-yl)methylidene]amino}-phenylferrocene</b>	<b>87</b>
Abstract	88
1. Introduction	89
2. Experimental	90
3. Results and discussion	91
3.1. Effect of carbon source	94
3.2. Effects of growth temperature	95
3.2.1. The nitrogen-doping percentage	96
3.2.2. N-CNTs yield and general morphology	97
3.2.3. Graphitic nature/crystallinity	98
4. Conclusion	100
Acknowledgement	101

References	101
<b>Chapter Five: Effect of boron concentration on physicochemical properties of boron-doped carbon nanotubes</b>	<b>106</b>
Abstract	107
1. Introduction	108
2. Experimental	109
2.1 Materials and synthesis of B-CNTs	109
2.2. Characterisation	110
3. Results and discussion	112
3.1. Effect of boron on morphology and composition of products	112
3.2. Determination of % boron concentration in the samples	116
3.3. Effect of % boron concentration on graphitic nature and thermal stability of the samples	117
3.4. Variation of textural properties of B-CNTs and B-CNF with % boron concentration in the sample	119
3.5. Effect of % boron concentration on conductivity of B-CNTs	122
3.6. Effect %boron concentration on magnetic properties of B-CNTs	124
3.7. Effect of % boron concentration in B-CNTs on surface energy properties	125
4. Conclusion	130
Acknowledgement	131
References	131
<b>Chapter Six: Bulk heterojunction solar cell with nitrogen-doped carbon nanotubes in the active layer: Effect of nanocomposite synthesis technique on photovoltaic properties</b>	<b>135</b>
Abstract	135
1. Introduction	136
2. Experimental	138
2.1. Materials	138
2.2. Synthesis of nitrogen-doped CNTs and nanocomposites	138
2.3. Characterization of the nanocomposites	139



2.4. Device preparation	141
3. Results and discussion	141
3.1. Morphology and structure of the nanocomposite	141
3.2. Vibrational and spectral characteristics of P3HT and the nanocomposite	144
3.3. Thermal stability of the nanocomposites	148
3.4. Surface energy analysis of nanocomposites	149
3.5. Photovoltaic properties	151
4. Conclusion	155
Acknowledgement	155
References	155
<b>Chapter Seven: Performance of organic solar cells P3HT:PCBM with boron- or nitrogen-doped carbon nanotubes in the photoactive layer</b>	<b>159</b>
Abstract	159
1. Introduction	160
2. Experimental	162
2.1. Materials and methods	162
2.2. Preparation of B- and N-CNTs/P3HT:PCBM solution	164
2.3. Device preparation	164
2.4. Characterisation techniques	164
3. Results and discussion	166
3.1. Structure of B- and N-CNTs	166
3.2. Effect of B- or N-CNTs on the spectro properties of the photoactive layer	170
3.3. Photovoltaic properties	172
3.4. Morphology of the films	174
3.5. Recombination dynamics in the film blends	175
4. Conclusion	178
Acknowledgement	179
References	179

<b>Chapter Eight: Boron- or -Nitrogen doped CNT as charge extracting and transporting layer in bulk heterojunction organic solar cell</b>	<b>182</b>
Abstract	182
1. Introduction	183
2. Experimental	184
3. Results and discussion	187
3.1. Characterisation of doped CNTs	187
3.2. Electrical characteristics	189
4. Conclusion	193
Acknowledgements	193
References	193
<b>Chapter Nine: Conclusion and future work</b>	<b>196</b>
1. Summary	196
2. Future work	199

## LIST OF ABBREVIATIONS AND SYMBOLS

Ac	Amorphous carbon
AFM	Atomic force microscope
AM	Air mass
B-CNTs	Boron-doped carbon nanotubes
BET	Brunauer–Emmett–Teller
BHJ	Bulk heterojunction
CdS	Cadmium sulphide
CdTe	Cadmium telluride
CHNS	Carbon, hydrogen, nitrogen and sulphur
CNFs	Carbon nanofibres
CNTs	Carbon nanotubes
Co	Cobalt
COMs	Conjugated organic molecules
CSP	Concentrating solar power
CPs	Conducting polymers
CS	Carbon spheres
CuInGaSe	Copper indium gallium selenium
CVD	Chemical vapour deposition
D-A	Donor-acceptor
D-CNTs	Doped-carbon nanotubes
D-band	Disorder-band
DFT	Density functional theory
DWCNTs	Double-wall carbon nanotubes
EDX	Electron dispersive X-ray spectroscopy
EQE	External quantum efficiency
FESEM	Field emission scanning electron microscope
FeTMMP-Cl	Iron tetramethoxyphenyl-orphyrin chloride
FF	Fill factor
GaAs	Gallium arsenide
G-band	Graphitic-band
Hf	Hafnium

HiPCO	High pressure carbon monoxide
HOMO	Highest occupied molecular orbital
HRTEM	High resolution transmission electron microscope
ICBA	Indene -C <sub>60</sub> bisadduct
ICP-OES	Inductively coupled plasma-optical emission spectroscopy
ID	Internal diameter
I <sub>D</sub> /I <sub>G</sub>	Intensity of D compared to intensity of G
IGC	Inverse gas chromatography
I <sub>MAX</sub>	Maximum current
InP	Indium phosphite
I <sub>SC</sub>	Short circuit current
ITO	Indium tin oxide
J <sub>SC</sub>	Short circuit current density
J-V	Current density-voltage
KBr	Potassium bromide
LiF	Lithium fluoride
LUMO	Lowest occupied molecular orbital
MEH-PPV	Poly[2-methoxy-5-(2-ethylhexyloxy)-1,4-phenylenevinylene]
Mo	Molybdenum
M <sub>R</sub>	Magnetic remanent
M <sub>S</sub>	Saturation magnetization
MWCNTs	Multiwall carbon nanotubes
Nb	Niobium
N-CNTs	Nitrogen-doped carbon nanotubes
Ni	Nickel
OD	Outer diameter
OPV	Organic photovoltaic
OSCs	Organic solar cells
P3HT	Poly(3-hexylthiophene)

P3OT	Poly(3-octylthiophene)
PCBM	[6,6]-phenyl-C <sub>61</sub> -butyric acid methyl ester
PCE	Percentage cell efficiency
PEDOT:PSS	Poly(3,4-ethylenedioxythiophene):poly-(styrenesulfonate)
PID	Proportional-integral-derivative
PI	Photoluminescence
PM	N-(1-pyrenyl)maleimideQTF <sub>12</sub> 2,7-Bis-(3,3'''-didodecyl-[2,2',5',2'';5'',2''']quarter-thiophen-5-yl)-fluoren-9-one
Re	Rhenium
Sc	Scandium
SCNMs	Shaped carbon nanomaterials
SEM	Scanning electron microscope
SPV	Solar photovoltaic
SSC	Silicon solar cells
SWCNTs	Single-wall carbon nanotubes
Ta	Tantrum
TAS	Transient absorption spectroscopy
TCO	Transparent conductive oxide
TEM	Transmission electron microscope
TGA	Thermogravimetric analysis
Ti	Titanium
T <sub>MAX</sub>	Maximum temperature
UV-Vis	Ultra violet-visible
V	Vanadium
V <sub>MAX</sub>	Maximum voltage
V <sub>OC</sub>	Open circuit voltage
VSM	Vibrating sample magnetometer
W	Tungsten
XPS	X-ray photoelectron spectroscopy

# Chapter One

## Introduction

Shaped carbon nanomaterials (SCNMs), especially carbon nanotubes (CNTs), are among the most extensively researched materials today. The production of CNTs has recently increased exceeding several thousand tons per year [1]. The increasing production of CNTs is largely attributed to their wide application in manufacturing of products, such as, rechargeable batteries [2], automotive parts [1], sporting goods [3], boat hulls [4] and water filters [5], among others. They are also being considered for applications in supercapacitors [6], optoelectronics [7], and lightweight electromagnetic shields [1]. The commercialization of CNTs has been made possible by improved synthesis, purification and chemical modifications, which have made incorporation of CNTs into other materials easier. In the proceeding sections of this chapter, the synthesis of CNTs and their applications are discussed. Finally, the objectives and overview of this thesis will be presented.

### 1. History and discovery of carbon nanotubes

Although the discovery of CNTs in most academic and popular journals is attributed to Sumio Iijima in 1991 [8], their history dates back to 1952. Radushkevich and Luckyanovich [9] published clear images of carbon nanotubes with a diameter of about 50 nm in the Soviet Journal of Physical Chemistry. In 1976, Endo and co-workers [10] published a paper on a vapour grown hollow carbon fibre with a diameter in the nanometre range. Abrahamson and Rhodes [11] also presented evidence of fibrous carbon at Penn State University in 1979 at a Biennial conference. More results of carbon nanofibres were published by a group of Soviet scientists in 1981 and were reported as multi-layer tubular crystals formed by rolling up graphene layers into a cylinder [12]. These hollow carbon fibres reported by these researchers resemble what are referred to as CNTs today.

Kroto *et al.* [13] in 1985 discovered fullerenes ( $C_{60}$  and  $C_{70}$ ), which were named Buckminster fullerenes. This allotrope of carbon (other than the known allotropes) started the move towards the study of other possible carbon allotropes. This discovery earned

these researchers the Nobel Prize in 1996 [14]. In the process of synthesizing fullerenes, by means of an arc discharge set-up, Iijima observed finite carbon structures consisting of needle-like tubes. These needle-like structures comprised about 2-50 coaxial tubes of graphitic sheets which were named multiwalled carbon nanotubes (MWCNTs). Ever since, CNTs have attracted interest for both academic and industrial purposes. This interest is due to their outstanding properties, such as high mechanical strength, high surface area, electrical and thermal conductivities, and thermal stability [15]. Their properties are also being extensively studied and this is evident from the number of publications and application patents reported on the subject [14,16-21]. These have been increasing linearly every year as shown in Figure 1. The data was obtained from Thomson Reuters™ ISI Web of Science.

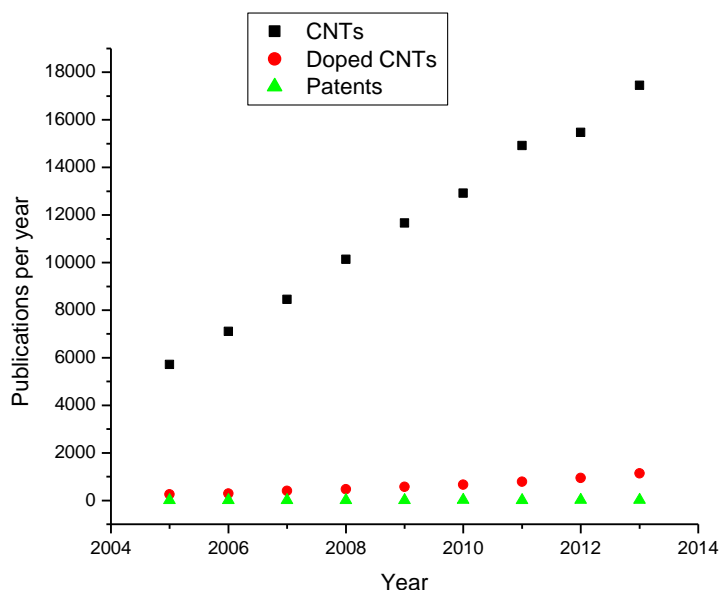


**Figure 1:** Publications on CNTs from the year 2005 to 2013.

## 2. Structure of CNTs

CNTs can be visualised as a graphene sheet rolled up into a seamless tube (Figure 2) [22]. The rolling up of the graphene sheet also defines the chirality of the nanotube.

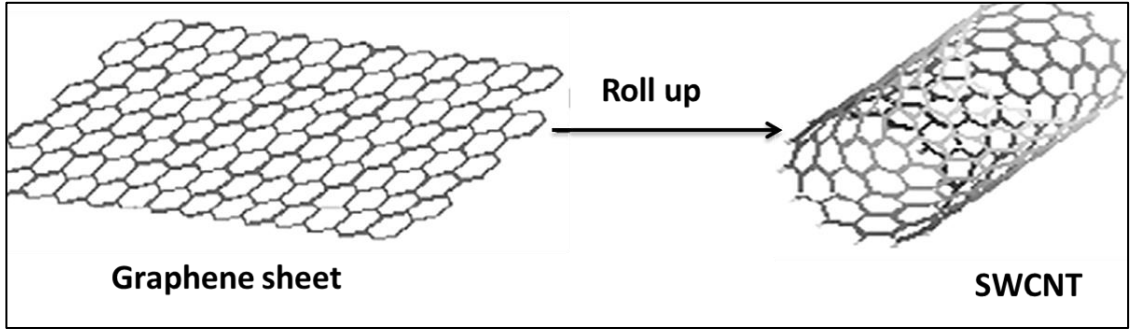


**Figure 2:** Diagram showing how a graphene sheet can be rolled up into a single-walled carbon nanotube (SWCNT) [22].

Rolling up of the graphene sheet is defined by a chiral vector that is determined by two integers  $m$  and  $n$  [23]. Two carbon atoms are chosen in the graphene sheet whereby one acts as the origin while the other acts as a chiral vector  $C$  pointed to the next carbon (Figure 3). The chiral vector  $\vec{c}$  is defined by;

$$\vec{c} = n\vec{a}_1 + m\vec{a}_2 \quad (1)$$

where,  $n$  and  $m$  are integers and  $\vec{a}_1$  and  $\vec{a}_2$  are the unit cell vectors.

Three types of CNT structures are formed, for example, when  $m = n$ , and the angle  $\theta$  is equal to  $0^\circ$ , an armchair structure is formed,  $\theta$  is defined by;

$$\theta = \tan^{-1}\left(\frac{m\sqrt{3}}{m+2n}\right) \quad (2)$$

When  $m$  or  $n = 0$  and  $\theta = 30^\circ$ , a zigzag structure is formed whilst when  $n \neq m$  and  $\theta > 0 < 30^\circ$ , a chiral CNT is formed. Figure 4 illustrates the formation of these three types of structures.



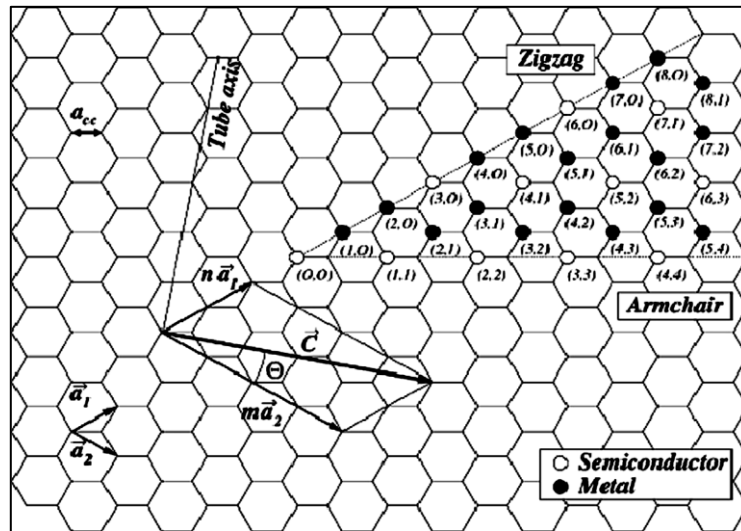


**Figure 3:** Diagram of graphene sheet and vector structure classification that is used to define CNT structures [24].

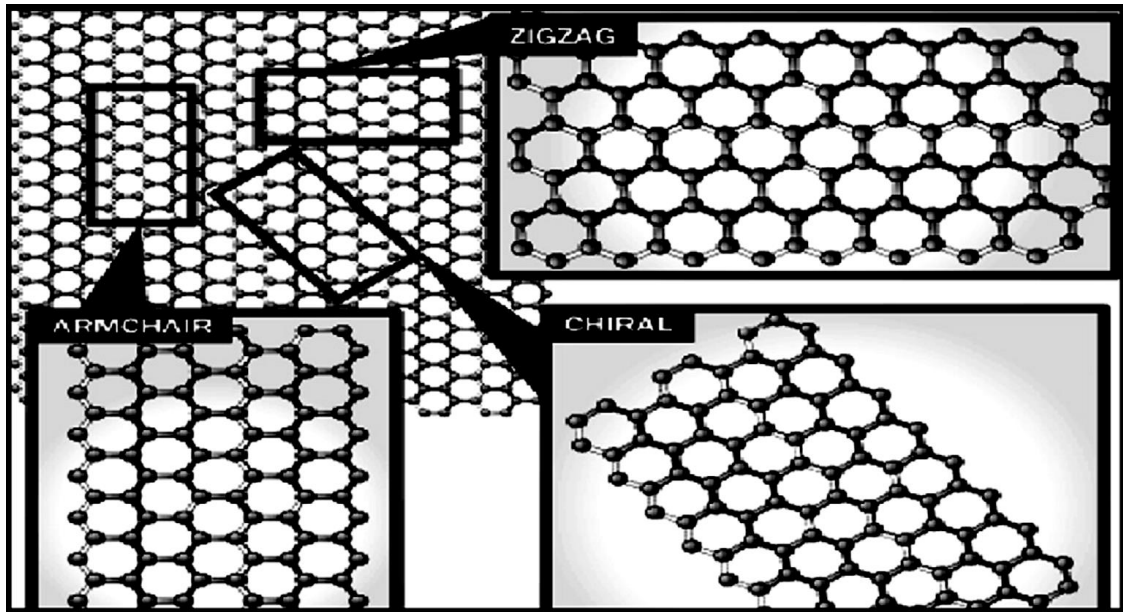


**Figure 4:** Formation of the three types of CNT structures [14].

Additionally, the values of  $n$  and  $m$  affect the properties of CNTs, such as optical, mechanical and electronic properties. For example;

$$|n - m| = 3i \quad (3)$$

is observed in metallic CNTs. For semi-conducting CNTs, they are defined by

$$|n - m| = 3i \pm 1 \quad (4)$$

where,  $i$  is an integer [25].

## 2.1. Types of CNTs

Depending on the number of coaxial structures present, CNTs can generally be classified into single-walled carbon nanotubes (SWCNTs), double-walled carbon nanotubes (DWCNTs) and multiwalled carbon nanotubes (MWCNTs). SWCNTs are made up of a single graphene sheet which is rolled into a seamless cylinder with a diameter ranging between 0.2 to 1 nm [26]. DWCNTs are composed of two concentric cylinders, whereas MWCNTs are made up of more than two concentric cylinders with diameters ranging between 2 to 100 nm [27]. An example of a SWCNT and a MWCNT is shown in Figure 5.

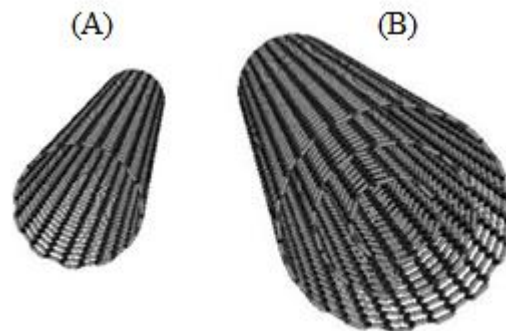


**Figure 5:** Types of CNT: (A) SWCNT and (B) MWCNT [24].

### 3. Synthesis of CNTs

CNTs can be synthesized by three methods, namely, arc discharge, laser ablation and chemical vapour deposition (CVD). Nevertheless, intensive research is on-going for more economical methods of producing CNTs. The subsequent sections will discuss these methods.

#### 3.1. Arc discharge method

In this technique, an electric arc is generated between two graphite electrodes (Figure 6). The temperature rises to about 3000 °C to create a plasma. This vaporizes the graphite at the anode and, if metal nanoparticles are present, CNTs deposit on the cathode [28]. The high temperature used in this method requires an inert atmosphere to prevent oxidation of the graphite electrodes plus metal catalyst present [29].

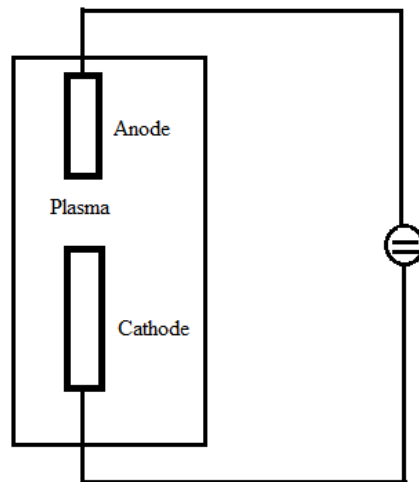


**Figure 6:** Schematic diagram of arc discharge.

Some examples where arc-discharge methods have been used for the synthesis of CNTs include MWCNTs of between 2–50 cylinders which were synthesized by Iijima [8] in 1991 in the process of synthesising fullerenes. Also, Ebbesen and Ajayan [30] reported the large scale synthesis of MWCNTs with diameters ranging between 2-20 nm by arc discharge. Similarly, SWCNTs have also been synthesized by using arc discharge. For instance, Iijima and Ichihashi [26], as well as Bethune *et al.* [31], reported almost at the same time

the maiden synthesis of SWCNTs by arc discharge. The major disadvantages of arc discharge are low yields and high levels of impurities such as soot and metal catalyst residues which eventually require cleaning. Also, it is an energy intensive method and this is not favourable. Nevertheless, it has the advantage that it forms highly crystalline CNTs [32]. Consequently, as illustrated in Table 1, arc discharge is used commercially for the synthesis of SWCNTs.

### 3.2. Laser ablation method

The laser ablation method requires the use of a laser to ablate a graphite target filled with metal powder catalyst into vapour [33]. The commonly used metal catalysts are cobalt and nickel. Vaporisation of the graphite target forms CNTs that are deposited on a cooled collector as illustrated in Figure 7.

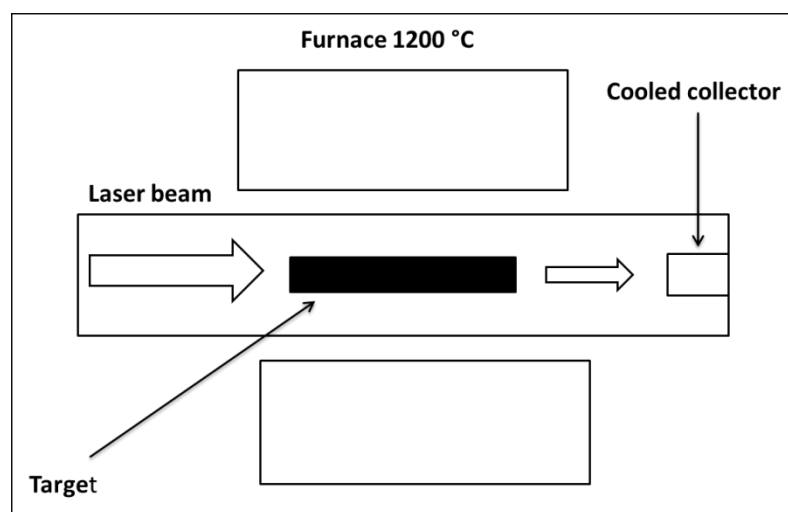


**Figure 7:** Schematic illustration of laser ablation.

The high temperature in the furnace anneals the product making it highly crystalline, hence, the method is efficient for the synthesis of high quality SWCNTs. Eklund *et al.* [34] reported the large scale synthesis of SWCNTs *via* this method. An important limitation and characteristic to this method is the high amount of energy required for synthesis.

**Table 1:** Methods of synthesis of CNTs in the market from different commercial suppliers.

Carbon nanotube supplier	Type of CNT	Method of synthesis*
Ad-nano technologies	MWCNTs	CVD
Carbon Nanomaterial Technologies Co, Ltd.	SWCNTs	CCVD
	MWCNTs	CCVD
Cheaptube.com	SWCNTs	CCVD
	DWCNTs	CCVD
	MWCNTs	CCVD
Cnano Technology	MWCNT	CVD
Southwest Nanotechnologies, Inc.	SWCNTs	CCVD
	MWCNTs	CCVD)
Nanolab	SWCNTs	PECVD
	DWCNTs	PECVD
	MWCNTs	CVD
Carbon Solution, Inc.	SWCNTs	Arc discharge
Reinste.com	SWCNTs	Arc discharge
Nanolab	SWCNTs	Arc discharge
	DWCNTs	CVD
	MWCNTs	CVD
Nanocyl	DWCNTs	CCVD
	MWCNTs	CCVD
Sigma Aldrich	SWCNTs	CCVD
	MWCNTs	Arc discharge
Vacuum release	MWCNTs	PECVD

\*CVD (chemical vapour deposition), CCVD (catalytic CVD), PECVD (plasma enhanced CVD)

This poses a challenge for its application in large-scale production. Furthermore, this method, as well as arc discharge, requires solid graphite, which is not cheap, as a target to be evaporated to form CNTs. Moreover, the challenge is how to obtain a sufficiently large graphite target for large scale production of CNTs.

### **3.3. Chemical vapour deposition (CVD)**

Chemical vapour deposition (CVD), also known as catalytic vapour deposition, involves the decomposition of hydrocarbons in the presence of a catalyst. Depending on the conditions used, the method can produce SWCNTs, MWCNTs, plus other shaped carbon nanomaterials (SCNMs), such as, carbon spheres and carbon nanofibres. A temperature range between 300–1000 °C is often used to decompose the carbon source [35]. The carbon source can either be in a solid, liquid or gaseous phase. The decomposition of precursors and growth of CNTs takes place in the hot zone of the furnace. The carbon source is introduced into the furnace by controlled gas flow or as an aerosol. An example of a CVD setup is illustrated in Figure 8. The CNT growth is controlled by many factors which may include: temperature of the reaction, composition and flow rate of carrier gas, type of catalyst nanoparticles, and the kind of carbon source. The diameters of the CNTs depend on the size of the catalyst nanoparticles, therefore, catalyst deposition techniques should be done carefully to achieve the desired sizes of CNTs. Other morphologies of the CNTs, such as surface roughness and alignment of MWCNTs, can be altered by using different type of CVD, e.g. plasma-assisted CVD provides vertically aligned MWCNTs [36].

The advantage of CVD as a method for synthesis of CNTs is its simplicity, energy efficiency, capability to scale up, and high yield [37]. Transition metals, such as Fe, Co and Ni, are commonly used as catalysts. However, other metals, such as Sc, Ti, V, Cr, Mn, Y, Zr, Nb, Mo, Hf, Ta, W, Re or a combination, can also be used [38]. The synthesis of CNTs through the CVD method can be achieved by using either a solid metal catalyst supported on a substrate or by introducing the catalyst as an organometallic compound which vaporizes in the hot zone. The latter approach is also known as floating catalysis, which provides nano-size particles.



**Figure 8:** CVD set up at the University of KwaZulu-Natal, Nanochemistry Laboratory.

#### **4. Organometallic compounds as CVD catalyst for CNTs synthesis**

One of the most commonly used organometallic floating catalysts is ferrocene [39] and  $\text{Fe}(\text{CO})_5$  [40]. Other organometallic compounds that have also been investigated as catalysts for the synthesis of CNTs include ruthenocene [41], cobaltocene and nickelocene [42]. MWCNTs were successfully synthesised with cobaltocene and nickelocene. Metal nanoparticles are formed after the decomposition of the organometallic compound and reduction of the metal [43]. Apart from ferrocene, its derivatives can also be used as a source of metal nanoparticles. These ferrocenyl derivatives can be synthesized in such a way to serve as a source of active metal nanoparticles (catalyst), additional carbon source or even as a heteroatom source for CNT-doping. There are various methods that can be used to synthesise ferrocenyl derivatives. However, the current and more greener approach involves use of mechanochemical method.

Mechanochemical synthesis involves a reaction that is activated by co-grinding or milling of powdered materials. The reaction usually occurs under solvent-free conditions with the precursors in either the solid, liquid or vapour state [44]. The principles of green chemistry are usually applied in these reactions whereby the use of toxic flammable solvents that usually pollute the environment are eliminated. This method increases the yield and can

also affect the selectivity during synthesis [45]. In comparison with synthesis in a solvent, the solvent-free synthesis takes a short reaction time and it is also relatively easy to isolate the final products [46]. Such synthesis reactions have been used by different groups to synthesize ferrocenyl derivatives with water as the only by-product formed. For example, Ombaka *et al.* [45] used this mechanochemical approach to synthesize 1, 1'-ferrocenyldiacrylonitriles by grinding 1,1'-ferrocenylcarboxylaldehyde with phenylacetonitriles. The ferrocenyl derivatives were obtained within a short reaction time and water was the only by-product. Imrie *et al.* [47] also synthesized 1, 1'-ferrocenyldiimine and ferrocenylacrylonitriles with good yields when 1, 1'-ferrocenylcarboxylaldehydes with aromatic amines were ground together. These ferrocenyl derivatives can be used as a source of heteroatoms as a dopant (e.g. nitrogen) during the synthesis of doped-CNTs as stated earlier. The common doped-CNTs include nitrogen-doped CNTs (N-CNTs) and boron-doped CNTs (B-CNTs).

## **5. Boron- and nitrogen-doping of CNTs**

CNTs are known to possess remarkable electronic, magnetic, thermal, chemical and mechanical properties. Although the properties of CNTs are tremendous, there are still some areas where their performance can be improved. This has prompted researchers to think of ways of modifying CNTs, to enhance these properties to suit other applications [48]. This can be achieved by structural modification of CNTs to obtain defined morphologies and controlled properties. For example, electronic properties of CNTs are controlled by delocalization of electrons; therefore any form of chemical modification can affect this property. Structural modification can be achieved either by surface functionalization or substitution of carbon atoms by a foreign atom otherwise known as doping.

Doping is the deliberate replacement of carbon atoms with 'impurity' (foreign atoms) such as nitrogen or boron. Any atom whose charge and size is adequate can be inserted into the CNT lattice. Boron and nitrogen are the most popular dopants due to their position in the periodic table just next to carbon. However, other atoms such as lithium [49] and



phosphorous [50,51] have also been used. Doping CNTs with heteroatoms can be achieved in two ways, namely, post- and *in situ*-doping. Post-doping involves the use of thermal treatment on CNTs to force the dopant atoms into the carbon lattice [52]. On the other hand, *in situ* doping involves the mixing together of the carbon source, catalyst, and dopant during synthesis. For instance, Jiang *et al.* [53] post-doped CNTs with boron by heating a mixture of boron powder and MWCNTs and obtained B-CNTs with cone shaped morphologies similar to the ones in Figure 9 (B). Lee *et al.* [54] also used post-synthesis to dope MWCNTs with boron and nitrogen. Thermal treatment of MWCNTs with boron powder in the presence of Ar/NH<sub>3</sub> was used. NH<sub>3</sub> gas was used to etch the CNTs to induce defects by the formation of CN<sub>x</sub> and C<sub>x</sub>H<sub>y</sub> groups and the vacancies formed after etching are filled by substitution with boron. For nitrogen-doping, thermal treatment was performed without the boron source. Yang *et al.* [55] synthesised B-CNTs by *in situ*-doping with a mixture of benzene, triphenylborane and ferrocene. B-CNTs containing percentages ranging between 0-2.24% by weight were synthesized in this work. Nxumalo *et al.* [56] used *in situ*-doping to synthesize N-CNTs by using ferroceneaniline, or a mixture of ferrocene and aniline, as the catalyst as well as the nitrogen source, and apart from toluene it was also an additional source of carbon. Higher doping was reported for ferroceneaniline compared with the mixtures of ferrocene and aniline. When a dopant is inserted into the carbon network of CNTs, the symmetry, structure and properties are altered [57]. For example, structural changes are observed when boron or nitrogen is inserted in the CNT lattice. Whereas pristine CNTs are known to be hollow, insertion of heteroatoms such as boron and nitrogen introduces cone structures and bamboo compartments, respectively (Figure 9).

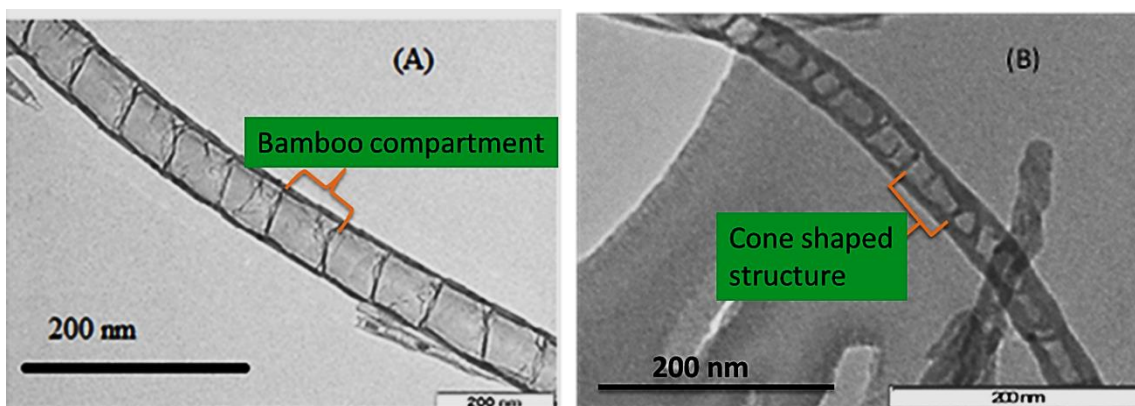


**Figure 9:** TEM images of (A) nitrogen-doped CNTs with bamboo compartments with very thin wall and (B) boron-doped CNTs with cone shaped structures that were synthesized in this study.

Boron-doping makes CNTs to be wavy and kinky as a result of the formation of “elbow joints”. Additionally, Terrones *et al.* [57] suggest that boron-doping increases the tube length as a consequence of it acting as surfactant, inhibiting closure of the tubes and promoting continued growth [58]. The inhibition of tube closure was also shown from density functional theory (DFT) calculations by Hashim *et al.* [59], who reported that boron-doping favours formation of heptagons. On the other hand nitrogen-doping favours the formation of pentagons which promote tube closure [60].

Boron has one electron less than carbon; hence, it acts as an acceptor when inserted into the carbon network of CNTs. This way, boron induces emptying of electronic states below the Fermi energy of pristine CNTs making them p-type conductors. On the other hand, nitrogen-doping brings an extra electron to the carbon network which makes the wall of the tube more reactive and, also makes the CNTs n-type conductors by raising the Fermi energy [61]. Insertion of nitrogen into the carbon network leads to the formation of two types of C-N bonds, i.e. one whereby nitrogen induces sharp localised state above the Fermi level owing to the extra electrons. This is usually in the form of quaternary or pyrrolic N-doping (Figure 10), which introduces donor states or makes CNTs n-type conductor. Alternatively, pyridinic type N-doping in which nitrogen is coordinated by two

carbon atoms and induces localised states below the Fermi level, thereby introducing metallic (p-type) behaviour depending on the level of doping obtained [62].

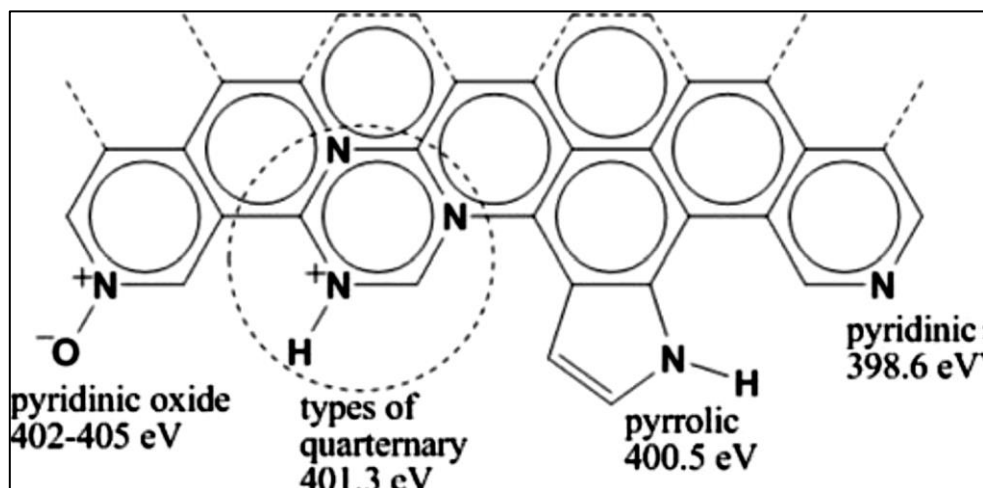


**Figure 10:** Types of nitrogen species that can be incorporated into the graphitic carbon network and the X-ray photoelectron spectroscopy (XPS) binding energies for each type [63].

Doping CNTs with boron or nitrogen enhances the properties of CNTs to suit their application, such as electrical properties. In the next section, some of these applications are discussed.

## 6. Application of CNTs

The nano-scale dimension of CNTs, their mechanical strength, chemical stability and high conductivity make them unique materials with a range of promising applications. CNTs are being used as fillers in plastics to increase stiffness, strength and toughness [1]. The suitability for use as fillers is controlled by the diameter, aspect ratio, alignment, dispersion and interfacial interaction of CNTs with the polymer matrix. Likewise, their high conductivity makes them suitable for use as conductive fillers in polymers. For instance, Chou *et al.* [64] reported a high conductivity of  $10000 \text{ S m}^{-1}$  for a composite with a 10% loading percolation threshold and attributed this to the conductive pathway introduced by CNTs.

CNTs are also applied in coatings and films, for example, paints containing MWCNTs are used as protective coats on ship hulls. This protects ships against attachment of algae and barnacles [4]. Additionally, CNT films are being used as anti-corrosion coating on metals [1]. In such coatings CNTs enhance stiffness, strength, and provide an electric pathway for cathodic protection. CNT films are also being proposed as alternatives to transparent conductive oxides, such as, indium tin oxide (ITO) [65]. Alternative replacements for ITO have been compelled by the increased demand for displays, touch screen and photovoltaic cells, which have made the price of indium very expensive. CNT films are becoming the best alternative owing to the ease of synthesis, flexibility and final deposition on the substrates by cost-effective techniques like spray painting, and slot and die, amongst many others.

CNTs have also been applied in microelectronics as transistors [7]. SWCNTs are attractive for transistors due to their low scattering effect and, also, compatibility with field effect transistors (FET). CNT thin film transistors are used to drive organic light emitting diode (OLED) displays. For instance, McCathy *et al.* [66] reported vertical FET with sufficient current to drive OLEDs at low voltage. In their findings, FET enabled emission of red-green-blue light through a transparent CNT network. Similarly, it is also anticipated that metallic CNTs with low defect density and contact resistance could replace copper in microelectronics interconnect. This is possible because of the low scattering effect, high current carrying capacity and migration resistance [1].

CNTs have found application in energy storage. For example, MWCNTs are being used in lithium ion batteries for mobile phones and notebook computers [67]. In fuel cells, the use of CNTs as catalyst supports has been reported to reduce the amount of platinum catalyst used when compared to carbon black [68]. For example, Le Goff *et al.* [68] reported the use of MWCNTs as supports for the Pt catalyst and reported a 60% platinum reduction compared with carbon black as the support.

CNTs in biotechnology are being used as sensors due to their high surface area and compatibility with biomolecules such as DNA and proteins. For example, Star *et al.* [69] reported CNT FET that were functioning as selective detectors for DNA immobilization and hybridization. Moreover, CNTs are also used as gas sensors and toxin detectors in food industries [1]. Esser *et al.* [70] reported the use of CNT-based devices to detect ethylene gas as a fruit ripening determinant. CNTs are also being investigated for application in drug delivery. This is more so because the drug binding onto CNTs and release can be controlled by varying the pH [1]. Liu *et al.* [71] reported more loading of drugs on CNTs as compared with conventional drug delivery systems. In their work, 60% of the anti-cancer drug doxorubicin was loaded on SWCNTs compared with 8-10 % in liposomes, the conventional drug delivery system. Drug release was fast and efficient in acidic media but more research is required to prevent accumulation of the CNTs in the body.

CNTs are also used in solar cells, for example, CNTs are being proposed for use in a hybrid p-n junction with silicon [72]. The basis of this is the superior optoelectronic property of CNTs and well established silicon technology. Thin films of CNTs can be deposited on Si wafers by simple and cost-effective deposition techniques. This is envisaged to reduce the cost of silicon p-n junctions due to the reduced size of silicon used. Moreover, high temperatures used in Si p-n junction manufacturing are avoided in these devices as it is carbon nanotubes that are deposited and not another silicon type [73]. Jung *et al.* [74] reported a SWCNTs/Si hybrid solar cell with high efficiency. A thin film of p-type SWCNTs was deposited on n-type Si wafers, to form a p-n junction with high power conversion (>11%). In organic solar cells (OSCs), CNTs are incorporated to reduce carrier recombination and improve charge carrier mobility [54]. Interfacial donor-acceptor structure in bulk heterojunction OSCs maximizes the opportunity for exciton dissociation [54]. However, the efficiency of these devices is still low due to a lack of dedicated pathways for charge carriers to the electrodes as they usually move *via* hopping mechanism through disordered organic materials [75]. The retarded carrier transport can be addressed

by incorporation of one dimensional nanomaterials such as CNTs within the semi-conducting materials [76,77]. More details on OSCs are discussed in the next section.

## **7. Organic solar cells**

The development of inexpensive renewable energy sources has stimulated a lot of research amongst both industrialists and academic scientists for low cost photovoltaic devices [78]. OSCs could provide the best alternative method for a cheap, and easy way of obtaining energy from solar radiation [79]. Scharber and Sariciftci [80] identified the following as the advantages of OSCs: low mass, flexible/stretchable modules, semi-transparent and aesthetically appealing, significantly lower manufacturing costs, continuous manufacturing processes using state of the art printing, and short energy payback time with low environmental impact during manufacture and operations. Additionally, the organic materials (OMs) used for making OSCs have properties such as the band gap that can be manipulated chemically by using easy and cheap processing techniques [81]. Similarly, these OMs have the ability to transport electric current and absorb light in the ultraviolet-visible region of the solar spectrum due to  $sp^2$  hybridization of carbon atoms [82]. Also, organic semi-conductors are known to have a relatively strong absorption coefficient usually  $\geq 10^5 \text{ cm}^{-1}$  [83].

Although OMs for solar cells have attractive properties as outlined above, they also have some limitations. For example, organic semi-conductors have relatively small diffusion lengths for photo-generated excitons. The diffusion length is  $\approx 10$  nm in amorphous and disordered OMs [84,85]. Photo-generated excitons are important in solar energy conversion processes, though, a strong electric field is required to dissociate them into free charge carriers [82]. However, photon-induced generated excitons in organic materials have high binding energies which are likely to favour geminate recombination. Furthermore, these OMs are known to have a high band gap  $\approx 2.0$  eV which limits their solar harvesting abilities to a greater extent.

For optimum utilization of OMs in solar cells, different device designs have emerged in an attempt to maximize the power conversion output. The first generation devices were made up of a single organic layer sandwiched between two metal electrodes [86]. These devices showed good rectification, and this was attributed to electron and hole injection to  $\pi^*$  and  $\pi$  orbitals respectively [87]. In addition, the Schottky-barrier was established by the p-type organic layer and the metal electrode of lower work function to produce a rectifying behaviour of the diode [88]. Low efficiencies in the order of  $10^{-3}$  to  $10^{-2}$  % were reported for these devices.

Single layer devices were improved with the introduction of the bilayer concept, whereby n-type and p-type organic semiconductor layers were sandwiched between two metal electrodes. The interface between p- and n-type organic semiconductors creates additional exciton dissociation sites for the generation of free charges, and this resulted in significant improvement of the efficiencies [82]. For example, Tang [78] reported a bilayer OSC, composed of a phthalocyanine p-type layer hole conductor and a perylene derivative n-type layer electron conductor and reported an efficiency of 1.0%. A breakthrough in OMs for solar cells was reported with the discovery of fullerenes  $C_{60}$  as electron acceptors, and also, improved properties of conjugated polymers [89]. A polymer-fullerene bilayer was made [84], and also, the bulk heterojunction concept was introduced [90]. In both cases photo-excited electrons from the polymer were transferred to the more electronegative  $C_{60}$ . Transfer of electrons from p-type hole conductors to electron receiving n-type fullerene electron conductors led to the formation of donor-acceptor interfaces [91] which enhanced the generation of free charge carriers.

The bulk heterojunction concept was developed by intermixing polymer donors with fullerene acceptors [54]. To date, this concept has proved to be the best design, as it has solved problems associated with the short diffusion length of excitons. Similarly, excitons dissociating into free charge carriers have been improved as observed from the effective quenching of the excitonic photoluminescence of the polymer [79]. Nevertheless, the efficiencies of these devices still remain low due to retarded movement of photo-generated

charge carriers by hopping through disordered and amorphous OMs. In this study, this problem was addressed by incorporating either B- or N-CNTs in the photoactive layer to enhance charge transfer, and collection at the electrodes.

Future application of polymer based OSCs in energy harvesting can be enhanced if they satisfy the following conditions; (i) Low band-gap to increase light absorption (ii) proper energy level match between LUMO of the donor molecules and acceptor to overcome exciton binding energy (iii) balanced charge carrier mobility for efficient charge transport (iv) optimized energy difference between HOMO of the donor polymer and LUMO of acceptor to maximize VOC. These properties are lacking in most of the 2nd generation thiophene-based polymers being used in OSCs [92]. It has to be noted that thiophene-based polymers are 2nd generation polymers and are less efficient than the recently proposed 3rd generation co-polymers such as polythieno-(3,4-b)-thiophene-co-benzodithiophene copolymer (PTB7) which has a band-gap of 1.6 eV. PTB7 is made of alternating electron rich benzodithiophene (BDT) unit and electron deficient thienothiophene (TT) [93]. These co-polymers have broad light absorption spectrum ranging from 550 nm to 750 nm [94] and have extended  $\pi$  system in BDT units that enable them form  $\pi$ - $\pi$  stacking with short distance between polymer backbone, leading to high charge mobility [93]. Additionally, charge separation rate in PTB7 is 2.7 times faster compared to the rate of annealed P3HT:PCBM film [95]. Density functional theory calculation of non-conformational and electronic properties of PTB7 revealed they have torsional potential almost independent of chain length. This is due to electronic delocalization, hydrogen bonding and absence of adjacent side chain to inter-conjugation unit [96]. Finally, side chain on the ester and benzodithiophene enables good solubility in organic solvent and suitable miscibility with fullerene acceptors [94].



## **8. Aim and objectives of this research**

The general aim of this research was to incorporate doped-CNTs (boron and nitrogen-doped CNTs) in the photoactive layer of bulk heterojunction OSCs to act as charge extractors and carrier pathways.

The specific objectives were to:

- i. Synthesize a novel ferrocene derivative with heteroatoms, such as nitrogen, that could be used as a catalyst and a nitrogen source in the synthesis of N-CNTs.
- ii. Determine the best conditions necessary for the synthesis of doped-CNTs in terms of the carbon source and temperature that can give the highest yield and largest amount of doping.
- iii. Synthesize, characterise and determine the effect of the boron concentration on the physicochemical properties of B-CNTs.
- iv. Synthesize composites of doped-CNTs and poly(3-hexylthiophene) by using different methods to determine which method yields a composite with the best interaction between the polymer and doped-CNTs, and also to investigate the effect of the synthesis method on the efficiency of the OSCs.
- v. Use boron- and nitrogen-doped CNTs as part of the photoactive layer in OSCs and compare the two dopants on cell efficiency.

## **9. Overview of thesis**

The thesis consists of nine chapters. Chapter One provides the introduction and background to the study. The subsequent chapters (Chapter Two to Eight) provide the findings of the research. These chapters are written in paper format and each has an abstract, introduction, experimental work, results and discussion, and a conclusion. Topics covered include the synthesis of B- and N-CNTs as well as other SCNMs, their characterization, and the application of B- or N-CNTs in solar energy harvesting with intent to generate electricity. The last chapter (Chapter Nine) provides a summary of the work carried out and discusses possible future work.

## **Chapter One (Introduction)**

This chapter introduces this thesis by giving the general background information on the research and also lays the foundation on the findings reported in this thesis. The research aim and objectives and the outline of this thesis are also given in this chapter.

## **Chapter Two (Paper One) [97]**

This chapter contains a literature review on how CNTs have been incorporated in the photoactive layer of organic solar cells. The chapter highlights the sources of energy in the world today and the advantages of using solar energy as an energy source. It also reviews photo-excitation in OSCs and free charge carrier generation with incorporation of CNTs. Effects of introducing CNTs containing a dopant, such as boron or nitrogen, on charge transfer in OSCs are also discussed. Additionally, techniques for the fabrication of OSCs, which include composite processing and film deposition techniques, are highlighted. Finally, examples of case studies of different types of CNTs in OSCs are mentioned.

## **Chapter Three (Paper Two) [98]**

In this chapter the crystal structure of a ferrocene derivative with nitrogen containing moieties, namely, 4-[(pyridin-4-yl)methylidene]amino}phenylferrocene ( $[\text{Fe}(\text{C}_5\text{H}_5)(\text{C}_{17}\text{H}_{13}\text{N}_2)]$ ), is reported. The aim was to synthesize a ferrocene derivative with heteroatoms which could be used as a catalyst and also as a source dopant for the synthesis of doped-CNTs. This ferrocene derivative was synthesised by using the principles of green chemistry. From this we were able to present the first report on the synthesis of this novel compound by means of a solvent-free mechanochemical synthesis method.

## **Chapter Four (Paper Three) [60]**

In this chapter we report the synthesis and characterization of nitrogen-doped SCNMs by using different synthetic conditions. The novel compound synthesized in Chapter Three was used as the catalyst and also as the nitrogen and carbon source for the synthesis of N-SCNMs. Two additional carbon sources, acetonitrile and toluene were also evaluated at three different reaction temperatures: 800, 850 and 900 °C. The main aim of this chapter

was to determine the optimum conditions that would give the highest yield of N-CNTs with high nitrogen-doping. We also report on the types of SCNMs synthesized from the different carbon sources and reaction temperatures. The best synthesis conditions for the highest yield of N-CNTs and high nitrogen-doping for this work was reported. We also report for the first time synthesis of N-CNTs by using a novel catalyst, 4-((pyridin-4-yl)methylidene]amino}phenylferrocene ( $[\text{Fe}(\text{C}_5\text{H}_5)(\text{C}_{17}\text{H}_{13}\text{N}_2)]$ ).

### **Chapter Five (Paper Four) [58]**

In this chapter we evaluated the effect of the boron concentration on the physicochemical properties of B-CNTs. We report the synthesis of B-CNTs by means of the CVD floating catalyst method with ferrocene as the catalyst, triphenylborane as the boron source as well as an extra source of carbon, and toluene as the carbon source. The amount of boron doped to the CNTs was determined by inductively coupled plasma-optical emission spectroscopy. The effect of the wt.% of the boron-containing precursor on the amount of boron-doped was also determined. Different characterization techniques, such as electron microscopy, Raman spectroscopy, thermogravimetric analysis, inverse gas chromatography, vibrating sample magnetometer and conductivity measurements were used to determine the effect of boron-doping on the physicochemical properties of B-CNTs. In this paper, we report for the first time, the characterization of surface properties of B-CNTs by use of inverse gas chromatography and how they were affected by boron concentration. Also, the ferromagnetic properties of B-CNTs determined from a vibrating sample magnetometer are reported for the first time.

### **Chapter Six (Paper Five)**

In this chapter the effects of the nanocomposites synthesis methods on the photovoltaic properties of OSCs were evaluated. These nanocomposites were composed of poly(3-hexylthiophene) and doped-CNTs. The two methods compared were *in situ* polymerization of 3-hexylthiophene monomers on the walls of CNTs and direct solution mixing of a polymer and N-CNTs in a suitable solvent. The nanocomposites that were synthesized were then used as the photoactive layers of OSCs and their photovoltaic properties were

determined by using a standard solar simulator operating at atmosphere (AM) 1.5 and 100 mW cm<sup>-2</sup>. To date most of the nanocomposites involving polymers and CNTs used in the photoactive layer of OSCs are synthesized by using direct solution mixing. The aim was to determine the method that would provide good interaction between N-CNTs and the polymer thereby improving the dispersion of N-CNTs in the polymer matrix and charge transfer processes. This would eventually result in good photovoltaic properties. Hence, a comparison of the performance of nanocomposites synthesized by using different techniques in the photoactive layer of OSCs is reported for the first time.

### **Chapter Seven (Paper Six)**

In this chapter we explore the effects on the performance on OSCs induced by incorporating either B- or N-CNTs in the photoactive. The doped-CNTs were mixed with the donor-acceptor components of the OSC to form the photoactive layer. Previous reports of incorporation of CNTs in the photoactive layer of OSCs have resulted in a positive effect while others have yielded a negative effect. Very few reports, if any, are available on why the presence of CNTs in the photoactive layer of OSCs results in either a positive or a negative effect on the performance. Therefore, the aim of this chapter was to determine the reasons why the presence of doped-CNTs in the photoactive layer of OSCs either produced a positive or a negative effect on performance. These effects were determined by the use of X-ray photoelectron spectroscopy, atomic force microscopy and transient absorption spectroscopy. Hence, in this chapter we report how presence of either B- or N-CNTs in the photoactive layer affects the performance of OSC devices. Additionally, this is the first report on the recombination of free charge carriers in OSCs with B-CNTs or N-CNTs in the photoactive layer of OSC investigation by transient absorbance spectroscopy.

### **Chapter Eight (Paper Seven)**

In this chapter we investigated B- or N-CNTs as a charge extracting and transporting layer in the bulk heterojunction of an organic solar cell. To understand the role of B- or N-CNTs in the photoactive layer of OSCs, different designs of devices were made. In these designs the position of the layer with B-CNTs and N-CNTs was changed and placed next to either

the hole or electron collecting electrodes. The position of these films was determined from the Hall coefficients of doped-CNTs, which for B-CNTs was positive and for N-CNTs negative. From these findings the best device design that improved the performance of the OSC was reported.

## **Chapter Nine (Conclusion and Future Work)**

This chapter gives the overall conclusion and summary of the thesis by putting together the major findings of each chapter. It also has future work emanating from the findings of this research work.

## **10. Conclusion**

In this chapter we reported on the history and types of CNTs. The methods that are used in the synthesis of CNTs were discussed. Doping of CNTs with either boron or nitrogen, and their effects on the structure of CNTs, were also highlighted. Potential application of CNTs, especially in OSC where CNTs are part of the photoactive layer, was explored further. Finally, the aim, objectives and overview of this thesis were outlined.

## **References**

- [1] M.F. De Volder, S.H. Tawfick, R.H. Baughman, A.J. Hart, *Science* 339 (2013) 535-539.
- [2] L. Dai, D.W. Chang, J.B. Baek, W. Lu, *Small* 8 (2012) 1130-1166.
- [3] J. Suhr, N. Koratkar, P. Keblinski, P. Ajayan, *Nature Materials* 4 (2005) 134-137.
- [4] S.M. Bennett, J.A. Finlay, N. Gunari, D.D. Wells, A.E. Meyer, G.C. Walker, M.E. Callow, J.A. Callow, F.V. Bright, M.R. Detty, *Biofouling* 26 (2010) 235-246.
- [5] X. Qu, J. Brame, Q. Li, P.J. Alvarez, *Accounts of Chemical Research* 46 (2012) 834-843.
- [6] J.-G. Wang, Y. Yang, Z.-H. Huang, F. Kang, *Electrochimica Acta* 75 (2012) 213-219.
- [7] A.D. Franklin, G.S. Tulevski, S.-J. Han, D. Shahrjerdi, Q. Cao, H.-Y. Chen, H.-S.P. Wong, W. Haensch, *ACS Nano* 6 (2012) 1109-1115.

- [8] S. Iijima, *nature* 354 (1991) 56-58.
- [9] L. Radushkevich, V. Lukyanovich, *Journal of Physical Chemistry(Moscow)* 26 (1952) 88-95.
- [10] A. Oberlin, M. Endo, T. Koyama, *Journal of Crystal Growth* 32 (1976) 335-349.
- [11] W.P. Abrahamson J, Rhodes B. , *Carbon* 37 (1999) 1873-1875.
- [12] L. Akadermiinauk, *Metals*, 3 (1982) (1982) 12-17.
- [13] H.W. Kroto, J.R. Heath, S.C. O'Brien, R.F. Curl, R.E. Smalley, *Nature* 318 (1985) 162-163.
- [14] A. Aqel, K.M. El-Nour, R.A. Ammar, A. Al-Warthan, *Arabian Journal of Chemistry* 5 (2012) 1-23.
- [15] M. Endo, T. Hayashi, Y.A. Kim, H. Muramatsu, *Japanese Journal of Applied Physics* 45 (2006) 4883.
- [16] V. Sujatha, M. Suresh, S. Mahalaxmi, *SRM University Journal of Dental Sciences* 2 (2011) 313.
- [17] J. Prasek, J. Drbohlavova, J. Chomoucka, J. Hubalek, O. Jasek, V. Adam, R. Kizek, *Journal of Materials Chemistry* 21 (2011) 15872-15884.
- [18] A.-C. Dupuis, *Progress in Materials Science* 50 (2005) 929-961.
- [19] J.-P. Tessonier, D. Rosenthal, T.W. Hansen, C. Hess, M.E. Schuster, R. Blume, F. Girgsdies, N. Pfänder, O. Timpe, D.S. Su, R. Schlögl, *Carbon* 47 (2009) 1779-1798.
- [20] J.P. Tessonier, D.S. Su, *ChemSusChem* 4 (2011) 824-847.
- [21] M. Kumar, Y. Ando, *Journal of Nanoscience and Nanotechnology* 10 (2010) 3739-3758.
- [22] T.W. Odom, J.-L. Huang, P. Kim, C.M. Lieber, *The Journal of Physical Chemistry B* 104 (2000) 2794-2809.
- [23] M. Dresselhaus, G. Dresselhaus, R. Saito, *Carbon* 33 (1995) 883-891.
- [24] M.S. Dresselhaus, G. Dresselhaus, P.C. Eklund, [www.Sciencedirect.com/science/-book/9780122218200](http://www.Sciencedirect.com/science/book/9780122218200). Accessed 11th August 2014.

- [25] M. Daenen, R. De Fouw, B. Hamers, P. Janssen, K. Schouteden, M. Veld, Eindhoven University of Technology 27 (2003) [www.oes.tamu.edu](http://www.oes.tamu.edu). (2003) Accessed 11th August 2014 .
- [26] S. Lijima, T. Ichihashi, *Nature* 364 (1993) 737.
- [27] J.N. Coleman, U. Khan, W.J. Blau, Y.K. Gun'ko, *Carbon* 44 (2006) 1624-1652.
- [28] Y. Saito, T. Yoshikawa, M. Okuda, N. Fujimoto, K. Sumiyama, K. Suzuki, A. Kasuya, Y. Nishina, *Journal of Physics and Chemistry of Solids* 54 (1993) 1849-1860.
- [29] H. Huang, H. Kajiura, S. Tsutsui, Y. Hirano, M. Miyakoshi, A. Yamada, M. Ata, *Chemical physics letters* 343 (2001) 7-14.
- [30] T. Ebbesen, P. Ajayan, *Nature* 358 (1992) 220-222.
- [31] D. Bethune, C. Klang, M. De Vries, G. Gorman, R. Savoy, J. Vazquez, R. Beyers, *Nature*, 363 (1993) 605.
- [32] X. Zhao, M. Ohkohchi, H. Shimoyama, Y. Ando, *Journal of Crystal Growth* 198 (1999) 934-938.
- [33] E. Munoz, W. Maser, A. Benito, M. Martinez, G. De la Fuente, Y. Maniette, A. Righi, E. Anglaret, J. Sauvajol, *Carbon* 38 (2000) 1445-1451.
- [34] P. Eklund, B. Pradhan, U. Kim, Q. Xiong, J. Fischer, A. Friedman, B. Holloway, K. Jordan, M. Smith, *Nano Letters* 2 (2002) 561-566.
- [35] Z.-h. Yuan, H. Huang, L. Liu, S.-s. Fan, *Chemical Physics Letters* 345 (2001) 39-43.
- [36] F. Ahmadzade, S. Safa, P. Balashabady, *Arabian Journal for Science and Engineering* 36 (2011) 97-103.
- [37] V. Shanov, Y.-H. Yun, M.J. Schulz, *Journal of the University of Chemical Technology and Metallurgy* 41 (2006) 377-390.
- [38] T. Susi, (2011) [http://urn.fi/URN:ISBN 978-952-60-4127-7](http://urn.fi/URN:ISBN%20978-952-60-4127-7). Accessed 14th August 2014. .
- [39] H. Zhu, C. Xu, D. Wu, B. Wei, R. Vajtai, P. Ajayan, *Science* 296 (2002) 884-886.
- [40] P. Nikolaev, M.J. Bronikowski, R.K. Bradley, F. Rohmund, D.T. Colbert, K. Smith, R.E. Smalley, *Chemical Physics Letters* 313 (1999) 91-97.

- [41] L. Panchakarla, A. Govindaraj, *Bulletin of Materials Science* 30 (2007) 23-29.
- [42] R. Sen, A. Govindaraj, C. Rao, *Chemical Physics Letters* 267 (1997) 276-280.
- [43] A. Cao, L. Ci, G. Wu, B. Wei, C. Xu, J. Liang, D. Wu, *Carbon* 39 (2001) 152-155.
- [44] D. Braga, S.L. Giaffreda, F. Grepioni, A. Pettersen, L. Maini, M. Curzi, M. Polito, *Dalton Transactions* (2006) 1249-1263.
- [45] L.M. Ombaka, P.G. Ndungu, B. Omondi, V.O. Nyamori, *Journal of Coordination Chemistry* (2014) 1-31.
- [46] A. McCluskey, P.J. Robinson, T. Hill, J.L. Scott, J.K. Edwards, *Tetrahedron Letters* 43 (2002) 3117-3120.
- [47] C. Imrie, P. Kleyi, V.O. Nyamori, T.I.A. Gerber, D.C. Levendis, J. Look, *Journal of Organometallic Chemistry* 692 (2007) 3443-3453.
- [48] L. Ci, Y. Li, B. Wei, J. Liang, C. Xu, D. Wu, *Carbon* 38 (2000) 1933-1937.
- [49] D. Quiñonero, A. Frontera, C. Garau, A. Costa, P. Ballester, P.M. Deyà, *Chemical Physics Letters* 411 (2005) 256-261.
- [50] E. Cruz-Silva, D.A. Cullen, L. Gu, J.M. Romo-Herrera, E. Muñoz-Sandoval, F. López-Urías, B.G. Sumpter, V. Meunier, J.-C. Charlier, D.J. Smith, *ACS Nano* 2 (2008) 441-448.
- [51] D. Larrude, M.M. Da Costa, F. Monteiro, A. Pinto, F. Freire Jr, *Journal of Applied Physics* 111 (2012) 064315.
- [52] F. Villalpando Paéz, [www.dspace.mit.edu/handle/1721.1/36215](http://www.dspace.mit.edu/handle/1721.1/36215) Accessed 11th August 2014..
- [53] Q. Jiang, L. Qian, J. Yi, X. Zhu, Y. Zhao, *Frontiers of Materials Science in China* 1 (2007) 379-382.
- [54] J.M. Lee, J.S. Park, S.H. Lee, H. Kim, S. Yoo, S.O. Kim, *Advanced Materials* 23 (2011) 629-633.
- [55] L. Yang, S. Jiang, Y. Zhao, L. Zhu, S. Chen, X. Wang, Q. Wu, J. Ma, Y. Ma, Z. Hu, *Angewandte Chemie* 123 (2011) 7270-7273.
- [56] E.N. Nxumalo, V.O. Nyamori, N.J. Coville, *Journal of Organometallic Chemistry* 693 (2008) 2942-2948.
- [57] M. Terrones, N. Grobert, H. Terrones, *Carbon* 40 (2002) 1665-1684.



- [58] G. Keru, P.G. Ndungu, V.O. Nyamori, *Materials Chemistry and Physics* 153 (2015) 323-332.
- [59] D.P. Hashim, N.T. Narayanan, J.M. Romo-Herrera, D.A. Cullen, M.G. Hahm, P. Lezzi, J.R. Suttle, D. Kelkhoff, E. Muñoz-Sandoval, S. Ganguli, A.K. Roy, D.J. Smith, R. Vajtai, B.G. Sumpter, V. Meunier, H. Terrones, M. Terrones, P.M. Ajayan, *Science Reports* 2 (2012) 1.
- [60] G. Keru, P.G. Ndungu, V.O. Nyamori, *Journal of Nanomaterials* 2013 (2013) 2.
- [61] M. Terrones, A.G. Souza Filho, A.M. Rao, In M.S. Dresselhaus, G. Dresselhaus, P.C. Eklund (Edn), Springer-Heidelberg, 2008, p. 531.
- [62] M. Terrones, P. Ajayan, F. Banhart, X. Blase, D. Carroll, J.-C. Charlier, R. Czerw, B. Foley, N. Grobert, R. Kamalakaran, *Applied Physics A* 74 (2002) 355-361.
- [63] G. Bepete, Z.N. Tetana, S. Lindner, M.H. Rummeli, Z. Chiguvare, N.J. Coville, *Carbon* 52 (2013) 316-325.
- [64] T.-W. Chou, L. Gao, E.T. Thostenson, Z. Zhang, J.-H. Byun, *Composites Science and Technology* 70 (2010) 1-19.
- [65] Z. Wu, Z. Chen, X. Du, J.M. Logan, J. Sippel, M. Nikolou, K. Kamaras, J.R. Reynolds, D.B. Tanner, A.F. Hebard, *Science* 305 (2004) 1273-1276.
- [66] M. McCarthy, B. Liu, E. Donoghue, I. Kravchenko, D. Kim, F. So, A. Rinzler, *Science* 332 (2011) 570-573.
- [67] K. Evanoff, J. Khan, A.A. Balandin, A. Magasinski, W.J. Ready, T.F. Fuller, G. Yushin, *Advanced Materials* 24 (2012) 533-537.
- [68] A. Le Goff, V. Artero, B. Jusselme, P.D. Tran, N. Guillet, R. Métayé, A. Fihri, S. Palacin, M. Fontecave, *Science* 326 (2009) 1384-1387.
- [69] A. Star, E. Tu, J. Niemann, J.-C.P. Gabriel, C.S. Joiner, C. Valcke, *Proceedings of the National Academy of Sciences of the United States of America* 103 (2006) 921-926.
- [70] B. Esser, J.M. Schnorr, T.M. Swager, *Angewandte Chemie International Edition* 51 (2012) 5752-5756.
- [71] Z. Liu, X. Sun, N. Nakayama-Ratchford, H. Dai, *ACS Nano* 1 (2007) 50-56.

- [72] R. Hirlekar, M. Yamagar, H. Garse, M. Vij, V. Kadam, *Asian Journal of Pharmaceutical and Clinical Research* 2 (2009) 17-27.
- [73] P. Castrucci, *Advances in Nano Research* DOI: 10.12989/anr.2014.2.1.023 (2014).
- [74] Y. Jung, X. Li, N.K. Rajan, A.D. Taylor, M.A. Reed, *Nano Letters* 13 (2012) 95-99.
- [75] G. Dennler, M.C. Scharber, C.J. Brabec, *Advanced Materials* 21 (2009) 1323-1338.
- [76] S. Chaudhary, H. Lu, A.M. Müller, C.J. Bardeen, M. Ozkan, *Nano Letters* 7 (2007) 1973-1979.
- [77] I. Lee, S. Lee, H. Kim, H. Lee, Y. Kim, *Open Physical Chemistry Journal* 4 (2010) 1.
- [78] C.W. Tang, *Applied Physics Letters* 48 (1986) 183-185.
- [79] N. Sariciftci, L. Smilowitz, A.J. Heeger, F. Wudl, *Science* 258 (1992) 1474-1476.
- [80] M. Scharber, N. Sariciftci, *Progress in Polymer Science* 38 (2013) 1929-1940.
- [81] H. Spanggaard, F.C. Krebs, *Solar Energy Materials and Solar Cells* 83 (2004) 125-146.
- [82] H. Hoppe, N.S. Sariciftci, *Journal of Materials Research* 19 (2004) 1924-1945.
- [83] H. Shirakawa, E.J. Louis, A.G. Macdiarmid, C.K. Chiang, A.J. Heeger, *Journal of the Chemical Society-Chemical Communications* (1977) 578-580.
- [84] J. Halls, K. Pichler, R. Friend, S. Moratti, A. Holmes, *Applied Physics Letters* 68 (1996) 3120-3122.
- [85] P. Peumans, A. Yakimov, S.R. Forrest, *Journal of Applied Physics* 93 (2003) 3693-3723.
- [86] D. Wöhrle, D. Meissner, *Advanced Materials* 3 (1991) 129-138.
- [87] B. Hu, Z. Yang, F. Karasz, *Journal of Applied Physics* 76 (1994) 2419-2422.
- [88] S. Karg, W. Riess, V. Dyakonov, M. Schwoerer, *Synthetic Metals* 54 (1993) 427-433.
- [89] R. Marks, J. Halls, D. Bradley, R. Friend, A. Holmes, *Journal of Physics: Condensed Matter* 6 (1994) 1379.

- [90] G. Yu, J. Gao, J. Hummelen, F. Wudl, A. Heeger, *Science-AAAS-Weekly Paper Edition* 270 (1995) 1789-1790.
- [91] S.H. Kareem, E. ABD-Al-Hussien, *Journal Baghdad Science* 9 (2012) 680-688.
- [92] L. Lu, L. Yu, *Advanced Materials* 26 (2014) 4413-4430.
- [93] Y. Liang, D. Feng, Y. Wu, S.-T. Tsai, G. Li, C. Ray, L. Yu, *Journal of the American Chemical Society* 131 (2009) 7792-7799.
- [94] Y. Liang, Z. Xu, J. Xia, S.T. Tsai, Y. Wu, G. Li, C. Ray, L. Yu, *Advanced Materials* 22 (2010) E135-E138.
- [95] J. Guo, Y. Liang, J. Szarko, B. Lee, H.J. Son, B.S. Rolczynski, L. Yu, L.X. Chen, *Journal of Physical Chemistry B* 114 (2010) 742-748.
- [96] R.S. Bhatta, D.S. Perry, M. Tsige, *The Journal of Physical Chemistry A* 117 (2013) 12628-12634.
- [97] G. Keru, P.G. Ndungu, V.O. Nyamori, *International Journal of Energy Research* 38 (2014) 1635-1653.
- [98] V.O. Nyamori, G. Keru, B. Omondi, *Acta Crystallographica Section E: Structure Reports Online* 68 (2012) m1535-m1535.

## Chapter Two

# A review on carbon nanotube/polymer composites for organic solar cells

Godfrey Keru, Patrick G. Ndungu and Vincent O. Nyamori\*

School of Chemistry and Physics, University of KwaZulu-Natal, Westville Campus, Private Bag X54001, Durban, 4000, South Africa

International Journal of Energy Research  
Volume 38, Issue 13, Article first published online 13 APR 2014  
Abstract | Full Article (HTML) | Enhanced Article (HTML) | References | Cited By

University of KwaZulu-Natal Libraries  
Wiley Online Library

International Journal of Energy Research

INTERNATIONAL JOURNAL OF ENERGY RESEARCH  
*Int. J. Energy Res.* 2014; **38**:1635–1653  
Published online 13 April 2014 in Wiley Online Library (wileyonlinelibrary.com). DOI: 10.1002/er.3194

REVIEW PAPER

**A review on carbon nanotube/polymer composites for organic solar cells**

Godfrey Keru, Patrick G. Ndungu and Vincent O. Nyamori\*†

School of Chemistry and Physics, University of KwaZulu-Natal, Westville Campus, Private Bag X54001, Durban, 4000, South Africa

**SUMMARY**

Carbon nanotubes (CNTs) have unique properties, such as their electrical conductivity, that enable them to be combined with conducting polymers to form composites for use in organic solar cells (OSCs). It is envisaged that the improved composite has a higher efficiency of green energy and will reduce the cost of these cells. The use of such alternative energy sources also drastically reduces overuse of fossil fuels and consequently limits environmental degradation. This review compares research and performance between conventional silicon solar cells and OSCs. It also discusses OSC photoexcitation and charge carrier generation with the incorporation of CNTs, physicochemical properties of the composites and other factors that affect the efficiencies of OSCs. In addition, properties of CNTs that favour their dispersion in polymer matrices as acceptors and charge carriers to the electrodes are covered. The effects of CNTs containing dopants, such as nitrogen and boron, on charge transfer are discussed. Also, the fabrication techniques of OSCs that include CNT/polymer composite processing and the methods of film deposition on the substrate are described. Finally, the case studies of OSCs containing polymers with single-walled CNTs, double-walled CNTs or multi-walled CNTs are evaluated. Copyright © 2014 John Wiley & Sons, Ltd.

**KEY WORDS**  
carbon nanotubes; conducting polymers; renewable green energy; CNT/polymer composites; organic solar cells

# **A review on carbon nanotube/polymer composites for organic solar cells**

Godfrey Keru, Patrick G. Ndungu and Vincent O. Nyamori\*

School of Chemistry and Physics, University of KwaZulu-Natal, Westville Campus, Private Bag X54001, Durban, 4000, South Africa

\*Correspondence - Vincent O. Nyamori, E-mail: nyamori@ukzn.ac.za

## **Summary**

Carbon nanotubes (CNTs) have unique properties, such as their electrical conductivity, and thus can be combined with conducting polymers to form composites for use in photovoltaic (PV) cells. It is envisaged that the improved composite has a higher efficiency of green energy and will reduce the cost of PV cells. The use of alternative energy sources such as PV also drastically reduces overuse of fossil fuels and consequently limits environmental degradation. This review compares research and performance between conventional silicon solar cells (SSCs) and organic solar cells (OSCs). It also discusses OSC photo-excitation and charge carrier generation with the incorporation of CNTs, physicochemical properties of the composites and other factors that affect the efficiencies of OSCs. In addition, properties of CNTs that favour their dispersion in polymer matrices as acceptors and charge carriers to the electrodes are covered. The effects of CNTs containing dopants, such as nitrogen and boron, on charge transfer are discussed. Also, covered in this review are fabrication techniques that include CNT/polymer composite processing and the methods of film deposition on the substrate are described. Finally case studies of OSCs containing polymers with single-walled CNTs, double-walled CNTs and multi-walled CNTs are evaluated.

**Keywords:** carbon nanotubes; conducting polymers; renewable green energy; CNT/polymer composites; photovoltaic cells.

## **1. Introduction**

Renewable energy accounts for approximately 16% of the primary energy sources used globally, whilst the rest is from less favourable options such as fossil fuels and nuclear power [1]. The primary factors in sourcing new and alternative sources of energy are ensuring positive and strong social economic development and the provision of abundant and reliable energy for domestic, industrial and various other economic sectors, and also, to harness enough energy to meet the demand of the growing population [2]. Globally, there is an intense interest and focus on the development of technologies that can use renewable sources of energy such as biomass [3,4], geothermal [5,6], solar [7], wind [8,9] and hydro-power [10,11]. Some of the reasons for this can be attributed to the concerns surrounding energy security, the environment, sustainability, the drive for affordable energy services and the need to increase accessibility to economically viable energy options, especially where they lack in developing countries [2].

The usage of fossil fuels leads to environmental pollution through release of greenhouse gases [12], land degradation during exploration and mining. This in turn has been linked to acid rain, depletion of the ozone layer, harsh and sometimes unpredictable climatic conditions, the occurrence and spread of tropical diseases, and other problems that not only adversely affect humans but also animals and plants. These appalling conditions can destroy fragile ecosystems, especially marine and aquatic life [2]. Despite these severe disadvantages of using fossil fuels, the implementation of renewable energy technology remains a challenge. This is mainly due to the intermittent nature of some renewable energy sources and geographically constricted environments (e.g. relatively lower solar insolation at higher latitudes or impossibility of hydroelectric generation in arid and semi-arid regions). Moreover, in developing nations, heavy investments in infrastructure development are a challenge and there is a fair amount of uncertainty and financial risk factors associated with renewable technologies and other immediate priorities [4,5,7].

Implementation of renewable energy technologies and utilization of renewable energy have several advantages including reliability and localization, diversification of energy supply, energy security, new wealth creation opportunities and a significantly smaller negative impact on the environment. In addition, harnessing renewable energy at the local level will negate the vulnerabilities due to distant political upheavals, encountered in fossil fuel-producing regions. Furthermore, increased energy security through alternative greener sources would be advantageous, especially when supplies of various non-renewable fuels dwindle and as demand increases. The 'norm' to circumvent this requires more costly explorations and potentially more dangerous extractions operations, which push up the cost of energy. This makes investment in renewable energy technologies a better and more timely option.

Renewable technologies have zero emission of pollutants and utilize relatively smaller amounts of water, thus de-stressing overburdened water resources. Moreover, they offer sustainable options for decentralization of energy supplies, and thereby provide new opportunities in rural development and boost various agricultural activities [2,3]. Interestingly, most investments on renewable energy are on materials and workmanship to build and maintain facilities, rather than more energy input. This also means that since most of the resources are spent locally there is a potentially huge foreign exchange savings which could be extremely beneficial especially in developing nations which are often cash-strapped [13].

Amongst all of the various options available as renewable sources of energy, solar energy has some key advantages, especially when considering developing nations within Africa. Africa has some of the highest solar insolation-receiving regions on the planet due to its location in the tropics where incoming solar radiation mostly strikes the ground at an angle of 90° almost throughout the year [14]. Solar energy is free and clean; it does not produce waste, it is ecologically acceptable and is directly convertible to other forms of energy. These advantages far outweigh the production of mild chemical waste that accompanies the manufacture of solar energy conversion technologies.

## **1.1 Solar energy**

The earth receives 120,000 TW every hour from the sun and the estimated global energy requirement per year is approximately 13 TW [15]. Therefore, harnessing 0.01% of the energy the earth receives from the sun every hour will meet and surpass the annual global requirement, and at the same time leave enough room for further growth and development to meet future needs. The technologies available for harnessing solar energy can be broadly categorised into two main areas. These are: concentrating solar power [16] and solar photovoltaic (SPV). In its simplest form, concentrating solar power focuses thermal energy from the sun into heat transfer fluid by using mirrors. The heat generated is recovered to produce steam, which eventually is used to drive turbines and generate electricity. On the other hand, in SPV, electromagnetic energy is converted directly to electricity. Photons from the sun excite electrons in donor molecules, and these electrons are transferred to electrodes to generate electricity.

In developing countries, SPV technologies are the most attractive and elegant options available to provide energy. This is especially true for Africa, where the population is scattered over vast regions and where different groupings have divergent and dynamic electricity needs within various rural areas. In addition, the provision and maintenance of conventional electricity grids would be extremely challenging due to environmental, economic, technical, or a combination of some or all of these factors.

## **1.2 Inorganic versus organic solar cells (OSCs)**

Currently, silicon-based cells have dominated commercial solar cell devices with approximately 90% of the global market share. Several factors account for this trend including both technical (e.g. silicon processing is a mature and reliable technology) and economic (widespread commercially available technologies for silicon device manufacture) reasons. However, in terms of efficiencies, current research efforts have demonstrated that multi-junction concentrator devices have overall efficiencies of about 30%, followed by crystalline silicon (~25%) [17], single-junction (~20.3%) [18], thin film technology (~15%) [19] and eventually emerging photovoltaic (PV) devices, which include dye-sensitized and



organic solar cells (OSCs) with efficiencies of less than 10% [13]. This is well illustrated in Figure 1, which shows efficiencies of different types of solar cells and their timelines on best research [13].

Silicon solar cells (SSCs), either crystalline (mono-crystalline [20-22], polycrystalline [23,24]) or amorphous [25,26], are generally expensive to manufacture and require a significant investment in labour and facilities. The main component, solar-grade silicon, is produced *via* several chemical steps and a detailed description of the process is beyond the scope of this review. However, a brief and basic procedure involves the reduction of raw quartz with carbon to produce metallurgical silicon, which is relatively cheap to produce, but this is an energy intensive process. The metallurgical silicon is then refined by converting the silicon to chlorosilanes (using HCl) and these are subsequently transformed, by using a CVD process, into electronic or solar-grade silicon (i.e. the well-known Siemens process). However, it should be noted that the cost of manufacturing for amorphous silicon (specifically by CVD) is relatively cheap compared to its crystalline counterparts. There are other recent techniques that use plasma, or direct metallurgical processes, but these current technologies are energy intensive, and can have detrimental effects on the environment [27-29]. These main drawbacks limit the implementation of silicon-based PV manufacturing within developing economies (many tropical countries, including South Africa). In the light of these challenges and circumstances, OSC technologies are favourable.

In general, OSCs can be described simply as PV devices made from polymers, small organic molecules, or a combination of both with or without some kind of nanomaterial incorporated into the overall device. Mostly, these devices are based on polymeric materials and can thus be assembled by using well-known polymer processing techniques. This means they are relatively simple to fabricate into various shapes and sizes (Figure 2 ) [30], easily adapted and designed for niche applications, and can be assembled on various substrates and produced cost-effectively [31].

# Best Research-Cell Efficiencies

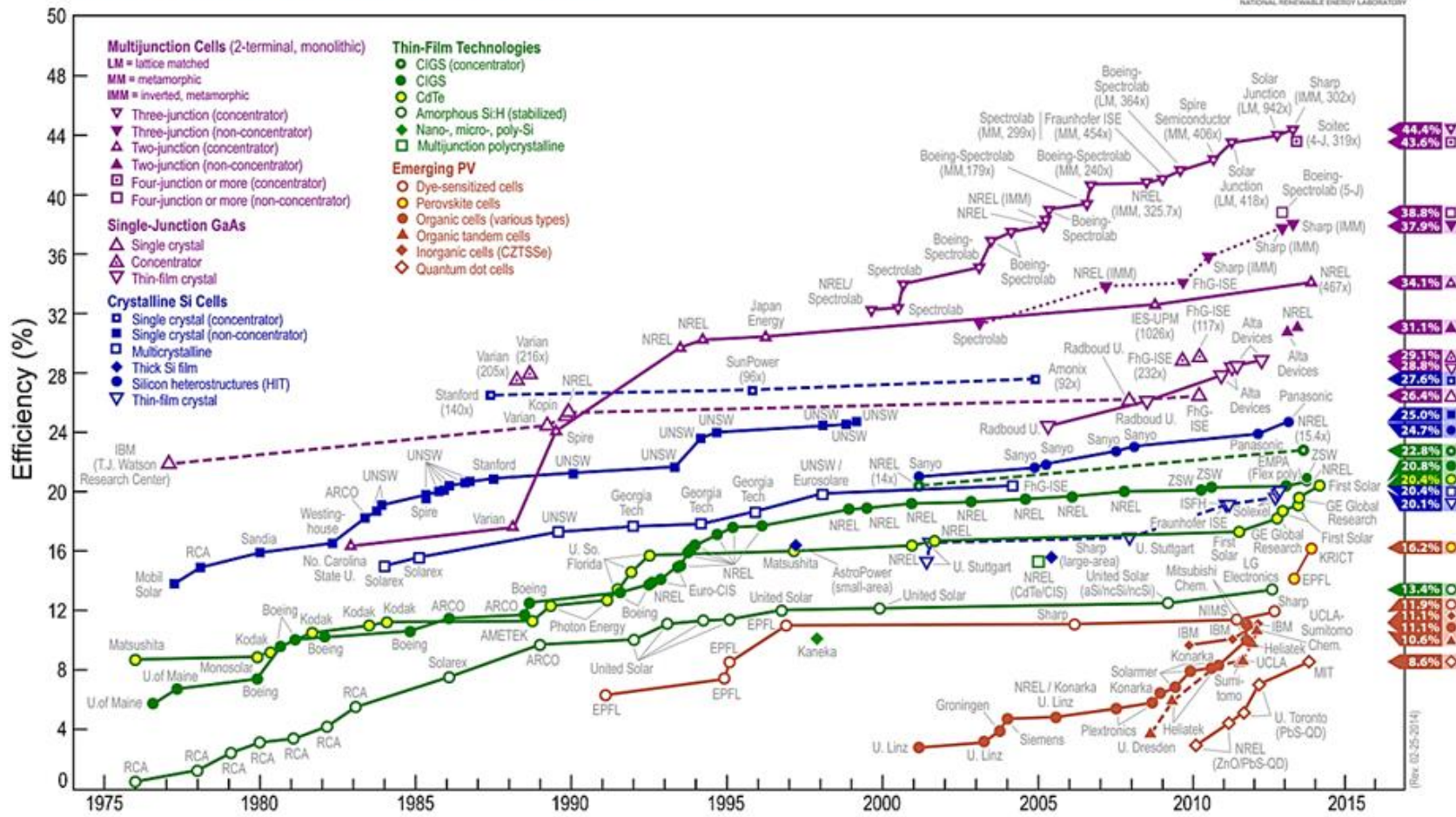
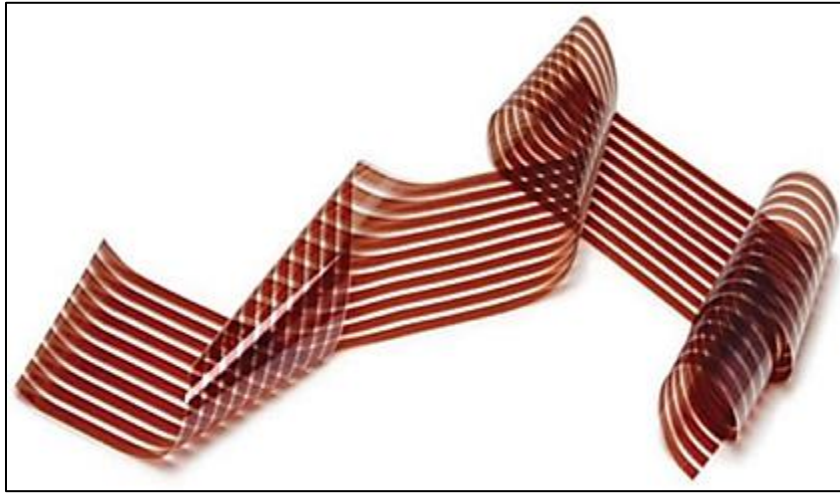


Figure 1: Timeline for different solar cells on best research and their best efficiencies reported so far [13].



**Figure 2:** Organic solar cell casted on a flexible substrate. It can be stretched, rolled or even curved in any direction [30].

The basic architecture of an organic-based solar cell includes an active layer sandwiched between two transport layers that conduct holes or electrons, and two electrodes that encase the whole structure, for harnessing the power generated. The active layer generates electron-hole pairs when excited by light, and at the interface between the transport layers and the active layer, the electron-hole pairs are separated and these charge carriers are eventually collected by the electrodes and used to power the system of interest [32-36].

With silicon-based solar cells, separation of charge carriers occurs across a p-n junction and this is enhanced by doping the material on either side of the junction. A similar scenario is encountered with other inorganic-based solar cells (e.g. CdTe, GaAs, CuInGaSe, etc.). With PV devices, ideally photon absorption excites an electron to the conduction band, which leads to the production of electron-hole pairs commonly known as excitons (electrostatically charged carriers). Excitons are characterized by a coulombic force [37].

$$F = \frac{q_1 q_2}{4\pi r^2 \epsilon \epsilon_0} \quad (1)$$

where  $q_1$  is the charge,  $r$  is the distance between charges,  $\epsilon$  is the dielectric constant and  $\epsilon_0$  is the permittivity in the free state.

### **1.3 Photo-excitation and carrier generation in OSCs**

With OSCs, the mechanism that leads to the separation of the electron-hole pair is a more complex process and is still an area under intensive investigation, but one of the key factors concerning their functionality is the heterojunction. The mechanism that leads to the generation of excitons, separation, and final production of a useful photocurrent has been discussed recently in the literature [17,32,33]. The research findings reported so far indicate that photons, with the requisite energy, excite electrons within the donor molecule from the highest occupied molecular orbital (HOMO) to the lowest unoccupied molecular orbital (LUMO). This produces excitons, polaron pairs, radical ion pairs, or more generally a charge transfer complex, which can be envisaged to be analogous to the electron-hole pair in inorganic PV materials. The photoexcited charge transfer complex must then move (by either migration or diffusion) to the donor-acceptor (D-A) interface. The transfer of energy via charge transfer complexes may involve one or more transformations within the donor molecule and similarly, there may be several energetic transition state complexes involving the donor, acceptor or combination of both at the D-A interface. The energy levels, HOMO and LUMO, within the donor are slightly higher than those of the acceptor. This is necessary to facilitate transfer of energy to the acceptor and reduce recombination within the donor. Thermal, radiative or electronic losses are possible near or at the D-A interface, but the generation of photocurrent occurs when the charge transfer complex separates into electron and hole charge carriers, with electrons in the acceptor material and holes in the donor and, eventually, they are collected at the electrodes [32,33,36].

#### **1.3.1 Calculating efficiencies in OSCs**

PV properties for OSCs and silicon solar cells (SSCs) are governed by determination of the current-voltage of the cell. This is achieved by calculating either the power conservation efficiency (PCE) or the external quantum efficiency (EQE) of the cell. EQE is the ratio of

collected charge carrier (electrons) per incident photon [38]. PCE of a cell is the efficiency of the cell under illumination of a standard light source or the percentage of solar energy exposed to a cell that is converted to electrical energy or electricity. A high PCE percentage translates to high output of that cell and this can be improved by the development of new materials (e.g. conducting polymers with low band gap) or device architecture (single-junction, tandem cell and bulk heterojunction) [33]. PCE is calculated from

$$\eta = \frac{V_{oc} I_{sc} FF}{P_{in}} \quad (2)$$

where  $V_{oc}$  is the open circuit voltage,  $I_{sc}$  is the short circuit current,  $P_{in}$  is the incident light power and FF is the fill factor. The fill factor measures the quality of a solar cell as a power source. It is the ratio between the maximum power delivered to an external circuit and the potential power of that cell and is defined

$$FF = \frac{V_{max} I_{max}}{V_{oc} I_{sc}} \quad (3)$$

where  $V_{max}$  is the maximum electromotive force in an electric circuit and  $I_{max}$  is the maximum rate of electron flow in an electric circuit.

A graphical relationship between  $V_{OC}$ ,  $I_{SC}$ ,  $V_{MAX}$  and  $I_{MAX}$  is shown in Figure 3.

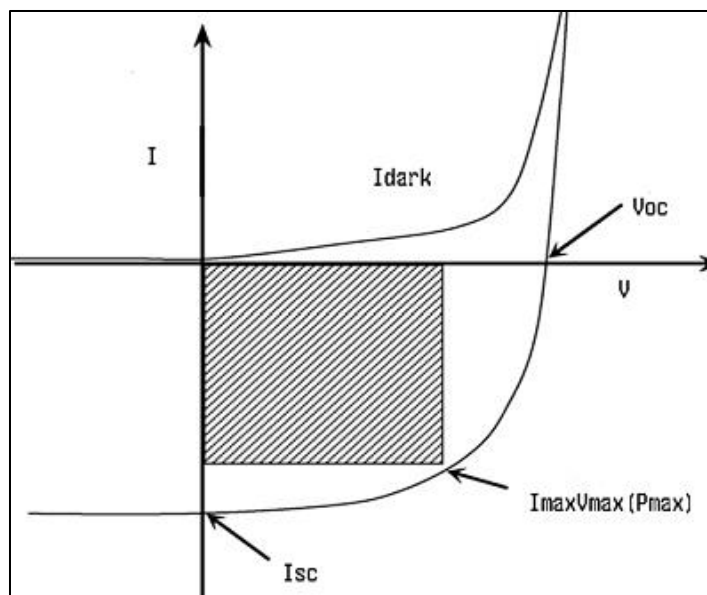


**Figure 3:** Relationship between  $V_{OC}$ ,  $I_{SC}$ ,  $I_{MAX}$  and  $V_{MAX}$  in the dark and under illumination. The shaded area is used to determine  $V_{MAX}$  and  $I_{MAX}$  [39].

### 1.3.2 Physicochemical factors that affect the efficiency of OSCs

OSCs have low PCE and are short-lived when compared to SSCs, and this limits their practical application [31]. The short lifetime is due to chemical and physical degradation of the active layers and electrodes. Chemical degradation involves chemical changes within the organic materials or on the electrodes due to the presence of oxygen and moisture (see Figure 4) [40]. Physical degradation is usually caused by charge accumulation, morphological changes or diffusion of metal into the active layer [31]. Electrodes degrade by oxidation, delaminating, de-doping and interfacial organometallic chemistry. Active layers degrade *via* photochemical reactions, thermo-chemical reactions, morphological changes and inclusion of impurities [41]. Degradation can also occur due to low photo-stability of the active layer-electrode interface and this can be minimized by depositing a thin film of electron extraction layer and hole extraction layer between the active layer and the electrodes [42]. It has been reported that an active layer with chemically active side groups is more susceptible to degradation than one without. Jorgensen *et al.* [34] were able

to show that degradation due to oxidation usually occurs at the side groups. Low PCE with OSCs can also be due to efficiency loss that occurs in the first few hours of exposure to the atmosphere known as burn-in [41]. This crucial loss in functionality can be ascribed to photochemical reactions in the active layer and the development of trap states within the band gap [41]. Performance also reduces because other mechanisms, which include, trap mediated recombination, reduced hole mobility and build-up of charge in various trap states.

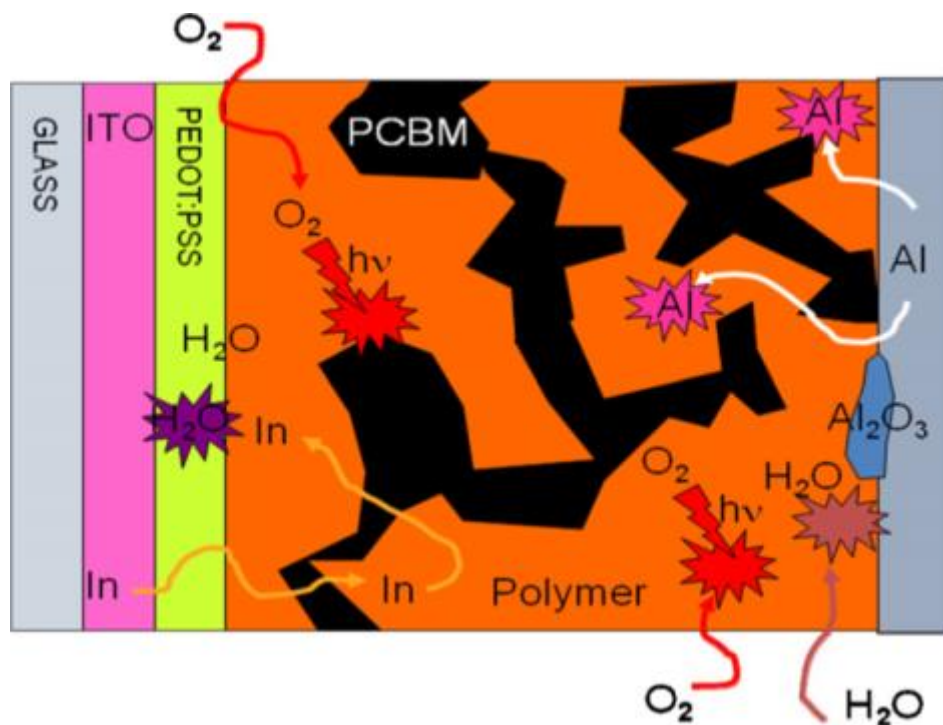


**Figure 4:** Degradation of the active layer due to the presence of oxygen and water, as well as diffusion of metal electrode particles into the active layer. Oxygen and water enter the device the during fabrication process [40].

One of the main limiting factors in achieving high PCE in OSCs is the recombination mechanisms that occur at the D-A interface. Some of the methods developed to minimize recombination include improving device morphology [43], using modified D-A materials [44], manipulation of electrode materials [45] and even enhancing optical absorption [46]. Zhang *et al.* [47] have reported a significant reduction in recombination losses by doping

the active layer poly(3-hexylthiophene) (P3HT)/ (6,6)phenyl-C<sub>61</sub>-butyric-acid methyl ester (PCBM) with ½ spin galvinoxyl radicals at the D-A interface, which increases the PCE of the device by ~340%.

Another factor that affects the efficiencies of OSCs is the band gap of the conjugated polymers. When the band gap of the semi-conducting conjugated polymer is large only a small portion of the incident solar energy is absorbed. For example, a polymer with band gap of ca. 2.0 eV can only absorb 25% of the solar energy. Reduction of the band gap to ca. 1.2 eV enhances absorption to between 70 and 80% [48] as shown in Figure 5. For maximum absorption, a smaller band gap is favourable. Of interest is to make use of low energy band gap materials with a value of band gap energy ( $E_g$ ) of 1.5 eV or less so that absorption will occur at 600 nm or greater in the neutral state [38].

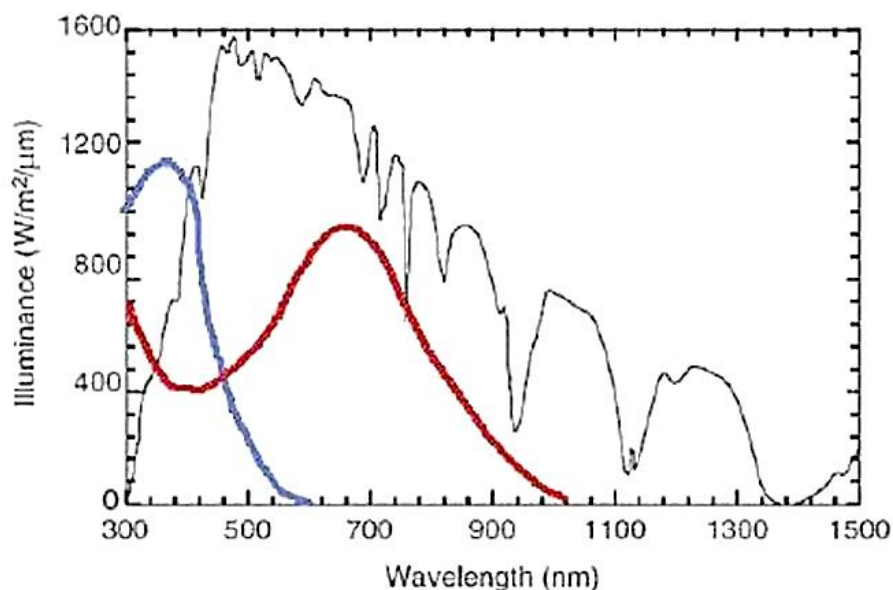


**Figure 5:** The solar spectrum together with the absorption spectra of various polymers showing the limitation of absorption due to the band gap size. The blue line shows the absorption of a polymer with a band gap of ca. 2 eV and the red of ca. 1.2 eV. The black line represent AM 1.5 illuminations [48].



Efficiencies of OSCs can be improved by incorporation of carbon nanotubes (CNTs) in the bulk heterojunction (BHJ). For example, Somani and co-workers [49] reported improvement of cell performance by many fold by incorporation of double-walled CNTs (DWCNTs) to P3HT. CNTs can be a good material at the interface because they have high affinity for electrons and also transport electrons to the electrodes unlike fullerenes, which are only good electron acceptors [50]. CNTs have also found use as transparent electrodes for hole collection owing to their high work function, replacing indium tin oxide (ITO). However, this is a topic of another review and we recommend the reader to references [51-55]. Arena and co-workers [56] reported that efficiency conversion of hybrid cells based on a conjugated polymer and doped silicon increased by 0.49% upon dispersion of CNTs in the conjugated polymer layer. Efficiencies of OSCs can be enhanced further by using CNTs with heteroatom dopants such as boron or nitrogen. Doping of CNTs with nitrogen or boron to form N-CNTs or B-CNTs introduces defects that changes structural, chemical and electronic properties [57]. Lee and co-workers [58] reported a high efficiency of 5.29% by incorporating N-CNTs in OSC. The cell had an efficiency of 4.68% before incorporation of N-CNTs.

## **2. Incorporation of carbon nanotubes in organic solar cells**

Inclusion of conducting nanostructures like CNTs in the BHJ enhances charge separation and improves transfer of charge carriers to the electrodes before they recombine. CNTs can combine with the  $\pi$ -electrons of conjugated polymers to form D-A-type solar cells [59]. Here, the CNTs do not only act as electron acceptors but also improve the dissociation of excitons by providing an enhanced electric field at the CNT/polymer interface, which suppresses recombination of photo-generated charges. CNTs in the BHJ of a polymer matrix result in high electron mobility, which exceeds that of any other semi-conductor [60]. Likewise, hole transport is also enhanced because of induced crystallinity of P3OT or other conducting polymers. Highly ordered supra-molecular organization of the conducting polymer ensures higher hole mobility *via* inter-chain transport [60].

Carbon nanotubes are dispersed in a solution of donor polymer before being spin-coated on the substrate. The substrate is usually a transparent electrode consisting of a transparent conductive oxide (TCO) of which indium tin oxide (ITO) is an example [30]. Firstly, a hole conducting layer of poly(3,4-ethylenedioxythiophene):poly(styrenesulfonate) (PEDOT:PSS) is deposited, which helps in selective hole injection to the ITO electrode as illustrated in Figure 6. An active layer consisting of the donor-acceptor is then deposited. Conjugated polymers, like P3HT or P3OT, are used as the donor components because of their ability to form semi-crystalline films when cast on a substrate [39], while fullerenes or CNTs can be the acceptor. Thermal annealing at a temperature above the polymer glass transition temperature allows the alignment of the polymer chains, thereby improving charge transfer. The top electrode is vacuum evaporated and is usually a metal of lower work-function (as compared to ITO), such as calcium or aluminium, and sometimes with an ultra-thin lithium fluoride under-layer [61].

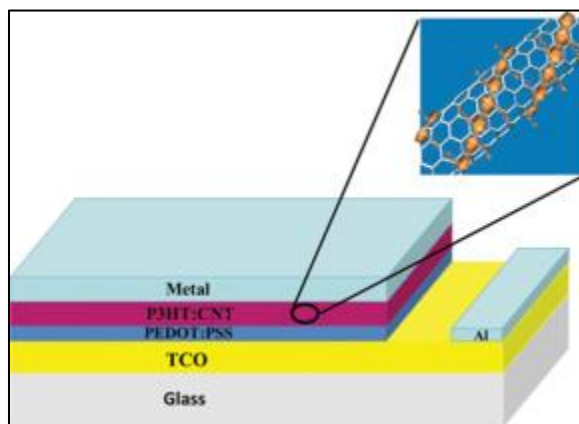


**Figure 6:** A schematic diagram showing the sandwiched active layer between the electrodes in OSCs with CNTs as acceptors within the active layer. Inset: high magnification of the active layer showing how polymer wraps onto CNTs [30].

Sometimes, a third component like a dye is incorporated in the active layer to improve the PV properties of a cell. Bhattacharyya *et al.* [62] used the dye N-(1-pyrenyl)maleimide

(PM) in the SWCNT/P3OT composite to form a cell ITO/P3OT-SWNCTs+PM/Al that improved the cell efficiency by two orders of magnitude. The group attributed this increase to efficient charge carrier transfer as illustrated in Figure 7.

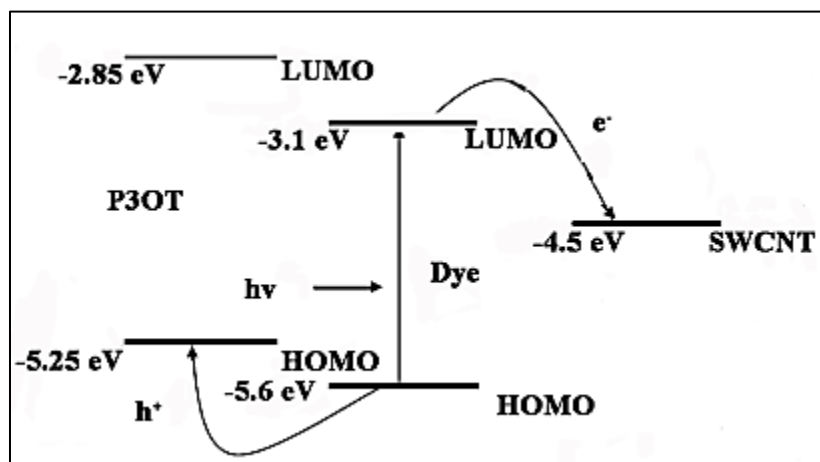


**Figure 7:** Movement of charge carriers between the energy levels of the donor polymer and dye with the eventual transfer of an electron to the SWCNT. Since the work function of the SWCNT is slightly lower than the LUMO of the dye the transfer of an electron is easy [62].

Doping CNTs with boron or nitrogen selectively enhances charge mobility, dispersibility in the polymer matrix and also tunes the work function [63]. For effective charge transfer, the work function of the CNTs should be close to the HOMO and LUMO of the donor and receiver respectively [64]. B-doping reduces the Fermi-level energy of the CNTs and at the same time increases the work function [65]. Upon B-doping, the work function increases to 5.2 eV from 4.6 eV of pristine CNTs, which is very close to the HOMO of P3HT (5.1 eV) donor [64]. This makes it very easy to inject a hole to the B-CNT for eventual transfer to the electrode. However, doping CNTs with electron rich nitrogen increases the Fermi-level energy and reduces the work function in comparison to pristine CNTs [63]. For N-CNTs the work function is 4.4 eV which is very close to the LUMO of the receiver PCBM (4.2 eV) in OSCs. An electron can easily move from LUMO of PCBM to N-CNTs because of

the short distance between the LUMO of PCBM and work function of N-CNTs ( $\sim 0.2$  eV), electrons are then to be transferred to the electrode. At the same time, use of either B- or N-doped CNTs in the bulk heterojunction of a polymer matrix makes charge recombination almost impossible. Mismatch of energies between the HOMO of the donor and N-CNTs, the LUMO of the receiver and B-CNTs makes it hard for dissociated charges to recombine as the hole is received by B-CNTs and electrons by N-CNTs [58]. B-doped or N-doped CNTs improve the short circuit current ( $I_{SC}$ ) and PCE of a cell and also help in the alignment of CNTs in the polymer matrix because of local polarities induced on the walls of CNTs and because the defects caused by the heteroatoms converts them from nonconducting to conducting materials [39,65].

## **2.1 Advantageous properties of carbon nanotubes for organic solar cells**

CNTs are synthesized in a number of different ways depending on the resources available and research objective. However, most methods are a variation on either the arc discharge [39], laser ablation [66] or chemical vapour deposition (CVD) method [67-69]. The CVD method is the most preferred technique since it is easy to implement and scale-up [70,71]. The synthesis technique has a direct impact on the final properties of the CNTs. The arc discharge and laser ablation techniques favour single-walled CNTs (SWCNTs) or highly graphitic multiwalled CNTs (MWCNTs). CVD methods usually produce MWCNTs; however, SWCNTs and DWCNTs can be grown.

When CNTs are incorporated into a polymer matrix, the resulting nanocomposites have significantly different physical-chemical properties than the original polymer material. The importance of the physical-chemical properties of CNTs in the polymer matrix and the significance of incorporating CNTs in OSCs are discussed in the next section.

## **2.2 Physicochemical properties of CNTs**

CNTs are good conductors of electricity, and their conductivity is 1000 times that of copper [70], and thus, when incorporated into a polymer matrix such as that for OSCs, they can

provide an excellent and robust network for the transfer of charge carriers to the electrodes by providing a percolating path [72]. Semiconducting CNTs also generate excitons upon absorption in the near infrared region of the electromagnetic spectrum [73]. This has the potential to increase the number of excitons generated within a device and results in a greater number of disintegrations to electrons and holes when incorporated in OSCs. CNTs have a high aspect ratio (>1000:1), and therefore, very little is required to form composites with physicochemical properties that are very different from those of the parent polymer [73]. They have outstanding mechanical properties [74], a high surface area to volume ratio [75], and relatively small diameters, which have made these materials very useful as additives to make high strength composites [76].

### 2.2.1 Electronic properties of CNTs

Single-wall CNTs can either have metallic or semi-conducting properties depending on the orientation of the graphene sheets which are rolled to make the individual tube [77]. In a perfectly aligned SWCNT, there is overlap of  $\pi$ -orbitals in the individual six-membered rings. This overlap provides a delocalized space for the movement of electrons and the SWCNTs are deemed conductors. The conductivity can change to semi-conducting when the alignment of the six-membered rings is distorted, and thus, the  $\pi$ -orbital overlap is changed. The direction of the graphene sheet plane and nanotube diameter are obtained from a pair of integers ( $n, m$ ) that denote the nanotube type [78]. In the *arm-chair* configuration the integers are equal ( $n = m$ ), and in the *zigzag* orientation one of the integers is equal to 0 ( $m$  or  $n = 0$ ), and when the tube is described as *chiral*, the integers are nonzero and non-equal ( $n \neq m$ ). Armchair-type tubes are metallic while all other orientations are semiconducting [79]. At high temperatures, the electrical conductivity of SWCNTs can be described by semi-classical models used with graphite, while at low temperature, they reveal 2D quantum transport features [80]. However, it is very difficult to predict the electrical properties of MWCNTs because rolling up of the graphene layers can differ from one layer to the other and their more complex structure increases the possibility of defects, which can alter the electronic properties.

In terms of electrical properties, some recent reviews have highlighted the limitations encountered when incorporating SWCNT structures into OSCs [81-84]. Nevertheless, the key consideration is the inhomogeneity of a sample of SWCNTs. Typically, after synthesizing and purifying SWCNTs, the samples contain a mixture of semiconducting and highly conducting tubes. Thus, some of the tubes may enhance charge carrier transfer to the electrodes, and some may act as sites for recombination of charge carriers. These limitations may be overcome in the near future, with improvements in the synthesis of SWCNTs to control chirality or in separation methods.

When CNTs, multiwalled or single-walled, are incorporated into a polymer matrix, the resulting nanocomposites can have electrical properties that differ from their parent materials. This depends on whether the loading or weight percent of CNTs is above or below the percolation threshold. Conductivity increases drastically when the amount of CNTs is at or above the percolation threshold. Bauhofer and Kovacs [85] have reviewed percolation thresholds for CNT/polymer composites. The percolation threshold is known to be influenced by dispersion, aspect ratio, purity and alignment of the CNTs [86]. Also, it has been suggested that it is easier for well-dispersed CNTs to form an electrical path owing to homogeneous dispersion [85]. Higher electrical conductivity leads to increased photocurrents which improve overall efficiency of the cell device [87].

The electrical properties of SWCNTs and MWCNTs can be tuned to a certain extent, whereby the HOMO and LUMO match the donor and acceptor polymers appropriately, and thus, these materials can be incorporated into the OSC architecture as electron or hole carriers within the donor or acceptor polymer matrix, or as transparent electrodes [88].

### **2.2.2 Mechanical properties of CNTs**

Carbon nanotubes are made of  $sp^2$  carbon-carbon bonds, and these continuous networks within a tubular shape make them some of the strongest and most resilient materials known to exist. CNTs have a theoretical Young's modulus on the scale of terapascals, and the tensile strength of these materials has been measured to be upwards of 100s of gigapascals.

To offer some perspective on such numbers, CNTs are often compared to steel, with simple descriptors stating they are 100 times stronger than steel but weigh six times less [78,89-91]. In addition, CNTs are also very flexible and can bend over 90° several times without breaking [92]. They undergo permanent structural changes at high pressures (>1.5 GPa), but below these values deformation is usually totally elastic [80]. Also in the radial direction, CNTs have a much lower Young's modulus of 10s of GPa, and the tensile strength in the radial direction is lower with values of ~1 GPa. The mechanical strength of CNTs increases the strength of the CNT/polymer composite [78,89-91,93,94], and can be of interest to OSCs [72]. The transfer of the mechanical properties of the CNTs to the polymer matrix or the change in mechanical properties from those of the parent materials to the new composite offers new possibilities in the design and implementation of solar cells in general. The use of lighter and stronger materials means that larger-surface-area PV systems can be assembled on structures that cannot support the weight of some inorganic systems. In addition, the flexibility would allow for greater options in design and implementation, for example, OSCs on a bridge column or any other highly curved surface. However, in order to achieve excellent mechanical properties with polymer/CNT nanocomposites, the CNTs need to be functionalized in order to debundle them and to facilitate dispersion in a solution or polymer matrix.

### **2.2.3 Thermal properties of CNTs**

Among the carbonaceous materials, CNTs are more stable to oxidation than activated carbon or amorphous carbon at high temperature. The thermal behaviour is different in SWCNTs and MWCNTs. SWCNTs are more thermally stable than MWCNTs since they have more defined structure and less deformations [90]. The thermoconductivity of CNTs in the axial direction is higher while in the radial direction, it is an insulator. The estimated thermoconductivity at room temperature is 7000 W m<sup>-1</sup> K<sup>-1</sup> [95]. This is comparable with that of diamond, therefore, inclusion of CNTs in the polymer matrix forms a thermally conductive percolating network enhancing thermal conductivity [96]. For OSCs, this can improve thermal conductivity, and hence, it may reduce thermal degradation problems.

#### **2.2.4 Chemical properties of CNTs**

Generally, CNTs are chemically inert, but the curvature on the surface of the tubes enhances their reactivity compared to a flat graphene sheet [97]. Mismatch between the  $\pi$ -orbital in the CNT walls brings about reactivity enhancements. CNTs with small diameters are more reactive than ones with bigger diameters [97]. The slight reactivity of CNTs allows surface modification, and this is accomplished by acid oxidation to introduce oxygen-containing group functionalities on the wall surfaces [98] which increases solubility in polar solvents and also increases their compatibility with some polymeric matrixes [93]. Further modification is possible through covalent chemistry and examples include fluorination, ozonolysis or acrylation [78]. These modifications of CNTs are known as functionalization and are discussed in the next section.

#### **2.3 Functionalization of CNTs**

Raw CNTs are not usually used to make CNT/polymer composites without treatment to eliminate impurities like amorphous carbon, metal particles and graphitic nanoparticles, all of which interfere with the desired properties or end product [99]. These impurities can be removed by gas-phase oxidation [100], acid treatment [101], annealing and thermal treatment [102,103], ultrasonication [99], magnetic separation [99], microfiltration [102], or a combination of two or more of the aforementioned methods [104].

As previously mentioned, incorporation of CNTs in a conjugated polymer has potential use in OSC fabrication as it improves mechanical, thermal and electrical properties of the polymer [62]. However, for improved interfacial bonding and good dispersion of the CNTs in a conjugated polymer or solvent, surface modification is required. Surface modification can either be covalent or non-covalent [105]. Table 1 shows how these two types of functionalization are achieved.



**Table 1:** Surface functionalization of CNTs.

Type of functionalization	Method of functionalization	Reagents	Damaging effect on CNTs	References
Non-covalent	sonication followed by <i>in situ</i> polymerization	dianhydride monomer	yes	[106]
	surfactant aided modification	sodium dodecyl sulfonate	no	[107,108]
	wrapping	polyvinylpyrrolidone	no	[109]
Covalent	solution treatment (usually acid oxidation)	conc H <sub>2</sub> SO <sub>4</sub> :HNO <sub>3</sub> 3:1	yes	[110,111]
	ball milling	gases, e.g. H <sub>2</sub> S, NH <sub>3</sub> , CO, COCl <sub>2</sub>	yes	[112,113]
	plasma treatment	N <sub>2</sub> /Ar microwave plasma treatment to introduce N <sub>2</sub> on the wall	no	[114]

### 2.3.1 Non-covalent functionalization

Non-covalent modification involves physical adsorption of the polymer chain on the walls of the CNTs through interaction of the delocalized  $\pi$ -electronic structure of CNTs and the delocalized  $\pi$ -electronic structure of conjugated polymer chains [109]. Interaction between the  $\pi$ -electronic systems of the polymer chains and the CNT walls breaks the van der Waals forces between individual CNTs. Typically, CNTs aggregate into bundles owing to the dispersion forces between individual tubes, and the high aspect ratio means the bundles can

be very difficult to break-up; hence, the use of ultrasound probe techniques during processing. The interaction between the polymer chain and individual CNTs modifies the conformation of the polymer and can lead to helical wrapping around the CNT. Non-covalent functionalization does not interfere with the conjugated system of the CNTs and therefore the desired properties are retained [115].

### **2.3.2 Covalent functionalization**

Covalent functionalization or a chemical modification introduces functional groups covalently bonded to the backbone structure of the CNTs and contributes to better dispersion of CNTs within the polymer matrix. It also improves the chemical affinity of CNTs, which assists in the processing of the CNT/polymer composite, and improves the mechanical and electrical properties of the composite [115]. However, covalent functionalization can alter the electronic properties of CNTs in an un-favourable manner and this can have an unfavourable effect on the final OSCs.

## **3. Assembling solar cells**

The processing of OSCs with CNTs involves a number of steps including, processing of the conjugated polymer/CNT composites and deposition of these composites onto a suitable substrate.

### **3.1 Processing conjugated polymer/CNT composites**

Good dispersion and adhesion of CNTs with the polymer matrix plays an important role in incorporating the excellent properties of CNTs in the polymer matrix [86]. There are several methods of processing CNT/polymer composites, which include solution mixing, melt blending and *in situ* polymerization. Effective utilization of CNTs in composite applications depends on their ability to disperse individually and homogeneously within the polymer matrix. Interfacial interaction between the CNTs and the polymer matrix, results in efficient load transfer. It also affects the alignment of individual tubes in the polymer matrix [115]. Well-aligned tubes are reported to interact well with the polymer matrix which, enhances conductivity and increase mechanical strength of the composite [116].

### 3.1.1 Solution processing

The general procedure involves dispersion of CNTs in a suitable solvent by energetic agitation, followed by mixing of polymer and nanotubes in solution by mechanical agitation. The solvent is then allowed to evaporate under controlled conditions and the CNT/polymer composite is left behind [86]. Energetic agitation can be brought about by shear intensive mechanical stirring, magnetic stirring or ultrasonication [115]. Prolonged use of high-powered ultrasonication can introduce defects on the nanotube walls and reduce their sizes, which affects their properties [86]. Bhattacharyya *et al.* [62] processed a poly(3-octylthiophene) (P3OT)/SWCNT composite by solution processing. The CNTs were dispersed in chloroform by high-powered ultrasonication, the P3OT solution in chloroform was added to this dispersion and the mixture was then sonicated. The chloroform solution was left to evaporate. Geng and Zeng [117] similarly prepared a composite P3HT with SWCNTs by solution processing.

Nogueira and co-workers [118] prepared a composite of SWCNTs and thiophene by using solution processing. However, in their case, they first dried the oxidized SWCNTs followed by refluxing them with 3 M nitric acid to introduce carboxylic acid groups. Thionyl chloride was then added and the mixture stirred to introduce acyl chloride groups. Thereafter, 2(2-thienyl)ethanol was added to form an ester named SWCNT-THIOP. The product was dispersed in toluene, the polymer P3OT was added, the mixture stirred and the toluene evaporated leaving the composite which they characterised.

### 3.1.2 Melt processing

This method involves heating the polymer above its melting point to form a viscous liquid and introducing the CNTs by shear mixing. The method is good for insoluble polymers that are impossible to prepare by solution processing. It is the most compatible method with current industrial practices such as injection moulding, blow moulding, extrusion and internal mixing. In particular, this technique is very useful when dealing with thermoplastic polymers which soften when heated [119]. Socher *et al.* [120] used melt

mixing to incorporate MWCNTs and carbon black together as a fillers in polyamide 12. The aim was to study the synergistic interaction effect of the two conductivity fillers. They reported higher volume conductivities for samples with the two fillers together although no synergistic effect was reported at the percolation threshold.

### **3.1.3 *In situ* processing**

The method involves dispersion of CNTs in a monomer solution. Polymerization takes place to form the polymer/CNT composite and is usually good for polymers that are not soluble or are thermally unstable. *In situ* polymerization can prepare composites that are covalently or non-covalently bound to the nanotubes [86]. Because of the small size of monomer molecules, the homogeneity of the resulting composite adducts is much higher than solution mixing of polymer and CNTs. It also allows preparation of composites with a high CNT weight fraction [115]. The advantage of this method is the high reactivity of monomers that makes it efficient and controllable and enables designable tailored processing.

Koizhaiganova *et al.* [121] synthesized a P3HT/DWCNT composite by *in situ* polymerization to enable interfacial bonding and proper dispersion of the CNTs in the polymer matrix. They reported impressive conductivity values and recommended the use of the composite as a PV cell material. The same group had earlier reported the synthesis of P3OT/DWCNTs by *in situ* polymerization [122], and reported that the inner walls of the DWCNTs retained their intrinsic properties while the outer walls were involved in the formation of the composite with the polymer. This explains why the composites are popular in solar cells. Kim *et al.* [123] synthesized MWCNT/P3HT composites by *in situ* polymerization. They reported that the MWCNTs provide good conductivity even at low loading. Impressive conductivities and mobility values of the composite make it suitable for use in PV materials.

## **3.2 Film deposition techniques**

CNT/polymer composite processing is followed by deposition or coating onto a suitable substrate in order to fabricate OSCs. Deposition techniques involve depositing a thin film of material on a substrate or previously deposited layers. The key issue is to have control on the layer thickness to a few tens of nanometres. The following are some of the methods used to deposit the organic films on the substrates.

### **3.2.1 Spin coating method**

This involves dosing CNT/polymer composite on the substrate that rotates, distributing the composite homogeneously on the surface due to centrifugal forces. The substrate spins until the composite dries up, and the final thickness is controlled by frequency of spin, composition and properties of the material as well as the drying conditions. Spin-coating parameters are interdependent on each other; for example, an increase in spin frequency results in a lower film thickness, higher drying rate and higher shear rate [124]. Nagata *et al.* [125] used spin coating to prepare a BHJ OSC with co-planer interdigitized electrodes. Vairavan and co-workers [126] used spin coating to deposit the active layer of Poly[2-methoxy-5-(2-ethylhexyloxy)-1,4-phenylenevinylene], CdTe and CdS hybrid on a substrate, and the PCE of the device increased by 0.05%. Singh *et al.* [127] used spin coating of P3HT, functionalized SWCNTs and PCBM composite on a substrate at ambient conditions and formed a cell with a photoefficiency of ~1.8%.

### **3.2.2 Knife-coating and slot-die coating method**

These techniques involve continuous deposition of a wet layer along the length of web without contact with the coating head and the web. Coating is a result of feeding the CNT/polymer composite suspension to a meniscus that stands between the coating head and the web (Figure 8). Coat thickness control is superior to printing. Knife-coating is very similar to doctor blading, and laboratory results show that it can be transferred quite readily to roll-to-roll knife coating [128]. An ink reservoir before the knife in the knife coating process serves as a supply to the meniscus with new ink; as the web passes by it gradually deposits.

In the case of slot-die coating, the suspension is supplied to the meniscus *via* a slot and a pump. With this method it is also possible to coat stripes of a well-defined width along the web direction and hence, it one of the only film-forming techniques that inherently allows for 1D patterning. This aspect has enabled the very convincing demonstration of slot-die coating for the manufacture of polymer solar cells. It is possible to control and adjust the coat layer by controlling the speed of the web or the CNT/polymer suspension supply. Wengeler and co-workers [124] investigated knife- and slot-die coating to process a polymer nanoparticle composite for hybrid polymer solar cells. They reported that knife-coated solar cells showed efficiencies comparable to spin-coated, which demonstrates scalability since knife-coating is compatible with the roll-to-roll technique.

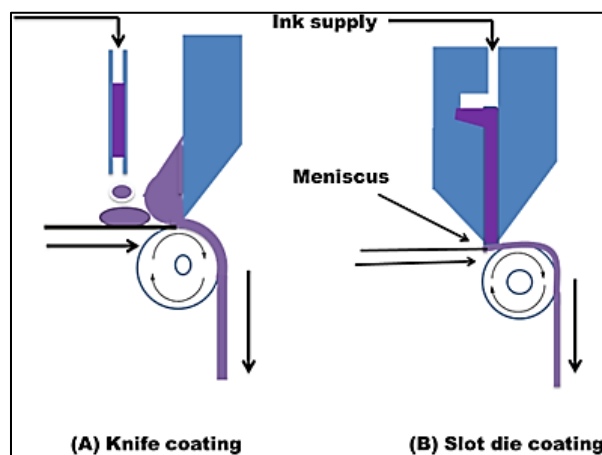


**Figure 8:** Illustration of knife-coating (A) and slot-die coating (B). The coat is deposited on the web as it passes [128].

### 3.2.3 Inject printing and spray-coating method

With these types of wet-film techniques, a coat is formed without contact between the substrate and the printing head. CNT/polymer composite suspension droplets are ejected into the free space that exists between the nozzle and substrate. The coat thickness can be controlled by printing multiple layers or adding more composite suspension to one spot [128]. Giroto *et al.* [129] used both spray and spin coating to compare composite performance. They demonstrated that spray coating is an excellent alternative to spin

coating. Peh *et al.* [130] reported spray coating as a high-throughput coating technique that is scalable and adaptable for OPV manufacturing. They argued that, to ensure uniform coating of the organic layer, the wettability, surface tension and boiling point of the solvent require optimization. Kang and co-workers [131] used a spray coating process to deposit electron- and hole-selective layers in an inverted OSC.

### **3.2.4 Dip coating technique**

Materials to use for dip coating are dissolved in an appropriate solvent such as toluene, chloromethane or chlorobenzene [132]. The substrate is soaked upright by allowing full coverage by the solution. Then the substrate is removed slowly from the solution and the liquid allowed to flow by gravity. A natural drying process follows and the film coat on the underside is erased.

### **3.2.5 Other printing techniques**

Other techniques include gravure printing [133,134], flexographic printing [135], screen-printing [136] and rotary screen-printing [128]. They involve transferring the motif to a substrate by physical contact between the object carrying the motif and the substrate.

## **4. Case studies**

There are several examples in the open literature where authors have investigated the use of CNTs in OSCs. Case studies where CNT/polymer are briefly highlighted, and some important developments in the field, based on SWCNTs, DWCNTs or MWCNTs as examples, are discussed in the subsequent section

### **4.1 Single-walled carbon nanotubes**

A composite consisting of a polycarbonate polymer and a 5 wt.% loading of SWCNTs was found to increase the conductivity by four orders of magnitude compared with the pristine polymer [137]. SWCNTs combined with poly(2-methoxyl-5-(2-ethoxylhexyloxy)-1,4-henylenevinylene) in the ratio 1:1 and with a  $V_{OC}$  of 0.4 V and  $J_{SC}$  of  $1 \mu\text{m A cm}^{-1}$  achieved a FF of 43% [138]. A SWCNT composite with P3OT was synthesized to determine the

effect of the SWCNT loading. A 15% loading was found to be the most favourable because the hole mobility increased 500 times compared with pristine P3OT [139]. Acid functionalized SWCNTs were found to enhance the conjugation length of P3HT thereby improving the absorption capacity. A device fabricated from these materials had a photo-conversion of ~1.8% [127]. SWCNTs when combined with P3HT-b-PS formed a device with increased photoresponse. This could be attributed to enhanced exciton dissociation and charge carrier separation [140]. Acid-treated SWCNTs covalently combined with aminothiophene through amide bonds to form a SWCNT-CONHTh composite showing an efficiency of 1.78%, while pristine SWCNTs had an efficiency of 1.48% and thiophene without SWCNT had an efficiency of 1% [141]. Integration of SWCNTs by simple and direct thermocompression in a polyethylene polymer formed a composite with good optical transparency and conductivity [142]. When SWCNTs form a composite with P3HT, charge carriers were found to be long-lived in the polymer matrix owing to the improved interfacial electron transfer [143].

#### **4.2 Double-walled carbon nanotubes**

Double-walled CNT/P3OT composite conductivities were compared with CNT loadings between 1 and 20% to determine the suitability of the composite as a photoactive material. The conductivity increased with CNT loading, and 20% was reported to have the highest conductivity of  $1.52 \times 10^{-3} \text{ S cm}^{-1}$ . The high conductivity of the composite makes it suitable for use as a photoactive layer in a PV cell [122]. Inclusion of DWCNTs in the active layer consisting of P3HT/C-60 increased the performance of the cell owing to increased charge transport and reduced recombination [59].

#### **4.3 Multiwalled carbon nanotubes**

A composite of MWCNTs and doped polyaniline (PANI) in its emeraldine salt MWCNT/PANI-ES was synthesized by *in situ* polymerization. The conductivity increased by 50–70% compared to pristine PANI. The increase was attributed to the presence of carboxylic acid groups on the wall of MWCNT which improved dispersion [144]. To determine the best MWCNT loading in the polymer matrix for efficient conductivity, a



composite of PANI and MWCNTs was synthesized by oxidative *in situ* polymerization. A 2 wt.% loading of acid-functionalised MWCNT gave the highest conductivity [145]. Polymer composites of poly(3,4-dihexyloxythiophene) and poly(3,4-dimethyloxythiophene-co-3,4-dihexyloxythiophene) with MWCNTs, conjugated by low energy band gap, were synthesized. A high conductivity of  $16 \text{ S cm}^{-1}$  was attained at 30% loading [38]. Sulfonated PANI forms a water-soluble and conducting composite with MWCNTs that were surface functionalized with phenylamine groups by *in situ* polymerization. The conductivity increased by two orders of magnitude compared with pristine MWCNTs [146]. A composite of pristine MWCNTs and poly[(2-methoxy-5-(2'-ethylhexyloxy)-1,4-phenylene)] was formed by solution mixing [147]. Photoluminescence quenching and increased absorbance, were some of the attributes of the composite formed. The electrical conductivity threshold of this composite was noted at 0.5% MWCNT loading; however, higher loading than this formed a dense network of nanotubes that acted as a nanomeric heat sink. Additional examples are given in Table 2.

## 5. Conclusion

From the discussion CNT/polymer composites have been shown to possess improved mechanical, conduction and electrical properties than the original polymer from which they were made. CNTs have also been found to enhance OSC efficiency due to improved dissociation of excitons and electron transfer to the electrodes. However, these efficiencies are still very low when compared to SSCs and more research is required to improve on the same. The research should focus more on the synthesis of copolymers, whose absorption will cover a wider range of the solar spectrum, and with improved environmental stability, which is another challenge in OSCs. Further research is also required on synthesis of CNTs, especially SWCNTs, to ensure metallic and semi-conductor is synthesized as different products. When the product is a mixture of metallic and semi-conductors, post-synthesis separation is difficult. In addition, when a mixture of the two is used to form a composite for OSCs, metallic type is reported to short circuit lowering efficiency. Easier and more efficient methods of synthesizing DWCNTs also need to be explored.

**Table 2:** Examples of CNT/polymer composites in OSCs.

Type of CNT used	CNT treatment / functionalization	CNT loading	Polymer used	CNT dopant	Additional composite additives	Position within the device	$V_{oc}$ /mV	$J_{sc}$ /mA cm <sup>-2</sup>	FF	$\eta$ /%	Illumination	Ref.
MWCNT	Oxidation (mix of H <sub>2</sub> SO <sub>4</sub> & HNO <sub>3</sub> )	2.0 wt%	poly(3-hexylthiophene-1,3-diyl) (P3HT)	N/A	Graphene	Active layer	670	4.7	0.32	1.05	100 mW cm <sup>-2</sup>	[38]
MWCNT	Alkyl amide side chains (octyldecylamine)	0.2 wt%	Poly(3-hexylthiophene) (P3HT)	N/A	PCBM	Active layer	560	14.79	0.52	4.39	AM 1.5 G,95 mW cm <sup>-2</sup>	[87]
SWCNT	carboxylated and sulfonated	0.4 wt%	poly(3-hexylthiophene) (P3HT)	N/A	C60	Active layer	386	2.72	0.51 2	0.57	AM 1.5 G,95 mW cm <sup>-2</sup>	[88]
SWCNT	Covalent functionalization with 2-(2-thienyl)ethanol	5.0 wt%	regioregular Poly(3-octylthiophene) (P3OT)	N/A	N/A	Active layer	750	0.009 5	NR	0.18 4	AM 1.5, 150 W	[118]
MWCNT	Oxidation (mix of H <sub>2</sub> SO <sub>4</sub> & HNO <sub>3</sub> )	1.0 wt%	Poly(3-hexylthiophene) (P3HT)	B	PCBM	Active layer	570	11.47	61.3	4.1	AM 1.5 G,95 mW cm <sup>-2</sup>	[64]
MWCNT	Oxidation (mix of H <sub>2</sub> SO <sub>4</sub> & HNO <sub>3</sub> )	1.0 wt%	Poly(3-hexylthiophene) (P3HT)	N	PCBM	Active layer	550	10.41	63.8	3.7	AM 1.5 G,95 mW cm <sup>-2</sup>	[64]

MWCNT	Oxidation (mix of H <sub>2</sub> SO <sub>4</sub> & HNO <sub>3</sub> )	1.0 wt%	poly 3-hexylthiophene (P3HT)	N/A	PCBM	Active layer	580	8.52	65.3	3.2	AM 1.5 G,95 mW cm <sup>-2</sup>	[64]
MWCNT	Oxidation (mix of H <sub>2</sub> SO <sub>4</sub> & HNO <sub>3</sub> )	0.2 wt%	poly(3-hexylthiophene) (P3HT) indene – C60 bisadduct (ICBA)	B-, & N-	PCBM	Active layer	560	9.29	57.5	3	AM 1.5 G,95 mW cm <sup>-2</sup>	[64]
MWCNT	Oxidation (mix of H <sub>2</sub> SO <sub>4</sub> & HNO <sub>3</sub> )	N/A	poly(2-methoxy-5-(2'-ethylhexyloxy) 1-4-phenylenevinylene) (MEHPPV)	N	InP	Active layer	790	11.9	65	6.11	AM 1.5 G, 100 mW cm <sup>-2</sup>	[58]
SWCNT	N/A	1:1	poly(3-octylthiophene) (P3OT)	N/A	N/A	electron donor layer	400	0.001	43	NR		[138]
SWCNT	acid treatment, and then dispersed with SDS	1.0 wt%	poly(3-hexylthiophene) (P3HT)	N/A	N/A	Active layer	750	0.5	NR	NR	AM 1.5, 100 mW cm <sup>-2</sup>	[139]
SWCNT	Oxidation (mix of H <sub>2</sub> SO <sub>4</sub> & HNO <sub>3</sub> )	N/A	poly(3-hexylthiophene) (P3HT)	N/A	PCBM	Active layer	520	5.53	0.49	1.8	80mW cm <sup>-2</sup>	[127]
SWCNT	Amidation with 2-aminothiophene	0.5 wt%	poly(3-hexylthiophene) (P3HT)	N/A	PCBM	photoactive layer	550	5.6	0.58	1.78	AM 1.5, 100 mWcm <sup>-2</sup>	[141]

MWCNT	Oxidation (mix of H <sub>2</sub> SO <sub>4</sub> & HNO <sub>3</sub> )	0.01 wt%	regioregular poly (3-hexylthiophene) (rr-P3HT)	N/A	PCBM	Active layer	520	11.33	54.6	3.47	AM 1.5 G, 100 mW CM <sup>-2</sup>	[144]
SWCNT	Non-covalent functionalization with the polymer	N/A	Separate layer in the device	N/A	N/A	Donor layer	580	8.36	69.4	3.36	AM 1.5 G	[148]
SWCNT	N/A	0.75wt%	poly(3-hexylthiophene) (P3HT)	N/A	N/A	Separate layer	509.6	8.2	24.6	3.52	AM 1.5 G	[149]
SWCNT	N/A (CNTs were semiconducting)	3.0 wt%	poly(3-hexylthiophene) (P3HT)	N/A	N/A	Active layer	1040	1.99	NR	0.72	AM1.5	[150]
MWCNT	Oxidation (mix of H <sub>2</sub> SO <sub>4</sub> & HNO <sub>3</sub> )	0.04 wt%	poly(3,4-ethylene dioxylthiophene)	N/A	polystyrenesulfonic acid	Active layer	560	9.03	47.4	2.39	100 mW cm <sup>-2</sup> , AM 1.5 G	[151]
DWCNT	37% HCl treatment	1.0 wt%	2,7-Bis-(3,3'-didodecyl-[2,2',5',2'';5'',2''']quaterthiophen-5-yl)fluoren-9-one (QTF12)	N/A	PCBM	Active layer	530	2.37	0.37	0.43	100 mW cm <sup>-2</sup> ,	[152]

Doped-CNTs in polymer composites could be better conductors than pristine CNTs when used in OSCs and thus, should be intensively investigated as currently data on these is limited.

### **Acknowledgements**

The authors thank the University of KwaZulu-Natal (UKZN), the National Research Foundation (NRF) and the India, Brazil and South Africa (IBSA) energy project for financial assistance. G. Keru thanks the UKZN College of Agriculture, Engineering and Science for award of a postgraduate bursary. We are grateful to Prof B.S. Martincigh for her critical comments and also proofreading the manuscript.

### **References**

- [1] Pegels A. Renewable energy in South Africa: Potentials, barriers and options for support. *Energy Policy*. 2010;**38**:4945-4954.
- [2] Spolding-Fecher R, Winker H, Mwakasonda S. Energy and the world summit on sustainable development. What next? *Energy Policy*. 2005;**33**:99-112.
- [3] Miah D, Ahmed R, Beleal MU. Biomass fuel use by the rural households in Chittagong region, *Bangladesh*. *Biomass and Bioenergy*. 2003;**24**:277-283.
- [4] Posten C, Schaub G. Microalgae and terrestrial biomass as source for fuels. A process view. *Journal of Biotechnology*. 2009;**142**:64-69.
- [5] Haehnlein S, Bayer P, Blum P. International legal status of the use of shallow geothermal energy. *Renewable and Sustainable Energy Reviews*. 2010;**14**:2611-2625.
- [6] Lund JW, Freeston DH, Boyd TL. Direct utilization of geothermal energy 2010 worldwide review. *Geothermics*. 2011;**40**:159-180.
- [7] Solangi KH, Islam MR, Saidur R, Rahim NA, Fayaz H. A review on global solar energy policy. *Renewable and Sustainable Energy Reviews*. 2011;**15**:2149-2163.
- [8] Sesto E, Casale C. Exploitation of wind as an energy source to meet the world's electricity demand. *Journal of Wind Engineering and Industrial Aerodynamics*. 1998;**74-76**:375-387.

- [9] Bhutto AW, Bazmi AA, Zahedi G. Greener energy: issues and challenges for Pakistan wind power prospective. *Renewable and Sustainable Energy Reviews*. 2013;**20**:519-538.
- [10] Yüksel I. Hydropower for sustainable water and energy development. *Renewable and Sustainable Energy Reviews*. 2010;**14**:462-469.
- [11] Gokcol C, Dursun B, Alboyaci B, Sunan E. Importance of biomass energy as alternative to other sources in Turkey. *Energy Policy*. 2009;**37**:424-431.
- [12] Farhat AAM, Ugursal VI. Greenhouse gas emission intensity factors for marginal electricity generation in Canada. *International Journal of Energy Research*. 2010;**34**:1309-1327.
- [13] Asim N, Kamaruzzaman S, Shideh A, Kasra S, Alghoul MA, Saadatian O, Zaidi SA. Review on the role of materials science in solar cells. *Renewable and Sustainable Energy Reviews*. 2012;**16**:5834–5847.
- [14] Davidson O. Energising Africa. *Science in Africa*; 2009; <http://www.sciencein africa.com>. Retrived 30 march 2013.
- [15] Lewis NS, Nocera DG. Powering the planet: Chemical challenges in solar energy utilization. *Proceedings of the National Academy of Sciences*. 2006;**103**:15729-15735.
- [16] Wang C, Abdul-Rahman H, Rao SP. A new design of luminescent solar concentrator and its trial run. *International Journal of Energy Research*. 2010;**34**:1372-1385.
- [17] Huang X, Han S, Huang W, Liu X. Enhancing solar cell efficiency the search for luminescent materials as spectral converters. *Chemical Society Reviews*. 2013;**42**:173-201.
- [18] Zhang X, Wang X, Xiao H, Yang C, Ran J, Wang C, Hou Q, Li J. Simulation of In<sub>0.65</sub>Ga<sub>0.35</sub>N single-junction solar cell. *Journal of Physics D: Applied Physics*. 2007;**40**:7335-7338.
- [19] Matin MA, Mannir-Aliyu M, Quadery AH, Amin N. Prospects of novel front and back contacts for high efficiency cadmium telluride thin film solar cells

- from numerical analysis. *Solar Energy Materials and Solar Cells*. 2010;**94**:1496-1500.
- [20] Choi SJ, Yu GJ, Kang GH, Lee JC, Kim D, Song H-E. The electrical properties and hydrogen passivation effect in mono crystalline silicon solar cell with various pre-deposition times in doping process. *Renewable Energy*. 2013;**54**:96-100.
- [21] Kwon TY, Yang DH, Ju MK, Jung WW, Kim SY, Lee YW, Gong DY, Yi J. Screen printed phosphorus diffusion for low-cost and simplified industrial mono-crystalline silicon solar cells. *Solar Energy Materials and Solar Cells*. 2011;**95**:14-17.
- [22] Yahia IS, Yakuphanoglu F, Azim OA. Unusual photocapacitance properties of a mono-crystalline silicon solar cell for optoelectronic applications. *Solar Energy Materials and Solar Cells*. 2011;**95**:2598-2605.
- [23] Yang B, Lee M. Fabrication of honeycomb texture on poly-Si by laser interference and chemical etching. *Applied Surface Science*. 2013;**284**:565-568.
- [24] Xue C, Rao J, Varlamov S. A novel silicon nanostructure with effective light trapping for polycrystalline silicon thin film solar cells by means of metal-assisted wet chemical etching. *Physica Status Solidi (A) Applications and Materials Science*. 2013 1–4 (2013) / DOI 10.1002/pssa.201330204.
- [25] Misra S, Yu L, Foldyna M, Roca i Cabarrocas P. High efficiency and stable hydrogenated amorphous silicon radial junction solar cells built on VLS-grown silicon nanowires. *Solar Energy Materials and Solar Cells*. 2013;**118**:90-95.
- [26] Jovanov V, Xu X, Shrestha S, Schulte M, Hüpkes J, Zeman M, Knipp D. Influence of interface morphologies on amorphous silicon thin film solar cells prepared on randomly textured substrates. *Solar Energy Materials and Solar Cells*. 2013;**112**:182-189.
- [27] Adomaitis RA, Schwarm A. Systems and control challenges in photovoltaic manufacturing processes: a modeling strategy for passivation and antireflection films. *Computers & Chemical Engineering*. 2013;**51**:65-76.

- [28] Braga AFB, Moreira SP, Zampieri PR, Bacchin JMG, Mei PR. New processes for the production of solar-grade polycrystalline silicon: A review. *Solar Energy Materials and Solar Cells*. 2008;**92**:418-424.
- [29] Pizzini S. Towards solar grade silicon: Challenges and benefits for low cost photovoltaics. *Solar Energy Materials and Solar Cells*. 2010;**94**:1528-1533.
- [30] Abdulrazzaq OA, Saini V, Bourdo S, Dervishi E, Biris AS. Organic solar cells: A review of materials, limitations, and possibilities for improvement. *Particulate Science and Technology*. 2013;**31**:427-442.
- [31] Jeon SO, Lee JY. Improved lifetime in organic solar cells using a bilayer cathode of organic interlayer/Al. *Solar Energy Materials and Solar Cells*. 2012;**101**:160-165.
- [32] Deibel C, Strobel T, Dyakonov V. Role of the charge transfer state in organic donor–acceptor Solar Cells. *Advanced Materials*. 2010;**22**:4097-4111.
- [33] Janssen RAJ, Nelson J. Factors limiting device efficiency in organic photovoltaics. *Advanced Materials*. 2012; **25**(13) 1847-1858.
- [34] Jørgensen M, Norrman K, Gevorgyan SA, Tromholt T, Andreasen B, Krebs FC. Stability of polymer solar cells. *Advanced Materials*. 2012;**24**:580-612.
- [35] Scharber MC, Mühlbacher D, Koppe M, Denk P, Waldauf C, Heeger AJ, Brabec CJ. Design rules for donors in bulk-heterojunction solar cells towards 10% energy conversion efficiency. *Advanced Materials*. 2006;**18**:789-794.
- [36] Weickert J, Dunbar RB, Hesse HC, Wiedemann W, Schmidt-Mende L. Nanostructured organic and hybrid solar cells. *Advanced Materials*. 2011;**23**:1810-1828.
- [37] Kim TH, Yang SJ, Park CY. Carbon nanomaterials in organic photovoltaic cells. *Carbon letters*. 2011;**12**:194-206.
- [38] Liu Z, He D, Wang Y, Wu H, Wang J, Wang H. Improving photovoltaic properties by incorporating both SPFGraphene and functionalized multi-walled carbon nanotubes. *Solar Energy Materials and Solar Cells*. 2010;**94**:2148-2153.



- [39] Skompska M. Hybrid conjugated polymer/semiconductor photovoltaic cells. *Synthetic Metals*. 2010;**160**:1-15.
- [40] Jørgensen M, Norrman K, Krebs FC. Stability/degradation of polymer solar cells. *Solar Energy Materials and Solar Cells*. 2008;**92**:686-714.
- [41] Peters CH, Sachs-Quintana IT, Mateker WR, Heumueller T, Rivnay J, Noriega R, Beiley ZM, Hoke ET, Salleo A, McGehee MD. The mechanism of burn-in loss in a high efficiency polymer solar cell. *Advanced Materials*. 2012;**24**:663-668.
- [42] Williams G, Wang Q, Aziz H. The photo-stability of polymer solar cells: contact photo-degradation and the benefits of interfacial layers. *Advanced Functional Materials*. 2013;**23**:2239-2247.
- [43] Wang DH, Moon JS, Seifert J, Jo J, Park JH, Park OO, Heeger AJ. Sequential processing: control of nanomorphology in bulk heterojunction solar cells. *Nano Letters*. 2011;**11**:3163-3168.
- [44] Price SC, Stuart AC, Yang L, Zhou H, You W. Fluorine substituted conjugated polymer of medium band gap yields 7% efficiency in polymer-fullerene solar cells. *Journal of the American Chemical Society*. 2011;**133**: 4625-4631.
- [45] Cox M, Gorodetsky A, Kim B, Kim KS, Jia Z, Kim P, Nuckolls C, Kymissis I. Single-layer graphene cathodes for organic photovoltaics. *Applied Physics Letters*. 2011;**98**: 123303,1-3.
- [46] Park SH, Roy A, Beaupre S, Cho S, Coates N, Moon JS, Moses D, Leclerc M, Lee K, Heeger AJ. Bulk heterojunction solar cells with internal quantum efficiency approaching 100%. *Nature Photonics*. 2009;**3**:297-302.
- [47] Zhang Y, Basel TP, Gautam BR, Yang X, Mascaro DJ, Liu F, Vardeny ZV. Spin-enhanced organic bulk heterojunction photovoltaic solar cells. *Nature Communications*. 2012;**3**:1043.
- [48] Ye Q, Chi C. Conjugated polymers for organic solar cells. In solar cells - new aspects and solutions, Prof. Leonid A. Kosyachenko (Ed.), ISBN: 978-953-307-761-1, *InTech*, DOI: 10.5772/23275. Available from: <http://www.intechopen.->

com/books/solar-cells-new-aspects-and-solutions/conjugated polymers for organic solar cells 2011:453-476.

- [49] Somani SP, Somani PR, Umeno M, Flahaut E. Improving photovoltaic response of poly(3-hexylthiophene)/n-Si heterojunction by incorporating double-walled carbon nanotubes. *Applied Physics Letters*. 2006;**89**: 223505,1-2.
- [50] Ferguson AJ, Blackburn JL, Kopidakis N. Fullerenes and carbon nanotubes as acceptor materials in organic photovoltaics. *Materials Letters*. 2013;**90**:115-125.
- [51] Kim YH, Müller-Meskamp L, Zakhidov AA, Sachse C, Meiss J, Bikova J, Cook A, Zakhidov AA, Leo K. Semi-transparent small molecule organic solar cells with laminated free-standing carbon nanotube top electrodes. *Solar Energy Materials and Solar Cells*. 2012;**96**:244-250.
- [52] Tune DD, Flavel BS, Quinton JS, Ellis AV, Shapter JG. Single-walled carbon nanotube network electrodes for dye solar cells. *Solar Energy Materials and Solar Cells*. 2010;**94**:1665-1672.
- [53] Xu F, Zhu WQ, Yan L, Xu H, Xiong LH, Li JH. Single-walled carbon nanotube anodes based high performance organic light-emitting diodes with enhanced contrast ratio. *Organic Electronics*. 2012;**13**:302-308.
- [54] Aitola K, Borghei M, Kaskela A, Kemppainen E, Nasibulin AG, Kauppinen EI, Lund PD, Ruiz V, Halme J. Flexible metal-free counter electrode for dye solar cells based on conductive polymer and carbon nanotubes. *Journal of Electroanalytical Chemistry*. 2012;**683**:70-74.
- [55] Aitola K, Halme J, Feldt S, Lohse P, Borghei M, Kaskela A, Nasibulin AG, Kauppinen EF, Lund PD, Bachloo G, Hagfeldt A. Highly catalytic carbon nanotube counter electrode on plastic for dye solar cells utilizing cobalt-based redox mediator. *Electrochimica Acta*. 2013;**111**:206-209.
- [56] Arena A, Daonato N, Saitta G. Photovoltaic properties of multi-walled carbon nanotubes. *Microelectronic journal*. 2008;**39**:1659-62.
- [57] Keru G, Ndungu PG, Nyamori VO. Nitrogen-doped carbon nanotubes synthesised by Pyrolysis of (4-[[pyridine-4-yl)methylidene]amino]phenyl)ferrocene. *Journal of Nanomaterials*. 2013;**2013**:1-7.

- [58] Lee JM, Kwon BH, Park HI, Kim H, Kim MG, Park JS, Yoo S, Jeon DY, Kim SO. Exciton dissociation and charge-transport enhancement in organic solar cells with quantum-dot/N-doped CNT hybrid nanomaterials. *Advanced Materials*. 2013;**25**:2011-2017.
- [59] Somani SP, Somani PR, Umeno M. Carbon nanotube incorporation: a new route to improve the performance of organic-inorganic heterojunction solar cells. *Diamond and Related Materials*. 2008;**17**:585-588.
- [60] Cataldo S, Salice P, Menna E, Pignataro B. Carbon nanotubes and organic solar cells. *Energy & Environmental Science*. 2012;**5**:5919-5940.
- [61] Guenes S, Neugebauer H, Sariciftci NS. Conjugated polymer-based organic solar cells. *Chemical Reviews*. 2007;**107**:1324-1338.
- [62] Bhattacharyya S, Kymakis E, Amaratunga GAJ. Photovoltaic properties of dye functionalized single-wall carbon nanotube/conjugated polymer devices. *Chemistry of Materials*. 2004;**16**:4819-4823.
- [63] Hwang SK, Lee JM, Kim S, Park JS, Park HI, Ahn CW, Lee KJ, Lee T, Kim SO. Flexible multilevel mesistive memory with montrrolled charge trap band N-doped carbon nanotubes. *Nano Letters*. 2012;**12**:2217-2221.
- [64] Lee JM, Park JS, Lee SH, Kim H, Yoo S, Kim SO. Selective electron- or hole-transport enhancement in bulk heterojunction organic solar cells with N- or B-doped carbon nanotubes. *Advanced Materials*. 2011;**23**:629-633.
- [65] Jana D, Sun C-L, Chen L-C, Chen K-H. Effect of chemical doping of boron and nitrogen on the electronic, optical, and electrochemical properties of carbon nanotubes. *Progress in Materials Science*. 2013;**58**:565-635.
- [66] Iijima S, Ichihashi T. Single-shell carbon nanotubes of 1-nm diameter. *Nature*. 1993;**363**:603-605.
- [67] Guo T, Nikolaev P, Thess A, Colbert DT, Smalley RE. Catalytic growth of single-walled manotubes by laser vaporization. *Chemical Physics Letters*. 1995;**243**:49-54.

- [68] Allouche H, Monthieux M, Jacobsen RL. Chemical vapor deposition of pyrolytic carbon on carbon nanotubes: Part 1. Synthesis and morphology. *Carbon*. 2003;**41**:2897-2912.
- [69] Danafar F, Fakhru'l-Razi A, Mohd-Salleh MA, Awang-Biak DR. Influence of catalytic particle size on the performance of fluidized-bed chemical vapor deposition synthesis of carbon nanotubes. *Chemical Engineering Research and Design*. 2011;**89**:214-223.
- [70] Kumar M. Carbon nanotube synthesis and growth mechanism: In Yellampalli, S (Edn) carbon nanotubes - synthesis, characterization, applications, ISBN 978-953-307-497-9, In Tech, Doi 10.5772/19331; 2011.
- [71] Bondi SN, Lackey WJ, Johnson RW, Wang X, Wang ZL. Laser assisted chemical vapor deposition synthesis of carbon nanotubes and their characterization. *Carbon*. 2006;**44**:1393-1403.
- [72] Kymakis E, Amaratunga GAJ. Single-wall carbon nanotube conjugated polymer photovoltaic devices. *Applied Physics Letters*. 2002;**80**:112-114.
- [73] Endo M, Strano MS, Ajayan PM. Carbon nanotubes In Jorio A, Dresselhaus MS, editors. Topics in applied physics, Springer: Berlin, 2008. pp. 13-62.
- [74] Coleman JN, Khan U, Blau WJ, Gun'ko YK. Small but strong: A review of the mechanical properties of carbon nanotube/polymer composites. *Carbon*. 2006;**44**:1624-1652.
- [75] Kim D-Y, Yun YS, Bak H, Cho SY, Jin H-J. Aspect ratio control of acid modified multi-walled carbon nanotubes. *Current Applied Physics*. 2010;**10**:1046-1052.
- [76] Endo M, Haruyashi T, Kim YA, Terrones M, Dresselhaus MS, Applications of carbon nanotubes. *Philosophical Transactions Royal Society London A*. 2004;**362**:2223–2238.
- [77] Oosthuizen RS, Nyamori VO. Carbon nanotubes as support for palladium and bimetallic catalyst for use in hydrogenation reactions. *Platinum Metals Review*. 2011;**55**:154–169.

- [78] Harris PJF. Carbon nanotube composites. *International Materials Reviews* 2004;**49**:31 - 43.
- [79] Jones WE Jr., Chiguma J, Johnson E, Pachamuthu A, Santos D. Electrically and thermally conducting nanocomposites for electronic applications. *Materials*. 2010;**3**:1478-1496.
- [80] Mohlala MS, Liu X-Y, Coville NJ. Synthesis of multi-walled carbon nanotubes catalyzed by substituted ferrocenes. *Journal of Organometallic Chemistry*. 2006;**691**:4768-4772.
- [81] Dubacheva GV, Liang C-K, Bassani DM. Functional monolayers from carbon nanostructures (fullerenes, carbon nanotubes, and graphene) as novel materials for solar energy conversion. *Coordination Chemistry Reviews*. 2012;**256**:2628-2639.
- [82] Guldi DM, Costa RD. Nanocarbon hybrids: the paradigm of nanoscale self-ordering/self-assembling by means of charge transfer/doping interactions. *The Journal of Physical Chemistry Letters*. 2013;**4**:1489-1501.
- [83] Kanemitsu Y. Multiple exciton generation and recombination in carbon nanotubes and nanocrystals. *Accounts of Chemical Research*. 2013;**46** (6):1358-1366.
- [84] Sliaužys G, Arlauskas K, Gulbinas V. Photogeneration and recombination of charge carrier pairs and free charge carriers in polymer/fullerene bulk heterojunction films. *Physica Status Solidi (A)*. 2012;**209**:1302-1306.
- [85] Bauhofer W, Kovacs JZ. A review and analysis of electrical percolation in carbon nanotube polymer composites. *Composites Science and Technology*. 2009;**69**:1486-1498.
- [86] Yang MJ, Koutsos V, Zaiser M. Interactions between polymers and carbon nanotubes: a molecular dynamics study. *Journal of Physical Chemistry B*. 2005;**109**:10009-10014.
- [87] Jun GH, Jin SH, Park SH, Jeon S, Hong SH. Highly dispersed carbon nanotubes in organic media for polymer:fullerene photovoltaic devices. *Carbon*. 2012;**50**:40-46.

- [88] Li C, Chen Y, Wang Y, Iqbal Z, Chhowalla M, Mitra S. A fullerene-single-wall carbon nanotube complex for polymer bulk heterojunction photovoltaic cells. *Journal of Materials Chemistry*. 2007;**17**:2406-2411.
- [89] Laird ED, Li CY. Structure and morphology control in crystalline polymer carbon nanotube nanocomposites. *Macromolecules*. 2013;**46**:2877-2891.
- [90] Ruoff RS, Qian D, Liu WK. Mechanical properties of carbon nanotubes theoretical predictions. *Comptes Rendus Physique*, 2003;**4**:993–1008.
- [91] Shokrieh MM, Rafiee R. A review of the mechanical properties of isolated carbon nanotubes and carbon nanotube composites. *Mechanics Composite Materials*. 2010;**46**:155-172.
- [92] Iijima S, Brabec C, Maiti, A, Bernholc, J. Structural flexibility of carbon nanotubes. *Journal of Chemistry and Physics* 1996;**104**:2089-2092.
- [93] Lin Y, Zhou B, Fernando KAS, Liu P, Allard LF, Sun YP. Polymeric carbon nanocomposites from carbon nanotubes functionalized with matrix polymer. *Macromolecules*. 2003;**36**:7199-7204.
- [94] Sakellariou G, Priftis D, Baskaran D. Surface-initiated polymerization from carbon nanotubes: strategies and perspectives. *Chemical Society Reviews*. 2013;**42**:677-704.
- [95] Padgett CW, Brenner DW. Influence of chemisorption on the thermal conductivity of single-wall carbon nanotube. *Nano Letters*. 2004;**4**:1051-1053.
- [96] Han Z, Fina A. Thermal conductivity of carbon nanotubes and their polymer nanocomposites: A review. *Progress in Polymer Science*. 2011;**36**:914-944.
- [97] Lin T, Bajpai V, Ji T, Dai LM. Chemistry of carbon nanotubes. *Australian Journal of Chemistry*. 2003;**56**:635-651.
- [98] Ozin GA, Arsenault AC. Nanochemistry: a chemical approach to nanomaterials. *Materials Today*. 2009;**12**:46.
- [99] Aqel A, El-Nour KMMA, Ammar RAA, Al-Warthan A. Carbon nanotubes, science and technology part (I) structure, synthesis and characterisation. *Arabian Journal of Chemistry*. 2012;**5**:1-23.

- [100] Rong H, Liu Z, Wu Q, Lee Y-H. A facile and efficient gas phase process for purifying single-walled carbon nanotubes. *Current Applied Physics*. 2010;**10**:1231-1235.
- [101] Edwards ER, Antunes EF, Botelho EC, Baldan MR, Corat EJ. Evaluation of residual iron in carbon nanotubes purified by acid treatments. *Applied Surface Science*. 2011;**258**:641-648.
- [102] Hou P-X, Liu C, Cheng H-M. Purification of carbon nanotubes. *Carbon*. 2008;**46**:2003-2025.
- [103] Andrews R, Jacques D, Qian D, Dickey EC. Purification and structural annealing of multi-walled carbon nanotubes at graphitization temperatures. *Carbon*. 2001;**39**:1681-1687.
- [104] Serp P, Corrias M, Kalck P. Carbon nanotubes and nanofibers in catalysis. *Applied Catalysis A: General*. 2003;**253**:337-358.
- [105] Ma PC, Siddiqui NA, Marom G, Kim JK. Dispersion and functionalization of carbon nanotubes for polymer-based nanocomposites: A review composites part A: *Applied Science and Manufacturing*. 2010;**41**:1345-367.
- [106] Park C, Ounaies Z, Watson KA, Crooks RE, Smith Jr J, Lowther SE, Connell JW, Siochi JE, Harrison JS, St Clair TL. Dispersion of single-wall carbon nanotubes by *in situ* polymerization under sonication. *Chemical Physics Letters*. 2002;**364**:303-308.
- [107] Zhang M, Su L, Mao L. Surfactant functionalization of carbon nanotubes (CNTs) for layer-by-layer assembling of CNT multi-layer films and fabrication of gold nanoparticle/CNT nanohybrid. *Carbon*. 2006;**44**:276-283.
- [108] Alpatova AL, Shan W, Babica P, Upham BL, Rogensues AR, Masten SJ, Drown E, Mohanty AK, Alocilja EC, Tarabara VV. Single-walled carbon nanotubes dispersed in aqueous media via non-covalent functionalization: effect of dispersant on the stability, cytotoxicity, and epigenetic toxicity of nanotube suspensions. *Water Research*. 2010;**44**:505-520.
- [109] Liu P. Modifications of carbon nanotubes with polymers. *European Polymer Journal*. 2005;**41**:2693-2703.

- [110] Yang ZL, Pu HT, Yin YL. Covalent functionalization of multi-walled carbon nanotubes by polyvinylimidazole. *Materials Letters*. 2005;**59**:2838-2841.
- [111] Jin F-L, Yop-Rhee K, Park S-J. Functionalization of multi-walled carbon nanotubes by epoxide ring-opening polymerization. *Journal of Solid State Chemistry*. 2011;**184**:3253-3256.
- [112] Kónya Z, Vesselenyi I, Niesz K, Kukovecz A, Demortier A, Fonseca A, Dehelle J, mekhalif Z, B-Naggy J, Koós AA, Osvàth Z, Kocsonya A, Biró LP, Kiricsi I. Large scale production of short functionalized carbon nanotubes. *Chemical Physics Letters*. 2002;**360**:429-435.
- [113] Chen L, Pang X-J, Zhang Q-T, Yu Z-l. Cutting of carbon nanotubes by a two-roller mill. *Materials Letters*. 2006;**60**:241-244.
- [114] Kalita G, Adhikari S, Aryal HR, Afre R, Soga T, Sharon M, Umeno M. Functionalization of multi-walled carbon nanotubes with nitrogen plasma for photovoltaic device application. *Current Applied Physics*. 2009;**9**:346-351.
- [115] Spitalsky Z, Tasis D, Papagelis K, Galiotis C. Carbon nanotube/polymer composites: Chemistry, processing, mechanical and electrical properties. *Progress in Polymer Science*. 2010;**35**:357-401.
- [116] Rahmat M, Hubert P. Carbon nanotube–polymer interactions in nanocomposites: A review. *Composites Science and Technology*. 2011;**72**:72-84.
- [117] Geng J, Zeng T. Influence of single-walled carbon nanotubes induced crystallinity enhancement and morphology change on polymer photovoltaic devices. *Journal of the American Chemical Society*. 2006;**128**:16827-16833.
- [118] Nogueira AF, Lomba BS, Soto-Oviedo MA, Correia CRD, Corio P, Furtado CA, Hummelgen IA. Polymer solar cells using single-wall carbon nanotubes modified with thiophene pedant groups. *Journal of Physical Chemistry C*. 2007;**111**:18431-18438.
- [119] Al-Saleh MH, Sundararaj U. Morphological, electrical and electromagnetic interference shielding characterization of vapour grown carbon



- nanofiber/polystyrene nanocomposites. *Polymer International*. 2013;**62**:601-607.
- [120] Socher R, Krause B, Hermasch S, Wursche R, Pötschke P. Electrical and thermal properties of polyamide 12 composites with hybrid fillers systems of multi-walled carbon nanotubes and carbon black. *Composites Science and Technology*. 2011;**71**:1053-1059.
- [121] Koizhaiganova R, Kim HJ, Vasudevan T, Kudaibergenov S, Lee MS. *In Situ* polymerization of 3-hexylthiophene with double-walled carbon nanotubes: studies on the conductive nanocomposite. *Journal of Applied Polymer Science*. 2010;**115**:2448-2454.
- [122] Koizhaiganova R, Kim HJ, Vasudevan T, Kudaibergenov S, Lee MS. *In Situ* polymerization of 3-hexylthiophene with double-walled carbon nanotubes: studies on the conductive nanocomposite. *Journal of Applied Polymer Science*. 2010;**115**:2448-2454.
- [123] Kim HJ, Koizhaiganova R, Vasudevan T, Sanjeeviraja C, Lee MS. Single step synthesis of poly(3-octylthiophene)/multi-walled carbon nanotube composites and their characterizations. *Polymers for Advanced Technologies*. 2009;**20**:736-741.
- [124] Wengeler L, Schmidt-Hansberg B, Peters K, Scharfer P, Schabel W. Investigations on knife and slot die coating and processing of polymer nanoparticle films for hybrid polymer solar cells. *Chemical Engineering and Processing: Process Intensification*. 2011;**50**:478-482.
- [125] Nagata S, Atkinson GM, Pestov D, Tepper GC, McLeskey Jr JT. Co-planar bi-metallic interdigitated electrode substrate for spin-coated organic solar cells. *SolarEnergy Materials and Solar Cells*. 2011;**95**:1594-1597.
- [126] Vairavan R, Mohamad Shahimin M, Juhari N. Fabrication and characterisation of MEH-PPV/CdTe/CdS. solar cell. 2011. <http://dx.doi.org/10.1109/CHU-SER.-2011.6163772> p. 454-458. *Retrieved 15<sup>th</sup> Feb 2013*.
- [127] Singh RK, Kumar J, Kumar A, Kumar V, Kant R, Singh R. Poly(3-hexylthiophene): Functionalized single-walled carbon nanotubes: (6,6)-phenyl-

- C-61-butyric acid methyl ester composites for photovoltaic cell at ambient condition. *Solar Energy Materials and Solar Cells*. 2010;**94**:2386-2394.
- [128] Sondergaard R, Hosel M, Angmo D, Larsen-olsen TT, Krebs FC. Roll-to-roll fabrication of thin film. *Materials Today*. 2012;**15**:37-49.
- [129] Giroto C, Rand BP, Genoe J, Heremans P. Exploring spray coating as a deposition technique for the fabrication of solution-processed solar cells. *Solar Energy Materials and Solar Cells*. 2009;**93**:454-458.
- [130] Peh RJ, Lu Y, Zhao F, Lee C-LK, Kwan WL. Vacuum-free processed transparent inverted organic solar cells with spray-coated PEDOT:PSS anode. *Solar Energy Materials and Solar Cells*. 2011;**95**:3579-3584.
- [131] Kang J-W, Kang Y-J, Jung S, Song M, Kim D-G, Su Kim C, Su Kim C, Chang SK, Kim SH. Fully spray-coated inverted organic solar cells. *Solar Energy Materials and Solar Cells*. 2012;**103**:76-79.
- [132] Hu Z, Zhang J, Xiong S, Zhao Y. Performance of polymer solar cells fabricated by dip coating process. *Solar Energy Materials and Solar Cells*. 2012;**99**:221-225.
- [133] Kopola P, Aernouts T, Guillerez S, Jin H, Tuomikoski M, Maaninen A, Hast J. High efficient plastic solar cells fabricated with a high-throughput gravure printing method. *Solar Energy Materials and Solar Cells*. 2010;**94**:1673-1680.
- [134] Kopola P, Aernouts T, Sliz R, Guillerez S, Ylikunnari M, Cheyng D, Valimaki M, Tuomikoski M, Hast J, Jabbour G, Mylly R, Maaninen A. Gravure printed flexible organic photovoltaic modules. *Solar Energy Materials and Solar Cells*. 2011;**95**:1344-1347.
- [135] Krebs FC, Fyenbo J, Jorgensen M. Product integration of compact roll-to-roll processed polymer solar cell modules: methods and manufacture using flexographic printing, slot die coating and rotary screen printing. *Journal of Materials Chemistry*. 2010;**20**:8994-9001.
- [136] Krebs FC, Jørgensen M, Norrman K, Hagemann O, Alstrup J, Nielsen TD, Fyenbo J, Larsen K, Kristensen J. A complete process for production of flexible

- large area polymer solar cells entirely using screen printing-first public demonstration. *Solar Energy Materials and Solar Cells*. 2009;**93**:422-441.
- [137] Pradhan B, Kohlmeyer RR, Chen J. Fabrication of in-plane aligned carbon nanotube-polymer composite thin films. *Carbon*. 2010;**48**:217-222.
- [138] Ltaief A, Bouazizi A, Davenas J. Charge transport in carbon nanotubes-polymer composite photovoltaic cells. *Materials*. 2009;**2**:710-718.
- [139] Kymakis E, Servati P, Tzanetakis P, Koudoumas E, Kornilios N, Rompogiannakis I, Franghiadakis Y, Amaratunga GAJ. Effective mobility and photocurrent in carbon nanotube-polymer composite photovoltaic cells. *Nanotechnology*. 2007;**18**:435702.1-6.
- [140] Sarker BK, Arif M, Khondaker SI. Near-infrared photoresponse in single-walled carbon nanotube/polymer composite films. *Carbon*. 2010;**48**:1539-1544.
- [141] Stylianakis MM, Mikroyannidis JA, Kymakis E. A facile, covalent modification of single-wall carbon nanotubes by thiophene for use in organic photovoltaic cells. *Solar Energy Materials and Solar Cells*. 2010;**94**:267-274.
- [142] Nasibulin AG, Ollikainen A, Anisimov AS, Brown DP, Pikhitsa PV, Holopainen S, Penttila JS, Helisto P, Ruokohainen J, Choi M Kauppinen EI. Integration of single-walled carbon nanotubes into polymer films by thermo-compression. *Chemical Engineering Journal*. 2008;**136**:409-413.
- [143] Ferguson AJ, Blackburn JL, Holt JM, Kopidakis N, Tenent RC, Barnes TM, Heben JM, Rumble G. Photoinduced energy and charge transfer in P3HT:SWNT composites. *Journal of Physical Chemistry Letters*. 2010;**1**:2406-2411.
- [144] Wu M-C, Lin Y-Y, Chen S, Liao H-C, Wu Y-J, Chen C-W, Chen Y-F, Su W-F. Enhancing light absorption and carrier transport of P3HT by doping multi-wall carbon nanotubes. *Chemical Physics Letters*. 2009;**468**:64-68.
- [145] Choudhury A, Kar P. Doping effect of carboxylic acid group functionalized multi-walled carbon nanotube on polyaniline. *Composites Part B: Engineering*. 2011;**42**:1641-1647.

- [146] Xu J, Yao P, Li X, He F. Synthesis and characterization of water-soluble and conducting sulfonated polyaniline/para-phenylenediamine-functionalized multi-walled carbon nanotubes nano-composite. *Materials Science and Engineering: B*. 2008;**151**:210-219.
- [147] Bansal M, Srivastava R, Lal C, Kamalasanan MN, Tanwar LS. Low electrical percolation threshold and PL quenching in solution-blended MWNT-MEH PPV nanocomposites. *Journal of Experimental Nanoscience*. 2010;**5**:412-426.
- [148] Dabera GDMR, Jayawardena KDGI, Prabhath MRR, Yahya I, Tan YY, Nismy NA, Shiozawa H, Sauer M, Ruiz-Soria G, Ayala P, Stojan V, Domitha AA, Jorowski PO, Pichler PD, Silva SRP. Hybrid carbon nanotube networks as efficient hole extraction layers for organic photovoltaics. *Amerian Chemical Society Nano*. 2013;**7**:556-565.
- [149] Mallajosyula AT, Kumar S, Iyer S, Mazhari B. Increasing the efficiency of charge extraction limited poly-(3-hexylthiophene):[6,6] phenyl C61 butyric acid methyl ester solar cells using single-walled carbon nanotubes with metallic characteristics. *Journal of Applied Physics*. 2011;**109**:124908-124910.
- [150] Ren S, Bernardi M, Lunt RR, Bulovic V, Grossman JC, Gradečak S. Toward efficient carbon nanotube/P3HT solar cells: Active layer morphology, electrical, and optical properties. *Nano Letters*. 2011;**11**:5316-5321.
- [151] Li J, Liu J, Gao C, Chen G. Nanocomposite hole-extraction layers for organic solar cells. *International Journal of Photoenergy*. 2011; **2011**:Article ID 392832;1-5.
- [152] Picard L, Lincker F, Kervella Y, Zagorska M, DeBettignies R, Peigney A, Flahaut E, Louarn G, Lefrant S, Demadrille R, Pron A. Composites of double-walled carbon nanotubes with bis-quaterthiophene-fluorenone conjugated oligomer: spectroelectrochemical and photovoltaic properties. *Journal of Physical Chemistry C*. 2009;**113**:17347-17354.


## Chapter Three

### (4-[[pyridin-4-yl)methylidene]amino}phenyl)ferrocene

Vincent O. Nyamori, Godfrey Keru and Bernard Omondi\*

School of Chemistry and Physics, University of KwaZulu-Natal, Westville Campus,  
Private Bag X54001, Durban 4000, South Africa

\*Correspondence e-mail: [owaga@ukzn.ac.za](mailto:owaga@ukzn.ac.za)

 Acta Crystallographica Section E <b>Structure Reports</b> <b>Online</b> ISSN 1600-5368	<b>metal-organic compounds</b>	
<b>(4-[[Pyridin-4-yl)methylidene]amino}-phenyl)ferrocene</b>	<b>Experimental</b>	
Vincent O. Nyamori, Godfrey Keru and Bernard Omondi*	<b>Crystal data</b>	
School of Chemistry and Physics, University of KwaZulu-Natal, Westville Campus, Private Bag X54001, Durban 4000, South Africa Correspondence e-mail: <a href="mailto:owaga@ukzn.ac.za">owaga@ukzn.ac.za</a>	[Fe(C <sub>4</sub> H <sub>4</sub> )(C <sub>17</sub> H <sub>13</sub> N <sub>2</sub> )] <i>M<sub>r</sub></i> = 366.23 Monoclinic, <i>P</i> 2 <sub>1</sub> <i>a</i> = 10.7200 (3) Å <i>b</i> = 7.4015 (2) Å <i>c</i> = 20.8517 (6) Å <i>β</i> = 93.044 (1)°	<i>V</i> = 1652.12 (8) Å <sup>3</sup> <i>Z</i> = 4 Mo <i>K</i> α radiation <i>μ</i> = 0.92 mm <sup>-1</sup> <i>T</i> = 173 K 0.56 × 0.45 × 0.10 mm
Received 2 November 2012; accepted 21 November 2012	<b>Data collection</b>	36615 measured reflections 7976 independent reflections 7617 reflections with <i>I</i> > 2σ( <i>I</i> ) <i>R<sub>int</sub></i> = 0.021
Key indicators: single-crystal X-ray study; <i>T</i> = 173 K; mean σ(C–C) = 0.002 Å; <i>R</i> factor = 0.022; <i>wR</i> factor = 0.061; data-to-parameter ratio = 17.7.	<b>Refinement</b>	H-atom parameters constrained Δρ <sub>max</sub> = 0.35 e Å <sup>-3</sup> Δρ <sub>min</sub> = -0.26 e Å <sup>-3</sup> Absolute structure: Flack (1983), 3568 Friedel pairs

## (4-[(Pyridin-4-yl)methylidene]amino)phenylferrocene

Vincent O. Nyamori, Godfrey Keru and Bernard Omondi\*

School of Chemistry and Physics, University of KwaZulu-Natal, Westville Campus,  
Private Bag X54001, Durban 4000, South Africa

\*Correspondence e-mail: [owaga@ukzn.ac.za](mailto:owaga@ukzn.ac.za)

**Key indicators:** single-crystal X-ray study; T = 173 K; mean  $\sigma$  (C–C) = 0.002 Å; R factor = 0.022; wR factor = 0.061; data-to-parameter ratio = 17.7.

### Abstract

The asymmetric unit of the title compound, [Fe(C<sub>5</sub>H<sub>5</sub>)(C<sub>17</sub>H<sub>13</sub>N<sub>2</sub>)], contains two independent molecules whose conformations differ, especially in the 4-[(pyridin-4-yl)methylidene]amino)phenyl unit where one is flipped by almost 180°. The cyclopentadienyl rings of the ferrocene unit also exhibit different staggered conformations: in one molecule the conformation is staggered by 9.43 (2) and in the other by 24.46 (1) from an ideal eclipsed geometry. The plane of the benzene ring is tilted away from the ferrocene group in both molecules, with dihedral angles of 6.97 (1) and 10.30 (2). The benzene ring is also slightly twisted from the plane of the pyridine ring, with dihedral angles of 5.98 (2) and 6.51 (2) in the two molecules.

### 1. Related literature.

For related compounds, see: Nyamori *et al.* (2012); Nyamori and Moodley (2011). For the synthesis, see: Rajput *et al.* (2006).

### 2. Comment

As part of investigation of the title compound (I) (Fig. 1) as a catalyst for synthesis of nitrogen doped shaped carbon nanomaterials we have determined its crystal structure. The compound crystallized with two independent molecules in the asymmetric unit (Fig. 2).

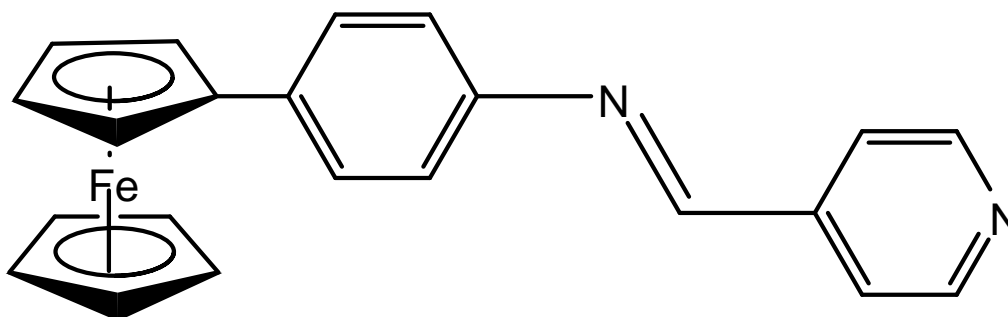


**Fig. 1:** Compound (1); ((4-[(Pyridin-4-yl)methylidene]amino)phenyl)ferrocene).

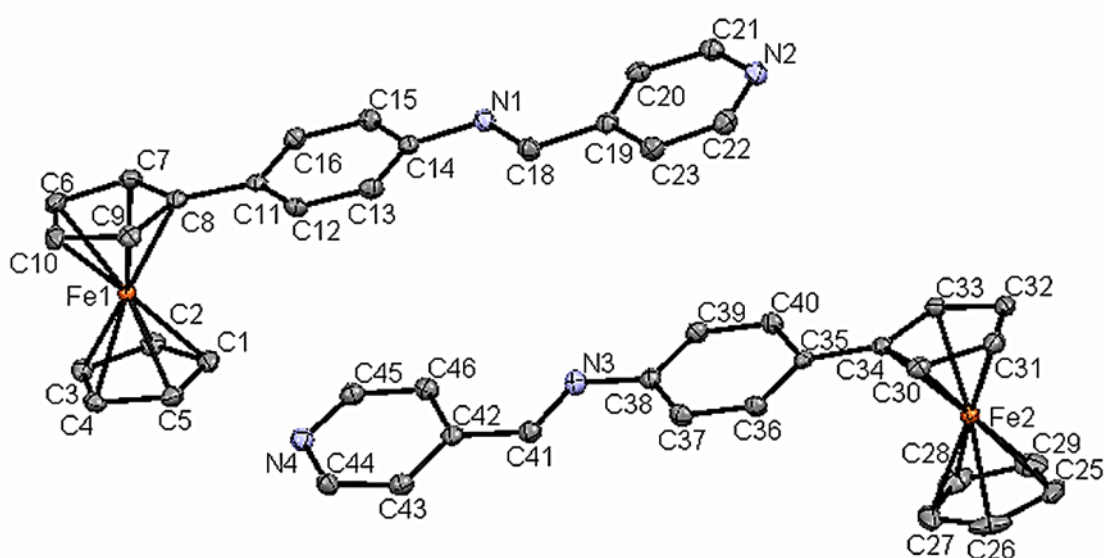


**Fig. 2:** The asymmetric unit of the title compound with displacement ellipsoids drawn at the 50% probability level.

In each molecule, the ferrocenyl moiety is linked to phenyl with imine and pyridine groups. The conformations of the two molecules are different especially in the staggering angles of each ones cyclopentadienyl ring and also in the (pyridin-4-ylmethylene) aniline moieties. The two cyclopentadienyl rings of the ferrocene moiety also exhibit different staggered geometries where in one the conformation is skewed by  $9.43(2)^\circ$  and in the other by  $24.46(1)^\circ$ . This differs from the value of  $15.9^\circ$  observed by Nyamori and Moodley, (2011) and  $2.17(2)^\circ$  by Nyamori *et al.*, (2012) in related

structures. The phenyl group is tilted away from the ferrocene group in one of the molecules by a dihedral angle of 6.97 (1) ° and by a dihedral angle of 10.30 (2) ° in the other molecule. The phenyl ring is also slightly twisted from the plane of the pyridinyl ring by a dihedral angle of 5.98 (2) ° in one and by 6.51 (2) ° in the other molecule.

### 3. Experimental

The title compound was prepared by a modification of the reported method (Rajput *et al.*, 2006). Into a Pyrex tube fitted with a ground glass joint 4-ferrocenylaniline (130 mg, 0.47 mmol) and pyridine-4-carboxyaldehyde (76 mg, 0.71 mmol) were added. The compounds were thoroughly ground. The mixture turned into a red solid which was subjected to column chromatography using a mixture of hexane: dichloromethane in the ratio 8:2. (162 mg, 94%) m.p. 199–201°C. IR (ATR cm<sup>-1</sup>) 3430, 3043, 2954, 2876, 1621, 1582, 1465, 1336, 1168, 1083, 1032, 889, 845, 741, 643, 549, 524, 491  $\delta$  1H (CDCl<sub>3</sub>) = 8.80 (2H, dd, J = 4.5 and 1.5 pyH), 8.54 (1H, s, CHN), 7.80 (2H, dd, J = 4.5 and 1.5 pyH), 7.54(2H, dd, J = 6.7 and 1.8 ArH), 4.69 (2H, t, J = 1.8 C5H4), 4.32 (2H, t, J = 1.8 C5H4), 4.06 (5H, s, C5H4).  $\delta$  13C (CDCl<sub>3</sub>) = 151.2, 148.5, 143.5, 138.9, 127.2, 122.9, 121.6, 96.5, 85.4, 77.1, 69.4, 66.4. m/z(%) 277.1 (23.9%) 367.2 (100%) Found: M<sup>+</sup>, 367.2 for C<sub>22</sub>H<sub>18</sub>FeN<sub>2</sub>, requires M, 366.2367.

### 4. Refinement

Carbon-bound H-atoms were placed in calculated positions [C—H = 1.00] for methine H atoms and 0.95 Å for aromatic.

H atoms;  $U_{\text{iso}}(\text{H}) = 1.2U_{\text{eq}}(\text{C})$  and were included in the refinement in the riding model approximation.

### 5. Computing details

Data collection: APEX2 (Bruker, 2008); cell refinement: SAINT-Plus (Bruker, 2008); data reduction: SAINT-Plus and XPREP (Bruker, 2008); program(s) used to solve structure: SHELXS97 (Sheldrick, 2008); program(s) used to refine structure: SHELXL97 (Sheldrick, 2008); molecular graphics: ORTEP-3 (Farrugia, 2012); software used to prepare material for publication: WinGX (Farrugia, 2012).



## 6. Crystal data

[Fe(C<sub>5</sub>H<sub>5</sub>)(C<sub>17</sub>H<sub>13</sub>N<sub>2</sub>)]

Mr = 366.23

Monoclinic, *P*21

Hall symbol: P 2yb

*a* = 10.7200 (3) Å

*b* = 7.4015 (2) Å

*c* = 20.8517 (6) Å

β = 93.044 (1) °

*V* = 1652.12 (8) Å<sup>3</sup>

*Z* = 4

*F*(000) = 760

D<sub>x</sub> = 1.472 Mg m<sup>-3</sup>

Mo *K*α radiation,

λ = 0.71073 Å

## 7. Cell parameters from 36615 reflections

θ = 1.9–28.3°

μ = 0.92 mm<sup>-1</sup>

*T* = 173 K

Plate, red 0.56 × 0.45 × 0.1 mm

## 8. Data collection

Bruker SMART APEXII CCD diffractometer

Graphite monochromator - φ and ω scans

Absorption correction: multi-scan

(SADABS; Bruker, 2008)

*T*<sub>min</sub> = 0.627, *T*<sub>max</sub> = 0.914

36615 measured reflections

7976 independent reflections

7617 reflections with *I* > 2σ(*I*)

*R*<sub>int</sub> = 0.021

θ<sub>max</sub> = 28.3°, θ<sub>min</sub> = 1.9°

*h* = -14→14

*k* = -9→9

*l* = -27→27

## 9. Refinement

Refinement on *F*<sup>2</sup>

Least-squares matrix: full

R[*F*<sup>2</sup> > 2σ(*F*<sup>2</sup>)] = 0.022

$$wR(F^2) = 0.061$$

$$S = 1.02$$

7976 reflections

451 parameters

1 restraint

Primary atom site location: structure-invariant direct methods.

Secondary atom site location: difference fourier map.

Hydrogen site location: inferred from neighbouring sites.

H-atom parameters constrained.

$$w = 1/[\sigma^2(F_o^2) + (0.0387P)^2 + 0.2134P]$$

$$\text{where } P = (F_o^2 + 2F_c^2)/3$$

$$(\Delta/\sigma)_{\max} = 0.004$$

$$\Delta\rho_{\max} = 0.35 \text{ e } \text{\AA}^{-3}$$

$$\Delta\rho_{\min} = -0.26 \text{ e } \text{\AA}^{-3}$$

## 10. Special details

### 10.1. Geometry

All estimated standard deviations (e.s.d.'s) (except the e.s.d. in the dihedral angle between two l.s. planes) are estimated using the full covariance matrix. The cell e.s.d.'s are taken into account individually in the estimation of e.s.d.'s in distances, angles and torsion angles; correlations between e.s.d.'s in cell parameters are only used when they are defined by crystal symmetry. An approximate (isotropic) treatment of cell e.s.d.'s is used for estimating e.s.d.'s involving l.s. planes.

### 10.2. Refinement

Refinement of  $F^2$  against all reflections. The weighted  $R$ -factor  $wR$  and goodness of fit  $S$  are based on  $F^2$ , conventional  $R$ -factors  $R$  are based on  $F$ , with  $F$  set to zero for negative  $F^2$ . The threshold expression of  $F^2 > \sigma(F^2)$  is used only for calculating  $R$ -factors(gt) *etc.* and is not relevant to the choice of reflections for refinement.  $R$ -factors based on  $F^2$  are statistically about twice as large as those based on  $F$ , and  $R$ -factors based on all data will be even larger. Fractional atomic coordinates and isotropic or equivalent isotropic displacement parameters (A2).

## **Acknowledgement**

The authors thank the University of KwaZulu-Natal and India, Brazil and South Africa (IBSA) energy initiative for financial support.

## **Supplementary data and figures**

Available from the IUCr electronic archives (Reference: HG5267)

## **References**

- Bruker (2008). APEX2, SAINT-Plus, XPREP and SADABS. Bruker AXS Inc., Madison, Wisconsin, USA.
- Farrugia, L. J. (2012). *J. Appl. Cryst.* 45, 849–854.
- Flack, H. D. (1983). *Acta Cryst.* A39, 876–881.
- Nyamori, V. O. and Moodley, N. N. (2011). *Acta Cryst.* E67, m1293.
- Nyamori, V. O., Zulu, S. M. and Omondi, B. (2012). *Acta Cryst.* E68, m353.
- Rajput, J., Hutton, A. T., Moss, J. R., Su, H. and Imrie, C. (2006). *J. Organomet. Chem.* 691, 4573–4588.
- Sheldrick, G. M. (2008). *Acta Cryst.* A64, 112–122.

## Chapter Four

# Nitrogen-doped carbon nanotubes synthesised by pyrolysis of 4-[[**(pyridin-4-yl)methylidene**]amino]phenyl)ferrocene

Godfrey Keru, Patrick G. Ndungu and Vincent O. Nyamori\*

School of Chemistry and Physics, University of KwaZulu-Natal, Westville Campus,  
Private Bag X54001, Durban, 4000, South Africa

Hindawi Publishing Corporation  
Journal of Nanomaterials  
Volume 2013, Article ID 750318, 7 pages  
<http://dx.doi.org/10.1155/2013/750318>



*Research Article*

## Nitrogen-Doped Carbon Nanotubes Synthesised by Pyrolysis of (4-[[**(Pyridine-4-yl)methylidene**]amino]phenyl)ferrocene

**Godfrey Keru, Patrick G. Ndungu, and Vincent O. Nyamori**

*School of Chemistry and Physics, University of KwaZulu-Natal, Westville Campus, Private Bag X54001, Durban 4000, South Africa*

Correspondence should be addressed to Vincent O. Nyamori; [nyamori@ukzn.ac.za](mailto:nyamori@ukzn.ac.za)

Received 3 June 2013; Accepted 13 August 2013

Academic Editor: Myoung-Woon Moon

Copyright © 2013 Godfrey Keru et al. This is an open access article distributed under the Creative Commons Attribution License, which permits unrestricted use, distribution, and reproduction in any medium, provided the original work is properly cited.

# Nitrogen-doped carbon nanotubes synthesised by pyrolysis of 4-[[pyridin-4-yl)-methylidene]amino}phenyl)ferrocene

Godfrey Keru, Patrick G. Ndungu and Vincent O. Nyamori\*

School of Chemistry and Physics, University of KwaZulu-Natal, Westville Campus, Private Bag X54001, Durban, 4000, South Africa

\*Vincent O. Nyamori, Email: nyamori@ukzn.ac.za

## Abstract

Nitrogen-doped carbon nanotubes (N-CNTs) were synthesized by pyrolysis of 4-[[pyridin-4-yl)methylidene]amino}phenyl)ferrocene in a solution of either acetonitrile or toluene as carbon source. This was achieved by testing three different growth temperatures (800, 850 and 900 °C), and the 850 °C was found to be the most favourable condition for N-CNT growth. At the lower temperature of 800 °C, amorphous carbon was mainly formed while at the higher temperature of 900 °C, the yield of carbon spheres (CSs) increased. Apart from the variation in temperature, the formation of other shaped carbon nanomaterials (SCNMs) was found to be carbon source dependent. Acetonitrile was found to produce mainly N-CNTs with 'bamboo' morphology while toluene formed a mixture of pristine CNTs and N-CNTs in the ratio of 1:1. N-CNTs and other SCNMs synthesized were characterized by means of TEM, SEM, Raman spectroscopy, TGA and elemental analysis.

**Keywords:** chemical vapour deposition; nitrogen-doped carbon nanotube; carbon sphere; acetonitrile; toluene; shaped carbon nanomaterials

## 1. Introduction

The introduction of heteroatoms into the backbone of carbon nanotubes (CNTs) changes their structural, chemical and electrical properties [1]. Doping CNTs with nitrogen creates superficial defects that alters the chemical properties of CNTs and creates a path to reactivity and applications [2]. Some of the potential applications of N-CNTs include lithium storage [3,4], biosensors [5,6], fuel cells [7,8], drug delivery [9], catalytic support [10], field emission [4,11] and electronic devices [12], among others.

Heteroatom doping was first reported by Stéphan *et al.* [13]. They doped CNTs with nitrogen and boron by means of the arc discharge method. Currently, nitrogen-doping is accomplished by either *in-situ* or *ex-situ* [14] methods whereby in the latter the walls of CNTs are functionalized with nitrogen-containing groups by use of molecules such as NH<sub>3</sub> [15] subsequent to CNT synthesis. Another useful example of *ex-situ* technique which does not involve a simple molecule but a complex has been illustrated by Schilling and Bron [16], where they functionalised multi-walled CNTs with the aid of a nitrogen-containing complex, iron tetramethoxyphenylporphyrin chloride (FeTMMP-Cl). On the other hand, nitrogen-doping using *in-situ* synthesis has been reported by means of arc discharge [17], laser ablation [18] and chemical vapour deposition (CVD) [19] techniques. In general, the CVD method is preferred since it is more economical, relatively easier to produce and scale-up the synthesis of N-CNTs. In this approach, the carbon source also provides the nitrogen source [2,20] however, the catalyst can also act as a source of nitrogen [9,21]. Additional examples include the use of nitrogen source that is completely separate from the carbon source and the catalyst [22].

N-CNTs can be identified by the characteristic “bamboo” morphology that arises due to the presence of nitrogen, which introduces defects and pentagon rings in the graphene network that results in a positive curvature of the tubular layer [1]. The distance between each bamboo compartment has been found to be directly proportional to the amount of nitrogen-doping with a smaller size compartment signifying a higher nitrogen-doping level [23]. Organometallic complexes, especially ferrocene and its derivatives, have been used as both catalysts and as carbon sources for the synthesis of CNTs and other shaped carbon nanomaterials (SCNMs) [24]. The use of ferrocene and

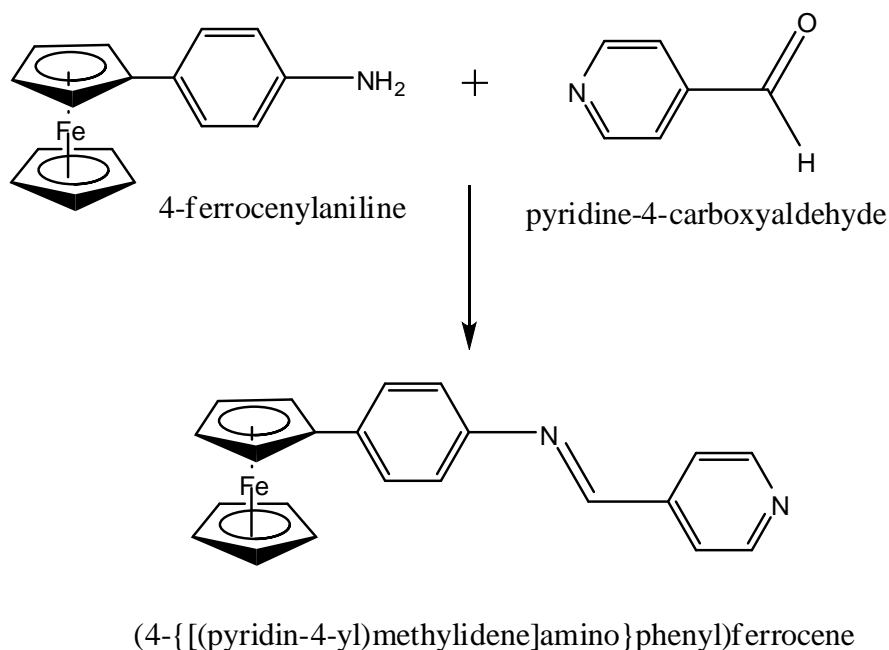
acetonitrile has also been investigated [25], however, in this paper we report on the use of an organometallic complex, (4-{{[(pyridin-4-yl)methylidene]amino}phenyl}ferrocene,  $[\text{Fe}(\text{C}_5\text{H}_5)(\text{C}_{17}\text{H}_{13}\text{N}_2)]$ , which is a novel ferrocenyl derivative as a catalyst for the synthesis of N-CNTs. It does not only act as the source of active metal iron nanoparticle but also as nitrogen and carbon source in a solution of acetonitrile or toluene. This paper also explores the variation of growth temperature and how it affects the yield, type of SCNMs formed and level of nitrogen-doping.

## 2. Experimental

All the chemicals used were of analytical grade and were used as received unless stated otherwise. The catalyst precursors were synthesized as previously reported: 4-nitrophenylferrocene [26] and 4-ferrocenylaniline by catalytic reduction of 4-nitrophenylferrocene as reported by Ataf *et al.* [27]. In brief, 2 g of 4-nitrophenylferrocene was dissolved in 100 mL of methanol and 2.62 g of zinc powder was slowly added to the mixture while stirring. Then 4 mL of formic acid was added drop-wise and thereafter the mixture heated to 70 °C. The reaction was monitored by thin layer chromatography (TLC) and the reaction product was isolated with a yield of 85%. (4-{{[(Pyridin-4-yl)methylidene]amino}phenyl}ferrocene was prepared as reported earlier by our group [28] under solvent-free conditions. Briefly, this involved mixing 4-ferrocenylaniline (130 mg, 0.47 mmol) and pyridine-4-carboxyaldehyde (76 mg, 0.71 mmol) in a Pyrex tube fitted with a ground glass joint (Scheme 1). The solid mixture was thoroughly ground leading to a melt, which solidified once it was left to stand under vacuum. The red solid was then subjected to column chromatography using a solvent mixture of hexane:dichloromethane in the ratio of 8:2. The pure product was isolated and obtained as red crystals.

An amount of 2.5 wt.% of (4-{{[(pyridin-4-yl)methylidene]amino}phenyl}ferrocene was used as a catalyst in the CVD floating catalyst method to synthesize N-CNTs. The setup of the reactor used was based on a previously reported design [29]. A quartz tube (inner diameter 27 mm and length 850 mm) used as the reactor vessel, was placed inside a muffle/tube furnace (model no. TSH12/50/610, Elite Thermal Systems Ltd) fitted with a main zone temperature controller (Eurotherm 2416). The temperature was

controlled and set to the desired maximum reaction temperature ( $T_{\max}$ ) that is 800, 850 or 900 °C. The purging and reducing gas was 10% H<sub>2</sub> in argon (v/v) set at a flow rate of 100 mL/min. When the desired temperature ( $T_{\max}$ ) was attained, a solution of 2.5 wt.% catalyst and the carbon source was injected at a rate of 0.8 mL/min with the aid of a New Era Inc. syringe pump (model no. NE 300). The carbonaceous materials obtained from the uniform hot zone were collected and weighed. The products were characterized by means of transmission electron microscopy (TEM) (JEOL, JEM 1010), scanning electron microscopy (SEM) (Carl Zeiss Ultra Plus), Raman spectroscopy (DeltaNu Advantage 532<sup>TM</sup> Raman spectrometer), thermogravimetric analysis TA Instrument Q series<sup>TM</sup> Thermal analyser DSC/TGA (Q600).and elemental analysis (CHNS).



**Scheme 1:** Solvent-free synthesis of (4-[[pyridin-4-yl)methylidene]amino]-phenyl)ferrocene.

### 3. Results and discussion

The catalyst, (4-[[pyridin-4-yl)methylidene]amino]phenyl)ferrocene was easily synthesized under solvent-free conditions to obtain an excellent yield (162 mg, 94%) and characterized as before [28]. The catalyst was further utilized in a solution of either



toluene or acetonitrile as the carbon source to synthesize shaped carbon nanomaterials (SCNMs) by means of the floating catalyst CVD method. Apart from the catalyst, acetonitrile was also used as an additional nitrogen source and the results obtained are shown in Table 1.

**Table 1:** Products obtained by pyrolysis of 4-[(pyridine-4-yl)methylidene]-amino}phenyl)-ferrocene (2.5 wt.%) in a solution of toluene or acetonitrile.

Temperature (°C)	Carbon source	Yield (mg)	Composition of the product*	Avg. I.D. (nm)	Avg. O.D. (nm)
800	Toluene	176	40% T; 60% Ac	10.19	60.19
	Acetonitrile	100	60% T; 40% Ac	31.309	50.64
850	Toluene	300	50% T; 45% CS; 5% Ac	15.62	68.31
	Acetonitrile	178	85% T; 15% Ac	54.248	60.709
900	Toluene	570	2% T; 98% CS	25.36	73.76
	Acetonitrile	240	20% T; 80% CS	65.69	76.47

\*The composition of the products is based on acceptable counting procedures using electron micrographs, at least 50 images were used in each case and over 200 SCNMs were counted per sample. T - carbon nanotubes; Ac - amorphous carbon; CS - carbon spheres; Avg. I.D. - average inner diameter; Avg. O.D. - average outer diameter.

From the results, three types of SCNMs were formed, i.e. CNTs, amorphous carbon (Ac), and carbon spheres (CS). These results are in agreement with the findings of Nxumalo *et al.* [30] who reported formation of similar products by pyrolysis of ferrocenylaniline or a mixture of ferrocene and aniline in different proportions by using toluene as the carbon source at 900 °C. However, in their case they also obtained carbon fibres. It is evident that the resultant products and their distribution is dependent not only on the catalyst and carbon source used, but also on the choice of reaction conditions such as reaction temperature ( $T_{MAX}$ ), reaction time, gas flow rate and pressure [31]. Figure 1 shows the TEM images of a representative samples of the SCNMs obtained.

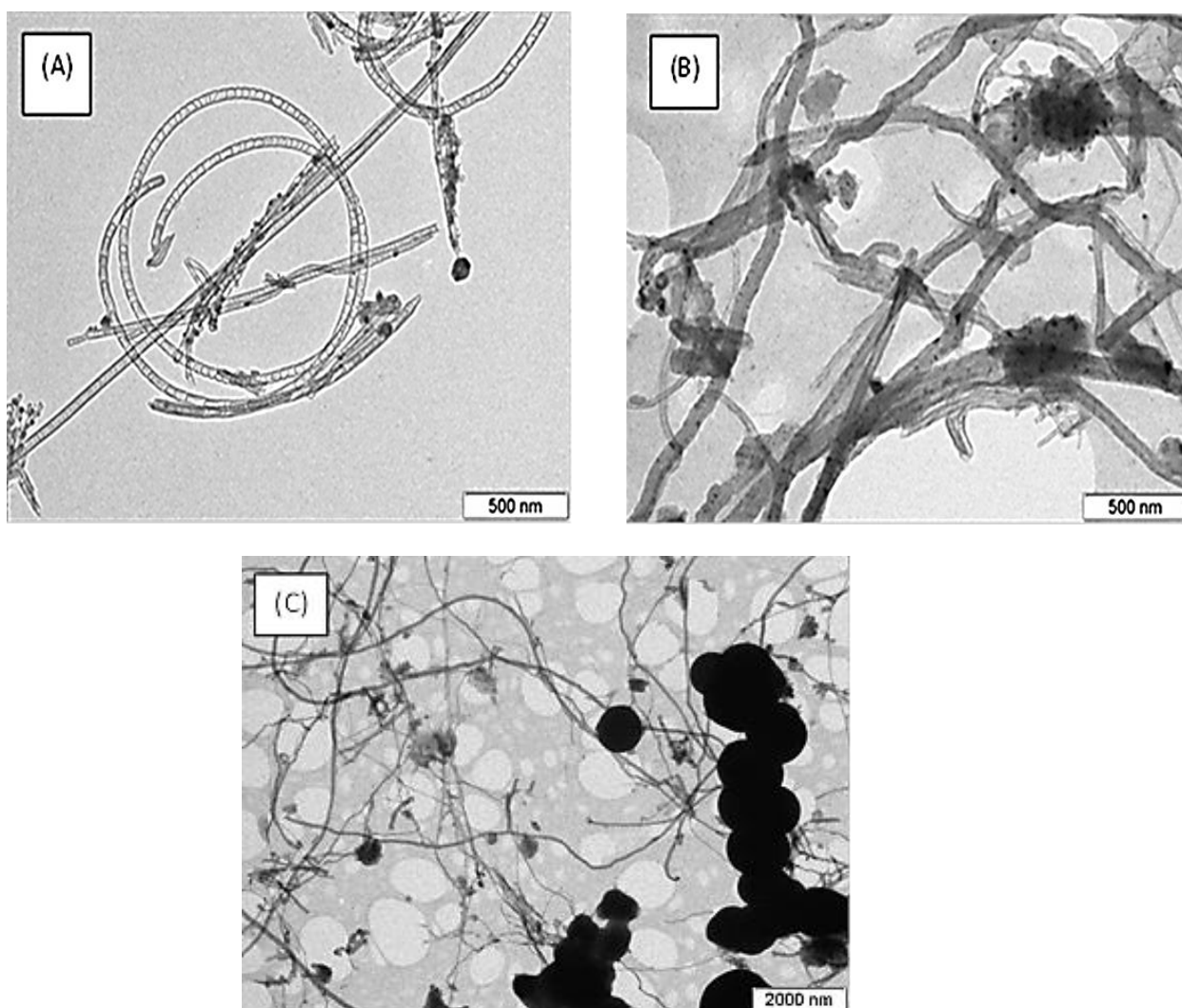


**Figure 1:** TEM images of SCNMs synthesized from a solution of (A) acetonitrile at 850 °C, (B) acetonitrile at 800 °C and (C) toluene at 850 °C.

The TEM images in Figure 1 show that the CNTs formed have “bamboo” shaped compartments which usually signifies nitrogen-doping. Bamboo compartments arise due to formation of pentagonal rings in the graphene network, which induces positive curvature in the graphene layer [1]. Inclusion of nitrogen or oxygen in the carbon graphene network is relatively easy. This is more so due to similarities in their hybridisation and bond length, i.e. C=C, C=O and C=N being 1.38 Å, 1.36 Å and 1.34 Å respectively. However, the C=N bond length is shorter than that of C=C and hence it distorts the order in the graphene matrix by introducing pentagons which cause strain in the structure [32]. These distortions created by the nitrogen atoms cause defects and are

seen to be more concentrated in the inner layer than other layers and hence the bamboo morphology is more pronounced inside the tube [33].

### 3.1 Effect of carbon source

The effect of the carbon source on the size of individual bamboo compartments, wall thickness and general morphology of CNTs was investigated. This was accomplished by comparing the type of CNTs formed when a solution of acetonitrile or toluene was used as the carbon source. Figure 2 shows some TEM images of N-CNTs grown from a solution of either acetonitrile or toluene.

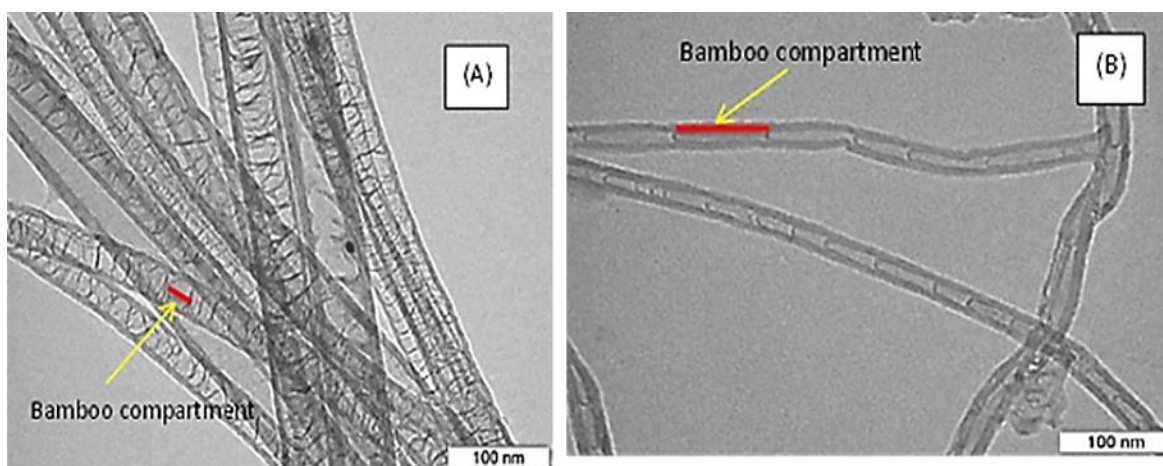


**Figure 2:** TEM images of N-CNTs synthesized at 850 °C from a solution of (A) acetonitrile and (B) toluene. The red lines and arrows on the images indicate the individual bamboo compartments.

The sizes of each bamboo compartment were different and this has a direct relationship to the amount of nitrogen from the nitrogen source. N-CNTs synthesized from a solution of acetonitrile formed shorter bamboo compartments compared with the ones formed from a solution of toluene. A possible explanation could be that more nitrogen atoms are incorporated into the structure since apart from the ferrocenyl derivative which contains nitrogen, the acetonitrile solvent also introduces additional nitrogen which would also be involved in the doping process. These findings concur with those of Nxumalo *et al.*[30], who observed a decrease in bamboo compartment size and more individual compartments in each tube, which was an indication of the increased extent

of nitrogen-doping. Chen *et al.* [8] also reported a positive correlation between higher nitrogen content in the carbon source and higher nitrogen-doping in the N-CNTs.

In addition to the bamboo compartment size, the use of acetonitrile formed N-CNTs with bigger internal diameters and smaller wall thicknesses. The increased internal diameter and reduced wall thickness could be due to the level of nitrogen-doping. Our findings concur with those of Ionescu *et al.* [34] who reported an increase in internal N-CNT diameter and decrease in wall thickness with increased nitrogen-doping.

Some of the CNTs synthesised in a solution of toluene lacked bamboo structures, indicating that effective nitrogen-doping did not readily take place in the graphene network. The number of N-CNTs (with bamboo structures) and pristine CNTs were in the ratio 1:1. This was determined by counting tubes in at least 50 images. Koós and co-workers [31] made a similar observation when they synthesized N-CNTs in a solution of toluene in 5% benzylamine. This suggests that nitrogen-doping significantly depends on both the choice of carbon source and catalyst [35]. It was noted that N-CNTs synthesized from a solution of acetonitrile were well aligned (Figure 3A). On the other hand the pristine CNTs (as determined by lack of bamboo structures) synthesised from a solution of toluene were observed to have kinks, were wavy and not aligned (Figure 3B). A possible reason could be that products derived from the latter approach were not only less ordered, but also intermingled with a mixture of pristine CNTs and N-CNTs, and hence distorting the alignment of the tubes [31].

### **3.2 Effect of growth temperature**

Varying the growth temperature was found to have an effect on the level of nitrogen-doping, yield and the graphitic nature or crystallinity of N-CNTs.

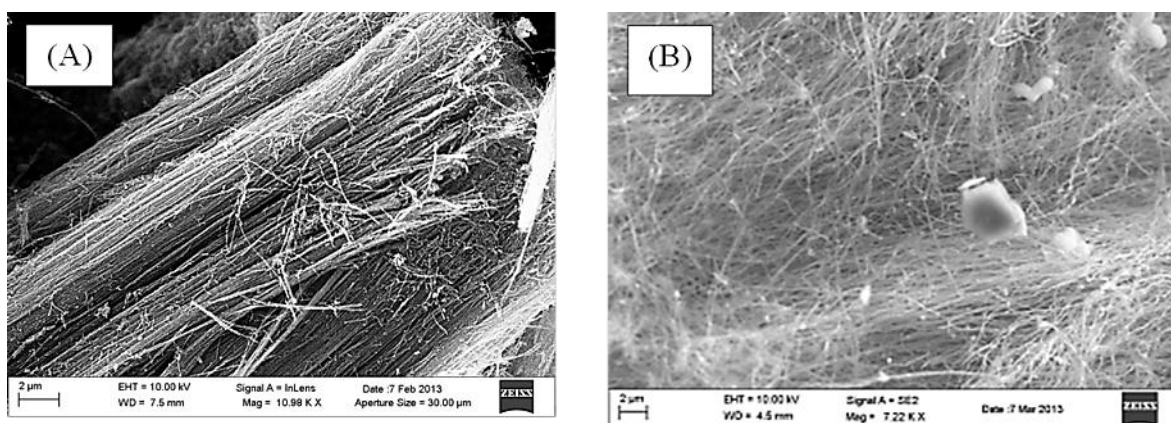


**Figure 3:** SEM images of CNTs synthesized at 850 °C from a solution of (A) acetonitrile and (B) toluene showing the former to be well aligned and the latter to be wavy.

### 3.2.1 The nitrogen-doping percentage

Elemental analysis by carbon, hydrogen, nitrogen and sulphur (CHNS) analyser was used to study the relationship between growth temperature and nitrogen-doping. Figure 4 show a CHNS spectrum for the sample grown at 850 °C and the extracted results. It was observed that the nitrogen-doping percentage increased from zero to 2.21% in N-CNTs synthesized in a solution of toluene as the growth temperature increased from 800 to 850 °C. When a solution of acetonitrile was used a similar, but more effective, doping trend was observed, that is, the nitrogen-doping percentage increased from 3.96% to 17.57% in the same temperature range. However, a different trend was observed when the growth temperature was increased to 900 °C when acetonitrile was used as a carbon source. The doping percentage decreased to 3.47%. A possible explanation of this reduction could be that as the growth temperature was raised to 900 °C, elemental nitrogen that is usually incorporated into the graphene structure did not react but escaped through the exhaust system and this was evident from the water trap showing more vigorous bubbling. Our findings concur with Tang *et al.* [35], who reported that the level of nitrogen-doping decreased by half when the temperature was increased from 800 to 900 °C. The highest nitrogen-doping was noted at 850 °C in a solution of acetonitrile indicating a direct relationship between nitrogen-doping, growth temperature and amount of nitrogen in the carbon sources. Furthermore, in terms of the

extent of nitrogen-doping, the elemental analysis at 850 °C, strongly correlates with the TEM observations (Figure 2) and results discussed above.

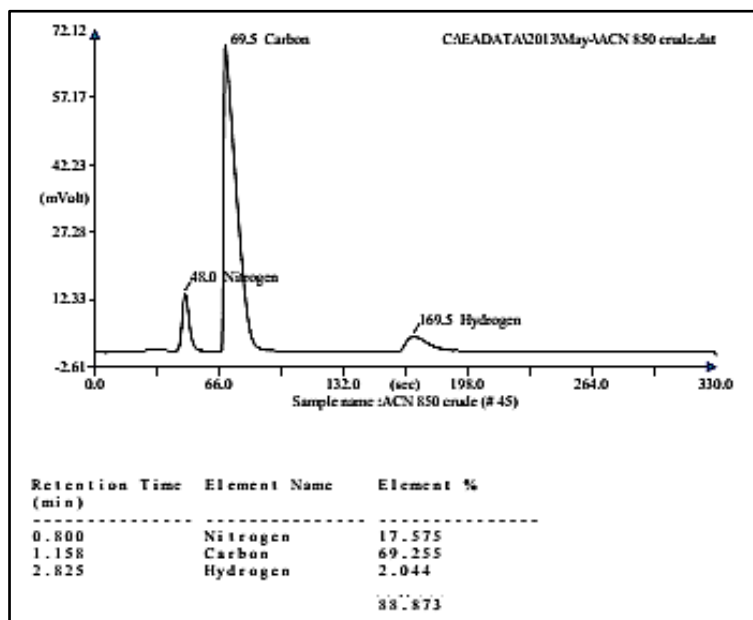


**Figure 4:** CHNS spectra of N-CNTs synthesized from a solution of acetonitrile at 850 °C and the extracted results.

### 3.2.2 N-CNT yield and general morphology

Generally the yield of N-CNTs increased with growth temperature for both acetonitrile and toluene. A solution of toluene gave a higher yield (176, 300, and 570 mg) compared with acetonitrile (100, 178, and 240 mg) at 800, 850 and 900 °C respectively (Table 1). It was also evident that the type of SCNMs formed changed with growth temperature. At 800 °C a lot of Ac formed but the amount decreased as the growth temperature increased to 900 °C. However, the percentage of CS increased with growth temperature. A possible reason could be due to agglomeration of catalyst nanoparticles into bigger particles at higher temperatures (note catalyst concentration was kept constant) and hence favouring the growth of other nanomaterials other than CNTs [36]. Seah *et al.* [37] also observed a similar trend at high temperature, however and in addition, higher catalyst/carbon ratio would also lead to catalyst particles agglomerating at a higher rate, becoming too large and thus resulting in unfavourable conditions for CNT growth.

The morphology of the N-CNTs such as the outer diameter (O.D.) was observed to change with growth temperature. The O.D. of the tubes was observed to increase with increase in growth temperature for acetonitrile (Table 1). However, when using a solution of toluene it was only possible to compare samples at temperatures of 800 and 850 °C and the trend was similar. A possible explanation for the increase in outer diameter with increase in temperature could be due to agglomeration and increase in catalysts particle sizes which favour formation of CNTs with large outer diameters. N-CNTs synthesised with a solution of acetonitrile at 850 °C had larger outer diameters (60.79 nm) compared with those grown from a solution of toluene (55.3 nm). In contrast, at 800 °C N-CNTs from toluene had bigger outer diameters than in acetonitrile (60.19 nm compared to 50.64 nm respectively). As for the internal diameter (I.D.), N-CNTs synthesized from acetonitrile were larger compared with ones grown from toluene. The opposite was observed for the wall thickness of N-CNTs synthesized from toluene that showed thicker walls compared with those grown from acetonitrile as the carbon source.

### 3.2.3 Graphitic nature/crystallinity

Raman spectroscopy was used to study the effect of growth temperature on the graphitic nature of N-CNTs. Two major peaks were observed: the G-band (between 1560 and 1599  $\text{cm}^{-1}$ ) which originates from the Raman  $E_{2g}$  mode and the D-band (between 1347 and 1363  $\text{cm}^{-1}$ ) which is the disorder-induced band. The intensities of the G-band and D-band were observed to differ and evidence can be seen from the  $I_D/I_G$  ratio (Figure 5).

This ratio is an indicator of the graphitic nature of the N-CNTs or degree of disorder, and was observed to increase from 800 to 850 °C for tubes synthesised with acetonitrile. Nitrogen-doping in N-CNTs increased as the growth temperature rose from 800 to 850 °C which implies a higher level of disorder, and this agrees with the results from elemental analysis and the TEM observations. In contrast, the  $I_D/I_G$  ratio of tubes synthesized from toluene decreased between 800 and 850 °C, which is an indication of the formation of more graphitic tubes.

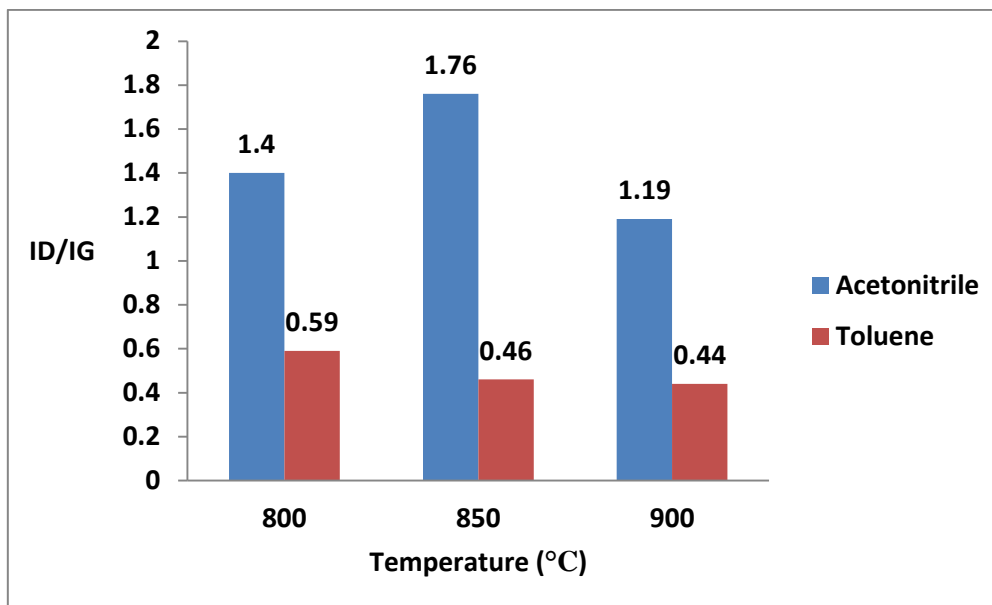


**Figure 5:** Raman chart comparing  $I_D/I_G$  ratio at the different growth temperatures.

However, Table 1 shows a reduction of Ac product as the growth temperature increases and this could also be a possible reason for the increase in the graphitic nature of the product at higher temperature. Generally, the N-CNTs synthesised in a solution of acetonitrile were found to be more disorderly at all growth temperatures and this is possibly due to the level of nitrogen-doping.

Thermogravimetric analysis was used to investigate the thermal stability of SCNMs synthesized at different growth temperatures in a solution of acetonitrile or toluene. Figure 6 shows the thermograms. SCNMs synthesized from a solution of toluene were thermally more stable compared with those grown from acetonitrile as confirmed by observing the initial decomposition temperature. A possible explanation is that toluene provided more pristine CNTs, which are more structured with fewer defects, while acetonitrile mainly formed N-CNTs, which is in-line with our elemental analysis results, TEM observations, and Raman analysis. N-CNTs synthesized at a temperature of 850 °C which had the highest level of nitrogen-doping, showed the least thermal stability. The decomposition temperature increased from 481 °C to 600 °C for N-CNTs synthesized from acetonitrile at growth temperatures of 850 and 900 °C respectively.



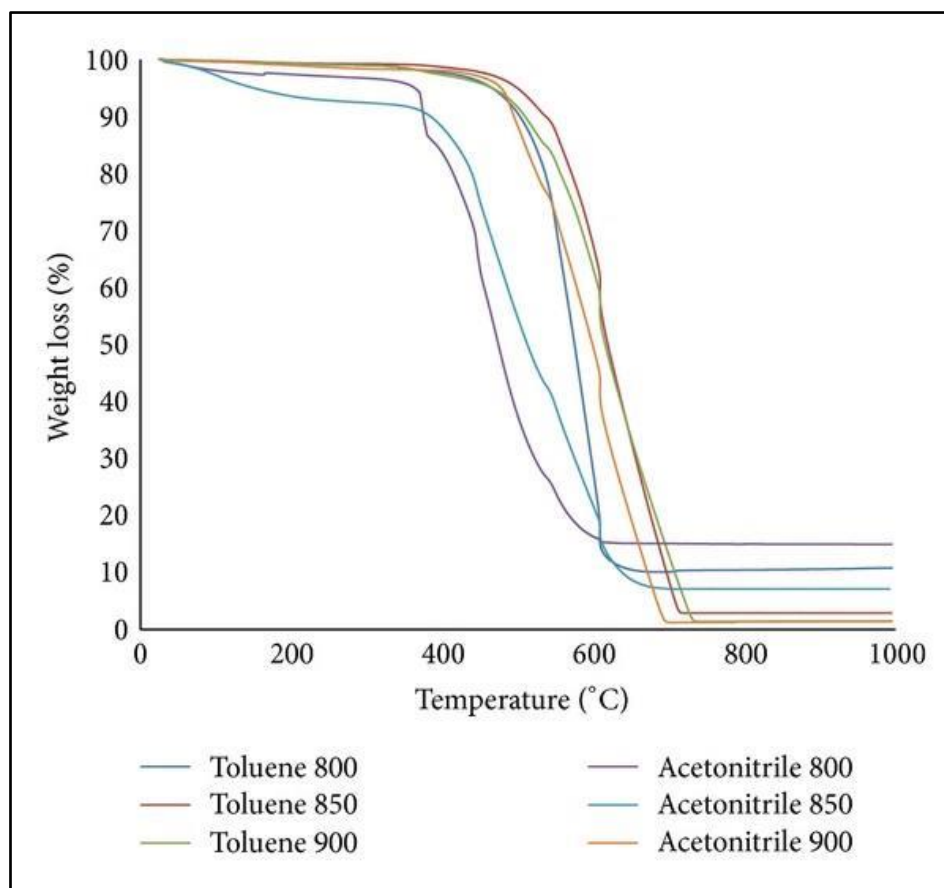


**Figure 6:** Thermogravimetric analysis of SCNMs at different growth temperatures (°C) in a solution of either toluene or acetonitrile.

This shows that the thermal stability increased as the growth temperature increased from 850 to 900 °C which supports the decrease in the level of nitrogen-doping.

#### 4. Conclusion

N-CNTs were synthesized by pyrolysis of (4-[(pyridine-4-yl)methylidene]amino-phenyl)ferrocene in a solution of either toluene or acetonitrile. Acetonitrile formed N-CNTs with mainly bamboo morphology indicative of nitrogen-doping. The N-CNTs were found to be generally less thermally stable and less graphitic. Also the thermal stability decreases as the level of nitrogen-doping increases. A solution of toluene formed a mixture of nitrogen-doped and pristine CNTs. In general, the growth temperature was found to affect the yield, type of SCNMs formed and level of nitrogen-

doping. Hence, this study has shown that the SCNMs synthesised depend on the conditions of synthesis and the precursors used.

### **Acknowledgement**

The authors wish to thank the University of KwaZulu-Natal, National Research Foundation (NRF) and the India, Brazil and South Africa (IBSA) energy project for financial assistance.

### **References**

- [1] X. Li, G. Zhu, and Z. Xu, "Nitrogen-doped carbon nanotube arrays grown on graphene substrate," *Thin Solid Films*, vol. 520, pp. 1959-1964, 2012.
- [2] P. Ayala, R. Arenal, M. Rummeli, A. Rubio, and T. Pichler, "The doping of carbon nanotubes with nitrogen and their potential applications," *Carbon*, vol.48, pp. 575-586, 2010.
- [3] W.H. Shin, H.M. Jeong, B.G. Kim, J.K. Kang, and J.W. Choi, "Nitrogen-doped multiwall carbon nanotubes for lithium storage with extremely high capacity," *Nano Letters*, vol. 12, pp. 2283-2288, 2012.
- [4] G. Zhang, W.H. Duan, and B.L. Gu, "Effect of substitutional atoms in the tip on field-emission properties of capped carbon nanotubes," *Applied Physics Letters*, vol. 80, pp. 2589-2591, 2002.
- [5] S. Boncel, K.H. Mueller, J.N. Skepper, K.Z. Walczak, and K.K.K. Koziol, "Tunable chemistry and morphology of multiwall carbon nanotubes as a route to non-toxic, theranostic systems," *Biomaterials*, vol. 32, pp. 7677-7686, 2011.
- [6] X. Feng, R. Li, Y. Ma, R. Chen, Q. Mei, Q. Fa, and W. Huang, "Nitrogen-doped carbon nanotube/polyaniline composite: Synthesis, characterization, and its application to the detection of dopamine," *Science China-Chemistry*, vol. 54, pp. 1615-1621, 2011.
- [7] Y. Shao, J. Sui, G. Yin, and Y. Gao, "Nitrogen-doped carbon nanostructures and their composites as catalytic materials for proton exchange membrane fuel cell," *Applied Catalysis B: Environmental*, vol. 79, pp. 89-99, 2008.

- [8] Z. Chen, D. Higgins, and Z. Chen, "Nitrogen-doped carbon nanotubes and their impact on the oxygen reduction reaction in fuel cells," *Carbon*, vol. 48, pp. 3057-3065, 2010.
- [9] Y. Zhao, Y. Tang, Y. Chen, and A. Star, "Corking carbon nanotube cups with gold nanoparticles," *American Chemical Society Nano*, vol. 6, pp. 6912-6921, 2012.
- [10] Y. Chen, J. Wang, H. Liu, M. N. Banis, R. Li, X. Sun, T. shem, S. Ye, and S. Knightsl, "Nitrogen-doping effects on carbon nanotubes and the origin of the enhanced electrocatalytic activity of supported Pt for proton-exchange membrane fuel cells," *Journal of Physical Chemistry C*, vol. 115, pp. 3769-3776, 2011.
- [11] L.G. Bulusheva, O.V. Sedelnikova, and A.V. Okotrub, "Substitutional sites of nitrogen atoms in carbon nanotubes and their influence on field-emission characteristics," *International Journal of Quantum Chemistry*, vol. 111, pp. 2696-2704, 2011.
- [12] A. Oikonomou, T. Susi, E.I. Kauppinen, and A. Vijayaraghavan," Growth, dispersion, and electronic devices of nitrogen-doped single-wall carbon nanotubes," *Physica Status Solid in B-Basic Solid State Physics*, vol. 249, pp. 2416-2419, 2012.
- [13] O. Stéphan, P.M. Ajayan, C. Colliex, P. Redlich, J.M. Lambert, P. Bernier, and P. lefin, "Doping graphitic and carbon nanotube structures with boron and nitrogen," *Science*, vol. 266, pp. 1683-1685, 1994.
- [14] J.D. Wiggins-Camacho, "Effect of nitrogen-doping on the electronic and catalytic properties of carbon nanotube electrode materials," <http://hdl.handle.net/2152-ETD-UT-2011-05-2669>, accessed 20<sup>th</sup> January 2013.
- [15] L. Jiang, and L.Gao, "Modified carbon nanotubes: an effective way to selective attachment of gold nanoparticles," *Carbon*, vol. 41, pp. 2923-2929, 2003.
- [16] T. Schilling, and M. Bron, "Oxygen reduction at Fe–N-modified multi-walled carbon nanotubes in acidic electrolyte," *Electrochimica Acta*, vol. 53, pp. 5379-5385, 2008.

- [17] M. Glerup, J. Steinmetz, D. Samaille, O. Stéphan, S. Enouz, A. Loiseau, S. Roth, and P. Bernier, "Synthesis of N-doped SWNT using the arc-discharge procedure," *Chemical Physics Letters*, vol. 387, pp. 193-197, 2004.
- [18] D. Golberg, Y. Bando, L. Bourgeois, K. Kurashima, and T. Sato, "Large-scale synthesis and HRTEM analysis of single-walled B- and N-doped carbon nanotube bundles," *Carbon*, vol. 38, pp. 2017-2027, 2000.
- [19] E.N. Nxumalo, P.J. Letsoalo, L.M. Cele, and N.J. Coville, "The influence of nitrogen sources on nitrogen doped multiwalled carbon nanotubes," *Journal of Organometallic Chemistry*, vol. 695, pp. 2596-2602, 2010.
- [20] L. Chen, K. Xia, L. Huang, L. Li, L. Pei, and S. Fei, "Facile synthesis and hydrogen storage application of nitrogen-doped carbon nanotubes with bamboo-like structure," *International Journal of Hydrogen Energy*, vol. 38, pp. 3297-3303, 2013.
- [21] E.N. Nxumalo, V.P. Chabalala, V.O. Nyamori, M.J. Witcomb, and N.J. Coville, "Influence of methylimidazole isomers on ferrocene-catalysed nitrogen-doped carbon nanotube synthesis," *Journal of Organometallic Chemistry*, vol. 695, pp. 1451-1457, 2010.
- [22] G-P. Dai, J-M. Zhang, and S. Deng, "Synthesis and characterization of nitrogen-doped monolayer and multilayer graphene on TEM copper grids," *Chemical Physics Letters*, vol. 516, pp. 212-215, 2011.
- [23] S.D. Mhlanga, E.N. Nxumalo, N. Coville, and V.V. Srinivasu, "Nitrogen-doping of CVD multiwalled carbon nanotubes: Observation of a large g-factor shift," *Materials Chemistry and Physics*, vol. 130, pp. 1182-1186, 2011.
- [24] V.O. Nyamori, S.D. Mhlanga, and N.J. Coville, "The use of organometallic transition metal complexes in the synthesis of shaped carbon nanomaterials," *Journal of Organometallic Chemistry*, vol. 693, pp. 2205-2222, 2008.
- [25] R.M. Yadav, P.S. Dobal, T. Shripathi, R.S. Katiyar and O.N. Srivastava, "Effect of growth temperature on bamboo-shaped carbon–nitrogen (N-C) nanotubes synthesized using ferrocene acetonitrile precursor," *Nanoscale Research Letters*, vol. 4, pp 197-203, 2009.

- [26] P. Hu, K-Q. Zhao, and H-B. Xu, "4-Nitrophenylferrocene," *Molecules*, vol. 6, pp. 249, 2001.
- [27] A.A. Altaf, N. Khan, A. Badshah, B. Lal, Shafiqullah, S. Anwar, and M. Subhan, "Improved synthesis of ferrocenylaniline," *Journal of the Chemical Society of Pakistan*, vol. 33, pp. 691-693, 2011.
- [28] V.O. Nyamori, G. Keru, and B. Omondi. "(4-[(Pyridin-4-yl)methylidene]amino)-phenyl)ferrocene," *Acta crystallographica Section E*, Structure reports online, vol. 68, m1535, 2012.
- [29] V.O. Nyamori, E.N. Nxumalo, and N.J. Coville, "The effect of arylferrocene ring substituents on the synthesis of multiwalled carbon nanotubes," *Journal of Organometallic Chemistry*, vol. 694, pp. 2222-2227, 2009.
- [30] E.N. Nxumalo, V.O. Nyamori, and N.J. Coville, "CVD synthesis of nitrogen-doped carbon nanotubes using ferrocene/aniline mixtures," *Journal of Organometallic Chemistry*, vol. 693, pp. 2942-2948, 2008.
- [31] A.A. Koós, F. Dillon, E.A. Obraztsova, A. Crossley, and N. Grobert, "Comparison of structural changes in nitrogen- and boron-doped multiwalled carbon nanotubes," *Carbon*, vol. 48, pp. 3033-3041, 2010.
- [32] S.V. Dommele, "Nitrogen-doped carbon nanotubes synthesis, characterization and catalysis," DOI:dissertations/2008-0702-200251/UUindex.html, accessed 04-02-2013.
- [33] S.Y. Kim, J. Lee, C.W. Na, J. Park, K. Seo, and B. Kim, "N-doped double-walled carbon nanotubes synthesized by chemical vapor deposition," *Chemical Physics Letters*, vol. 413, pp. 300-305, 2005.
- [34] M.I. Ionescu, Y. Zhang, R. Li, H. Abou-Rachid, and X. Sun, "Nitrogen-doping effects on the growth, structure and electrical performance of carbon nanotubes obtained by spray pyrolysis method," *Applied Surface Science*, vol. 258, pp. 4563-4568, 2012.
- [35] C. Tang, Y. Bando, D. Golberg, and F. Xu, "Structure and nitrogen incorporation of carbon nanotubes synthesized by catalytic pyrolysis of dimethylformamide," *Carbon*, vol. 42, pp. 2625-2633, 2004.

- [36] M. Kumar, and Y. Ando," Chemical Vapor Deposition of Carbon Nanotubes: A review on growth mechanism and mass production," *Journal of Nanoscience and Nanotechnology*, vol. 10, pp. 3739-3758, 2010.
- [37] C.M. Seah, S.P. Chai, and A.R. Mohamed, "Synthesis of aligned carbon nanotubes,"*Carbon*, vol. 49, pp. 4613-4635, 2011.

## Chapter Five


# Effect of boron concentration on physicochemical properties of boron-doped carbon nanotubes

Godfrey Keru, Patrick G. Ndungu, and Vincent O. Nyamori\*

School of Chemistry and Physics, University of KwaZulu-Natal, Westville Campus,  
Private Bag X54001, Durban 4000, South Africa

Materials Chemistry and Physics 153 (2015) 323–332

---




**ELSEVIER**


Contents lists available at [ScienceDirect](#)

**Materials Chemistry and Physics**

journal homepage: [www.elsevier.com/locate/matchemphys](http://www.elsevier.com/locate/matchemphys)



---

**Effect of boron concentration on physicochemical properties of boron-doped carbon nanotubes** 

Godfrey Keru, Patrick G. Ndungu, Vincent O. Nyamori\*

*School of Chemistry and Physics, University of KwaZulu-Natal, Westville Campus, Private Bag X5-4001, Durban, 4000, South Africa*

---

**H I G H L I G H T S**

- Boron-doping of carbon nanotubes (CNTs) changes their physicochemical properties.
- Amount of boron-doping was dependent on the wt.% of boron precursor used.
- Boron-doping changed CNTs surfaces and the distribution of dispersive energy sites.
- Boron-doping affected the conductivity and ferromagnetic properties.
- Increased boron-doping results in a more favourable interaction with polar probes.

# Effect of boron concentration on physicochemical properties of boron-doped carbon nanotubes

Godfrey Keru, Patrick G. Ndungu, and Vincent O. Nyamori\*

School of Chemistry and Physics, University of KwaZulu-Natal, Westville Campus, Private Bag X54001, Durban 4000, South Africa

\*Correspondence: Vincent O. Nyamori; Tel: +27 031 260 8256. Email-[nyamori@ukzn.ac.za](mailto:nyamori@ukzn.ac.za)

## Abstract

Boron-doped carbon nanotubes (B-CNTs) were synthesized using chemical vapour deposition (CVD) floating catalyst method. Toluene was used as the carbon source, triphenylborane as boron as well as the carbon source while ferrocene was used as the catalyst. The amount of triphenylborane used was varied in a solution of toluene and ferrocene. Ferrocene was kept constant at 2.5 wt.% while, a maximum temperature of 900 °C was used for the synthesis of the shaped carbon nanomaterials (SCNMs). SCNMs obtained were characterized by the use of transmission electron microscope (TEM), scanning electron microscope (SEM), high resolution-electron microscopy, electron dispersive X-ray spectroscopy (EDX), Raman spectroscopy, inductively coupled plasma-optical emission spectroscopy (ICP-OES), vibrating sample magnetometer (VSM), nitrogen adsorption at 77 K, and inverse gas chromatography. TEM and SEM analysis confirmed SCNMs obtained were a mixture of B-CNTs and carbon nanofibres (B-CNF). EDX and ICP-OES results showed that boron was successively incorporated into the carbon hexagonal network of CNTs and its concentration was dependent on the amount of triphenylborane used. From the VSM results, the boron doping within the CNTs introduced ferromagnetic properties, and as the percentage of boron increased the magnetic coectivity and squareness changed. In addition, boron doping changed the conductivity and the surface energy among other physicochemical properties of B-CNTs.

**Keywords:** boron-doped carbon nanotubes; carbon nanofibres; physiochemical properties; chemical vapour deposition; ferrocene



## 1. Introduction

Doping carbon nanotubes is a process of introducing foreign atoms into the carbon backbone structure to deliberately fine tune their physicochemical properties. Doping of carbon nanotubes (CNTs) with heteroatoms such as boron or nitrogen alters their chemical [1], electrical [2], mechanical [3] and physical properties [4]. In addition, it also increases the number of defects on the walls of the CNTs; breaking inertness and enhancing reactivity [5]. Mousavi and Moradian [6] reported increased electrical conductivity of CNTs with increased nitrogen- or boron-dopant concentration. The increase in boron-doping has been found to enhance crystallinity [7] and improve field emission properties when compared to pristine and nitrogen-doped CNTs [8]. Enhanced properties after doping CNTs with boron has resulted in the application of these materials in; hydrogen storage [9], oxygen reduction reactions [10], transparent conducting film [2], secondary batteries [11] and field emitters [12] among others.

Boron-doping of CNTs can be achieved through either; post- or direct-synthesis. In post-synthesis doping, already synthesized CNTs are mixed with the boron-dopant, normally at high temperature, inducing substitution of carbon with the boron [13]. However, this has a disadvantage of introducing undesirable by-products such as nano-rods that form during this high temperature process [14]. On the other hand, direct-synthesis boron-doping can be achieved by heating a mixture of boron-dopant, carbon source and the catalyst. Examples of boron sources in direct-synthesis doping include boron trioxide [15], boron fluoride [16], organoboranes [7,17-19] or diborane [20]. This process can be achieved by the arc discharge [21,22], laser ablation [13,23] and chemical vapour deposition (CVD) [16,24] methods. Organoboranes are more popular with the CVD method because they do not only supply boron but can also be an additional source of carbon. CVD is the most preferred synthesis method because it is economical, possible to scale up and easier to fine tune doping levels by simply controlling various physical parameters such as temperature and pressure while also the chemical aspect such as concentration of the dopant in the precursors mixture [7].

It is also possible, with the CVD method, to synthesize preferred dimensions and the level or concentration of boron within the boron-doped CNTs (B-CNTs). For example

Lyu *et al.* [7] synthesized double-walled CNTs with boron concentration ranging between 0.8 to 3.1 atomic % (at.%) by catalytic decomposition of tetrahydrofuran, triisopropylborane over Fe-Mo/MgO catalyst. Alternatively, B-CNTs were synthesized by CVD using benzene, triphenylborane and ferrocene as catalyst with boron content ranging between 0-2.24% [10].

In this paper we report for the first time effect of boron concentration in the B-CNTs on the surface energy properties of these materials. To the best of our knowledge the influence of boron-doping on the surface energy of B-CNTs has not been reported. Inverse gas chromatography (IGC) is a very versatile and reliable technique for determination of surface characteristics of a material since they can be compared and quantified. From these results energetic properties of sample surfaces and functional groups attached can be determined. CNTs can be used as fillers with other compounds such as polymers, or as components in other types of nanocomposites. Surface energy properties can be linked to various physical-chemical properties that can provide some insights into which compounds (gases, liquids, or solids) can interact with CNTs to ensure their unique properties can be well utilised.

## **2. Experimental**

### **2.1. Materials and synthesis of B-CNTs**

All the chemicals used in this study were of analytical grade and were used as received unless stated otherwise. Both triphenylborane (98%) and ferrocene (98%) were purchased from Sigma Aldrich Co. (St Louis, USA) and toluene (97%) from BDH chemicals (Poole England). For all samples ferrocene catalyst weight percent (wt.%) was constant i.e. at 2.5 wt.% while, triphenylborane concentration was varied 1.0, 2.5 and 5.0 wt.%. Toluene as a carbon source was added to make 100 wt.%. The total mass of the mixture was 10 grams and was placed in a 20 mL plastic syringe. Reactor set-up used was based on a previously reported design [25]. In brief, a quartz tube (inner diameter 27 mm and length 850 mm) was used as the reactor vessel. This was placed inside a tube furnace (model no. TSH12/50/610, Elite Thermal Systems Ltd.) fitted with a main zone furnace controller (Eurotherm 2416). The furnace was heated to a maximum temperature ( $T_{MAX}$ ) of 900 °C, and a mixture of toluene, triphenylborane

and ferrocene was injected at a flow rate of  $0.8 \text{ mL min}^{-1}$  using a syringe pump (New Era Inc. syringe pump, model no. NE 300). The carrier gas used was a mixture of 10% hydrogen in argon (v/v) and was set at a flow rate of 100 mL/min. The product was obtained from the part of quartz tube reactor that was in the hot zone of tube furnace, weighed, before being characterised. Iron catalyst nanoparticles and amorphous carbons were purified from as-synthesized products by refluxing with 6M  $\text{HNO}_3$ . 200 mg of as-synthesized products was mixed with 50 mL 6M  $\text{HNO}_3$  in a round bottomed flask. The mixture was stirred at  $80 \text{ }^\circ\text{C}$  for 12 hours; vacuum filtered, washed with distilled water several times until the pH of the filtrate was seven then dried in a vacuum at  $100 \text{ }^\circ\text{C}$  for 12 hours.

## 2.2. Characterizations

The carbon products obtained were characterised using several instruments. Initial analysis on the surface morphology was conducted using a field emission scanning microscopy (Carl Zeiss Ultra Plus). Samples were pressed onto double sided carbon tape mounted on aluminium stubs, placed within the microscope and then analysed using an accelerating voltage of 10 kV. Images were captured using the Zeiss ultra plus FEGSEM software. Further structural and morphological characterizations were done using a JEOL transmission electron microscopy (JEOL, JEM 1010) and a high-resolution transmission electron microscopy (HR-TEM) (JEOL, JEM 2100) using accelerating voltages of 100 and 200 kV respectively. Before TEM or HR-TEM analysis, samples were dispersed in ethanol using a bath sonicator and then were drop dried on carbon coated copper grids. On the TEM, images were captured using Megaview 3 camera and then analysed using iTEM software. On the HR-TEM, Gatan digital micrograph software was used for imaging while electron dispersive X-ray spectroscopy (EDX) which was coupled to the instrument (INCA 4.15 by Oxford instrument) was used for qualitative elemental analysis.

Raman spectroscopy on the carbon products was done using a DeltaNu Advantage 532<sup>TM</sup> Raman spectrometer. The excitation source was a Nd: YAG solid state crystal class 3b diode laser at 532 nm excitation wavelength. Nuspec<sup>TM</sup> software was used to capture generated spectra. Thermogravimetric analysis (TGA) was done using TA

Instrument Q series <sup>TM</sup> Thermal analyser DSC/TGA (Q600). The carbon products obtained were heated at a rate of 10 °C min<sup>-1</sup> using an air flow rate of 50 mL min<sup>-1</sup>, and the data was captured and analysed using the TA instrument universal analysis 2000 software.

The boron content and its percentage or concentration in the carbon products were determined using inductively coupled plasma-optical emission spectroscopy (ICP-OES) on a Perkin Elmer Optima 5300 DV. 10 mg of B-CNTs samples were digested in piranha solution (a mixture of conc sulphuric acid and 30% v/v hydrogen peroxide in the ratio 3:1). The WinLab 32 software was used to analyse the data.

Magnetic properties were determined using a vibrating sample magnetometer (VSM) and the data was analysed by the VSM system software. Conductivity was calculated from resistivity obtained by four probe resistivity measurements (Scientific equipment and service, India). Samples were prepared by dispersing 30 mg of carbon products in 10 mL of ethanol using bath sonication for 30 minutes. The dispersion was vacuum filtered with a hitch funnel to form a thin film of about 0.15 mm ( $\pm$  0.01) on the filter paper. The film thickness was determined using micrometre screw gauge. In brief, the samples were fixed on the four probes then inserted in proportional-integral-derivative (PID) controlled oven. The controller minimizes the temperature error by adjusting upward or downward in case of over shoot. Temperature was varied between room temperature and 110 °C at 3° interval each time recording change in voltage while current was kept constant.

Textural characteristics were determined using Micrometrics TriStar II surface area and porosity while the data was captured and analysed using TriStar II 3020 Version 2 Software. Samples were weighed (200 mg) and vacuum degassed for 12 hours before determining surface area and pore size/volume. IGC surface energy analyzer (SEA) was used to determine surface energy properties of the samples. About 30 mg of the sample was packed in IGC salinized glass column 300 mm length and 4 mm internal diameter. The column was filled with salinized glass wool on both ends of the sample

until it was well packed Cirrus control software was used for analysis control and Cirrus Plus software was used for data analysis.

### **3. Results and discussion**

#### **3.1. Effect of boron on morphology and composition of products**

Fig. 1 shows the TEM images of the products synthesized at 900 °C. Two types of shaped carbon nanomaterials (SCNMs) were observed and these were mainly carbon nanotubes (B-CNTs) and carbon nanofibres (B-CNFs) (Fig. 1A). From Fig. 1B, image was of MWCNTs and had cone-shaped structures on the internal surfaces and this were a qualitative indicator that boron-doping was achieved. This is also reported in literature where the B-CNTs have cones and the centre of the tube was not as hollow as in pristine MWCNTs [26,27]. The product was also observed to be wavy and kinky, formed “elbow” joints and had thick walls. This distinguishes them from nitrogen-doped CNTs (N-CNTs) which have “bamboo” structures and thin walls [28]. Hashim *et al.* [29] reported that boron-doping of CNTs favours formation of “elbow” joints (responsible for waviness and kinkiness) and other multi-junction like Y-junctions. Formation of B-CNFs was found to increase as the wt.% of triphenylborane (boron source) was increased (Table 1). This could be due to the fact that, at higher boron concentration and the 900 °C temperature used in this study, catalyst agglomeration is enhanced hence favouring the formation of other SCNMs rather than CNTs [30]. Under similar temperature conditions (900 °C), we have previously reported the synthesis of nitrogen-doped CNTs (N-CNTs) by use of toluene as the carbon source and a ferrocene derivative, (4-[(pyridin-4-yl)methylidene]amino}phenyl)ferrocene as a catalyst and nitrogen source. In this case a mixture of N-CNTs and carbon spheres were formed [28]. From the weight of the products we also noted that yield increased by using high wt.% of boron precursor (Table 1).

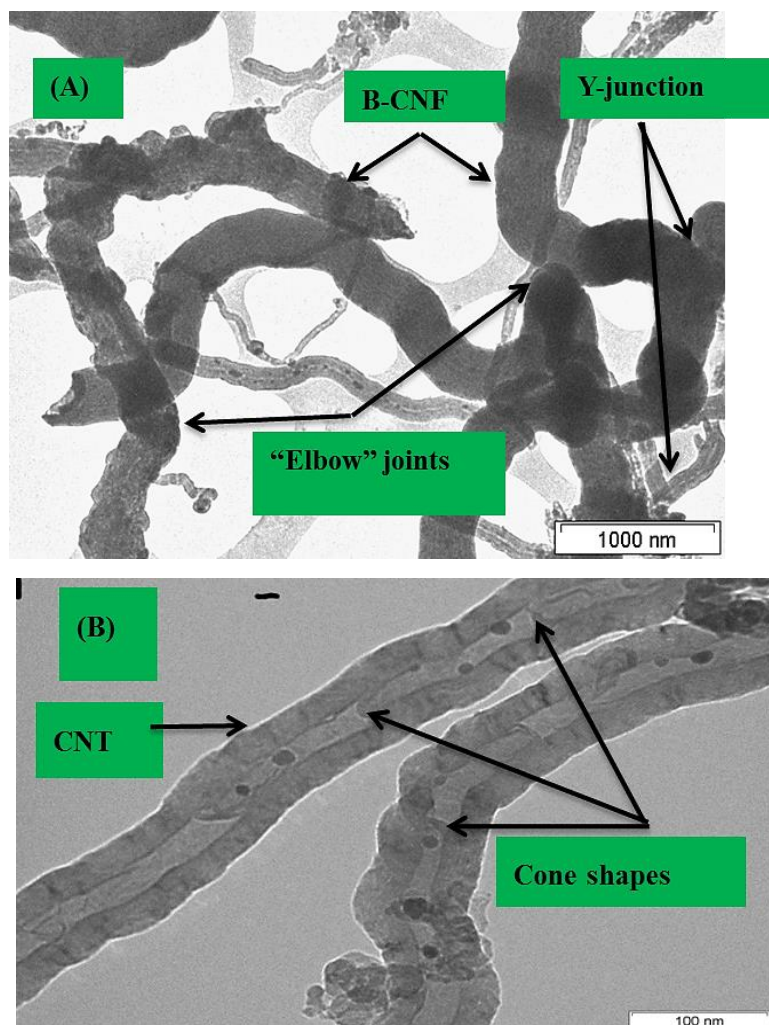


**Fig. 1:** TEM images of (A) products obtained B-CNTs with very small diameter and B-CNF with have large diameter. (B) High magnification of B-CNTs showing cone-shaped compartment, thick walls and kinks.

FESEM image, Fig. 2 shows the surface morphology of SCNMs synthesized and the wavy and kinky morphology within the samples in the image. Samples were composed of B-CNTs and B-CNF.

Formation of B-CNTs and B-CNFs observed in this study (Figs. 1 and 2) concur with results of Jiang *et al.* [31] who post-doped CNTs with boron by heating a mixture of CNTs and boron powder at high temperatures and reported that, apart from formation of B-CNTs with cone shaped compartments, some nanotubes changed to solid nanofibres.

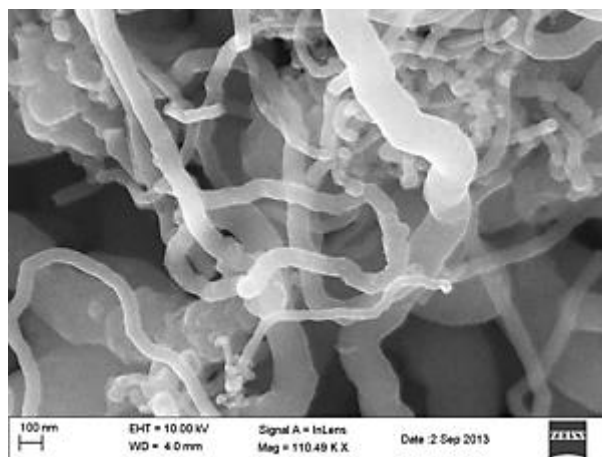


**Fig. 2:** FESEM image of the synthesized CNTs and B-CNFs with wavy and kinky structure.

The composition and distribution of the products was determined by counting not less than 50 TEM images and over 200 carbon nanotubes and fibres, then reported as an average [32]. Also, the inner- and outer-diameter of B-CNTs as well as, outer-diameter of B-CNFs were determined with similar approach from several TEM images.

**Table 1:** Composition of the products obtained at 900 °C.

Wt.% boron precursor	Yield (mg)	Composition (T = BCNTs, F = B-CNF)
1.0	200	85% T, 15% F
2.5	340	75% T, 25% F
5.0	660	60% T, 40% F

The inner- and outer-diameters of B-CNTs as well as, outer-diameter of B-CNF were determined from TEM images. It was observed that the outer diameter of both B-CNTs and B-CNFs decreased as the wt.% of boron precursor was increased (Fig. 3).

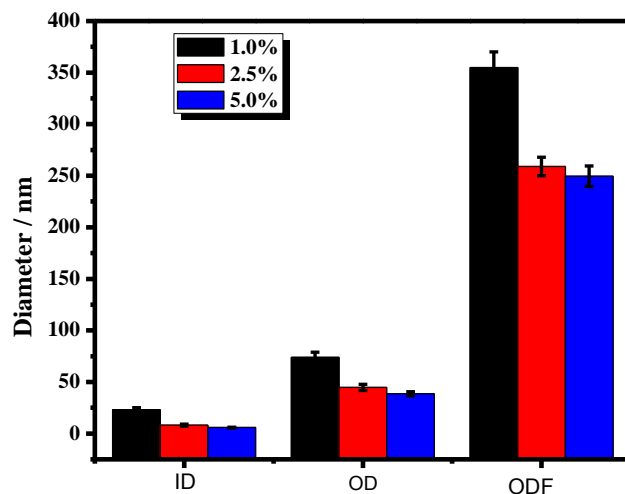


**Fig. 3:** Change of CNTs inner-diameter (ID) and CNTs outer-diameter (OD) of B-CNTs while ODF is the outer-diameter of B-CNF. This was determined from a minimum of 50 TEM images and reported as an average.

Reduction of the outer diameters could be due to interaction of boron with the catalyst to generate smaller nanoparticles. Boron has poor solubility with iron catalyst nanoparticle at high temperatures therefore, it is segregated on the surface of the catalyst [33]. This reduces the amount of carbon dissolving in the catalyst and eventually, precipitated to form B-CNTs. Our findings on reduction of outer diameter of B-CNTS from 73.8 nm to 38.5 nm (Fig. 3) agree with findings by Koo's *et al.* [17] who reported a decrease from 77 nm to 47 nm by increasing boron precursor from 5.0 to 10.0 wt.%. The length of B-CNTs synthesised was estimated to be between 4–6  $\mu\text{m}$  from TEM images. This long length could be due to boron acting as surfactant [33] that inhibit closure of the tubes and promote continued tube growth. Hashim *et al.* [29] used DFT calculations to prove that boron doping favours formation of heptagons which also inhibits tube closure as opposed to pentagons which favour closure. Our previous work has shown that nitrogen-doping within CNTs, does promote tube closure and this is because the nitrogen heteroatom forms “bell-shaped” structures which are due to pentagon as well as, nitrogen occupying edges of the tubes as opposed to hexagon or heptagons [28].



### 3.2. Determination of % boron concentration in the samples

We attempted to determine the concentration of boron using EDX; Fig. 4 represents the spectrums and Table 2 values obtained by this characterization technique. No boron was detected in samples prepared with 1.0 wt.% boron precursor using this method, the possible reason could be concentration of boron was below detection limits of this instrument.

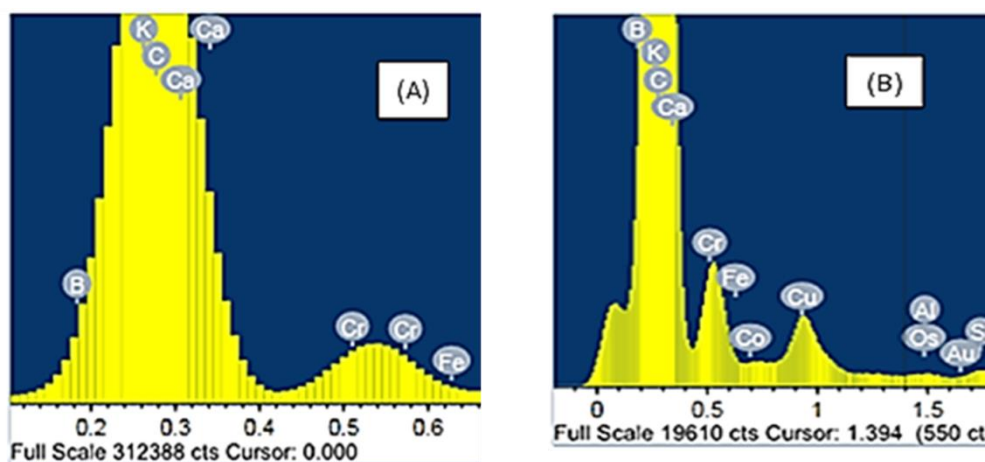


**Fig. 4:** Boron concentration as determined by EDX, (A) B-CNTs synthesized from 2.5 wt.% and (B) from 5.0 wt.% triphenylborane (boron containing precursor).

**Table 2:** Values of Boron concentrations obtained form EDX for 2.5% and 5.0% wt. % triphenylborane.

Wt. % of triphenylborane	elements	weight %	atomic %
2.5	boron	2.3	2.7
	carbon	92	96
5.0	boron	3.3	3.9
	carbon	87	94

EDX was attached to HR-TEM, at high magnification different sections of the same tube were analysed while, at low magnification different sections of the samples were analysed. From EDX analysis we noted boron was heterogeneously doped on the tubes (from one tube to another and also in different sections of the same tube) and followed no regular pattern. Hashim *et al.* [29] experimentally mapped boron-doping on samples

synthesized by aerosol assisted CVD with triethylborane as boron source using electron loss spectroscopy and reported that boron was concentrated on “ elbow” joints only. Varied boron-doping in different sections of the sample was also reported by Nichollas *et al.* [27] and thus our results, and those from the literature, show that EDX could not be used as a quantitative technique for determining the overall level of boron within the samples. However, quantification of boron concentration in the samples was done by use of ICP-OES. Table 3 gives the results obtained.

Boron concentration was between 0.4–2.5%, which was dependant on the wt.% of boron precursor used. From the quantitative data obtained by ICP-OES we observed that the % boron concentration increased as the wt.% of boron precursor increased; and it was possible to tune the amount of boron-doped by varying the amount triphenylborane used.

**Table 3:** Boron concentration as determined by ICP-OES.

Boron precursor (wt.%)	Boron concentration (%)
1.0	0.4
2.5	1.2
5.0	2.5

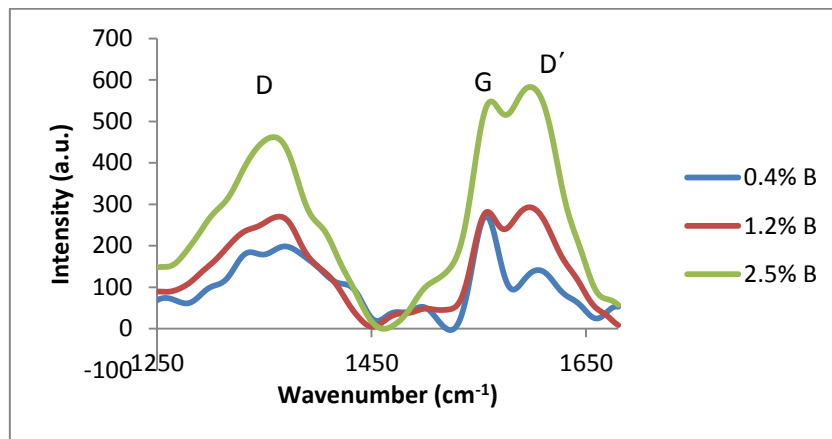
### **3.3. Effect of % boron concentration on graphitic nature and thermal stability of the samples**

Raman spectroscopy was used to investigate the changes in the graphitic structure of the B-CNTs with boron concentration in the products. Two major peaks were identified, the G-band between 1500–1600  $\text{cm}^{-1}$  and the D-band between 1300–1400  $\text{cm}^{-1}$ . The D-band is associated with structural disorder along the graphene sheet that makes up the walls of the tubes, while the G-band is due to C-C stretching mode as a result of tangential vibration of carbons within the walls of the nanotube. Table 4 highlights results from Raman spectroscopy analysis.

**Table 4:** Raman shift of for B-CNTs with boron concentration.

Boron concentration (%)	D-band ( $\text{cm}^{-1}$ )	G-band ( $\text{cm}^{-1}$ )	D'-Band ( $\text{cm}^{-1}$ )	$I_D/I_G$
0.4	1352	1556	1601	0.52
1.2	1358	1559	1600	0.72
2.5	1356	1564	1600	0.77

It was observed that the G-band shifted to longer wavelength as the boron concentration increased. Shift of the G-band to higher wavelength was attributed to substitution of carbon from its network by boron [34]. In all the samples D'-band was observed (Table 4 and Fig. 5), D'-band is double resonance Raman feature induced by disorder and defects by insertion of some boron atoms between graphitic carbon layers especially where it is concentrated in the “elbow” joint [35]. The peaks area were observed to broaden (Fig. 5) with increased boron concentration and this is also reported in literature [34]. Increased peak sizes with boron concentration could be due to increased defects and also, high concentration of B-CNF as observed in TEM images.

**Fig. 5:** Raman D and G peaks for the sample. Appearance of D' on G-peak was also observed.

Ratio of intensity of G-band and D-band ( $I_D/I_G$  ratio) was calculated from the integrated intensity of the Raman peaks between  $1300\text{--}1400\text{ cm}^{-1}$  and  $1500\text{--}1600\text{ cm}^{-1}$ . An increase of  $I_D/I_G$  was observed from sample with 0.4% to 1.2% boron concentration (Table 3) this could be due to increased amount of B-CNFs and defects as the diameter

reduces due decreased number of walls. Several researchers have reported increased  $I_D/I_G$  ratio, as a measure of disorder level, as dopant concentration increases [12,17,28]. The small change of  $I_D/I_G$  ratio in samples with 1.2% - 2.5% boron concentration relates well with their decrease in outer diameter, which was also minimal and both samples had high amount of B-CNFs which are less graphitic. Schuster *et al.* [36] used XPS to compare graphitic nature of CNT and CNF and reported that CNF are less graphitic. This supports our observation that samples with high amount of B-CNFs had more disorders and less graphitic (Tables 3 and 4).

Thermal stability and purity of the samples were analysed using thermogravimetric analysis, a widely used method in the literature for the analysis of CNTs [32,37,38], and the results are shown in Fig. 6 A and B. We observed that the sample with 0.4% boron concentration as-synthesized was the most thermally stable but also had the highest amount of residual mass. This high residual mass could be due to iron catalyst nanoparticles encapsulated inside the B-CNTs. After acid purification the iron catalyst nanoparticles were removed and the residue mass decreased but thermal stability also decreased. Fig. 6B derivative % weight loss shows clearly that sample with 2.5% boron concentration was a mixture.

#### **3.4. Variation of textural properties of B-CNTs and B-CNF with % boron concentration in the sample**

The effect of percentage boron content on the textural characteristics of the B-doped SCNMs; surface area and porosity, was calculated using the BET and Barrett-Joyner-Helanda (BJH) equations respectively. Table 5 summarizes the results obtained which shows the sample with 0.4 % boron concentration had the highest BET-surface area which can be attributed to the fact that the sample had the least amount of B-CNFs (see Table 5). Fig. 7 presents the pore size distributions (small and large pores) for the various samples. Small pores are due to inner channels of B-CNTs while large pores are as a result of entanglement of CNTs [36].

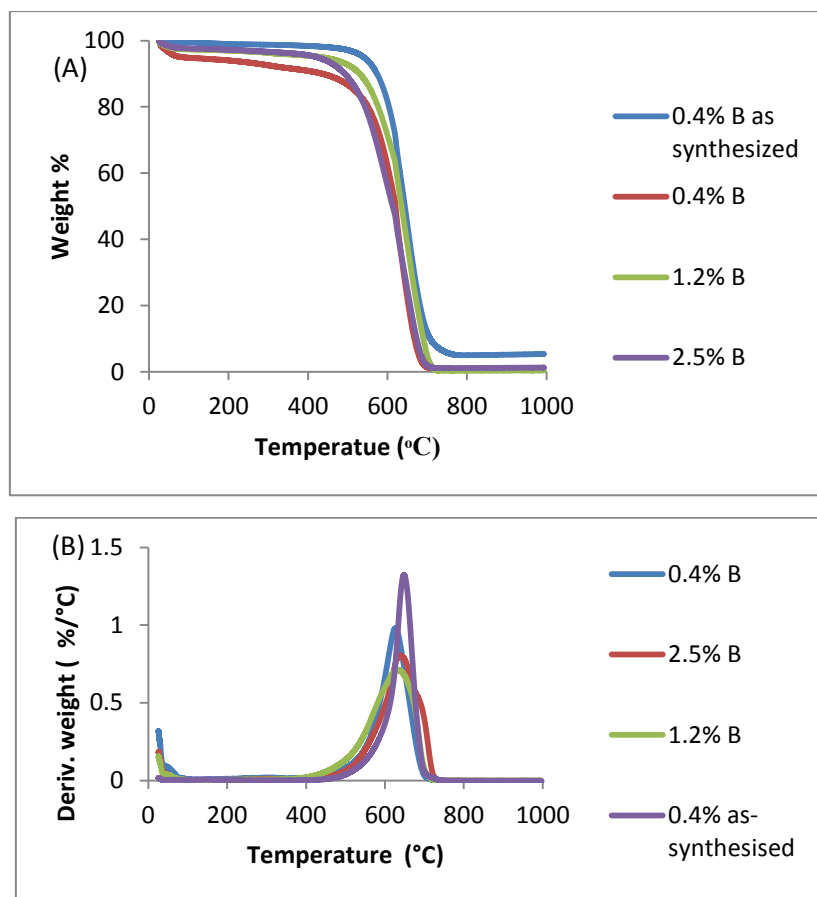


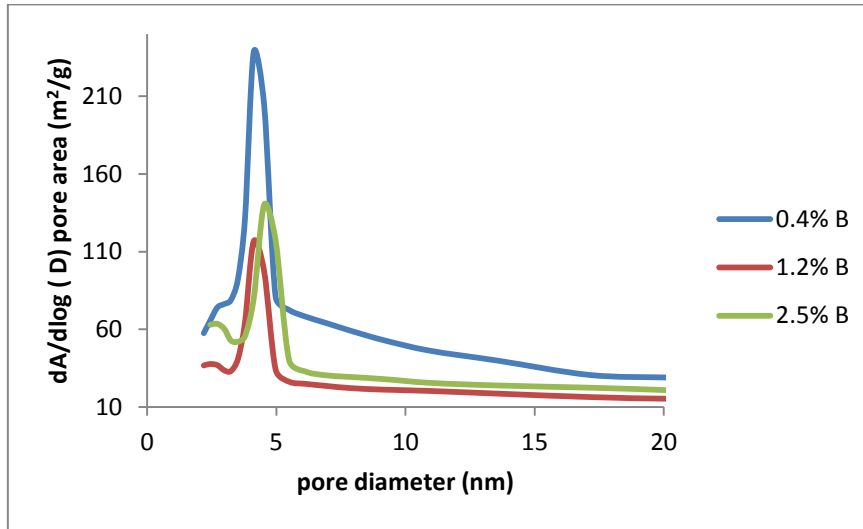
**Fig. 6.** Thermogravimetric analysis of B-CNTs and B-CNFs (A) showing amount of residue remaining on the purified samples was very little and (B) their derivative % weight loss.

We observed the sample with 0.4 % boron concentration had high contribution of both small pores (1–10 nm) and large pores (11-20 nm). High contribution of small pores supports our earlier observation in the TEM that this sample had high amount of tubes with open ends.

Also, this contribution of both small and large pores (Fig. 7) increased amount of nitrogen gas adsorption on the samples making this sample to have the highest BET surface area and porosity. Small pores in samples with 1.2% and 2.5% boron concentration are an indication of reduced number of B-CNTs and increased B-CNFs, reduced entanglement and thereby reducing large pores.

**Table 5:** Summary of textual characteristics of B-MWCNTs.

Boron concentration (% )	Surface area (m <sup>2</sup> /g)	Pore volume (cm <sup>3</sup> /g)	Pore size (nm)
0.4	102.507	0.228	10.926
1.2	63.8421	0.1414	13.279
2.5	81.3456	0.1430	10.515

**Fig. 7:** Pore size distribution.

We observed a good trend of BET surface area and pore sizes for samples with 1.2% and 2.5% boron concentration in relation to OD, ID and ODF as the amount of B-CNFs increased the BET surface area decreased as well as the outer diameter. Adsorption isotherms (Fig. 8) show that the 0.4% and 1.2% boron concentration samples had type IV isotherm with a defined hysteresis loop. In contrast the 2.5% boron concentration sample had a small and almost ill-defined hysteresis loop. The differences can be linked to the B-CNF content increase with increased doping. Tessonier *et al.* [36] reported similar observations for commercial carbon nanostructures with carbon fibres.

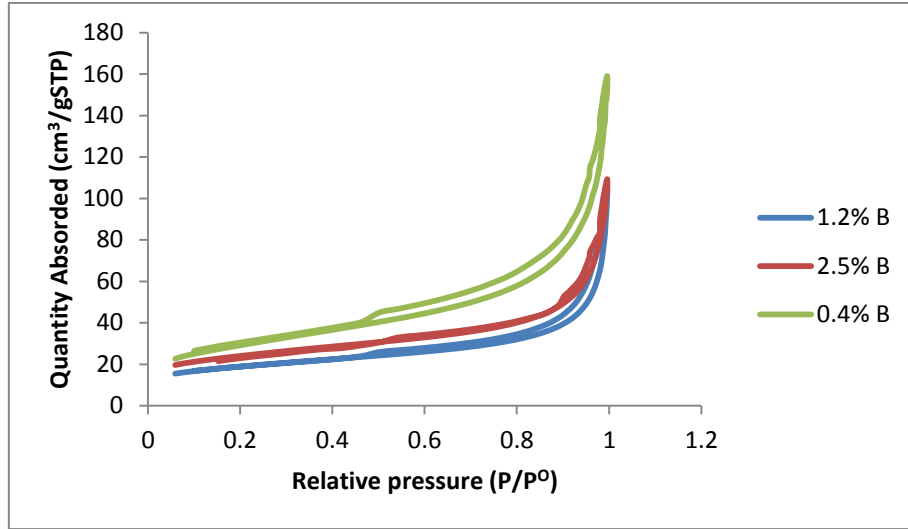


**Fig. 8:** B-MWCNTs isotherm plots for 0.4%, 1.2% and 2.5% boron concentration.

### 3.5. Effect of % boron concentration on conductivity of B-CNTs

The conductivity of the materials was calculated from their resistivity as determined by four probe method. Resistivity ( $\rho$ ) by four probe method was calculated as follows

$$\rho = \frac{\pi h}{\ln 2} \left( \frac{\Delta V}{I} \right) \quad \text{for } h \ll a \quad (1)$$

where  $h$  is the film thickness and  $a$  is the distance between the probes. This equation is used mainly when the film thickness ( $h$ ) is smaller than the distance between the probes ( $a$ ). In our case  $h$  was  $0.15 (\pm 0.01)$  mm while  $a$  was 0.2 cm. Conductivity ( $\delta$ ) was calculated from resistivity ( $\delta = 1/\rho$ ) of the samples and it was observed that conductivity increased with temperature and also with % boron concentration. Samples with 2.5%, 1.2% and 0.4% boron concentration showed a minimum of 0.836, 0.549 and  $0.266 \Omega^{-1} \text{cm}^{-1}$  respectively (Fig. 9). This observation concurs with finding of Kim *et al.* [39], who reported increased conductivity of CNTs by increasing the amount of substitutional boron.

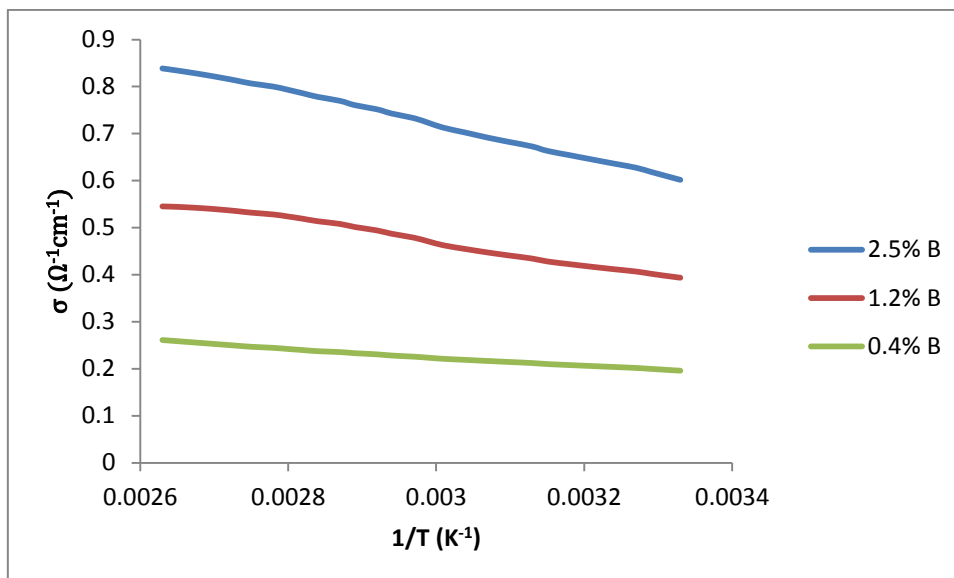


**Fig: 9.** Conductivity of B-CNTs against 1/T. Conductivities increases as % B boron concentration and temperature increases.

Boron-doping increases hole type charge carriers in the carbon network which intern increased conductivity [12], however, increased boron-doping has been reported to act as scattering centres which reduces current flow [26]. Jana *et al.* [40] reported theoretical calculations showing predictions that BC<sub>3</sub> nanotubes are low band-gap semi-conductors irrespective of diameter or chirality. Hence, we could assume the increase conductivity is due to change of chirality where boron incorporation favours formation of *zigzag* CNTs. Also the localization of boron at the tips [12] and “elbow” joints [29] reduces the scattering effect. We also observed that conductivity increased with temperature, which could indicate that B-CNTs samples were semi-conducting. Semi-conducting behaviour in CNTs is normally seen in the *zigzag* chirality which in this case was induced by boron-doping [41,42]. We also observed conductivity to increase with % B-CNFs in the sample, which had helical-like morphology. High conductivity for the sample with 2.5% boron concentration could be due to contribution of B-CNFs [43]. Generally, conductivity is expected to decrease as the diameter of B-CNTs reduced due to decreased mean free charge carrier path [44] (Fig. 3) but, in our case it was increasing which we attribute to the presence of B-CNFs in the sample which were composed of walls parallel to the axis increasing mean carrier path.



### 3.6. Effect %boron concentration on magnetic properties of B-CNTs

Magnetic properties; coercivity ( $H_C$ ), magnetic remanent ( $M_R$ ), saturation magnetization ( $M_S$ ) and squareness (Table 6) of B-CNTs were determined by VSM. Ferromagnetic properties were observed in all the samples with 0.4% as-synthesised showing the highest hysteresis loop, coercivity and squareness. The possible reason for this could be due to iron (known to be highly ferromagnetic) catalyst nanoparticles trapped inside the B-CNTs (Fig. 1) and this was also supported by thermogravimetric analysis seen in Fig. 6.

**Table 6:** Magnetic properties as determined by VSM.

Boron concentration (%)	Coercivity (G)	Magnetic remanent [MR] ( $\text{emu g}^{-1}$ )	Saturation magnetization [MS] ( $\text{emu g}^{-1}$ )	Squareness
0.4 – as synthesized	264	0.184	2.49	0.074
0.4	153	-0.143	4.67	0.004
1.2	227	0.070	1.46	0.048
2.5	254	0.061	1.06	0.057

It was also observed that coercivity and squareness increased with % boron concentration (Table 6). Hysteresis loop was observed in all samples but was very weak for the sample with 0.4% boron concentration which was almost showing superparamagnetic property however, the size and shape of the loop was dependent on the % boron concentration (Fig. 10).

Fig. 6 (thermogravimetric analysis) shows that some residue remained after thermal degradation of the sample with 0.4% B as-synthesized, the other samples were showing almost negligible amount. This was due to presence of some impurities that were likely to be iron metal catalyst nanoparticles trapped inside the B-CNTs and B-CNFs.

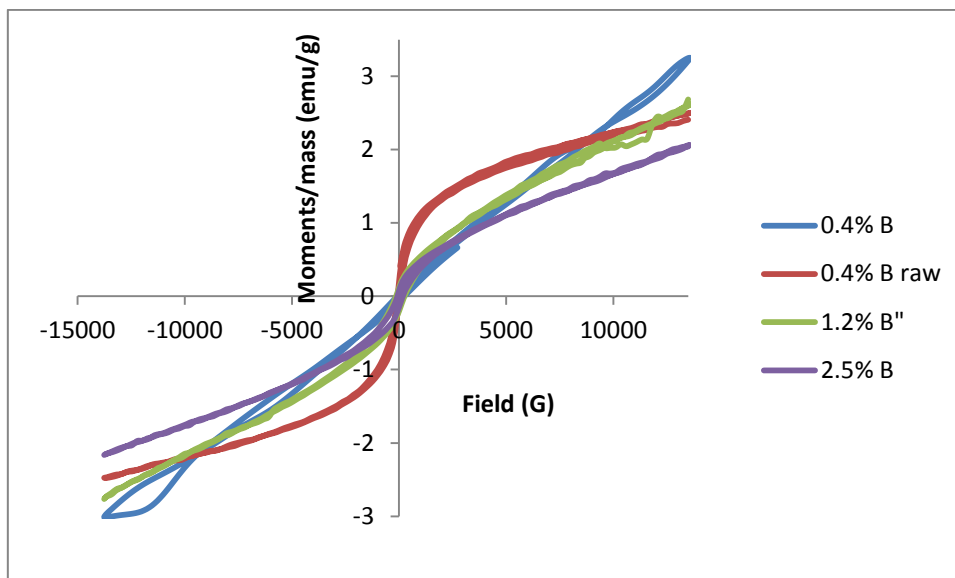


**Fig.10:** Magnetization of B-CNTs showing hysteresis loops. 0.4% B as synthesised had the highest loop (red) and 0.4% B (blue) lowest.

However; the ferromagnetic properties observed cannot be wholly attributed to remnant iron only, since samples with 0.4% and 2.5% B had almost the same amount of residue (Fig. 6A) but, high coercivity and squareness values were observed for the sample with high % B (Table 3). Likodimos *et al.* [45] synthesized B-CNTs without using metal catalyst and reported sample with 1% boron-doping with relatively high ferromagnetic signal from a dc magnetization. Saturation magnetization of their samples was in the range  $0.1\text{--}0.08\text{ emu g}^{-1}$  in the temperature ranging 2-200 K. These values are lower than what we observed in our samples at 300 K. Okanda and Oshiyama used DFT calculations and reported ferromagnetic ordering in hexagonally bonded honeycombs consisting of boron, nitrogen and carbon [46].

### 3.7. Effect of % boron concentration in B-CNTs on surface energy properties

Surface energy properties of B-CNTs were determined using inverse gas chromatography using a surface energy analyzer (SEA), from surface measurement systems, that was equipped with flame ionization detector. Helium was the carrier gas and methane reference gas. Dispersive component surface energy ( $\gamma_s^d$ ) was determined from the retention time ( $t_r$ ) of volume of a series of normal alkanes  $C_5\text{--}C_8$  at a flow rate

of 10 mL/min and 5% surface coverage. All of the data was analysed using the Cirrus Plus SEA data analysis software (Version 1.2.3.1). The  $\gamma_s^d$  was calculated from a slope of a straight line drawn from  $RT \ln V_N$  against the number of carbon atoms in n-alkanes using the Doris and Gray [47] or Schultz [48] methods at maximum peak time. Where, R is gas constant, T absolute column temperature and  $V_N$  is the net retention volume of non-polar probes as well as polar probes and can be calculated from the equation;

$$V_N = Fj(t_R - t_M) \left( \frac{P_O - P_W}{P_O} \right) \left( \frac{T_C}{T_{meter}} \right) \quad (2)$$

where F is the flow rate,  $t_R$  and  $t_M$  are the retention and dead times measured with a specific probe and a non-adsorbing probe (such as methane) respectively,  $P_0$  is the pressure at the flow meter,  $P_w$  is the vapour pressure of pure water at the temperature of the flow meter ( $T_{meter}$ ), and  $T_c$  is the column temperature [49]. For j it was James-Martin correction factor of gas compressibility when the column inlet ( $P_i$ ) and outlet ( $P_o$ ) pressures are different given by equation.

$$j = 3/2 \left[ \frac{\left( \frac{P_i}{P_o} \right)^2 - 1}{\left( \frac{P_i}{P_o} \right)^3 - 1} \right] \quad (3)$$

The polar probes used to determine the acid/base properties of B-CNTs surfaces were acetone; acetonitrile, ethanol, ethyl acetate and dichloromethane. The  $\gamma_s^d$  was determined at 100 °C (10 hours run) for all of the samples using four alkanes; pentane, hexane, heptane and octane.

There was no clear trend relating % boron concentration with  $\gamma_s^d$ , at 0.4% was 39.64 mJ m<sup>-2</sup>, 1.2% was 191.10 mJ m<sup>-2</sup> and 2.5% boron concentration was 157.81 mJ m<sup>-2</sup>. However, we observed that B-CNTs and B-CNFs in our samples had high surface energies that compared well with values reported elsewhere for un-doped CNTs [50]. The retention time of the various solvents can give some insight on the differences in the distribution of surface groups on the samples. For instance, Shaffer *et al.* [51], demonstrated that the differences in the retention time of a polar probe (pentanol) by

oxidised CNTs and annealed CNTs was due to the types and amounts of polar groups on the surfaces of the different types of CNTs. Table 7 provides the results of the retention time taken at the peak maximum, and the ratio of the retention time taken at the centre of mass (COM) of the peak to the maximum retention time with the non-polar and polar probes. The non-polar probes show some variation with the retention times, as the carbon length decreases the retention time with each sample decreases, which is an expected result and can be attributed to the smaller cross-sectional area of each probe as the carbon chain length gets smaller (from octane – pentane) and thus there will be less interaction between the shorter probes and the surface of the nanotubes when compared with the longer probes. An interesting result is the large increase with the retention time of the non-polar probes when comparing 0.4% and 1.2% B samples and then a subsequent decrease when comparing 1.2% and 2.5% B samples.

An increase in retention time is an indication that the surface chemistry of the nanotubes changes from the 0.4% to the 1.2% B sample, in terms of adsorption sites for the probes. With the non-polar probes the interaction between the nanotube walls and the probes will be due to van der Waals forces between the delocalized electrons along the tube walls and the probes. Any disruption in the distribution of the delocalized electrons will result in shorter retention times especially with the larger probes. Such a disruption can be due to the distribution of the boron atom within the framework of the nanotubes. As previously noted in the literature, different dopant levels will result in the boron atoms in fairly isolated positions, and at higher dopant levels the  $BC_3$  domains formed will be much closer together [10,27,39,42].

This change will result in different surface properties with the different % boron concentration and hence the difference in the interactions between probes and samples. It is interesting to note that Nicholls *at al.* [27], observed that nanotube morphologies change with the boron doping level. Thus, besides the change from dominantly CNT to B-CNF morphology with the 2.5% boron concentration sample, there may be a change with the CNT overall structure within the samples and hence a change in the retention times with the non-polar probes.

**Table 7.** The maximum retention time taken at the peak maximum, and the ratio of the retention time taken at the centre of mass (COM) of the peak to the maximum retention time of the various solvents used to probe the 3 samples.

Solvents	0.4% boron concentration		1.2% boron concentration		2.5% boron concentration	
	Peak Max [min]	Peak Com/Max	Peak Max [min]	Peak Com/Max	Peak Max [min]	Peak Com/Max
Octane	0.570	1.062	16.389	2.118	8.949	2.570
Heptane	0.536	0.986	4.155	2.748	2.479	2.957
Hexane	0.495	0.975	1.188	2.313	0.935	2.106
Pentane	0.498	1.019	0.590	1.213	0.583	1.198
Acetone	0.507	1.086	0.953	3.108	2.223	2.997
Acetonitrile	0.503	1.384	0.978	3.167	1.688	2.766
Ethanol	0.518	1.156	1.198	4.127	2.767	2.698
Ethyl acetate	0.508	1.065	1.866	3.665	4.333	2.821
Dichloromethane	0.685	1.033	0.600	1.212	0.623	1.344

Specific free energy  $\Delta G^{AB}$  of adsorption for acid-base specific interaction was used to study surface polarity. Interaction with polar probes was high for bi-functional probes e.g. acetonitrile, ethyl acetate and ethanol in all the samples showing the surfaces of B-CNTs and B-CNFs were covered by amphoteric functional groups [52]. These groups were assumed to be  $-\text{OH}$  and  $-\text{COOH}$  groups introduced during acid purification. In addition, a large ratio of peak max/peak COM (Table 6) is indicative of a nanotube surface with a significant number of polar moieties and a variety of polar groups [51]. The ratios, from Table 6, for the polar probes acetone, acetonitrile, ethanol, and ethyl acetate are larger than the non-polar probes and dichloromethane, which can be indicative of a surface with various polar groups. However, the  $\text{BC}_3$  domains may also play a role in acid base chemistry of these materials. Surface chemistry of the samples were assed using the Gutmann acid ( $K_a$ ) and base ( $K_b$ ) constant and in all the samples,

the base constant  $K_b$  values was observed to be higher than acid constant  $K_a$  values showing the surfaces were more basic or contained donor groups. Although, with boron-doping Lewis acid property (acceptor) was introduced, its effect was overshadowed by that of oxygenated groups introduced during acid purification. These groups have lone pair of electrons which bring about Lewis base properties and hence, this was the main reason for the surfaces being basic.

The dispersive surface energy and the specific free energy ( $\Delta G_{sp}$ ) at different surface coverage were also determined in order to assess surface heterogeneity of the samples. Usually this can be influenced by different aspects, such as, surface functional groups, surface topography, surface irregularities and impurities [53]. Figure 11 (a) shows dispersive surface energy distribution for the low and high (0.4 and 2.5%) B for surface coverage between 0.02-0.08  $n/n_m$ . ( $n$  is the no. of moles of solute adsorbed and  $n_m$  is the monolayer capacity) at 100 °C.

From Figure 11 we observed that the increase in boron-doping in the samples changed the nanotubes from surfaces with a narrow distribution to a wider distribution of dispersive surface energy sites. This can be attributed to the increase in  $BC_3$  domains on the nanotube walls. The changes with the specific free energy, Figure 11 (a) and (b), show that the increased doping results in a more favourable interactions with the polar probes, since the distribution of  $\Delta G_{sp}$  values are all negative with the 2.5% boron concentration sample.

The polar probes ethanol, ethyl acetate, and acetonitrile had a much wider variation in the values of  $\Delta G_{sp}$  with the 0.4% boron concentration sample, which indicates at the lower doping level there are a wide variety of polar groups.

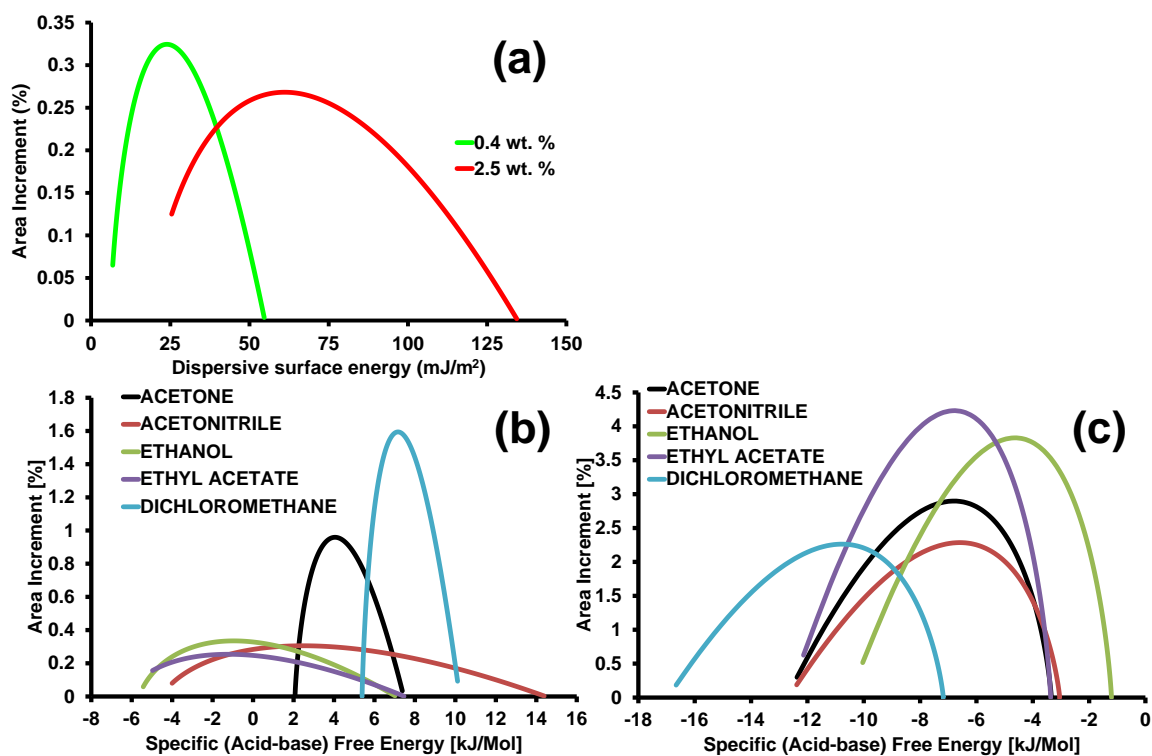


**Fig. 11:** Dispersive surface energy component surface energy at different surface coverage.

However, ethanol is considered slightly acidic and acetonitrile is slightly basic, thus a similar wide distribution indicates the presence of surface groups that can interact favourably with both probes. With the 2.5% boron concentration sample the range of values with the dichloromethane probe increased but decreased with all other probes. This indicates the heterogeneity of the nanotube surface was altered by the doping levels, and since dichloromethane has a relatively large acceptor number (3.9) and a low donor number (0.0) this does highlight the dominance of the  $BC_3$  domains on the surface properties of the nanotubes at higher doping levels.

#### 4. Conclusion

B-CNTs with boron concentration 0.4%, 1.2% and 2.5% were successfully synthesized. It was possible to vary boron concentration by use of different amount of triphenylborane as the boron source. Physicochemical properties, composition and yield of the products were found to be dependent on the amount of triphenylborane used. Increased amounts of triphenylborane lead to a high yield of the products but

percent of B-CNFs increased. High % boron concentration was found to favour formation of B-CNFs. Properties such as conductivity, magnetic, specific surface area and porosity and surface energy were observed to change with boron concentration. Ferromagnetic properties which are as a result of boron-doping should be explored further to determine suitability of B-CNTs as raw materials for applications such as memory, detectors and sensors among other electronic devices.

### **Acknowledgements**

The authors wish to thank the University of KwaZulu-Natal, the National Research Foundation (91529 and 76635) (NRF) and India, Brazil, and South Africa (IBSA) energy project for financial assistance. We are also grateful to Dr T. Moyo and Dr Hafiz Abdallah (UKZN Westville campus Condensed Matter Physics Lab) for assistance in VSM and conductivity measurements. G. Keru also thanks the UKZN College of Agriculture, Engineering and Science for award of a postgraduate bursary.

### **References**

- [1] Y. Chen, J. Wang, H. Liu, M.N. Banis, R. Li, X. Sun, T.-K. Sham, S. Ye, S. Knights, *The Journal of Physical Chemistry C* 115 (2011) 3769-3776.
- [2] W.K. Hsu, T. Nakajima, *Carbon* 40 (2002) 462-465.
- [3] S.D. Mhlanga, E.N. Nxumalo, N.J. Coville, V.V. Srinivasu, *Materials Chemistry and Physics* 130 (2011) 1182-1186.
- [4] X. Li, G. Zhu, Z. Xu, *Thin Solid Films* 520 (2012) 1959-1964.
- [5] P. Ayala, R. Arenal, M. Rummeli, A. Rubio, T. Pichler, *Carbon* 48 (2010) 575-586.
- [6] H. Mousavi, R. Moradian, *Solid State Sciences* 13 (2011) 1459-1464.
- [7] S.C. Lyu, J.H. Han, K.W. Shin, J.H. Sok, *Carbon* 49 (2011) 1532-1541.
- [8] F.H. Monteiro, D.G. Larrude, M.E.H. Maia da Costa, L.A. Terrazos, R.B. Capaz, F.L. Freire, *The Journal of Physical Chemistry C* 116 (2012) 3281-3285.
- [9] M. Sankaran, B. Viswanathan, *Carbon* 45 (2007) 1628-1635.
- [10] L. Yang, S. Jiang, Y. Zhao, L. Zhu, S. Chen, X. Wang, Q. Wu, J. Ma, Y. Ma, Z. Hu, *Angewandte Chemie* 123 (2011) 7270-7273.
- [11] U. Tanaka, T. Sogabe, H. Sakagoshi, M. Ito, T. Tojo, *Carbon* 39 (2001) 931-936.



- [12] W.K. Hsu, S. Firth, P. Redlich, M. Terrones, H. Terrones, Y.Q. Zhu, N. Grobert, A. Schilder, R.J.H. Clark, H.W. Kroto, D.R.M. Walton, *Journal of Materials Chemistry* 10 (2000) 1425-1429.
- [13] W. Han, Y. Bando, K. Kurashima, T. Sato, *Chemical Physics Letters* 299 (1999) 368-373.
- [14] D. Golberg, Y. Bando, L. Bourgeois, K. Kurashima, T. Sato, *Carbon* 38 (2000) 2017-2027.
- [15] H.J. Ceragioli, A.C. Peterlevitz, J.C.R. Quispe, A. Larena, M.P. Pasquetto, M.A. Sampaio, V. Baranauskas, *Journal of Physics: Conference Series* 100 (2008).
- [16] K.C. Mondal, N.J. Coville, M.J. Witcomb, G. Tejral, J. Havel, *Chemical Physics Letters* 437 (2007) 87-91.
- [17] A.A. Koós, F. Dillon, E.A. Obraztsova, A. Crossley, N. Grobert, *Carbon* 48 (2010) 3033-3041.
- [18] J.-J. Adjizian, R. Leghrib, A.A. Koos, I. Suarez-Martinez, A. Crossley, P. Wagner, N. Grobert, E. Llobet, C.P. Ewels, *Carbon* 66 (2014) 662-673.
- [19] Y. Cao, H. Yu, J. Tan, F. Peng, H. Wang, J. Li, W. Zheng, N.-B. Wong, *Carbon* 57 (2013) 433-442.
- [20] R.B. Sharma, D.J. Late, D.S. Joag, A. Govindaraj, C.N.R. Rao, *Chemical Physics Letters* 428 (2006) 102-108.
- [21] K. McGuire, N. Gothard, P.L. Gai, M.S. Dresselhaus, G. Sumanasekera, A.M. Rao, *Carbon* 43 (2005) 219-227.
- [22] B. Wang, Y. Ma, Y. Wu, N. Li, Y. Huang, Y. Chen, *Carbon* 47 (2009) 2112-2115.
- [23] J.L. Blackburn, Y. Yan, C. Engtrakul, P.A. Parilla, K. Jones, T. Gennett, A.C. Dillon, M.J. Heben, *Chemistry of Materials* 18 (2006) 2558-2566.
- [24] P. Ayala, W. Plank, A. Gruneis, E.I. Kauppinen, M.H. Rummeli, H. Kuzmany, T. Pichler, *Journal of Materials Chemistry* 18 (2008) 5676-5681.
- [25] V.O. Nyamori, S.D. Mhlanga, N.J. Coville, *Journal of Organometallic Chemistry* 693 (2008) 2205-2222.
- [26] Z. Aslam, R. Nicholls, A. A. Koos, V. Nicolosi, N. Grobert, *The Journal of Physical Chemistry C* 115 (2011) 25019-25022.
- [27] R.J. Nicholls, Z. Aslam, M.C. Sarahan, A. Koós, J.R. Yates, P.D. Nellist, N. Grobert, *ACS Nano* 6 (2012) 7800-7805.

- [28] G. Keru, P.G. Ndungu, V.O. Nyamori, *Journal of Nanomaterials* 2013 (2013) 1-7.
- [29] D.P. Hashim, N.T. Narayanan, J.M. Romo-Herrera, D.A. Cullen, M.G. Hahn, P. Lezzi, J.R. Suttle, D. Kelkhoff, E. Muñoz-Sandoval, S. Ganguli, A.K. Roy, D.J. Smith, R. Vajtai, B.G. Sumpter, V. Meunier, H. Terrones, M. Terrones, P.M. Ajayan, *Scientific Reports*. 2, 363 (2012) 1-8.
- [30] R.S. Oosthuizen, V.O. Nyamori, *Applied Organometallic Chemistry* 26 (2012) 536-545.
- [31] Q. Jiang, L. Qian, J. Yi, X. Zhu, Y. Zhao, *Frontiers of Materials Science in China* 1 (2007) 379-382.
- [32] M.S. Mohlala, N.J. Coville, *Journal of Organometallic Chemistry* 692 (2007) 2965-2970.
- [33] S.M. Enouz-Védrenne, O. Stéphan, M. Glerup, J.-L. Cochon, C. Colliex, A. Loiseau, *Journal of Physical Chemistry C* 112 (2008) 16422-16430.
- [34] S. Ishii, T. Watanabe, S. Ueda, S. Tsuda, T. Yamaguchi, Y. Takano, *Physica C: Superconductivity* 468 (2008) 1210-1213.
- [35] S. Osswald, M. Havel, Y. Gogotsi, *Journal of Raman Spectroscopy* 38 (2007) 728-736.
- [36] J.-P. Tessonnier, D. Rosenthal, T.W. Hansen, C. Hess, M.E. Schuster, R. Blume, F. Girgsdies, N. Pfänder, O. Timpe, D.S. Su, R. Schlögl, *Carbon* 47 (2009) 1779-1798.
- [37] A.A. Koos, F. Dillon, E.A. Obraztsova, A. Crossley, N. Grobert, *Carbon* 48 (2010) 3033-3041.
- [38] J.H. Lehman, M. Terrones, E. Mansfield, K.E. Hurst, V. Meunier, *Carbon* 49 (2011) 2581-2602.
- [39] Y.A. Kim, S. Aoki, K. Fujisawa, Y.-I. Ko, K.-S. Yang, C.-M. Yang, Y.C. Jung, T. Hayashi, M. Endo, M. Terrones, M.S. Dresselhaus, *The Journal of Physical Chemistry C* 118 (2014) 4454-4459.
- [40] D. Jana, C.-L. Sun, L.-C. Chen, K.-H. Chen, *Progress in Materials Science* 58 (2013) 565-635.
- [41] J.W. Mintmire, C.T. White, *Synthetic Metals* 77 (1996) 231-234.
- [42] S.-S. Yu, W.-T. Zheng, *Nanoscale* 2 (2010) 1069-1082.

- [43] Z.R. Ismagilov, A.E. Shalagina, O.Y. Podyacheva, A.V. Ischenko, L.S. Kibis, A.I. Boronin, Y.A. Chesalov, D.I. Kochubey, A.I. Romanenko, O.B. Anikeeva, T.I. Buryakov, E.N. Tkachev, *Carbon* 47 (2009) 1922-1929.
- [44] E.M.M. Ibrahim, V.O. Khavrus, A. Leonhardt, S. Hampel, S. Oswald, M.H. Rümmeli, B. Büchner, *Diamond and Related Materials* 19 (2010) 1199-1206.
- [45] V. Likodimos, S. Glenis, C.L. Lin, *Physical Review B* 72 (2005) 045436.
- [46] S. Okada, A. Oshiyama, *Physical Review Letters* 87 (2001) 146803.
- [47] G.M. Dorris, D.G. Gray, *Journal of Colloid and Interface Science* 77 (1980) 353-362.
- [48] J. Schultz, L. Lavielle, C. Martin, *The Journal of Adhesion* 23 (1987) 45-60.
- [49] X. Zhang, D. Yang, P. Xu, C. Wang, Q. Du, *Journal of Materials Science* 42 (2007) 7069-7075.
- [50] R. Menzel, A. Lee, A. Bismarck, M.S.P. Shaffer, *Langmuir* 25 (2009) 8340-8348.
- [51] R. Menzel, A. Bismarck, M.S.P. Shaffer, *Carbon* 50 (2012) 3416-3421.
- [52] J. Khoo, D. Burnett, R. Menzel, M.S. Shaffer. [www. the sorption solution.com](http://www.the-sorption-solution.com). Retrieved 24-04-2014.
- [53] P.P. Ylä-Mäihäniemi, J.Y.Y. Heng, F. Thielmann, D.R. Williams, *Langmuir* 24 (2008) 9551-9557.

## Chapter Six

### **Bulk heterojunction solar cell with nitrogen-doped carbon nanotubes in the active layer: Effect of nanocomposite synthesis technique on photovoltaic properties**

Godfrey Keru, Patrick G. Ndungu, Genene T. Mola and Vincent O. Nyamori\*

School of Chemistry and Physics, University of KwaZulu-Natal, Private Bag X54001, Durban, 4000, South Africa

\*Corresponding author – Vincent O. Nyamori, email – nyamori@ukzn.ac.za

#### **Abstract**

Nanocomposites of poly(3-hexylthiophene) [P3HT] and nitrogen-doped carbon nanotubes (N-CNTs) have been synthesized by two methods; specifically, direct solution mixing and *in situ* polymerization. The nanocomposites were characterized by means of transmission electron microscopy (TEM), scanning electron microscopy (SEM), X-ray dispersive spectroscopy, UV-Vis spectrophotometry, photoluminescence spectrophotometry (PL), Fourier transform infrared spectroscopy (FTIR), Raman spectroscopy, thermogravimetric analysis and dispersive surface energy analysis. The nanocomposites were used in the active layer of a bulk heterojunction organic solar cell with composition ITO/PEDOT:PSS/P3HT:N-CNTS:PCBM/LiF/Al. TEM and SEM analysis showed that the polymer successfully wrapped the N-CNTs. FTIR results indicated good  $\pi$ - $\pi$  interaction within the nanocomposite synthesized by *in situ* polymerization as opposed to samples made by direct solution mixing. Dispersive surface energies of the N-CNTs and nanocomposites supported the fact that polymer covered the N-CNTs well. J-V analysis show that good devices were formed from the two nanocomposites, however, the *in situ* polymerization nanocomposite showed better photovoltaic characteristics.

**Keywords:** polythiophene; nitrogen-doped carbon nanotubes; nanocomposites; photovoltaic properties

## 1. Introduction

The electrical conductivity of a linear chain organic polymer (polyacetylene) was first discovered by Shirikawa *et al.* in 1977 [1]. Later, a number of other organic molecules particularly polythiophene groups emerged as alternative conducting polymers (CPs) with potential applications in the area of opto-electronic devices. The advantages of CPs over inorganic semi-conductors in opto-electronic applications include the ease of processability, tuneable properties of the molecules, flexibility and light weight [2]. CPs consist of alternating single and double bonds; the  $\pi$ -electrons in their double bonds are mobile due to overlap of  $\pi$ -orbitals [3]. Electronic properties of CPs can be tuned during synthesis and they also have good magnetic and optical properties [4]. Of late CPs have been considered as one of the best alternatives for the production of solar cells. This realisation stems from the fact that solar cells fabricated by use of inorganic materials can be expensive and also the processes that are utilised during their manufacture can be extensively energy intensive [5]. For CPs to function well in solar cells they should possess the following characteristics: soluble in common organic solvents, can form a thin film on substrates, low band-gap to enhance absorption, partially miscible with electron acceptors, a good hole conductor and chemically stable in ambient conditions [3]. Polythiophenes not only have several of the characteristics named above but also have efficient electronic conjugation as well as synthetic versatility [3]. Polythiophenes are made by linking thiophene rings, which are insoluble, and then improving their solubility by introducing alkyl chains, i.e. hexyl and octyl groups. Polythiophenes have been studied for various applications which include organic field effect transistors [6], solar cells [7], sensors and light emitting diodes [8].

Although CPs have unique properties their applications in various fields are hampered by their poor environmental stability and mechanical strength. This problem can be overcome by introducing different fillers within the CPs to form nanocomposites [9,10]. Among the different fillers available, carbon nanotubes (CNT) have attracted a lot of interest due to their unique structural, electrical and mechanical properties [11]. Further enhancement of these unique properties can be achieved by doping CNTs with boron or nitrogen to form boron- and nitrogen-doped CNTs (B-CNTs or N-CNTs). Nitrogen-doping creates defects on the walls of CNTs that improves the ability of the surfaces to

undergo various covalent chemistries, provide good anchoring sites for nanoparticles, introduces a variety of functional groups, and more importantly, it also improves the electrical conductivity of CNTs [12]. For example, Panchakarla *et al.* [13] reported higher electrical conductivity for N-CNTs than for pristine CNTs. CNTs/N-CNTs in polymer nanocomposites enhance Young's modulus, the tensile strength and electrical conductivity [14]. Additionally, the incorporation of CNTs can be an effective route to synthesize low density, high performance thermoelectric materials [15]. Nanocomposites of CNTs coated with CPs have found use in organic field emission devices [16], light emitting diodes [8,17], electronic devices and sensors [18], and organic solar cells (OSC) [19]. However, effective utilization of CNTs in the polymer nanocomposites strongly depends on the dispersion. For example, poorly dispersed CNTs in the active layer of OSC can act as recombination sites and also can lead to short-circuiting [20].

OSCs have gained a lot of attention in recent years due to the high expectation of producing relatively cheap devices for converting solar energy directly to electricity [10]. Some of the advantages of OSCs over inorganic solar cells include low-cost manufacturing, high-throughput production and high flexibility, and therefore OSCs can be cast on flexible substrates or on curved surfaces [19]. Although CNTs have many advantages when well dispersed in the polymer matrix, the performance of OSCs with CNTs in the active layer have continued to perform poorly when compared to polymer/fullerene systems, e.g. poly(3-hexylthiophene) (P3HT) and [6,6]phenyl-C<sub>61</sub>-butyric acid methyl ester (PCBM). This has been attributed to short-circuiting as a result of a mixture of semiconducting and metallic CNTs [21], and filamentary short-circuiting due to CNTs extending outside the active layer [22]. Poor performance could also be due to unbalanced charge mobility for a device with CNTs, as one charge carrier will be transferred very fast while the other is subjected to hopping in disordered organic materials [23].

Jun *et al.* [24] fabricated a solar cell with CNTs functionalised with alkyl-amides in an active layer of P3HT:PCBM. The efficiency of this device increased by 30% from 3.2 to 4.4% compared with a device without CNTs. They attributed this increase to wide

band absorption, high charge carrier mobility and improved dispersion in the polymer matrix. Kalita *et al.* [25] used plasma oxygen-functionalized CNTs in the active layer of P3HT:PCBM and reported an 81.8% efficiency increase from 1.21 to 2.2% compared with a device without CNTs. They attributed this increase to improved hole mobility and increased surface area for excitons dissociation.

In this paper we compare the effect of synthesis technique for nanocomposites on their photovoltaic properties. The two techniques compared are: oxidative *in situ* polymerization, and direct solution mixing of P3HT and N-CNTs. We also report on a unique characterization technique whereby dispersive surface energy was used to determine how effective the polymer wrapped/covered the walls of N-CNTs. Finally, the results on the use of nanocomposites in the active layer of organic solar cells (OSC) is presented and discussed.

## **2. Experimental**

### **2.1. Materials**

Chemicals used in this study were of analytical grade and were used as received unless stated otherwise. Anhydrous ferric chloride (99%), [6,6]-phenyl-C<sub>61</sub>-butyric acid methyl ester (PCBM) (98%), regioregular poly (3-hexylthiophene-2,5-diyl) (99.0%) and 3-hexylthiophene (99%) were purchased from Sigma Aldrich (St Louis, USA) while, chloroform (99%) was sourced from an alternative supplier (Merck Chemicals, S.A). Indium tin oxide (ITO) coated glasses slide was purchased from Merck, Germany. Chloroform was dried before being used.

### **2.2. Synthesis of nitrogen-doped CNTs and nanocomposites**

N-CNTs were synthesised in our laboratory by a chemical vapour deposition floating catalyst method as reported elsewhere [26]. Briefly, 2.5 wt.% of (4-[[pyridinyl-4-amino}methylidene]phenyl}ferrocene catalyst was dissolved in acetonitrile solvent to make 100 wt.% solution. This was followed by pyrolysis at 850 °C. The crude N-CNTs obtained were purified by, firstly, calcining at 400 °C in air to remove amorphous carbon, and then refluxing with 6 M HNO<sub>3</sub> for 24 hours at 80 °C to remove any iron residue used as catalyst during the N-CNTs synthesis.

The nanocomposites were synthesized by the means of two techniques, namely, oxidative *in situ* polymerization and direct solution mixing. For oxidative *in situ* polymerization of 3-hexylthiophene monomers on the walls of N-CNTs, this was achieved by use of a similar method as reported by Karim [27]. In brief, 1 wt.% (of the weight of 3HT monomers) of N-CNTs (6.8 mg) was weighed, 50 mL of dry chloroform was added and the mixture was placed in a two-necked round-bottomed flask with a stirrer. The mixture was sonicated for 1 hour to disperse the N-CNTs. Thereafter, 0.648 g (4 mmol) of anhydrous ferric chloride in 50 mL of dry chloroform was added to the above dispersion and further sonicated for 30 min. Then 673.2 mg (2 mmol) of 3-hexylthiophene monomers in 25 mL of dry chloroform solution was placed in a pressure equalised funnel and added dropwise to the above mixture with constant stirring. Stirring continued under the same conditions for the next 24 hours. The nanocomposite was precipitated with methanol; vacuum filtered, washed with methanol, 0.1 M HCl, deionised water, acetone, and then eventually vacuum dried for 24 hours at room temperature.

The direct solution mixing method to synthesize the nanocomposite was adapted from a method reported by Lee *et al.* [28]. In brief, P3HT was dissolved in dry chloroform to make 20 mg mL<sup>-1</sup> solution, and 1 wt.% of N-CNT (of the weight of P3HT) were added to the solution of P3HT in chloroform. The mixture was sonicated for 1 hour then stirred for 12 hours in the dark to protect it from light. This solution was spin coated directly on ITO glass substrate.

The active layer for the solar cell device was prepared by mixing the N-CNTs/P3HT nanocomposite with [6,6] phenyl-C<sub>61</sub>-butyric acid methyl ester (PCBM) at a ratio of 1:0.8 by mass to make 20 mg mL<sup>-1</sup> solution in chloroform. The mixture was sonicated for two hours before spin-coating onto ITO coated glass substrates.

### **2.3. Characterization of the nanocomposites**

The morphology and structure of the nanocomposites was characterised by; transmission electron microscopy (TEM), (JEOL JEM 1010) at 200 kV. The nanocomposite samples were dispersed in ethanol by sonication before being deposited



on carbon-coated copper grids. A scanning electron microscope (Carl Zeiss ultra plus field emission electron microscope (FEGSEM)) was used at 5 kV accelerating voltage. Samples were placed on aluminium stubs by using carbon tape.

Raman spectra of N-CNTs and the nanocomposites were recorded with a DeltaNu Advantage 532™ Raman spectrometer. The excitation source was a Nd:YAG solid state crystal class 3b diode laser at 532 nm excitation wavelength. Nuspec™ software was used to capture generated spectra. Thermogravimetric analysis (TGA) was performed with a TA Instruments Q series™ thermal analyser DSC/TGA (Q600). The P3HT, nanocomposites and N-CNTs were heated at a rate of 10 °C min<sup>-1</sup> under an air flow rate of 50 mL min<sup>-1</sup> and the data was captured and analysed using the TA Instrument Universal Analysis 2000 software.

An inverse gas chromatography (IGC) surface energy analyzer (SEA) was used to determine the surface energy properties of N-CNTs and the nanocomposites. About 30 mg of the sample was packed in IGC salinized glass column of 300 mm length and 4 mm internal diameter. The column was filled with salinized glass wool on both ends of the sample until it was well packed. Cirrus control software was used to control the analysis and Cirrus Plus software was used for data analysis. FTIR spectra were recorded with KBr pellets on a Perkin-Elmer Spectrum 1 FTIR spectrometer equipped with spectrum Rx software. Photoluminescence spectra were obtained with a Perkin Elmer Spectro Fluorimeter equipped with FL Winlab software at an excitation wavelength of 298 nm in chloroform solution. UV-Vis spectra were recorded in a chloroform solution with a Perkin Elmer Lambda 35 dual-beam UV-Vis spectrophotometer and data analysed with FL Winlab software. Samples for the Photoluminescence and UV-Vis were prepared using a modified method as reported by Goutam *et al.* [14] briefly, 10 mg of P3HT and nanocomposites were dissolved in dry chloroform to make 100 mL solutions. Necessary equivalent dilutions were made using micropipette to record spectra.

## 2.4. Device preparation

Devices were prepared in ambient conditions on ITO-coated glass substrates with a shunt resistance of 15  $\Omega$ . Half of the ITO coat was etched with a mixture of water, HCl and HNO<sub>3</sub> in the ratio of 12:12:1 by volume, respectively, and then placed in deionised water. Etching was necessary to provide a non-conductive part to prevent short circuiting and also, allow flow of electrons. The etched substrate was thereafter cleaned by sonication for 10 minutes each with separate solution of detergent, distilled water, acetone, and finally with isopropanol. Thereafter, the substrate was dried at 50 °C for 10 minutes. The hole transport layer Poly(3,4-ethylenedioxythiophene): poly(styrenesulfonate) (PEDOT:PSS) was spin-coated on the clean substrate at 3000 rpm for 50 seconds, and then annealed for 10 minutes at 120 °C. The active layer, a mixture of P3HT/N-CNTs:PCBM was spin-coated at 1500 rpm for 30 seconds, and then annealed for 20 minutes at 120 °C. Before vacuum evaporation of the counter electrode, 0.6 nm of lithium fluoride (LiF) was also vacuum evaporated on top to serve as a hole blocking layer. A 60 nm counter electrode consisting of Al metal was thermally evaporated at  $2.22 \times 10^{-7}$  mbar in an HHV Auto 306 vacuum evaporator equipped with INFICON SQM-160 thin film deposition thickness and rate monitor. Current-voltage characterization was determined by using a standard solar simulator model # SS50AAA (Pet Photoemission Tech. Inc.), with a Keithley 2420 source meter.

## 3. Results and discussions

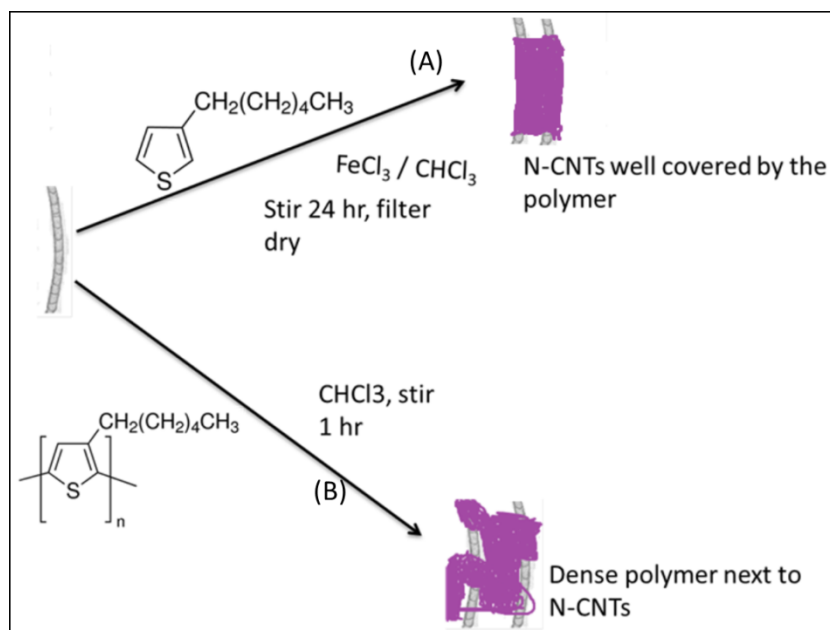
Scheme 1 illustrates how the synthesis of the nanocomposites was achieved. In *in situ* polymerization technique monomers were polymerized directly on the surface of the N-CNTs. However, in the direct solution mixing, a solution of N-CNTs was mixed with a solution of the polymer.

### 3.1. Morphology and structure of the nanocomposite

Figure 1 shows the structure of the N-CNTs before and after formation of the nanocomposites with poly(3-hexylthiophene). From the TEM images it was observed that the polymer coated the surface of the N-CNTs. From the bamboo structures observed it can be deduced that the tubular inner part consist mainly of N-CNTs and the

coated surface is conducting P3HT. The smooth surfaces of the N-CNTs (Figure 1A) became rough after they were covered by the polymer (Figure 1B).

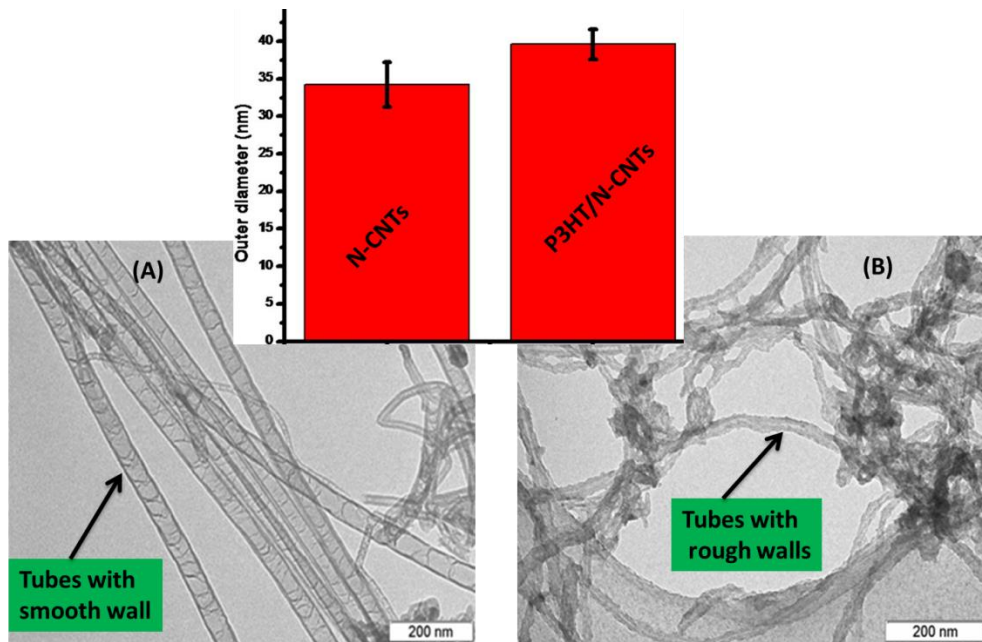
**Scheme 1:** Synthesis of the nanocomposites, (A) *in situ* polymerization, and (B) direct mixing.



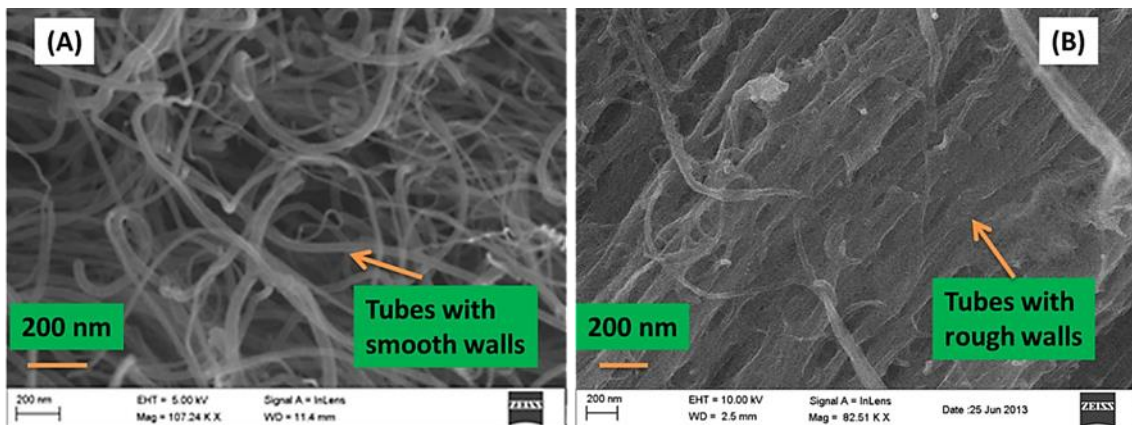
From Figure 2(A), the N-CNTs appear as an entangled mat of tubular structures with smooth surfaces which are a characteristic of carbon-based nanotubes. However, in Figure 2(B) a few thick tubular structures with rough surfaces and agglomerated mat-like structures were observed, and this is indicative of the polymer wrapping onto the nanotubes to form a nanocomposite. EDX, which was coupled with FEGSEM provided further evidence of the nanocomposite elemental composition which consisted of carbon, sulphur and oxygen. Oxygen observed in the nanocomposite could be due to the introduction of oxygenated groups during acid purification and functionalization of N-CNTs. The at.% of carbon increased with the formation of the nanocomposite as compared to that in polymer. Karim [27] reported similar results when they synthesised P3HT/MWCNTs nanocomposites by *in situ* polymerization.

Figure 2 shows the morphology of the N-CNTs and nanocomposite synthesized by *in situ* polymerization as observed in SEM.

**Figure 1.** TEM images of (A) purified N-CNTs, and (B) N-CNT/P3HT nanocomposite synthesized by *in situ* polymerization (inset comparison of outer diameters).



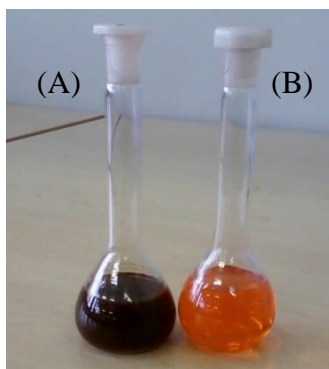
**Figure 2.** Morphology of (A) N-CNTs, and (B) nanocomposite of N-CNTs/P3HT synthesized by *in situ* polymerization.



Further evidence of the polymer wrapping the N-CNTs was obtained by measuring the outer diameters of the N-CNTs and nanocomposite from their TEM images, (inset Figure 1). This was determined from not less than 50 TEM images and over 200 tubes per sample. The diameters were observed to increase with formation of the nanocomposites. An increase of  $\approx 15.9\%$  was observed; a good indication that the N-CNTs were wrapped by the polymer.

Figure 3 further confirms formation of a nanocomposite whereby, the brown colour of pristine P3HT changed to dark brown. Our observations concur with what is reported elsewhere in the literature [29].

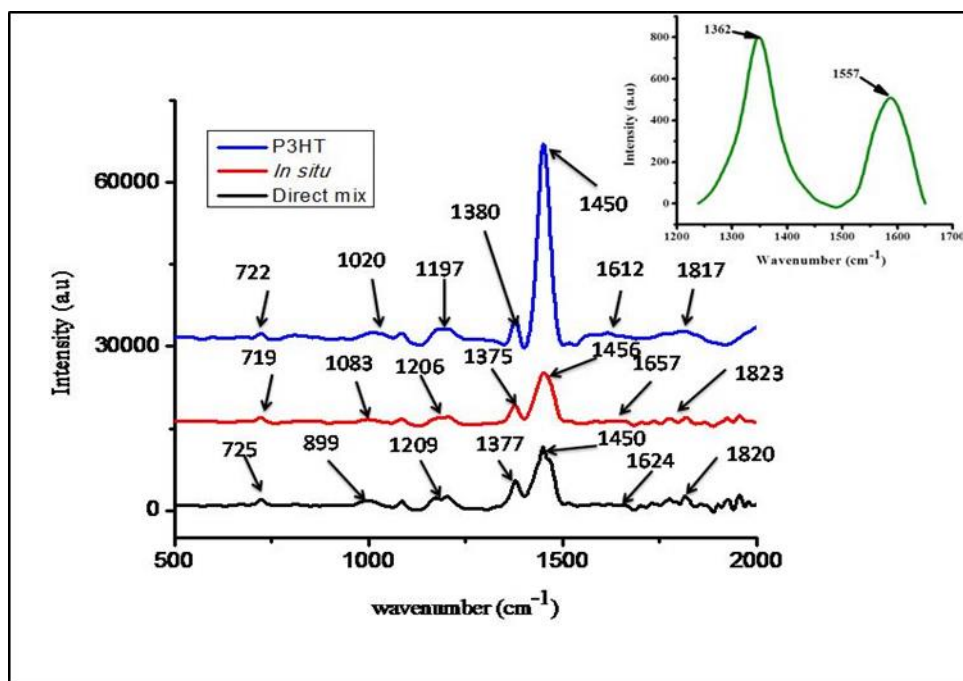
**Figure 3.** Colour of P3HT in chloroform solution (A) after formation of nanocomposite and (B) pristine P3HT under white light.



### 3.2. Vibrational and spectral characteristics of P3HT and the nanocomposite

Interaction between P3HT and N-CNTs in the two nanocomposites was assessed by means of Raman spectroscopy. Figure 4 shows Raman vibration peaks of the nanocomposites. For the N-CNTs (Figure 4 inset) the peak at  $1593\text{ cm}^{-1}$  represents the G-band which originates from the Raman  $E_{2g}$  mode while the one at  $1356\text{ cm}^{-1}$  is the disorder-induced band. The  $I_D/I_G$  ratio for N-CNTs was 1.55 which was an indication of high disorder due to nitrogen-doping. Both peaks were consequently absent in the nanocomposites.

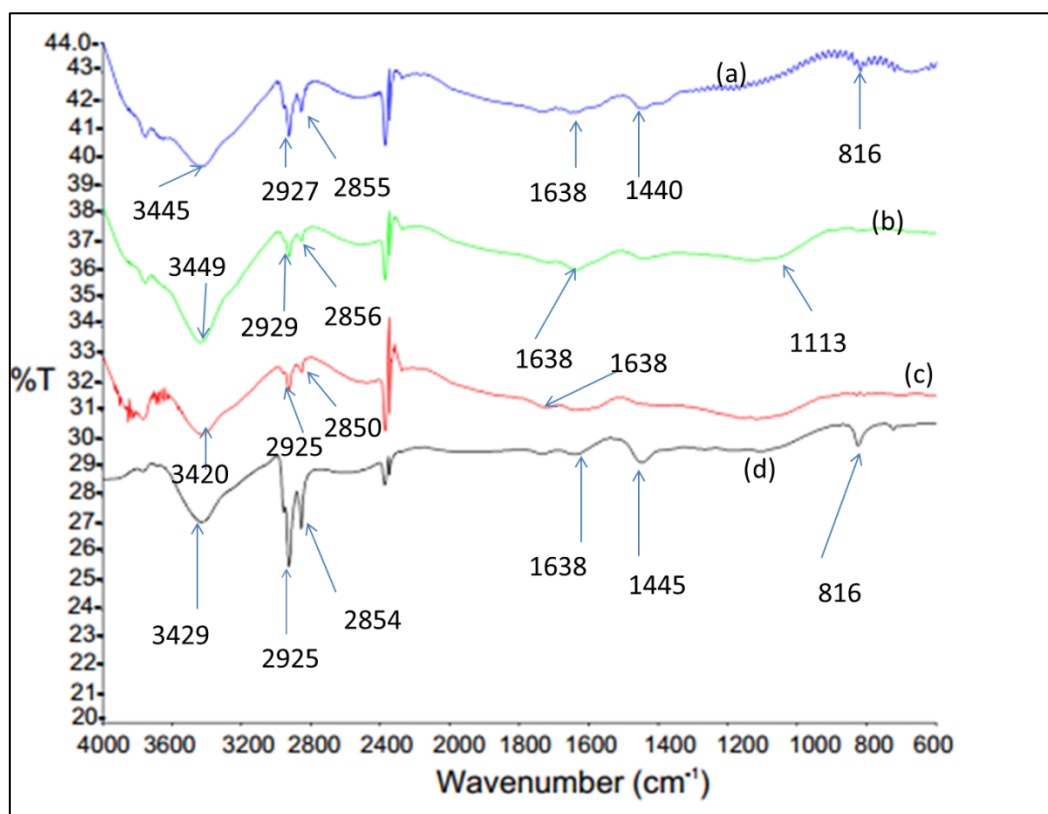
**Figure 4:** Raman spectroscopy results of nanocomposites, (A) direct mixing and (B) *in situ* polymerization (inset position of D-band and G-band for N-CNTs).



The observed peaks for both nanocomposites were almost in similar position and can be assigned as follows; peak at 704-719  $\text{cm}^{-1}$  is the C-S-C ring deformation for thiophene rings while that at around 1198  $\text{cm}^{-1}$  is the C-C symmetric stretching and C-H bending vibrations. The peak in the range of 1373-1377  $\text{cm}^{-1}$  is the C-C stretch deformation in organic thiophene rings while that around 1438-1454  $\text{cm}^{-1}$  is the symmetric C-C stretch deformations in alkyl chain and 1800-1850  $\text{cm}^{-1}$  is the asymmetric C-C stretching deformation for of thiophene ring [30].

FTIR spectroscopy results for P3HT and P3HT/N-CNTs nanocomposites synthesized by both techniques are presented in Figure 5. P3HT shows a peaks at 2925 and 2844  $\text{cm}^{-1}$  assigned to C-H stretching vibrations, the peak at 1645  $\text{cm}^{-1}$  is assigned to the aryl substituted C=C of the thiophene ring, the peak at 1440  $\text{cm}^{-1}$  is attributed to the vibrational stretch of the thiophene ring and peaks between 900-670  $\text{cm}^{-1}$  are due to the C-H out-of-plane deformation of thiophene [30].

**Figure 5:** FTIR absorption frequencies for P3HT and nanocomposites (a) P3HT, (b) *in situ*, (c) N-CNTs and (d) direct mixing.

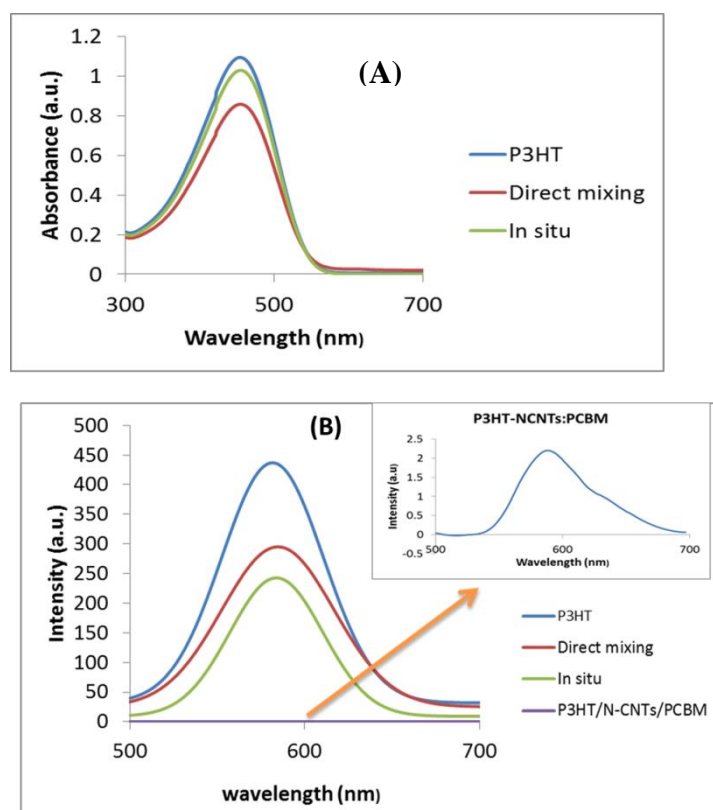


The nanocomposites synthesized by direct solution mixing gave almost all the peaks as for P3HT which was an indication of poor interaction between the polymer and N-CNTs. However, for the nanocomposite synthesized by *in situ* polymerization the C-H stretch vibration peak shifted slightly to higher wavenumbers from 2925 to 2929  $\text{cm}^{-1}$ . A slight shift to longer wavenumbers can be attributed to CH- $\pi$  interaction between N-CNTs and P3HT [31]. Additionally, the peak at 1440  $\text{cm}^{-1}$  was not observed for this nanocomposite which was an indication that stretching vibration of thiophene ring was interfered with and also, evidence of  $\pi$ - $\pi$  interaction between N-CNTs and the thiophene rings of P3HT [31].

UV-visible absorption spectra of pristine P3HT and the nanocomposites in chloroform solution are presented in Figure 6 A. The absorption maximum ( $\lambda_{\text{max}}$ ) for P3HT was observed at 442 nm, an indication of extensive  $\pi$ -conjugation [14]. The absorption peak

for P3HT that we observed compared well with values reported in the literature [27]. From the figure it was noted that N-CNTs did not make significant contribution to the spectra but a small red shift was noted to  $\lambda_{\text{max}}$  of 445 nm for the nanocomposites synthesized with both techniques. Slight red shift of  $\lambda_{\text{max}}$  can be attributed to an increased conjugation length of the polymer due to strong  $\pi$ - $\pi$  interaction with N-CNTs as a result of increased organization of the polymer chains on the nanotube surface [32].

**Figure 6.** (A) Uv-Vis absorption spectra, (B) photoluminescence emission for P3HT and P3HT/N-CNTs nanocomposites in chloroform solution. Inset in B is enlarged photoluminescence spectrum of a mixture of P3HT/N-CNTs:PCBM showing almost complete quenching of P3HT emission.



Photoluminescence (PL) spectra of P3HT and the nanocomposites are shown in Figure 6 B. The emission peak of P3HT was observed at 581 nm and those of the nanocomposites were slightly red shifted to 585 nm, but the intensity of the emission

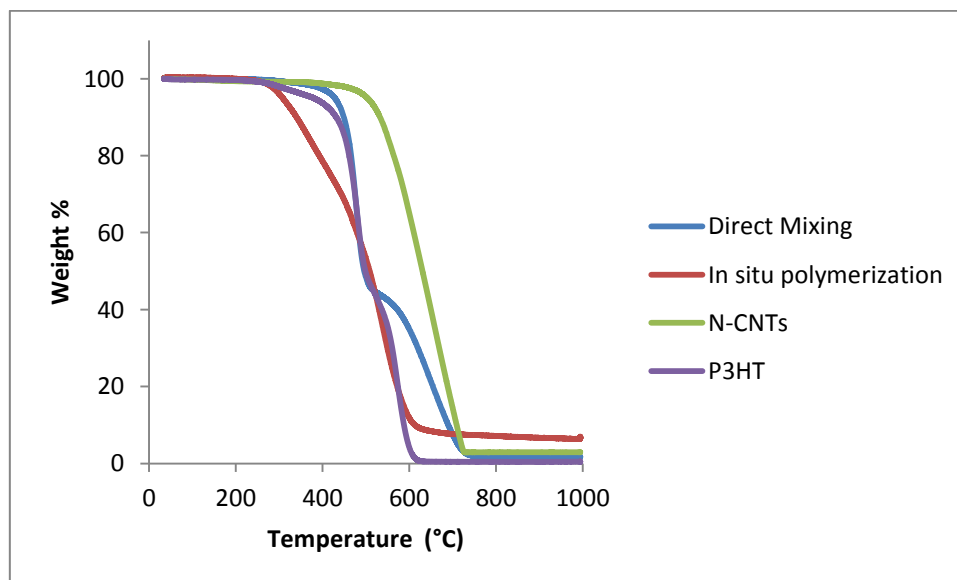


peak for P3HT was higher than that of nanocomposites. This was attributed to quenching as a result of charge transfer between N-CNTs and P3HT reducing electron-hole recombination. Quenching was high for the nanocomposite synthesized by *in situ* polymerization. This can be due to better  $\pi$ - $\pi$  interaction between the P3HT and N-CNTs surfaces enhancing the charge transfer process. Addition of PCBM to the mixture almost completely quenches PL emission of P3HT. This is an indication of the high capacity of PCBM to accept electron from the donor polymer. Kuila *et al.* [31] attributed PL quenching to  $\pi$ - $\pi$  interaction between the polymer and CNTs introducing additional deactivation paths for the excited electrons.

### 3.3. Thermal stability of the nanocomposites

The TGA thermograms for N-CNTs and the nanocomposites are presented in Figure 7. Both nanocomposites exhibit a two-step weight loss process and this could suggest that they are mixtures. The initial decomposition temperature for the nanocomposites is lower than for N-CNTs and indicates that they are less thermally stable.

**Figure 7.** Thermogravimetric analysis of N-CNTs, P3HT and P3HT/N-CNTs nanocomposites.



The nanocomposite formed by *in situ* polymerization is the least thermally stable. The possible reason for this could be due to high reactivity of monomers polymerizing and thus, forming more polymer on the surface of N-CNTs. The high amount of residue for *in situ* polymerization nanocomposite could be due to some remnant ferric oxide initiator remaining entrapped as the nanocomposite even after washing.

### 3.4. Surface energy analysis of nanocomposites

The effectiveness of the wrapping/covering of N-CNTs with the polymer was determined by comparing dispersive components of surface energy of the N-CNTs and the nanocomposites by using inverse gas chromatography equipped with a flame ionization detector. The dispersive component of surface energy ( $\gamma_s^d$ ) can be a useful tool to examine surfaces of a solid whereby changes in surface properties can easily be detected. The  $\gamma_s^d$  was obtained from the retention time ( $t_R$ ) of a given volume of a series of normal alkanes (C5–C9) at a flow rate of 10 mL min<sup>-1</sup> and 0.05 surface coverage. The  $\gamma_s^d$  was calculated from the slope of a straight line drawn from  $RT \ln V_N$  against the number of carbon atoms in the n-alkanes by using the Doris and Gray method at peak maximum time [33]. R is the gas constant, T is the absolute column temperature and  $V_N$  is the net retention volume of non-polar probes as well as polar probes and can be calculated from equation.

$$V_N = Fj(t_R - t_M) \left( \frac{P_o - P_w}{P_o} \right) \left( \frac{T_c}{T_{meter}} \right) \quad (1)$$

where; F is the flow rate,  $t_R$  and  $t_M$  are the retention and dead times measured with a specific probe and a non-adsorbing probe (such as methane) respectively,  $P_o$  is the pressure at the flow meter,  $P_w$  is the vapour pressure of pure water at the temperature of the flow meter ( $T_{meter}$ ), and  $T_c$  is the column temperature [34]. For j it was James-Martin correction factor of gas compressibility when the column inlet ( $P_i$ ) and outlet ( $P_o$ ) pressures are different given by the equation.

$$j = 3/2 \left[ \frac{(P_i/P_o)^2 - 1}{(P_i/P_o)^3 - 1} \right] \quad (2)$$

The polar probes acetone, acetonitrile, ethyl acetate and dichloromethane were used to determine the acid/base properties of N-CNTs and the nanocomposites surfaces. The  $\gamma_s^d$  was determined at 100 °C for the N-CNTs and the nanocomposites by using five alkanes namely, pentane, hexane, heptane, octane and nonane. Table 1 presents the data on the  $\gamma_s^d$ , the acid and base constants determined from the interactions with the polar probes, and the acid base ratio. The  $\gamma_s^d$  of N-CNTs was higher than that of the nanocomposite made by the direct mixing method and lower than those samples synthesised by *in situ* polymerization. The differences can be attributed to the slight difference in the final morphology of the nanocomposites.

**Table 1:**  $\gamma_s^d$ , acid-base constants determined from interaction with polar probes.

Sample	Surface Energy (mJ m <sup>-2</sup> )	Acid Constant - K <sub>a</sub>	Base Constant - K <sub>b</sub>	Acid - Bascity Ratio	Specific (Acid-base) Free Energy [kJ Mol <sup>-1</sup> ]			
					Acetone	Aceto-nitrile	Ethyl acetate	Dichloro-methane
N-CNTs	49.02	0.0275	0.4975	0.0552	6.75	11.8	5.20	8.14
<i>In Situ</i> Nano-composite	56.53	0.0622	0.5738	0.1084	11.1	15.7	7.74	8.49
Direct mixing Nano-composite	46.68	0.3031	0.4446	0.6819	26.3	26.4	24.5	7.35

When comparing the two nanocomposites only, the direct mixing method reduces the dispersive component of the surface energy by either effectively wrapping CNT bundles, leaving fewer exposed CNT tips, or through a combination of both factors. The *in situ* method has a slightly larger dispersive component than the N-CNTs due to the polymerization process and the combination of ultra sound effectively de-bundling the N-CNTs. This allows for a greater amount of individual N-CNTs to be wrapped by the polymer and also, allow for greater exposure of surface groups at the tips of the N-CNTs. The specific free energy  $\Delta G^{AB}$  of adsorption for acid-base specific interaction was high for bi-functional acetonitrile for both N-CNTs and the nanocomposites showing the surfaces are covered by donor groups. N-CNTs have extra electrons due to the lone pair of electrons on nitrogen and P3HT contain conjugated  $\pi$ -electrons which make them donor groups. The Gutmann acid (K<sub>a</sub>) and base (K<sub>b</sub>) constants were used to

determine the surface chemistry of the samples.  $K_b$  values were higher for both N-CNTs and nanocomposites than  $K_a$  showing that the surfaces were covered by donor groups.

### 3.5. Photovoltaic properties

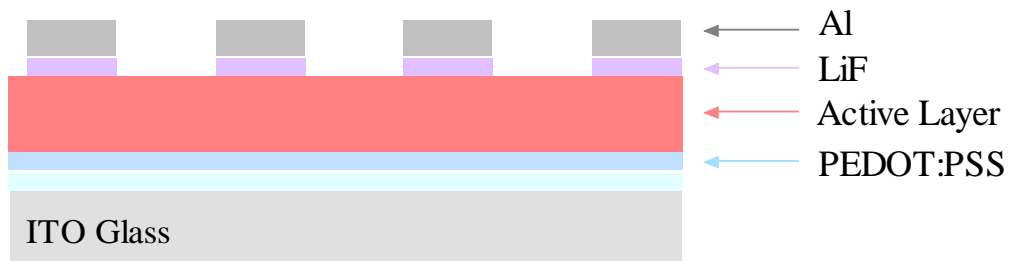
Several organic solar cells were fabricated by using a bulk heterojunction design in which the photoactive layer was composed of a blend of donor and acceptor molecules. Figure 8 shows a schematic diagram of the OSC device structure employed in this investigation. The electrical properties of the devices were studied by measuring the current-voltage (J-V) characteristics from each diode in the sample. The important parameters of the cell are derived from the diode equation which often describes the J-V characteristics of a diode. The fill factor (FF), which determines the quality of the device, and the power conversion efficiency (PCE), which provide the device output are defined as

$$FF = \frac{J_{Max} \times V_{Max}}{J_{sc} \times V_{oc}} \quad (4)$$

$$PCE = FF \frac{J_{sc} \times V_{oc}}{P_{in}} \quad (5)$$

where;  $J_{MAX}$  and  $V_{MAX}$  are current density and voltage at maximum power point,  $J_{SC}$  is short circuit current density,  $V_{OC}$  is open circuit voltage and  $P_{in}$  is incident light power [35].

**Figure 8.** Diagram of the OSC showing the arrangements of the thin layers.



Characterization of the cell under light illumination was performed by using a solar simulator operating at AM 1.5,  $100 \text{ mW cm}^{-2}$ . The photoactive layers of the devices were fabricated from the two different nanocomposites obtained by *in situ* polymerization and direct solution mixing. Figure 9 shows the measured J-V curves of the devices produced under the two types of photoactive layers. The parameters of the solar cells derived from the data indicate that the devices prepared by *in situ* polymerization generally out performed those fabricated by direct solution mixing. According to the summary given in Table 2 the  $J_{SC}$ , FF and PCE of the devices based on the nanocomposite synthesized by *in situ* polymerization are higher than those by direct mixing method.

The higher  $J_{SC}$  suggests that better charge transport properties are exhibited in the photoactive layer prepared by *in situ* polymerization. In other words, the medium has better carrier mobility of charge carriers which increases device performance. In fact, the SEM images of the two active layers given in Figure 10 partially explain difference in the devices performances. The measured parameters of the cells are summarized in Table 4.

**Figure 9.** J-V curves of the devices from the two nanocomposites.

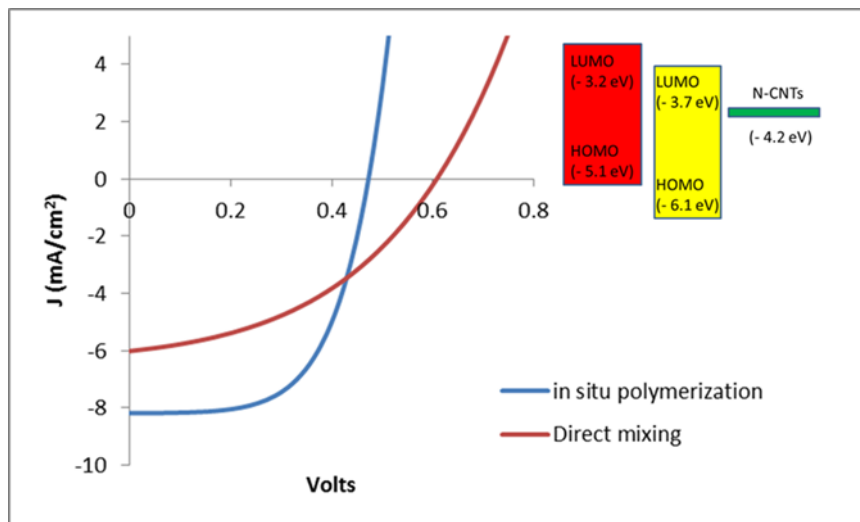


**Table 2.** Measured cell parameters.

Method of synthesis	Voc (volts)	Jsc (mA cm <sup>-2</sup> )	FF	Efficiency (%)
Direct mixing	0.61	5.084	29.26	0.51
<i>In situ</i> polymerization	0.48	7.731	41.63	1.66
Reference device (P3HT:PCBM)	0.55	6.97	54.4	2.09

However, the open circuit voltage of the OSC prepared by direct solution mixing is higher than the former by nearly 135 mV, but, it is very close to the value of  $V_{OC}$  of the reference cell. This is an indication for the existence of high non-radiative recombination of the free charge carriers in the medium formed by *in situ* polymerization. Despite the higher solar cell performance of the *in situ* polymerization it suffers from high charge recombination process which limits the potential ability of the medium for higher power conversion. The scanning electron microscopy (SEM) images were taken from various samples to investigate the morphologies of the active layers.

**Figure 10.** SEM images of the cell morphology showing N-CNTs (A) not well dispersed in the direct mixing nanocomposite and (B) well dispersed for the *in situ* polymerization nanocomposite.

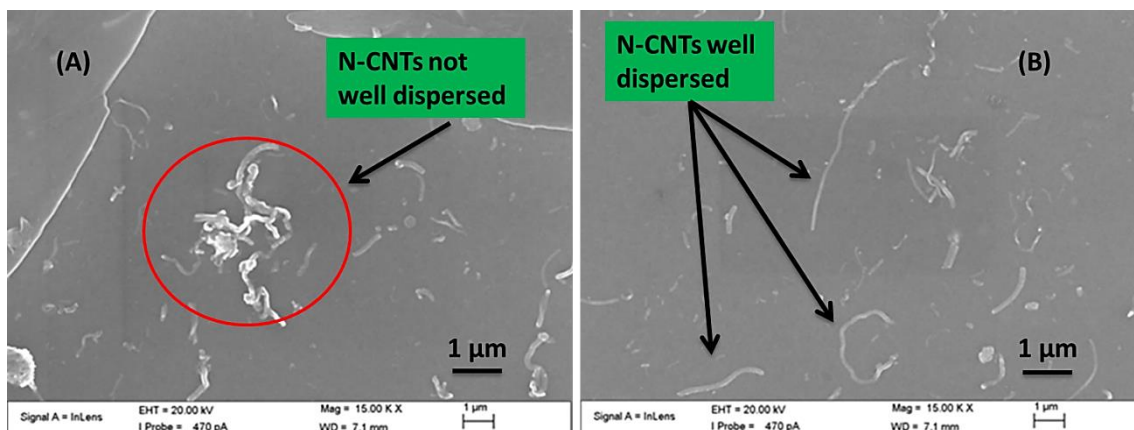


Figure 10 shows the surface morphologies captured from samples coated with the solutions of the active layer prepared both by direct solution mixing (Figure 10A) and *in*

*situ* polymerization (Figure 10B). The SEM images clearly showed that the dispersion of the N-CNTs in the polymer matrix was not good for the composite formed by direct solution mixing. This composite favours CNT agglomeration and entanglement that form various CNT clusters (Figure 10 A). On the other hand, good dispersion of N-CNTs was observed for the composite prepared by *in situ* polymerization (Figure 10B) which can be ascribed to the fact that the monomers were polymerized on the surface of the N-CNTs and this inhibits  $\pi$ - $\pi$  interaction of the tubes and thereby decrease agglomeration. Furthermore, good dispersion meant there was a continuous percolation path for free charge carriers and eventual collection at the electrodes thereby improving cell performance

The high PCE and FF from devices prepared by *in situ* polymerization can be attributed to the small size of monomer molecules making the composite adduct more homogeneous compared with the one prepared by mixing solutions of polymer and N-CNTs [5]. Lee *et al.* [28] reported an efficiency of 3.8% for a composites of N-CNTs and P3HT prepared by direct mixing. The high efficiency of their device compared with ours could be due to preparation conditions. The nanocomposite in this work was prepared under ambient conditions whereas theirs was prepared in an inert gas atmosphere. Javier and Werner [32] used direct mixing to prepare a nanocomposite of pristine multi-wall CNTs (MWCNTs) and P3HT in ambient conditions. Their device recorded lower  $J_{SC}$  and FF than what we observed in our device from nanocomposites by direct solution mixing. We attribute the high  $J_{SC}$  and FF of our device to improved charge transfer by N-CNTs. Wu *et al.* [36] mixed pristine MWCNTs with P3HT and reported a high efficiency of 3.47% for devices prepared in an inert gas atmosphere.

From the above examples it is to be noted that most of the nanocomposites used in solar cells are more often prepared by direct solution mixing. However, according to the results found from the current synthesis and characterization, using FTIR, PL and J-V, it appeared to us that *in situ* polymerization would be the best technique for preparation nanocomposite. The poor performance of the devices prepared from direct solution mixing could be due to energetic agitation brought about by shear intensive mechanical

stirring and ultrasonication used during nanocomposite preparation which initiates polymer chain breakage and degradation of opto-electrical properties [24].

#### 4. Conclusions

*In situ* polymerization and direct solution mixing techniques have been used successfully to synthesize conducting nanocomposite of P3HT and N-CNTs. N-CNTs formed extra exciton dissociation sites which were observed by PL quenching. The diodes formed from the nanocomposite had positive rectification confirming their conductive nature but, the efficiency observed was very low. The *in situ* polymerization technique was observed to be better method for synthesising nanocomposite for organic solar cells. More investigation is required to determine why nitrogen-doping of the N-CNTs that is expected to improve the conductivity of the composite, did not improve the cell efficiency as anticipated.

#### Acknowledgements

The authors wish to thank the University of KwaZulu-Natal (UKZN), the National Research Foundation (NRF) and India, Brazil and South Africa (IBSA) energy project for financial assistance. G. Keru also thanks the UKZN College of Agriculture, Engineering and Science for the award of a postgraduate bursary.

#### References

- [1] Shirakawa H, Louis EJ, Macdiarmid AG, Chiang CK, Heeger AJ. Synthesis of electrically conducting organic polymers-halogen derivatives of polyacetylene, (CH)<sub>x</sub>. *J Chem Soc Chem Comm.* **1977**,578-580.
- [2] Giulianini M, Waclawik ER, Bell JM, Scarselli M, Castrucci P, De Crescenzi M, Motta N. Microscopic and spectroscopic investigation of poly(3-hexylthiophene) interaction with carbon nanotubes. *Polymers.* **2011**,3,1433-1446.
- [3] Bounioux C, Katz EA, Yerushalmi-Rozen R. Conjugated polymers-carbon nanotubes-based functional materials for organic photovoltaics: a critical review. *Poly Advan Tech.* **2012**, 23,1129-1140.



- [4] Karim MR, Lee CJ, Lee MS. Synthesis and characterization of conducting polythiophene/carbon nanotubes composites. *J Poly Sci Part A: Poly Chem.* **2006**,44, 5283-5290.
- [5] Keru G, Ndungu PG, Nyamori VO. A review on carbon nanotube/polymer composites for organic solar cells. *Inter J Ener Res.* **2014**, 38, 1635-1653.
- [6] Tsumura A, Koezuka H, Ando T. Polythiophene field-effect transistor: Its characteristics and operation mechanism. *Syn Met.* **1988**, 25, 11-23.
- [7] Kim Y, Cook S, Tuladhar SM, Choulis SA, Nelson J, Durrant JR, Bradley DD, Giles M, McCulloch I, Ha C-S. A strong regioregularity effect in self-organizing conjugated polymer films and high-efficiency polythiophene: fullerene solar cells. *Nat Mater.* **2006**, 5, 197-203.
- [8] Burroughes JH, Bradley DDC, Brown AR, Marks RN, Mackay K, Friend RH, Burns PL, Holmes AB. Light-emitting diodes based on conjugated polymers. *Nature.* **1990**, 347, 539-541.
- [9] Choudhary V, Gupta A. Polymer/carbon nanotube nanocomposites. In: Yellampalli S (eds) Material Sciences, Polymer. In Tech, Rijeka, Croatia. **2011**, 65-90.
- [10] Ltaief A, Bouazizi A, Davenas J. Charge Transport in Carbon Nanotubes-Polymer Composite Photovoltaic Cells. *Materials.* **2009**, 2, 710-8.
- [11] Karim MR, Yeum JH, Lee MS, Lim KT. Synthesis of conducting polythiophene composites with multi-walled carbon nanotube by the  $\gamma$ -radiolysis polymerization method. *Mater Chem Phys.* **2008**, 112, 779-782.
- [12] Ayala P, Arenal R, Rummeli M, Rubio A, Pichler T. The doping of carbon nanotubes with nitrogen and their potential applications. *Carbon.* **2010**, 48, 575-586.
- [13] Panchakarla LS, Govindaraj A, Rao CNR. Boron- and nitrogen-doped carbon nanotubes and graphene. *Inorg Chim Acta.* **2010**, 363, 4163-4174.
- [14] Goutam PJ, Singh DK, Giri PK, Iyer PK. Enhancing the photostability of poly (3-hexylthiophene) by preparing composites with multiwalled carbon nanotubes. *J Phys Chem B.* **2011**, 115, 919-924.

- [15] Du Y, Shen SZ, Yang WD, Chen S, Qin Z, Cai KF, Casey PS. Facile preparation and characterization of poly (3-hexylthiophene)/multiwalled carbon nanotube thermoelectric composite films. *J Elec Mater.* **2012**, 41, 1436-1441.
- [16] Connolly T, Smith RC, Hernandez Y, Gun'ko Y, Coleman JN, Carey JD. Carbon-nanotube-polymer nanocomposites for field-emission cathodes. *Small.* **2009**, 5, 826-831.
- [17] Kim J-Y, Kim M, Kim H, Joo J, Choi J-H. Electrical and optical studies of organic light emitting devices using SWCNTs-polymer nanocomposites. *Opt Mater.* **2003**, 21, 147-151.
- [18] Philip B, Xie J, Chandrasekhar A, Abraham J, Varadan VK. A novel nanocomposite from multiwalled carbon nanotubes functionalized with a conducting polymer. *Smart Mater Struct.* **2004**, 13, 295.
- [19] Lee I, Lee S, Kim H, Lee H, Kim Y. Polymer solar Cells with polymer/carbon nanotube composite hole-collecting buffer layers. *Open Phys Chem J.* **2010**, 4, 1-3.
- [20] Miller AJ, Hatton RA, Silva SRP. Water-soluble multiwall-carbon-nanotube-polythiophene composite for bilayer photovoltaics. *Appl Phys Lett.* **2006**, 89, 123115-1-123115-3.
- [21] Kanai Y, Grossman JC. Role of semiconducting and metallic tubes in P3HT/carbon-nanotube photovoltaic heterojunctions: density functional theory calculations. *Nano Lett.* **2008**, 8, 908-912.
- [22] Berson S, de Bettignies R, Bailly S, Guillerez S, Jusselme B. Elaboration of P3HT/CNT/PCBM composites for organic photovoltaic cells. *Adv Func Mater.* **2007**, 17, 3363-3370.
- [23] Liming L, Stanchina WE, Guangyong L. Enhanced performance of bulk heterojunction solar cells fabricated by polymer:fullerene:carbon-nanotube composites. *Nano 8th IEEE Conference.* **2008**, 233-236.
- [24] Jun GH, Jin SH, Park SH, Jeon S, Hong SH. Highly dispersed carbon nanotubes in organic media for polymer: fullerene photovoltaic devices. *Carbon.* **2012**, 50, 40-46.

- [25] Kalita G, Wakita K, Umeno M. Efficient bulk heterojunction solar cells incorporating carbon nanotubes and with electron selective interlayers. *Photovoltaic Specialists Conference 35th IEEE*. **2010**, 90-94.
- [26] Keru G, Ndungu PG, Nyamori VO. Nitrogen-doped carbon nanotubes synthesised by pyrolysis of 4-[[pyridine-4-yl)methylidene]amino}phenyl)-ferrocene. *J Nanomater*. **2013**, 2013, 1-7.
- [27] Karim MR. Synthesis and characterizations of poly(3-hexylthiophene) and modified carbon nanotube composites. *J Nanomater*. **2012**, 2012, 1-8.
- [28] Lee JM, Park JS, Lee SH, Kim H, Yoo S, Kim SO. Selective electron- or hole-transport enhancement in bulk-heterojunction organic solar cells with N- or B-doped carbon nanotubes. *Adv Mater*. **2011**, 23, 629-633.
- [29] Goutam PJ, Singh DK, Iyer PK. Photoluminescence quenching of poly (3-hexylthiophene) by carbon nanotubes. *J Phys Chem C*. **2012**, 116, 8196-8201.
- [30] Louarn G, Trznadel M, Buisson JP, Laska J, Pron A, Lapkowski M, Lefrant S. Raman spectroscopic studies of regioregular poly(3-alkylthiophenes). *J Phys Chem*. **1996**, 100, 12532-12539.
- [31] Kuila BK, Malik S, Batabyal SK, Nandi AK. In-situ synthesis of soluble poly (3-hexylthiophene)/multiwalled carbon nanotube composite: Morphology, structure, and conductivity. *Macromolecules*. **2007**, 40, 278-287.
- [32] Arranz-Andrés J, Blau WJ. Enhanced device performance using different carbon nanotube types in polymer photovoltaic devices. *Carbon*. **2008**, 46, 2067-2075.
- [33] Dorris GM, Gray DG. Adsorption of n-alkanes at zero surface coverage on cellulose paper and wood fibers. *J Coll Inter Sci*. **1980**, 77, 353-362.
- [34] Zhang X, Yang D, Xu P, Wang C, Du Q. Characterizing the surface properties of carbon nanotubes by inverse gas chromatography. *J Mater Sci*. **2007**, 42, 7069-7075.
- [35] Günes S, Neugebauer H, Sariciftci NS. Conjugated polymer-based organic solar cells. *Chem Rev*. **2007**, 107, 1324-1338.
- [36] Wu M-C, Lin Y-Y, Chen S, Liao H-C, Wu Y-J, Chen C-W, Chen Y-F, Su W-F. Enhancing light absorption and carrier transport of P3HT by doping multiwall carbon nanotubes. *Chem Phys Lett*. **2009**, 468, 64-68.

## Chapter Seven

### **Performance of organic solar cells P3HT:PCBM with boron- or nitrogen-doped carbon nanotubes in the photoactive layer**

Godfrey Keru<sup>1</sup>, Patrick G. Ndungu<sup>2</sup>, Genene T. Mola<sup>1</sup>, Ana F. Nogueira<sup>3</sup> and Vincent O. Nyamori<sup>1\*</sup>

1. School of Chemistry and Physics, University of KwaZulu-Natal, Westville Campus, Private Bag X54001, Durban, 4000, South Africa

2. Department of Applied Chemistry, University of Johannesburg P.O. Box 17011, Doornfontein, Johannesburg, 2028 South Africa

3. Chemistry Institute, State University of Campinas, Campinas P. O. Box 6154, 13083970 Brazil

#### **Abstract**

In this study either boron- or nitrogen-doped carbon nanotubes (B- or N-CNTs) were incorporated in bulk heterojunction organic solar cells photoactive layer composed of poly(3-hexylthione) (P3HT):(6,6)-phenyl-C<sub>61</sub>-butyric acid methyl ester (PCBM). The physical and chemical properties were investigated using different spectroscopic techniques. The cell performance was followed from their current-voltage (J-V) characteristics. Recombination dynamics of the photo-generated free charge carriers were investigated using micro- to milli-seconds transient absorption spectroscopy (TAS). Transmission electron microscopy (TEM) images revealed presence of cone structures and bamboo compartments in B-CNTs and N-CNTs respectively. X-ray photoelectron spectroscopy (XPS) revealed very little boron was substituted in the carbon network and presence of pyrrolic, pyridinic and quaternary species of nitrogen in N-CNTs. J-V characteristics were found to be similar for the devices with B- and N-CNTs even though, boron- and nitrogen-doped CNTs are known to have different properties i.e. p-type and n-type, respectively. TAS results showed that all devices had long lived free charge carriers but the devices with B- or N-CNTs had low power conservation efficiency and low voltage.

**Keywords:** photoactive layer; photo-generated charges; recombination; carbon nanotubes

## 1. Introduction

The demand on energy supply has become a key concern with the advancement and development of nations. The current trend suggests that the future global economy is likely to consume even more energy. At the moment the main source of fuel is still the fossil fuel (oil, coal and gas). However, the dwindling size of global fossil fuel resources compounded with the unfavourable climatic changes due to emission of oxides of carbon by the use of these fuels, calls for the need to look for an alternative source of energy. Renewable sources which are environmentally friendly and inexhaustible are the best alternative [1,2]. Among the renewable resources of energy, solar energy is one of the most abundant and can easily be converted to electricity by use of photovoltaic cells [3]. Bulk heterojunction organic solar cells (OSCs) whose active layers are composed of p-type conjugated polymer and fullerene derivatives are the most promising device structure for solar energy conversion. The advantages of using OSCs over others include, low device manufacturing cost using solution processing to ultra-thin film, flexible and light weight substrates [4,5]. Recently, power conversion efficiencies above 10% have been reported for OSCs [1,6,7], which is the minimum value required for commercialization of OSC in the energy market [8].

One of the major limitations of OSCs is low diffusion length of the excitons that ranges between 10-15 nm which causes high recombination and low power conversion [9]. This difficulty has been eased by the introduction of bulk heterojunction (BHJ) design in which the donor and acceptor molecules are blended in the photoactive medium. Such mixture of donor-acceptor molecules increases the efficient dissociation of excitons in the medium by creating local donor/acceptor interfaces. Although free charge carrier generation is improved using BHJ, high efficiency cannot be achieved due to the disordered nature of the medium that prevents the smooth transport of charges. Instead charges are forced to use percolation paths *via* a hopping mechanism to reach electrodes [10,11]. Low charge carrier mobility in the bulk of organic materials can be addressed by the incorporation of one dimensional nanostructures such as carbon nanotubes (CNTs) which provide a high mobility pathway for charge carriers within the semi-conducting materials [12].

CNTs in the active layer of OSC do not only improve carrier mobility but also mechanical flexibility of the polymer materials and are also compatible with throughput solution processing [13]. Despite such attractive advantages of CNT their incorporation in the active layer of OSCs often have resulted in poor performances than those without CNTs [5]. Derbel-Habak *et al.* [14] investigated the cell efficiency by varying wt.% SWCNTs i.e. between 0 to 0.6 wt.% of ester functionalized HiPCo SWCNTs. Their findings indicated that the reduction was directly proportional to the percentage weight ratio of SWCNTs, with 0.6 wt.% having the highest reduction. Even when CNTs in the active layer are purported to enhance efficiencies, values reported are still very low for commercialization. For instance, Styliankis *et al.* [15] reported an improvement from 2.67 to 3.52% on addition of 0.5% functionalized singlewalled CNTs (SWCNTs). This enhancement was attributed to efficient excitons dissociation and improved hole mobility. Khatri *et al.* [16] reported enhanced photovoltaic properties by introducing a combination of SWCNTs and functionalized multiwalled CNTs (MWCNTs) in poly(3-octylthiophene) (P3HT)/n-silicon hybrid heterojunctions solar cells. SWCNTs assisted in excitons dissociation and electron transfer while MWCNTs in hole transfer. Kuila *et al.* [17] incorporated CNTs in the polymer matrix by grafting P3HT on the walls of CNTs *via* ester bonds and an efficiency of 0.29% was obtained for this cell.

On the other hand, there have been reports that suggests there are positive effects with the introduction of either B-CNTs or N-CNTs in the photo-active layer of OSCs [10,11]. The possible reason for this enhancement could be due to the B- or N-CNTs serving very specific role with regards to the transportation of the charges in the medium. B-CNTs usually behave as p-type semi-conductors with high work function (- 5.2 eV) that matches well with the highest occupied molecular orbital (HOMO) of the donor polymer (P3HT) (- 5.1 eV) and make them selective to hole transfer [10]. However, N-CNTs behave as n-type semi-conductor with work function (- 4.2 eV) close to the lowest occupied molecular orbital (LUMO) of the receiver materials, which are commonly fullerene derivatives such as 1-(3-methoxycarbonyl) propyl-1-phenyl[6,6] C<sub>61</sub> (PCBM) (- 3.7 eV) [10]. It is energetically favourable for electrons to move from the LUMO of the acceptor to N-CNTs therefore, they are electron selective. For example, Lee *et al.* [11] reported 13% increase in efficiency with the incorporation

of N-CNTs in the active layer poly(3-hexylthiophene): indene-C<sub>60</sub> bisadduct (P3HT:ICBA/N-CNTs) from 4.68 to 5.29%. The same group had earlier reported high efficiency by incorporating 1.0 wt.% of either B- or N-CNTs in the active layer of the cell P3HT:PCBM which resulted in an efficiency of 4.1% and 3.7% for B- and N-CNTs, respectively. These high efficiencies were attributed to selectivity of charge carrier transport in the medium.

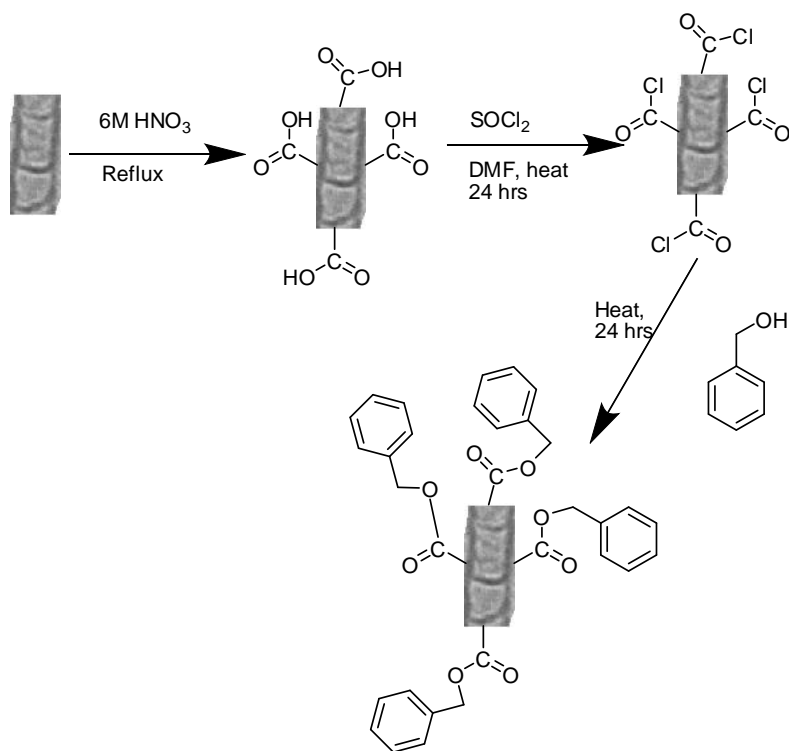
In this paper, we investigated the underlying reasons how doped-CNTs of either boron or nitrogen affects the performance of OSCs when incorporated in the photoactive layer of the cell composed either of P3HT/B- or N-CNTs:PCBM. X-ray photoelectron spectroscopy (XPS) was used to analyse the elemental composition as well as the chemical bonding environment of boron or nitrogen. Atomic force microscope (AFM) and scanning electron microscope (SEM) were used to determine the morphology of the active film layer. Ultraviolet-visible (UV-Vis) and photoluminescence (PL) were used to determine absorbance and emission of the film respectively. Transient absorption spectroscopy (TAS) was used to determine the life-time of dissociated charge carriers and the recombination dynamics. TAS is an excellent technique for investigating recombination dynamics in the active layer of a photovoltaic device. To the best of our knowledge this is the first report on reasons why despite enhancing properties of CNTs by doping with either boron or nitrogen, their performance in OSCs was opposite of the expectation.

## **2. Experimental**

### **2.1. Materials and methods**

Chemicals and solvents used in this study were of analytical grade and used as received unless otherwise stated. Benzyl alcohol (98%), thionyl chloride (98%), poly(3-hexylthiophene) 2,5-dyl (P3HT) (98%), 1-(3-methoxycarbonyl)propyl-1-phenyl-[6,6] C61) PCBM) (98%) and poly(3,4-ethelenedioxythiophene):polystyrene sulphonate [PEDOT:PSS] (98%) were purchased from Merck, Germany. 1,2-Dichlorobenzene (99%) and isopropyl alcohol (99%) were sourced from a different company, i. e. *Veiec quimica fina ltda*, Brasil.

B-CNTs were synthesized using a modified method previously reported in literature [18]. Briefly, a mixture of ferrocene (2.5 wt.%) as the catalyst, triphenylborane (5.0 wt.%) as the boron source and toluene (to make 100 wt.%) as the carbon source were pyrolysed at 900 °C in a quartz reactor tube in a muffle furnace. A mixture of 10 wt.% hydrogen gas in argon was used as a carrier gas as well as reducing agent. N-CNTs were synthesized as reported earlier by our group [19]. Briefly, 2.5 wt.% of 4-pyridinyl-4-aminomethylideneferrocene catalyst was dissolved in acetonitrile solvent to make 100 wt.% solution. This was followed by pyrolysis at 850 °C in a quartz reactor tube in a muffle furnace. As synthesized B- and N-CNTs were purified and functionalized by refluxing with 6 M nitric acid for 24 hr. To enhance the CNTs dispersion properties in solvents, the CNTs were further functionalized with benzyl alcohol as illustrated in Scheme 1.



**Scheme 1:** Functionalization of B- and N-CNTs with benzyl alcohol *via* ester bond.



## **2.2. Preparation of B- and N-CNTs/P3HT:PCBM solution**

Solution for the devices was prepared using a modified method previously reported in literature [10]. Briefly, 1.0 wt.% of B- or N-CNTs to the weight of P3HT was weighed and dispersed in 1.3 g of 1,2-dichlorobenzene and bath sonicated by using ultrasonic cleaner model UD150SH operating at 400 kHz for 1 hr. To this mixture, 10 mg of P3HT and 10 mg of PCBM were added to the dispersion and further sonicated for 1 hr. The mixture was then transferred to a stirring plate and stirred for 12 hr at 50 °C, in the dark. A solution of P3HT:PCBM without CNTs was also prepared in a similar manner.

## **2.3. Device preparation**

Devices were prepared on indium tin oxide (ITO) coated substrates (Lumtec, 15Ω). Part of the ITO was etched by putting a paste of zinc metal on the part that needed to be etched then put in a 6 M hydrochloric acid solution. The etched substrate was cleaned by sequentially sonicating with a detergent solution, distilled water, acetone and isopropyl alcohol, for 10 min in each case. Clean substrates were dried in a stream of dry nitrogen gas. A 20 μL of PEDOT:PSS was spin coated on the cleaned substrates at 3500 rpm for 50 s then, annealed for 10 min at 120 °C. A 20 μL active layer B- or N-CNTs/P3HT:PCBM was spin coated at 1500 rpm for 30 s then annealed in the dark for 20 min at 120 °C. A thin buffer layer of lithium fluoride (0.5 nm), and 60 nm thick aluminium electrodes were vacuum evaporated at  $1.5 \times 10^{-6}$  mbars. Thin film of the active layer was spin coated from the same solution and similar conditions on a glass substrate without ITO for TAS and AFM characterization. A similar solution of P3HT:PCBM without CNTs was also prepared to make devices for comparative purposes. In all the devices spin coating of the solutions was carried out in ambient conditions then quickly transferred into a glove box for annealing and characterization.

## **2.4. Characterization techniques**

As-prepared B- or N-CNTs structures were determined with transmission electron microscopy (TEM), JEOL JEM 1010 transmission electron microscope, at 200 kV. Images were captured using Megaview 3 camera and then analysed using iTEM software. Samples were dispersed in ethanol by sonication then deposited on carbon coated copper grids. Morphology of the thin film was determined with AFM, Agilent

Pico Scan 5500 microscope in a tapping mode. Images were acquired using Nanosurf Easyscan 2. For SEM, a JEOL-JSM-6360 LV operating at 20 kV was used. Images were acquired using JSM-6360 LV software.

The elemental composition, as well as the chemical bonding environment of boron- and nitrogen-doped in the CNTs, was analysed with X-ray photoelectron spectroscopy (XPS), Thermo VG Scientific Sigma Probe instrument. The monochromatic Al K $\alpha$  X-ray source (1486.6 eV) was focused on the sample (size 400  $\mu$ m). The high resolution spectra were collected by passing energy of 20 eV at energy step size of 0.1 eV with flood gun turned on to eliminate surface charge.

Absorption of the P3HT:PCBM films and for those with B- or N-CNTs were determined with UV-Vis, model Hp 8452A diode array spectrometer equipped with Hp UV-Vis Chemstation software. Photoluminescence quenching of P3HT by either B- or N-CNTs was determined using a dilute solution of P3HT/B- or N-CNTs in 1, 2 dichlorobenzene with a ISS-PC1 Spectrofluorimeter (using a Vinci software), at 440 nm excitation wavelength. Solution for photoluminescence was prepared as reported in the literature [20]. In brief, 20 mg of P3HT was dissolved in 1, 2 dichlorobenzene to make 100 mL solution. For solutions with B- or N-CNTs, 1.0 wt.% to the weight of P3HT of B- or N-CNTs was added then bath sonicated for one hour. Necessary equivalent dilutions were made to record spectra.

Charge recombination dynamics and the yield of free charge carrier pairs that were generated in the active films layer (B- or N-CNTs/P3HT:PCBM and P3HT:PCBM) were determined using microsecond to millisecond laser-based TAS following photo-excitation of the films. TAS kinetic traces were taken using a simultaneous pump and probe set up. A pulsed nitrogen laser (Photon Technology International GL-3300) was used to excite a dye laser (Photon Technology International GL-301), producing emission at 540 nm which was directed to the sample and this induced electronic excitation.

Hall Effect measurements were carried out using Ecopia Hall effect measurements system, model HMS 3000 equipped with HMS3000 VER 3.15.5 software in the presence of a 0.695 T permanent magnet. A thin film of B- or N-CNTs were deposited on a glass substrate by drop casting from 1,2 dichlorobenzene solution. Aluminium metal was thermo evaporated in van der Pauw geometry on top of the film to provide four probes contacts.

A quartz halogen lamp (Bentham IL1) and photodiode were used to measure the absorption characteristics of the samples at a typical probe wavelength of 950 nm. Monochromators (Photon Technology International) were employed to refine the probe wavelength. Current-voltage characteristics of the devices were determined using Keithley, model 2400 source meter, with a xenon lamp illumination at  $100 \text{ mW cm}^{-2}$ .

### **3. Results and discussion**

#### **3.1. Structure of B- and N-CNTs**

Pristine CNTs usually have tubular structures which are hollow and can be modified with the introduction of heteroatoms such as boron or nitrogen into the carbon network [21-23]. Fig. 1 presents typical TEM images of the B-CNTs and N-CNTs. From the figure, we observed cone shaped structures and thick walls ( $\approx 15 \text{ nm}$ ) for B-CNTs whereas N-CNTs had bamboo compartments and thin walls ( $\approx 6 \text{ nm}$ ). Formation of cone shaped structures and bamboo compartment were preliminary indicators of incorporation of boron and nitrogen heteroatoms in the hexagonal carbon network [24]. B-CNTs were also observed to have kinks and twisted compared to N-CNTs which were relatively straight. The kink and twist observed can be attributed to the size of B-C bonds which are larger than C-C bond by about 0.5% [25].

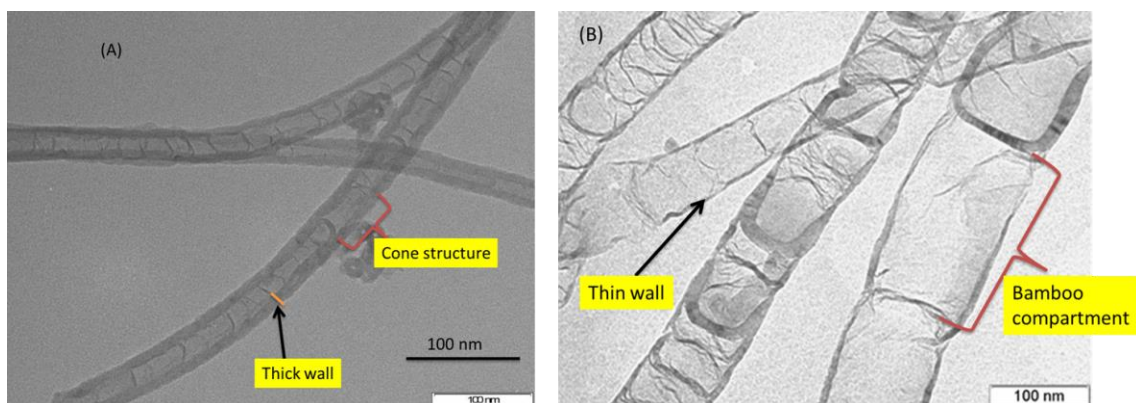


**Fig. 1:** Structure of (A) B-CNTs with cone shaped structures and thick walls. (B) N-CNTs with bamboo compartments and thin walls.

Incorporation of boron and nitrogen in the carbon network was further assessed using XPS. For B-CNTs, three peaks were identified i.e. a peak at  $\approx 190$  eV assigned to B 1s,  $\approx 284.5$  eV assigned to C 1s from  $sp^2$  hybridised carbon, and  $\approx 532.7$  eV for O 1s. For the N-CNTs, three peaks were also identified and assigned as follow; at  $\approx 284.7$  eV for C 1s, at  $\approx 401$  eV for N 1s and  $\approx 531.8$  eV for O 1s. Table 1 illustrates the atomic % of each and peak ranges as determined by XPS.

**Table 1:** Peak range for each and quantity (at. %) of boron, nitrogen, oxygen and carbon in B- and N-CNTs.

Type of CNTs	Peak position (eV)	Element	Atomic %
B-CNTs	186.0-193.5	B 1s	1.5
	282.0-293.0	C 1s	88.8
	528.0-537.0	O 1s	9.7
N-CNTs	283.0-293.9	C 1s	87.0
	396.5-407.5	N 1s	4.0
	527.5-407.5	O 1s	9.0

Oxygen could have originated from two sources namely; introduced during acid purification to remove impurities and also, oxygen molecules could have been

physisorbed on the rough surfaces that comes with doping of foreign atom on the smooth CNTs walls [26]. To determine the elemental composition as well as the chemical bonding environment of boron and nitrogen in B- and N-CNTs, B 1s and N 1s peaks were deconvoluted. The B 1s peak at 186–193.5 eV was deconvoluted into 4 peaks (Fig. 2). Lower peaks (186–189 eV) are associated with B-C bonding while the ones at high energy levels (190–194 eV) are associated with oxidised species of boron and correspond to  $BC_2O$ ,  $BCO_2$ , and  $B_2O_3$  [27].

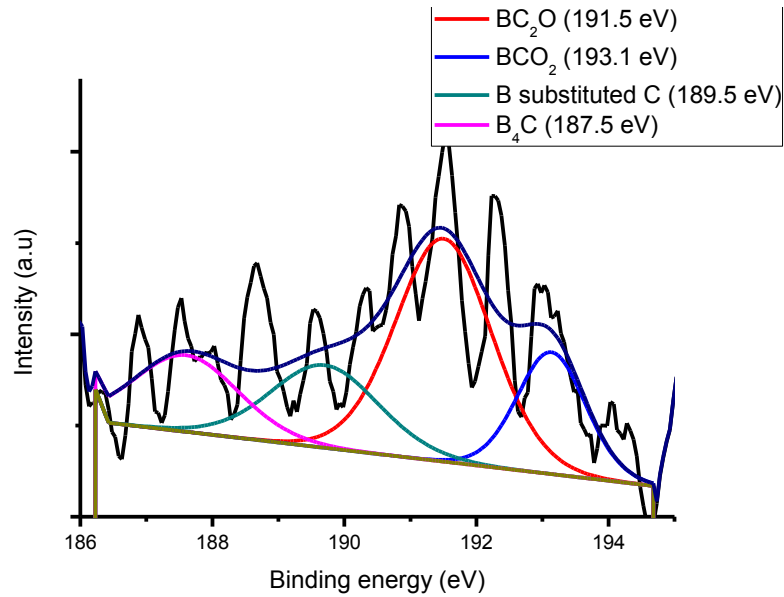


**Fig. 2:** Deconvoluted B 1s peaks showing the bonding environment of boron in B-CNTs.

From Fig. 2, substituted boron peak was the smallest indicating that very little boron was incorporated into the hexagonal network of carbon. B-CNTs with low boron concentration exhibit metallic character since insertion of boron in hexagonal carbon network results in large number of acceptors near the Fermi level [27]. Effect of this in the active layer of OSC will be discussed later in Section 3.3.

The N 1s peak at 396.5-407.5 eV was also deconvoluted into 4 peaks (Fig. 3) which corresponds to the 4 bonding environment of nitrogen in hexagonal carbon network. From Fig. 3, the highest peak obtained was that of pyrrolic nitrogen, followed by pyridinic, quarternary and lastly, the smallest represented the molecular nitrogen. The

carbon-nitrogen (C-N) bonds in quaternary or pyrrolic provide delocalised electrons into the  $sp^2$  hybridized carbon lattice. This induces sharp localised state above the Fermi level due to extra electrons and this, makes N-CNTs to behave like n-type semiconductor or donor states. However, in pyridinic type where nitrogen is coordinated by two carbon atoms induces localised states below the Fermi level. These make N-CNTs that were semi-conducting to show metallic (p-type) behaviour depending on the level of doping [28].

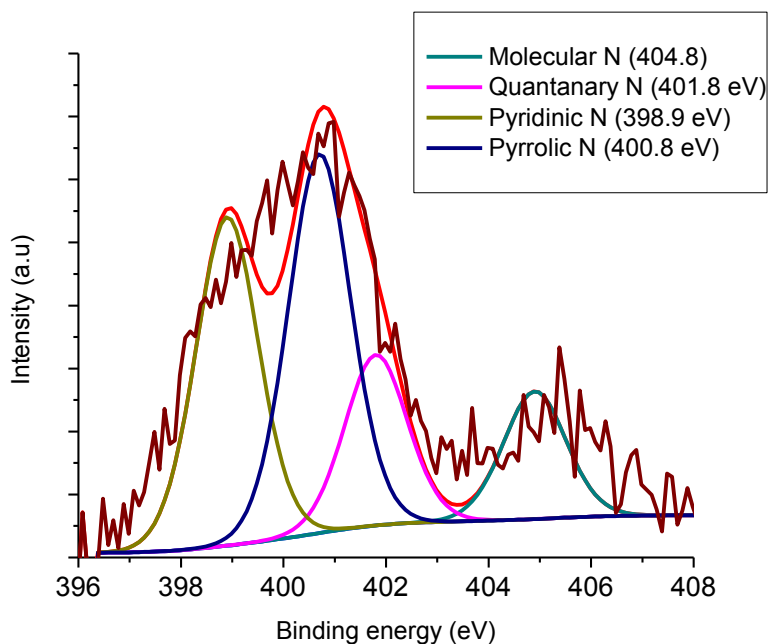


**Fig. 3:** The four peaks of N 1s after deconvolution.

Effect of this on the performance in OSCs will be discussed later in Section 3.3. B- or N-CNTs were mixed with polymer P3HT to form nanocomposites that were eventually, mixed with PCBM to form part of the photoactive layer in OSC. Behaviour of B-CNTs as a p-type and N-CNTs as n-type semi-conductors was further supported by Hall effect measurements (Table 2).

The negative value for bulk concentration in N-CNTs and positive in B-CNTs was an indicator that they were behaving as n-type and p-type, respectively, semi-conductors. Baumgartner *et al.* [29] studied a film of MWCNTs using Hall effect measurements and

in their findings, a positive Hall coefficient value was obtained and they concluded that the film as predominant hole conductor (p-type).

**Table 2:** Hall effects measurements and mobility of thin film of B- and N-CNTs.

Type of CNTs	Bulk concentration ( $\text{cm}^{-3}$ )	Sheet concentration ( $\text{cm}^{-2}$ )	Mobility ( $\text{cm}^2\text{V}^{-1}\text{s}^{-1}$ )
N-CNTs	$-1.962 \times 10^{21}$	$-4.905 \times 10^{16}$	$2.025 \times 10^{-1}$
B-CNTs	$1.592 \times 10^{19}$	$3.980 \times 10^{14}$	1.514

### 3.2. Effect of B- or N-CNTs on the spectro properties of the P3HT:CNTs blends

Photoluminescence of the nanocomposite (Fig. 4) was obtained from a solution of P3HT/B- or N-CNTs in 1,2 dichlorobenzene before PCBM was added. From the figure we observed  $\approx 50\%$  quenching of the emission spectra with the inclusion of N-CNTs. This was an indication of charge transfer between N-CNTs and P3HT. We also attribute this quenching to the position of P3HT LUMO (- 3.2 eV) and work function of N-CNTs (- 4.2 eV) which are close to each other [10]. This makes it energetically favourable for electrons transfer from P3HT LUMO to N-CNTs. Our observations differ with those of Lee *et al.* [11] who reported insignificant quenching for a solution of P3HT and N-CNTs. They attributed this to energy barriers between semi-conductor (P3HT) and conductor (N-CNTs). However, B-CNTs spectrum was almost a replica to that of P3HT. The possible reason for this was that B-CNTs do not accept electrons from the P3HT due to the mismatch between the work function of B-CNTs (- 5.2 eV) and the LUMO of P3HT (- 3.2 eV), hence, quenching was not possible.

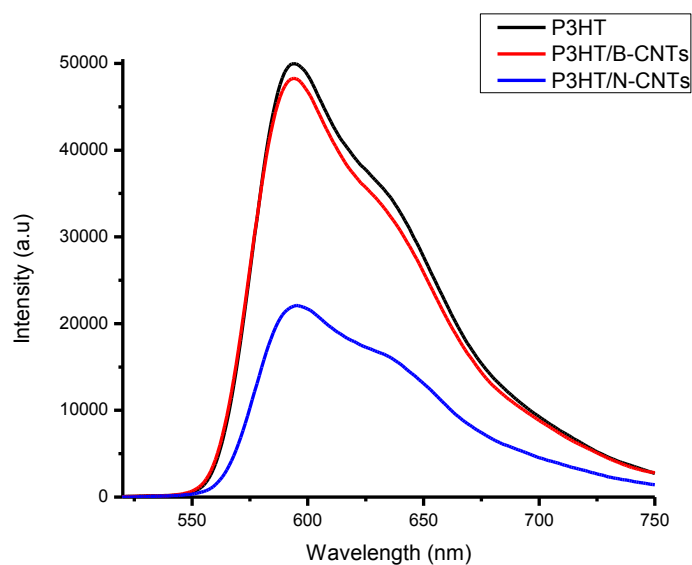


**Fig. 4:** Photoluminescence spectra for pristine P3HT (black curve), overlapped by P3HT/B-CNTs (red curve) and quenching by P3HT/N-CNTs (blue curve).

Absorbance of the nanocomposite was measured after mixing P3HT/B- or N-CNTs with PCBM then, spin coating thin films on a glass substrate and annealing at 120 °C for 10 min (Fig. 5).

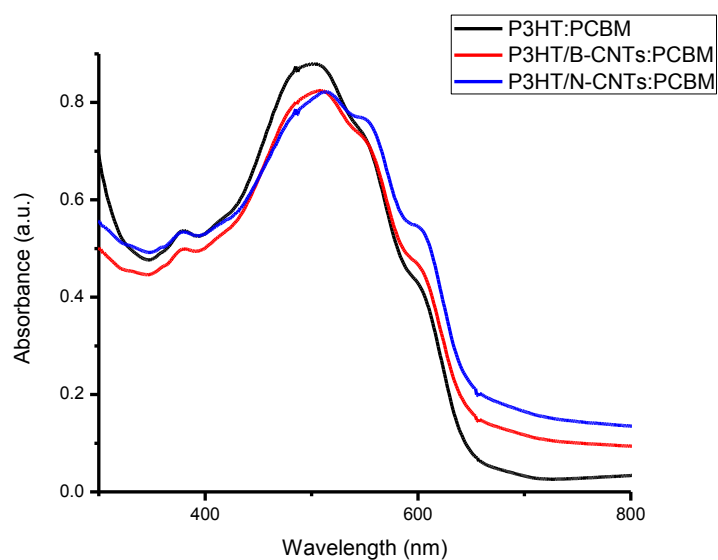


**Fig. 5:** UV-Vis absorbance of thin films black pristine P3HT, red P3HT/B-CNTs and blue P3HT/N-CNTs all the films had PCBM.



From Fig. 5 we noted a red shift for the absorbance of P3HT when B- or N-CNTs (from 500.5 nm to 507.9 nm and 514.3 nm for B-CNTs and N-CNTs) respectively, were added to the polymer. Similar observations were made by Karim [30] and attributed this to enhanced ground interaction between CNTs and the polymer. Due to this interaction we expected CNTs to create a good percolation pathway for the photo-generated charge carriers and eventual efficient collection at the electrodes. A maximum absorption ( $\lambda_{\text{max}}$ ) of 500.5 nm, 507.9 nm and 514.3 nm for P3HT, P3HT/B-CNTs and P3HT/N-CNTs was observed, respectively. The slight red shift of  $\lambda_{\text{max}}$  for the films with doped-CNTs was attributed to polymer wrapping on the CNTs surfaces which increase conjugation length as a result of  $\pi$ - $\pi$  interactions [31]. The  $\lambda_{\text{max}}$  observed for thin film was more red shifted compared to that of a solution of P3HT in 1,2-dichlorobenzene (not shown here) which was 442 nm. This red shift can be due to enhanced polymer structure ordering by annealing [32]. Additionally, annealing increases  $\pi$ - $\pi$  overlap in the polymer chains and causes phase segregation between the donor polymer and acceptor PCBM which increases  $\lambda_{\text{max}}$  of the polymer [33].

### 3.3. Photovoltaic properties

Bulk heterojunction organic solar cells were produced in a sandwich type device structure consisting of different layers of materials (Fig. 6). The photoactive layer was composed of P3HT/B- CNT/PCBM or P3HT/N-CNT/PCBM.

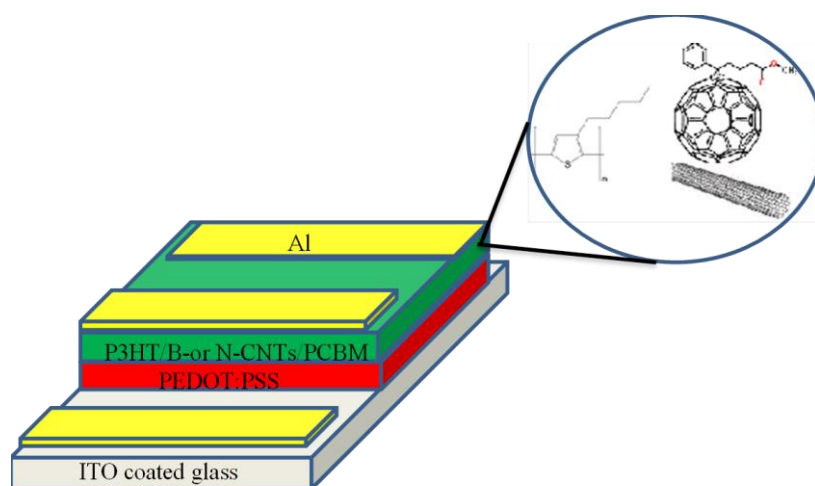


**Fig. 6:** Schematic diagram of the device.

The current-voltage (J-V) curves given in Fig. 7 are typical representatives of the OSC diodes under investigation.

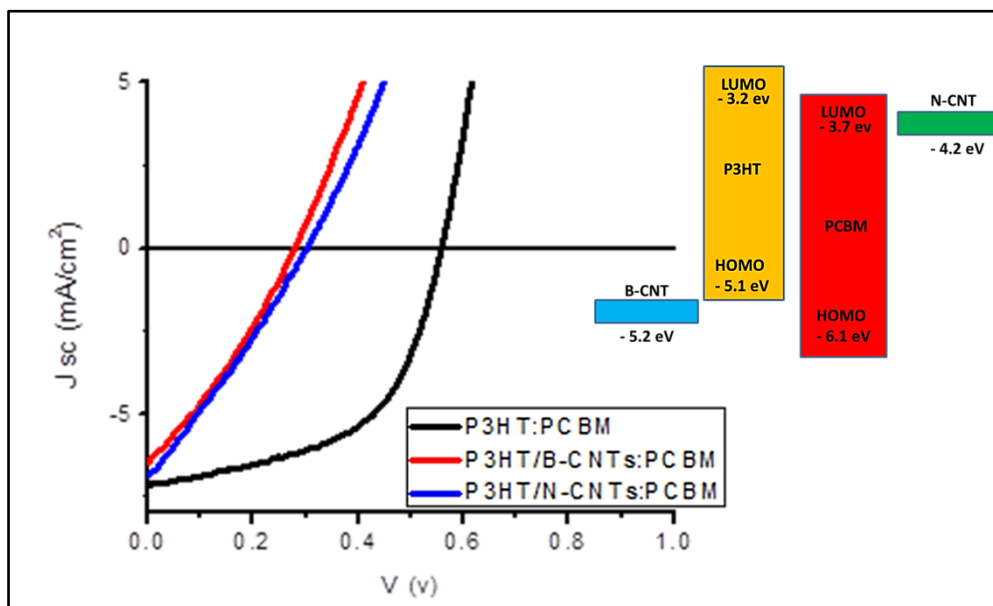


**Fig. 7:** I-V Curves of devices with and without doped-CNTs and the energy band diagram.

According to the cell parameters provided in Table 3, the performance of the devices did not improve as expected after blending the active layer with B- or N-CNTs.

**Table 3:** Photovoltaic characteristics of the devices.

OSC	$V_{oc}$ (V)	$I_{sc}$ (A)	$J_{sc}$ ( $\text{mA}/\text{cm}^2$ )	$P_{MAX}$ ( $\text{mW}/\text{cm}^2$ )	FF (%)	$\eta$ (%)
P3HT:PCBM	0.557	0.00064	7.114	2.15	54.2	2.15
P3HT/B-CNTs:PCBM	0.277	0.00058	6.452	0.54	30.2	0.54
P3HT/N-CNTs:PCBM	0.302	0.00062	6.863	0.58	28.1	0.58

The device without doped-CNTs had an efficiency of 2.15% while the ones with B-CNTs and N-CNTs had 0.54% and 0.58%, respectively. Despite the fact that the two types of CNTs used had different properties (i.e. the N-CNTs behaving like n-type and B-CNTs as p-type semi-conductors), they had similar behaviour in the devices. By intermixing the P3HT donor, PCBM electron acceptor with either B- or N-CNTs was

expected to improve the efficiency of charge separation at the D-A interfaces. These was to take place in the photoactive medium by a way of enhanced charge transfer as a result of high mobility in doped-CNTs [34]. However, the samples with doped-CNTs exhibited drastic reduction in the values of the  $V_{OC}$  and FF which might be attributed to high recombination in the devices. Similar behaviour was manifested in both types of doped-CNTs which could also be associated with the metallic character induced by low B-doping in B-CNTs and high level of pyridinic-nitrogen in N-CNTs. In all the devices, it was anticipated to have almost the same  $V_{OC}$  as it mainly depends on the difference between the HOMO level of the donor and the LUMO level of the acceptor [35,36]. Major factors for the observed low  $V_{OC}$  can be attributed to recombination in the devices and shunt resistance due to CNTs protruding out of the active layer causing current leak in the form of short circuit. Derbal-Habak *et al.* [14] reported that the presence of metallic CNTs in the photoactive layer favours recombination of free charge carriers. Additionally, Halt *et al.* [37] used time-resolved microwave conductivity to show that metallic SWCNTs in P3HT blend was unfavourable to photovoltaic performance.

According to the results given in Table 3 the devices had similar  $J_{SC}$  which is known to depend on device quantum efficiency (QE). QE of a device depends on light absorption of the polymer, excitons dissociation at the D-A interfaces as well as the efficiency of charge collection. From Table 3, we can conclude that the charge collection was not good for the devices with doped-CNTs among the three factors listed above and this affected the device efficiency [11]. To try and understand why these devices had low efficiency compared with results of Lee and co-workers [10,11] who, reported impressive efficiency of 5.29% and 4.11% using N-CNT and B-CNTs, respectively, further studies on the thin film based samples were carried out.

### **3.4. Morphology of the films**

Morphology and size of photoactive layer films of the devices were analysed using AFM and SEM. Fig. 8 shows AFM images of these films. From the images, it was observed that films with N-CNTs were rougher compared to the one without doped-CNTs. This roughness decreased as the film thickness increased, i.e. from 114.2 nm to

278.2 nm. Similar observations were made for 257 nm and 160 nm thick films with B-CNTs. The average size of the photoactive layer was 250 nm. We observed sharp pointed filaments protruding on the surface of the films with doped-CNTS. These filaments could be the cause of short circuiting of these devices. This has also been suggested by Berson *et al.* [5] who attributed reduction in  $V_{OC}$  and FF in their devices P3HT/CNT/PCBM to the formation of filamentary electrical short circuiting which was as a result of CNTs extending across the photoactive layer.

The SEM image in Fig. 9 shows that the doped-CNTs were well dispersed in the film. Therefore, we ruled out bundling of CNTs in these devices. Hence, we attribute the good dispersion to covalent functionalization of our doped-CNTs with benzyl alcohol *via* ester groups. This has been reported by other authors where the covalent functionalization of CNTs with ester groups promotes dispersion in the polymer matrix [14].

From Fig. 9, the size of the doped-CNTs was bigger compared to the thickness of the film  $\approx 250$  nm. Hence, there is a possibility that the doped-CNTs were extending across the photoactive layer.

### **3.5. Recombination dynamics in the film blends**

Although intermixing of polymer donor and fullerene acceptor results in significant enhancement of photo-induced charge generation, it can also increase interfacial area available for bimolecular recombination. Transient absorption spectroscopy (TAS) was used to study recombination dynamics in P3HT:PCBM, P3HT/B- or N-CNTs films blend. TAS was used to provide information on the yield of photo-generated charges (polarons). This was achieved by monitoring optical absorption which directly relates to the yield of photo-generated charges [38].

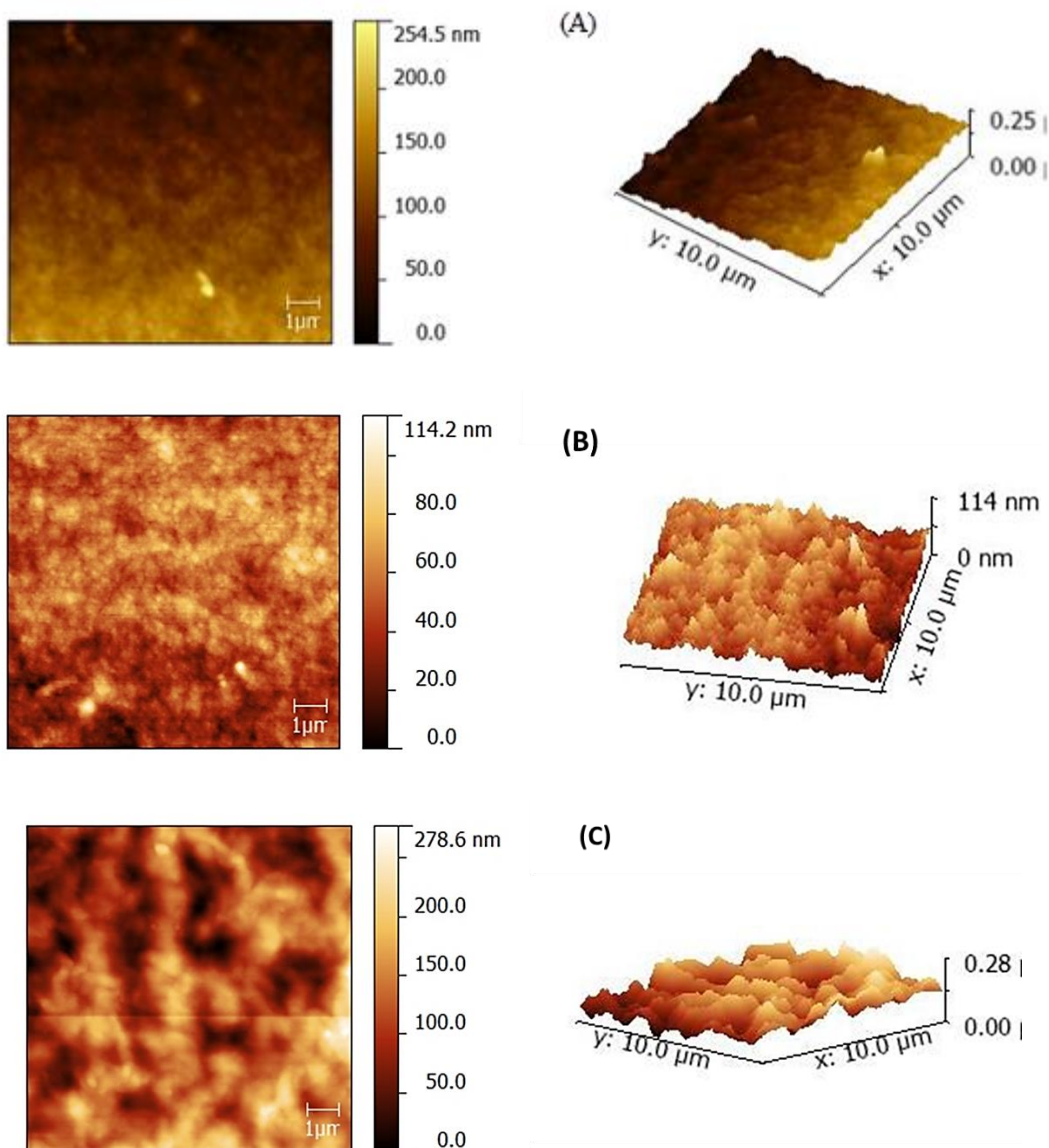


**Fig. 8:** AFM film images of (A) P3HT:PCBM, (B) 114.2 nm thick film of P3HT/N-CNTs:PCBM and (C). 278.6 nm thick film of P3HT/ N-CNTs:PCBM.

Fig. 10 shows TAS signal for the blend films at 540 nm pump wavelength and 950 nm probe wavelength at 1 s time delay. The probe wavelength was set at 950 nm in order to correspond with transient absorption of P3HT positive polarons ( $\text{P3HT}^+$ ). Additionally, low intensity excitation was employed to ensure photo-generated charge carriers were comparable with those generated under solar illumination.

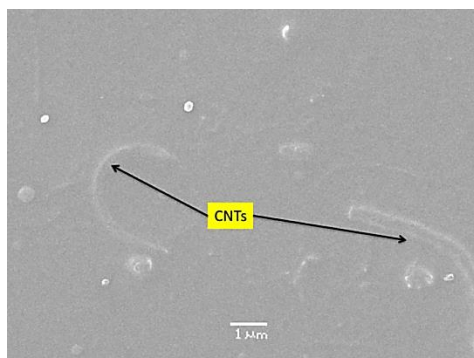


**Fig. 9:** SEM image showing dispersion of doped-CNTs. The length of the doped-CNTs is in microns scale.

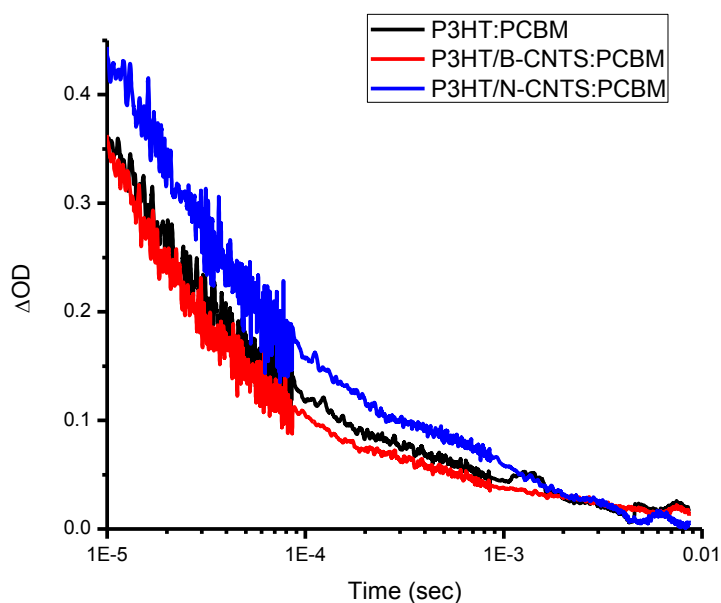


**Fig. 10:** The transient absorption decay kinetics of a P3HT:PCBM (1:1) blend film and a similar blend containing 1.0 wt. % of either B- or N-CNTs obtained as a function of laser excitation density with a pump wavelength of 540 nm and a probe wavelength of 950 nm.

We observed the films transient signal decay corresponding to power law decay ( $\Delta OD \propto t^{-\alpha}$ ) suggesting trap-limited recombination extending to millisecond time scale [38,39]. This long-lived power law decay is a characteristic of bimolecular charge recombination of dissociated charged species [40]. TAS excitation was undertaken in a nitrogen

atmosphere (films were put in a culvert then filled with nitrogen gas). To rule out the formation of triplet state, the same experiment was also done under oxygen atmosphere and it was observed that the signal was not quenched. This has also been observed by Ohkita *et al.* [41].

Despite the fact the blend with N-CNTs had the highest percent of photo-generated charge carriers which also had the longest life time (average time a free charge carrier lives before recombining non-geminate), this did not result into a good photovoltaic output. We anticipated good efficiency from this device due to high yield of long-lived dissociated polarons. The TAS results of high yield of photo-generated free charge carriers for P3HT/N-CNTs:PCBM film correlates well with photoluminescence results, where excitons quenching was observed and this is an indication that N-CNTs provided extra excitons dissociation sites. The TAS results observed leads us to a conclusion that B- and N-CNTs in this study were acting as generated charge carriers traps which encouraged bimolecular recombination instead of acting as pathway to the electrodes. The possible reason for this could be due to the metallic nature of the doped-CNTs used and their sizes as compared to the thickness of photoactive film. This encouraged shunting, which caused energy loss and a decreasing  $V_{OC}$  of the devices. Other authors such as Liu *et al.* [42], have analysed intensity dependent photocurrents in P3HT/SWCNTs:PCBM and attributed the poor performance of their device to the bimolecular recombination which was due to presence of metallic SWCNTs. Hence, metallic CNTs do encourage bimolecular recombination and this can be the major reason for efficiency deterioration for devices with CNTs.

#### **4. Conclusions**

The OSC devices with B- or N-CNTs in the photoactive layers were successfully fabricated. The devices recorded low cell efficiency compared to a standard P3HT:PCBM device. The devices behaved in a similar manner despite the fact that B- and N-doping made properties of photoactive layer different. The doped-CNTs were metallic in nature as a result of low concentration of substitutional boron in B-CNTs and pyridinic-nitrogen species in N-CNTs. Hence, this can be the main reason for similar behaviour. The size of B- or N-CNTs estimated to be between 10-20 microns

encouraged them to extend across and even protruded on both sides of the photoactive layer. From the findings controlled doping is necessary to prevent metallic species of B- and N-CNTs and this will assist to improve their implementation in the photoactive layer of OSCs.

### **Acknowledgements**

The authors thank Nanotechnology and Solar cell Laboratory, Chemistry Institute, University of Campinas where the major part of this work was undertaken through the courtesy of Prof Dr Ana Flavia, Brazilian Nanotechnology National Laboratory (LNNano) for the XPS facility (proposal - XPS-17582), the University of KwaZulu-Natal (UKZN), the National Research Foundation (NRF) and the India, Brazil and South Africa (IBSA) energy project for financial assistance. G. Keru also thanks the UKZN College of Agriculture, Engineering and Science for award of a postgraduate bursary.

### **References**

- [1] C.M. Proctor, M. Kuik, T.-Q. Nguyen, *Progress in Polymer Science* 38 (2013) 1941-1960.
- [2] E.A. Arbab, B. Taleatu, G.T. Mola, *Journal of Modern Optics* (2014) 1-5.
- [3] G. Keru, P.G. Ndungu, V.O. Nyamori, *International Journal of Energy Research* 38 (2014) 1635-1653.
- [4] G.H. Jun, S.H. Jin, S.H. Park, S. Jeon, S.H. Hong, *Carbon* 50 (2012) 40-46.
- [5] S. Berson, R. de Bettignies, S. Bailly, S. Guillerez, B. Jousset, *Advanced Functional Materials* 17 (2007) 3363-3370.
- [6] C. Liu, C. Yi, K. Wang, Y. Yang, R.S. Bhatta, M. Tsige, S. Xiao, X. Gong, *ACS Applied Materials & Interfaces* 7 (2015) 4928-4935.
- [7] J.-D. Chen, C. Cui, Y.-Q. Li, L. Zhou, Q.-D. Ou, C. Li, Y. Li, J.-X. Tang, *Advanced Materials* 27 (2015) 1035-1041.
- [8] O. Pachoumi, C. Li, Y. Vaynzof, K.K. Banger, H. Siringhaus, *Advanced Energy Materials* 3 (2013) 1428-1436.
- [9] B. Ratier, J.-M. Nunzi, M. Aldissi, T.M. Kraft, E. Buncel, *Polymer International* 61 (2012) 342-354.



- [10] J.M. Lee, J.S. Park, S.H. Lee, H. Kim, S. Yoo, S.O. Kim, *Advanced Materials* 23 (2011) 629-633.
- [11] J.M. Lee, B.H. Kwon, H.I. Park, H. Kim, M.G. Kim, J.S. Park, E.S. Kim, S. Yoo, D.Y. Jeon, S.O. Kim, *Advanced Materials* 25 (2013) 2011-2017.
- [12] S. Chaudhary, H. Lu, A.M. Müller, C.J. Bardeen, M. Ozkan, *Nano Letters* 7 (2007) 1973-1979.
- [13] S.H. Lee, J.S. Park, B.K. Lim, C.B. Mo, W.J. Lee, J.M. Lee, S.H. Hong, S.O. Kim, *Soft Matter* 5 (2009) 2343-2346.
- [14] H. Derbal-Habak, C. Bergeret, J. Cousseau, J.M. Nunzi, *Solar Energy Materials and Solar Cells* 95, Supplement 1 (2011) S53-S56.
- [15] M.M. Stylianakis, E. Kymakis, *Applied Physics Letters* 100 (2012) 093301.
- [16] I. Khatri, S. Adhikari, H.R. Aryal, T. Soga, T. Jimbo, M. Umeno, *Applied Physics Letters* 94 (2009) 093509-093509-093503.
- [17] B.K. Kuila, K. Park, L. Dai, *Macromolecules* 43 (2010) 6699-6705.
- [18] S. Wang, L. Zhang, Z. Xia, A. Roy, D.W. Chang, J.B. Baek, L. Dai, *Angewandte Chemie International Edition* 51 (2012) 4209-4212.
- [19] G. Keru, P.G. Ndungu, V.O. Nyamori, *Journal of Nanomaterials* 2013 (2013) 2.
- [20] P.J. Goutam, D.K. Singh, P.K. Giri, P.K. Iyer, *The Journal of Physical Chemistry B* 115 (2011) 919-924.
- [21] E.N. Nxumalo, N.J. Coville, *Materials* 3 (2010) 2141-2171.
- [22] Y. Chen, J. Wang, H. Liu, M.N. Banis, R. Li, X. Sun, T.-K. Sham, S. Ye, S. Knights, *The Journal of Physical Chemistry C* 115 (2011) 3769-3776.
- [23] Q. Jiang, L. Qian, J. Yi, X. Zhu, Y. Zhao, *Frontiers of Materials Science in China* 1 (2007) 379-382.
- [24] G. Keru, P.G. Ndungu, V.O. Nyamori, *Materials Chemistry and Physics* 153 (2015) 323-332.
- [25] L. Yang, S. Jiang, Y. Zhao, L. Zhu, S. Chen, X. Wang, Q. Wu, J. Ma, Y. Ma, Z. Hu, *Angewandte Chemie* 123 (2011) 7270-7273.
- [26] F. Monteiro, D. Larrude, M. Maia da Costa, L. Terrazos, R.B. Capaz, F. Freire Jr, *The Journal of Physical Chemistry C* 116 (2012) 3281-3285.
- [27] S. Lyu, J. Han, K. Shin, J. Sok, *Carbon* 49 (2011) 1532-1541.

- [28] M. Terrones, N. Grobert, H. Terrones, *Carbon* 40 (2002) 1665-1684.
- [29] G. Baumgartner, M. Carrard, L. Zuppiroli, W. Bacsa, W.A. de Heer, L. Forró, *Physical Review B* 55 (1997) 6704-6707.
- [30] M.R. Karim, *Journal of Nanomaterials* 2012 (2012) 8.
- [31] J. Arranz-Andrés, W.J. Blau, *Carbon* 46 (2008) 2067-2075.
- [32] F. Padinger, R.S. Rittberger, N.S. Sariciftci, *Advanced Functional Materials* 13 (2003) 85-88.
- [33] K. Kim, J. Liu, M.A. Namboothiry, D.L. Carroll, *Applied Physics Letters* 90 (2007) 163511.
- [34] C.J. Brabec, N.S. Sariciftci, J.C. Hummelen, *Advanced Functional Materials* 11 (2001) 15-26.
- [35] M.C. Scharber, D. Mühlbacher, M. Koppe, P. Denk, C. Waldauf, A.J. Heeger, C.J. Brabec, *Advanced Materials* 18 (2006) 789-794.
- [36] F.B. Kooistra, J. Knol, F. Kastenberg, L.M. Popescu, W.J. Verhees, J.M. Kroon, J.C. Hummelen, *Organic Letters* 9 (2007) 551-554.
- [37] J.M. Holt, A.J. Ferguson, N. Kopidakis, B.A. Larsen, J. Bult, G. Rumbles, J.L. Blackburn, *Nano letters* 10 (2010) 4627-4633.
- [38] T.M. Clarke, F.C. Jamieson, J.R. Durrant, *The Journal of Physical Chemistry C* 113 (2009) 20934-20941.
- [39] A.F. Nogueira, I. Montanari, J. Nelson, J.R. Durrant, C. Winder, N.S. Sariciftci, C. Brabec, *The Journal of Physical Chemistry B* 107 (2003) 1567-1573.
- [40] I.-W. Hwang, D. Moses, A.J. Heeger, *The Journal of Physical Chemistry C* 112 (2008) 4350-4354.
- [41] H. Ohkita, S. Cook, Y. Astuti, W. Duffy, S. Tierney, W. Zhang, M. Heeney, I. McCulloch, J. Nelson, D.D. Bradley, *Journal of the American Chemical Society* 130 (2008) 3030-3042.
- [42] L. Liu, W.E. Stanchina, G. Li, *Applied Physics Letters* 94 (2009) 233309.

## **Chapter Eight**

# **Boron- or -nitrogen doped CNTs as charge extracting and transporting layer in bulk heterojunction organic solar cell**

Godfrey Keru<sup>1</sup>, Patrick G. Ndungu<sup>2</sup>, Vincent O. Nyamori<sup>1</sup> and Genene T. Mola<sup>1\*</sup>

1. School of Chemistry and Physics, University of KwaZulu-Natal, Westville Campus, Private Bag X54001, Durban, 4000, South Africa

2. Department of Applied Chemistry, University of Johannesburg, P.O. Box 17011, Doornfontein, Johannesburg, 2028, South Africa

\*Corresponding Author: Genene T. Mola. Email: mola@ukzn.ac.za

### **Abstract**

The effects of boron- or nitrogen-doped carbon nanotubes (B- or N-CNTs) have been investigated as photoactive layer of a bulk heterojunction solar cell composed of poly(3-hexylthiophene) [P3HT] and 1(3-methoxycarbonyl)propyl-1-phenyl-[6,6] C<sub>61</sub> (PCBM). Two types of device configurations were employed by casting the doped-CNTs close to either the hole or electron collecting electrodes next to a film of P3HT:PCBM. The electrical properties of OPV devices measured under standard 1.5 AM illumination, suggest that those devices with B-CNTs close to the hole collecting electrode improved by 141% while, the devices with N-CNTs next to electron collecting electrode improved only by 38%. The results are attributed to enhanced charge carriers transfer to the electrodes by reducing recombination at the interfaces. The incorporation of doped-CNTs layer near the photoactive medium of OPV significantly affected the cell parameters.

**Keywords:** bulk heterojunction; doped-carbon nanotubes; efficiency; recombination; solar cell

## 1. Introduction

Low cost and clean source of energy is highly sought at present in order to alleviate the challenges in environmental degradation associated with the use of fossil fuels and an abetting rise for the cost of energy [1]. Solar energy is one of the solutions but the mechanism of converting solar energy into electricity is continuously changing due to the development of new methods and materials. Conventional silicon based solar cells have been successfully utilized as an alternative green source of energy but the cost of fabrication of devices is still an affordable to the large majority of low-medium income segment of the world population [2]. Organic solar cells using conjugated organic molecules (COMs) are under intensive research as an alternative to silicon based devices due to their ease of processing, flexibility, low cost and tuneable properties [3]. There is a rapid development in recent years in organic electronics that utilize organic semiconductors due to their unique electrical and optical properties. However, the progress in the realization of large scale organic molecules based solar cell has slowed down because of their poor environmental stability and charge transport across photo-active medium [1].

The introduction of carbon nanotubes (CNT) into the photoactive layers of OPV were intended to mitigate the shortcomings of conjugated polymers discussed above [4]. Especially, CNTs and conjugated polymers have a similar  $sp^2$  type hybridization [5] and exhibits high electrical conductivity. Apart from attractive electrical and mechanical properties of the CNT, its geometrical structure is favourable to act as a pathway for photo-generated free charge carriers in the medium of bulk heterojunction OPV devices [6]. Initially, the CNTs were thought to serve as an additive or replacement of PCBM in BHJ design because of their better electron transfer, electrical conductivity, crystallinity, and improved photo-stability [7-14]. However, the integration of CNTs in photoactive layer was not straight forward as one expected from the attractive properties of the CNTs.

Several investigations were reported on the use of CNT both on the positive and negative contribution in the active layers of BHJ OPV. The studies that report on the positive effect of CNT in OPV and have attributed to the manufacturing techniques, size

and purity of CNTs, post-synthesis treatment, increased exciton dissociation and enhanced charge transfer to the electrodes among other reasons. For example Ren *et al.* [15] reported 80% efficiency increase with the inclusion of 0.5 wt.% of SWCNTs followed by annealing at 150 °C for 10 min. Generally, a number of research reports suggest that low concentration and use of mono- and bi-functionalised MWCNTs are essential for better performance of OPVs with CNTs [16-19]. More recently, Lau *et al.* [19] reported a 30% improvement in power conservation efficiency (PCE) with inclusion of short MWCNTs in the photoactive layer of the device P3HT:PCBM:MWCNTs. Another investigations by Lu *et al.* [11] found that 18% PCE increase with 1.5% N-CNTs inclusion in PTB7:PC71BM bulk heterojunction; the success of the result was attributed to enhanced light absorption, increased exciton dissociation sites and efficient charge collection.

On the other hand, the incorporation of CNTs in the photoactive layer of BHJ has been reported to be problematic and detrimental to the overall device performance [20]. The relatively long size and highly conducting nature of the CNTs might cause short circuiting and resulting failure of many OPV devices [21]. Moreover, the CNTs in BHJ active medium forms small and large CNTs clusters that behave like free charge carriers sinks which hinder the transport of charges across electrodes [20]. Based on the information available so far there is no conclusive evidence on the role of CNTs in bulk heterojunction composites. In this article, we employed doped-CNTs into P3HT:PCBM active as well as buffer layer between the active layer and the electrodes. Comparison of the various devices structures and results are presented and discussed.

## 2. Experimental

All chemicals used in this study were of analytical grade and were used as received unless stated otherwise. Poly(3-hexylthiophene)2,5-diyl (P3HT) 98%, 1-(3-ethoxycarbonyl)propyl-1-phenyl-[6,6]C61 (PCBM) 98% and poly(3,4-ethylenedioxythiophene): poly(styrenesulphonate) (PEDOT:PSS) 98%, were all purchased from Merck Germany. 1,2-dichlorobenzene (99%) was sourced from a different supplier – *Veiec Quimica Ltda* – Brazil.

Doped-carbon nanotubes, B- or N-CNTs, were synthesized and characterized in our laboratory as communicated earlier [22,23]. Nanocomposite solutions were prepared by firstly, mixing 0.2 mg of B- or N-CNTs with 1.3 g of 1, 2-dichlorobenzene. The mixture was bath sonicated with ultrasonic cleaner model UD150SH operating at 40 kHz for 1 hr to disperse the CNTs. Secondary, 20 mg of P3HT was then added to the dispersion and the mixture was sonicated for a further 1 hr, followed by stirring for 2 hr in the dark. For the solution with PCBM, after dispersion of CNTs, 20 mg of P3HT and 20 mg of PCBM were added and sonicated for an additional 1 hr, and thereafter stirred for 2 hr in the dark. For the solution without doped-CNTs, 20 mg of P3HT and 20 mg of PCBM were mixed with 1.3 g of 1,2-dichlorobenzene and sonicated for 1 hr and then stirred for 2 hr in the dark.

Devices were prepared on ITO coated glass substrates (resistance 15  $\Omega$ ). Part of the ITO was etched from the substrate by partially protecting it with a photoresist tape. Zinc paste was applied on unprotected part of the substrate and placed the samples in a 2 M HCl solution. After etching, the substrate was cleaned in ultrasonic bath using detergent, distilled water, acetone, and isopropyl, respectively, in 10 minutes holding time each. The clean substrates were then dried with pressurized dry nitrogen gas. Four types of stacking layers were prepared at various device structures denoted by 1, 2, 3 and 4 (FIG. 1). In all cases, hole transporting layer PEDOT:PSS was spin coated on the substrates at 3500 RPM and were annealed at 120 °C for 10 minutes. Devices 1 and 2 are designed in such a way that the active layers are composed of P3HT/B-CNTs/PCBM and P3HT/N-CNTs/PCBM, respectively, each film was spin coated on top of PEDOT:PSS at 1500 RPM (FIG. 1 A and B). In the case of device 3, additional thin layer of B-CNTs was spin coated at 3500RPM on PEDOT:PSS before P3HT:PCBM active layer at 1500 RPM (FIG. 1 C). Device 4 was prepared by spin coating N-CNTs at 3500 RPM on top of dried P3HT:PCBM layer casted at 1500 RP (FIG. 1 D). Finally, a buffer layer of LiF ( $\approx 5$  nm) and Al ( $\approx 60$  nm) top electrodes were thermally evaporated in vacuum ( $1.0 \times 10^{-6}$  mbars). Current-voltage properties of these devices were determined using a standard solar simulator (K.H. Steuernagel) with Keithly model 2400 source meter and a xenon lamp at  $100 \text{ mW cm}^{-2}$  illumination.

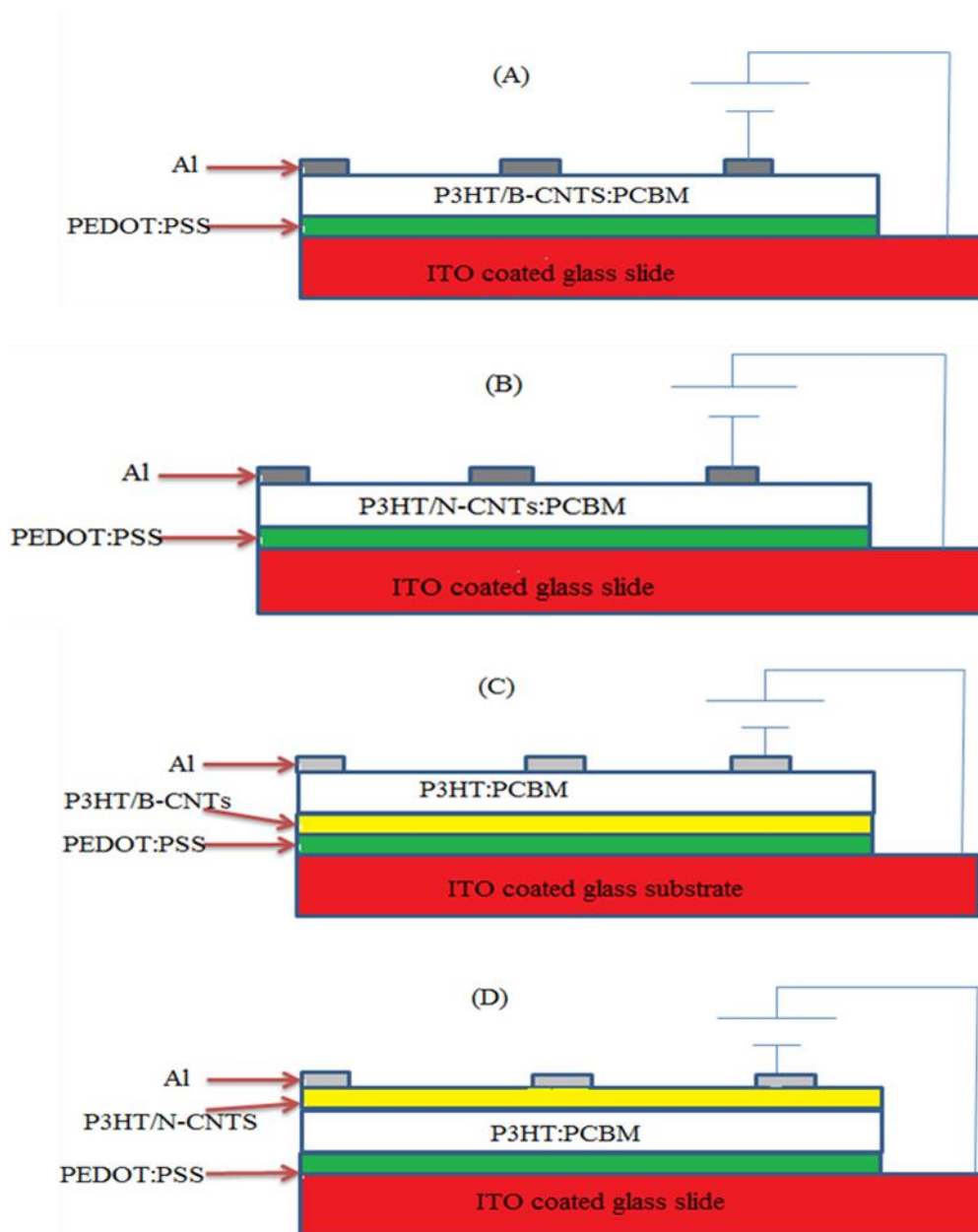


**FIG. 1:** Schematic diagrams of the devices tested (A) devices one B-CNTs intermixed with P3HT:PCBM (B) devices two N-CNTs intermixed with P3HT:PCBM (C) device three, B-CNTs/P3HT film was place next to hole collecting electrode and (D) device four, N-CNTs/P3HT film was place next to electron collecting electrode.

Bonding environment of nitrogen in N-CNTs was determined using X-ray

photoelectron spectroscopy (XPS) with a Thermo VG Scientific Sigma Probe instrument. A monochromatic Al K $\alpha$  X-ray source (1486.6 eV) was focused on the sample (size 400  $\mu$ m). The high resolution spectra were collected by passing energy of 20 eV, at energy step size of 0.1 eV with flood gun turned on to eliminate surface charge. Hall coefficient of B- or N-CNTs was determined by Hall Effect measurements using Ecopia Hall effect measurements system model HMS 3000 equipped with HMS3000 VER 3.15.5 software in the presence of a 0.695 T permanent magnet. A thin film of B-CNTs and N-CNTs were deposited on a glass substrate by drop casting from 1,2 dichlorobenzene solution. The dispersion was prepared by mixing 2 mg of B-CNTs or N-CNTs with 10 mL of 1, 2 dichlorobenzene, and bath sonicated for 2 hr. and then stirred for 12 hr. Silver metal was thermo-evaporated (van der Pauw geometry) on top of the film to provide contacts for the four probes.

### **3. Results and discussion**

#### **3.1. Characterization of doped CNTs**

The structures of B- and N-CNTs were determined using Transmission electron microscopy (TEM), (JEOL JEM 1010), operating at 200 kV. The images were captured using Megaview 3 camera and then analysed using iTEM software. Samples were dispersed in ethanol by sonication then deposited on carbon coated copper grids. Two distinct structures were found from the TEM images taken from the samples which are associated with the different types of doping. Bamboo like structures were observed in nitrogen-doped CNTs (N-CNTs) while in boron-doped samples (B-CNTs) the TEM image showed a cone shaped structures in the internal walls of the tubes (FIG. 2). These structures are the qualitative indicators for achieving nitrogen and boron-doping, respectively. The dopants, in the CNTs network, are basically the cause of alteration on the geometrical symmetry of the CNT structure resulting in changes in several physical properties.

For instance, doping the CNTs with either boron or nitrogen creates defects on the walls of the CNTs network that improves the ability of the surfaces to undergo various covalent chemistries, provide good anchoring sites for nanoparticles, introduces a



variety of functional groups [22,23]. More importantly, it improves the electrical conductivity of the CNTs.

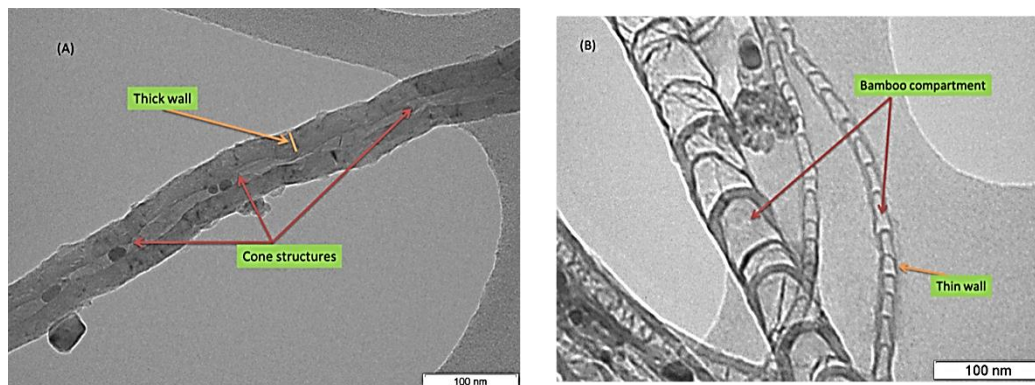


**FIG. 2:** TEM images of doped CNTs (A) boron-doped, cone shapes can be noted and (B) nitrogen-doped showing bamboo compartments with very thin wall.

In order to understand the carrier types on doped-CNTs we carried out four point probe Hall measurements on the films of doped-CNTs. The outcome of this experiment was intended to provide information to determine the position of thin layer with doped-CNTs in bulk heterojunction design. Thin layer of B-CNTs or N-CNTs was formed from a solution in order to carry out four probe Hall Effect measurement. However, a small quantity of P3HT was used with doped-CNTs in a solution of 1,2 dichlorobenzene to act as binder in CNTs dispersion which otherwise is difficult to cast CNTs on glass substrate.

The results of the Hall measurements on B-CNTs or N-CNTs are summarized on TABLE I. The average Hall coefficient found for the N-CNTs was negative which indicates that the N-CNTs are a good material for electron transport whereas, the positive coefficient for B-CNTs suggest hole charge carrier transport in the material. According to the results in the TABLE I the hole mobility in B-CNT layer is one order of magnitude higher than the electron mobility in N-CNT. The results were an encouraging indication to test the doped-CNTs as charge transport layer between photoactive medium and the electrodes. Indeed, both layers are highly conductive for transporting the photo-generated charges towards the electrodes. Therefore, a thin layer

of doped-CNTs were spin coated at 3500 RPM close to two electrodes as indicated in FIG. 1. That is, in device 3, a thin film of B-CNTs was spin coated next to ITO electrode while, in device 4, N-CNTs next to Al electrode. In both cases P3HT:PCBM thin layer was used as an photoactive medium and coated at a rate of 1500 RPM.

**TABLE I:** Results found from Hall measurements.

Doped-CNTs	Average Hall coefficient (cm <sup>3</sup> /C)	Conductivity (1/Ω cm)	Mobility (Ω cm)
B-CNTs	3.921 x 10 <sup>-1</sup>	3.860	1.514
N-CNTs	-3.882 x 10 <sup>-3</sup>	6.363 x10 <sup>1</sup>	2.025 x 10 <sup>-1</sup>

### 3.2. Electrical characteristics

The electrical characteristics of each device were measured in terms of J-V data. All the devices show the expected rectification suitable for solar cell application as depicted in FIGS. 2 and 3. FIG. 2 compares the electrical properties of devices 1 and 3, in which, device 1 active layer is composed of P3HT/B-CNT/PCBM blend whereas, in the case of device 3 the B-CNTs was spin coated on top PEDOT:PSS as in FIG. 1C. FIG. 2 clearly showed the deference between the two devices in terms fill factor, V<sub>OC</sub> and J<sub>SC</sub> of device 3 and device 1. Where device 3 outperformed device 1 in all cell parameters, for example, V<sub>OC</sub> and J<sub>SC</sub> of device 3 are increased by 53% and 31%, respectively. As a consequence, the power conversion efficiency also grew by 141% between the two device arrangements.

Similar experiments were also conducted using N-CNT layer between the top aluminium electrode and the photoactive layer P3HT:PCBM. The N-CNTs layer in this arrangement is intended to assist the extraction and the transport of electrons towards the aluminium electrode. FIG. 3 shows representative current-voltage characteristics of devices 2 and 4 with N-CNT in P3HT:N-CNT:PCBM blend (device 2) and N-CNT layer on top of P3HT:PCBM as in device 4 (FIG. 1D). TABLE II summarizes detailed photovoltaic characteristics for devices 1 to 4.

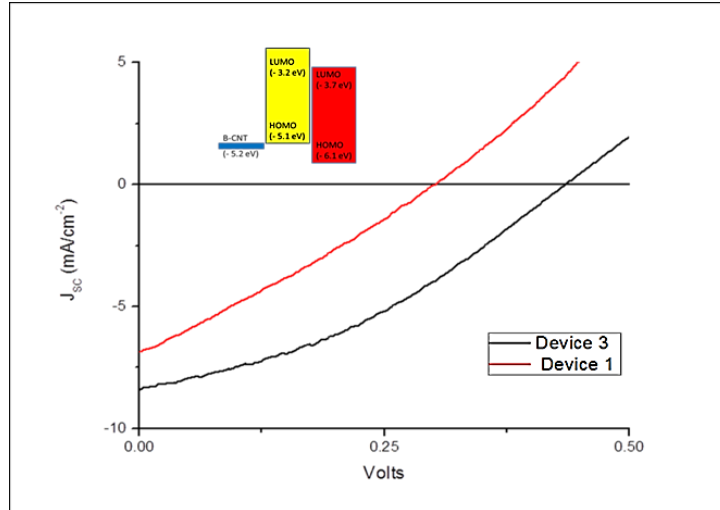


**FIG. 2:** J-V characteristics of devices prepared with B-CNTs where device 1 active layer is P3HT:B-CNT:PCBM and device 3 B-CNT layer between PEDOT:PSS and P3HT:PCBM layers. The energy levels of the donor, acceptor molecules and the work function of B-CNTs is also given in bar diagram.

**TABLE II:** Photovoltaic parameters of devices with B-CNTs or N-CNTs in the photoactive layer.

Device	Composition of the photoactive film(s)	$V_{OC}$ (V)	$J_{SC}$ (mA/cm <sup>2</sup> )	FF (%)	$\eta$ (%)
1	P3HT/B-CNTs:PCBM	0.28	6.45	30.2	0.54
2	P3HT/N-CNTs:PCBM	0.30	6.86	28.1	0.58
3	P3HT/B-CNTs P3HT:PCBM	0.43	8.43	35.0	1.30
4	P3HT:PCBM P3HT/B-CNTs	0.29	9.24	29.0	0.80

The J-V characteristics of device 2 and device 4 as depicted in FIG. 3 show that there is significant difference in the short circuit currents but the open circuit voltages of both devices remains almost unaffected by the devices structure (TABLE II).

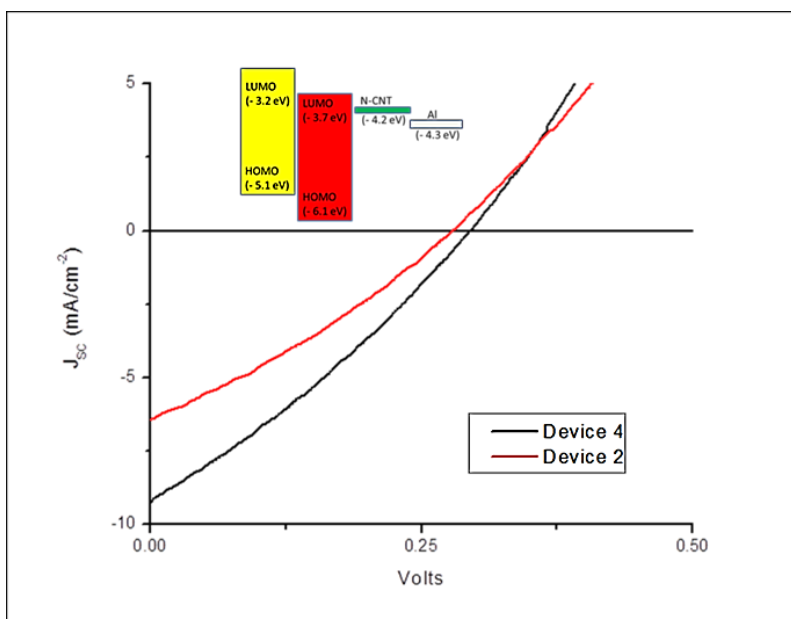


**FIG. 3:** J-V characteristics of devices with N-CNTs in P3HT:PCBM (device 2) and top of P3HT:PCBM photoactive layer (device 4). On left side of the diagram shows the energy levels diagram of donor and acceptor as well as the work function of N-CNTs.

According to the results given in FIG. 3, there was a 35% improvement with the  $J_{SC}$  which could be the main reason for 38% power conversion efficiency increase. These results concur with those of Zhong and co-workers [24] who reported direct relationship between  $J_{SC}$  and cell efficiency.

The open circuit voltage in N-CNTs is generally smaller than the one of B-CNTs device 4 suggesting either the energy bands mismatch of the molecules is unfavourable leading to reduced  $V_{OC}$  or the existence of enhanced recombination process. Carrier concentration is a result of exciton dissociation and the transport properties of the free charge carriers which ultimately determine recombination process [25]. Increased recombination with N-CNTs could be due to the bonding environment of nitrogen in the graphitic carbon network. In order to ascertain the nature of the nitrogen in the N-CNTs, XPS investigations were conducted and the results are presented in TABLE III. In our devices  $V_{OC}$  should have been dictated by the HOMO position of the donor (P3HT) and LUMO of the acceptor (PCBM).

**TABLE III:** Bonding environment of nitrogen in N-CNTs.

Type of nitrogen	Binding energy (eV)	Atomic %
Pyrrolic	400.7	37.67
Pyridinic	398.9	32.62
Quaternary	401.8	16.98
Molecular	404.9	12.73

The high atomic % of pyridinic-nitrogen could be the cause of enhanced recombination as it is reported to induce localized states below the Fermi level. This introduces metallic character to the CNTs that were semi-conducting [26]. Although it is difficult to control doping processes, the bonding environment of nitrogen in CNTs can be controlled. For example, Ombaka *et al.* [27] was able to reduce pyridinic nitrogen significantly by introducing oxygen during N-CNTs synthesis. The group reported increased atomic % of pyrrolic and reduced pyridinic as well as, molecular nitrogen species by changing atomic % of oxygen between (0-2) percent. Bepete *et al.* [28] reported that the incorporation of pyridinic and molecular nitrogen species in CNTs network is favoured at low temperature (700-800) °C and low oxygen environment. These species of nitrogen disappears at high synthesis temperature and high oxygen content, only quaternary nitrogen was incorporated at these conditions. If the conditions stated above are used during synthesis of N-CNTs incorporation of pyridinic species which encourages recombination can be minimized or eliminated completely.

Improved device performance by changing the position of B-CNTs and N-CNTs can be attributed to improved hole and electron mobility's which are 1.51 and  $2.025 \times 10^{-1} \text{ cm}^2/\text{V s}$ , respectively (TABLE I), compared to the mobility of hole and electrons in P3HT and PCBM which is reported to be  $< 10^{-4} \text{ cm}^2\text{V}^{-1} \text{ s}^{-1}$  [29]. Increased charge carrier mobility reduces recombination due to improved charge extraction [30]. Additionally, by having the layer with B- or N-CNTs separate from the donor-acceptor layer eliminates the problem of short circuiting as a result of CNTs spanning the entire active layer. For example Alley *et al.* [20] reported the likelihood of having 1  $\mu\text{m}$  SWCNTs protruding on either side of 100 nm thick active layer which resulted in short circuit and ohmic device character.

#### 4. Conclusions

We have investigated the effect of B- or N-CNTs both in photoactive layer and as a buffer layer between the electrodes and active layers in bulk heterojunction design. In all cases the introduction of B- or N-CNTs layers close to hole or electron extracting electrodes, respectively, improved charge extraction and reduced recombination. We found that enhanced PCE with B-CNT layer by 141% compared to the devices with P3HT:B-CNT:PCBM active layer. Nearly 38% PCE improvement was recorded using N-CNT layer between aluminium electrode and P3HT:PCBM than when it is incorporated in P3HT:N-CNT:PCBM blend. The device with N-CNTs had low  $V_{OC}$  which was attributed to enhanced recombination process as a result of nitrogen species present on the CNTs surfaces. It is, however, a good charge transporting medium assisting the collection of charges.

#### Acknowledgments

This work is based on the research supported by the National Research Foundation (NRF), South Africa and the India, Brazil and South Africa (IBSA) energy project. One of the authors G. Keru thanks the College of Agriculture, Engineering and Science, University of KwaZulu-Natal (UKZN) for the award of a postgraduate bursary.

#### References

- [1] B. Ratier, J.-M. Nunzi, M. Aldissi, T.M. Kraft and E. Buncel, *Poly. Intern.* (2012), 61 (3) 342.
- [2] G. Keru, P.G. Ndungu, V.O. Nyamori, *Intern. J. Ener. Res.*, (2014), 38 (13) 1635.
- [3] M. Giulianini, E.R. Waclawik, J.M. Bell, M. Scarselli, P. Castrucci, M. De Crescenzi and N. Motta, *Polymers*. (2011), 3 (3) 1433.
- [4] A. Ltaief, A. Bouazizi and J. Davenas, *Materials*, (2009), 2 (3) 710.
- [5] N.A. Nismy, K. Jayawardena, A. Adikaari and S.R.P. Silva, *Adv. Mater.* (2011), 23 (33) 3796.
- [6] J. Yan, T. Ni, F. Zou, L. Zhang, D. Yang, S. Yang and B. Zou, *Diam. Rel. Mater.* (2014) 41. 79.
- [7] C. Li, Y. Chen, Y. Wang, Z. Iqbal, M. Chhowalla and S. Mitra, *J. Mater. Chem.* (2007), 17 (23) 2406.

- [8] K.W. Johnston, A.G. Pattantyus-Abraham, J.P. Clifford, S.H. Myrskog, D.D. MacNeil, L. Levina and E.H. Sargent, *Appl. Phys. Lett.* (2008), 92 (15) 151115.
- [9] N.M. Dissanayake and Z. Zhong, *Nano lett.* (2010), 11 (1) 286.
- [10] Y.D. Park, J.A. Lim, Y. Jang, M. Hwang, H.S. Lee, D.H. Lee, H.-J. Lee, J.-B. Baek and K. Cho, *Org. Elec.* (2008), 9 (3) 317.
- [11] L. Lu, T. Xu, W. Chen, J.M. Lee, Z. Luo, I.H. Jung, H.I. Park, S.O. Kim and, L. Yu, *Nano lett.* (2013). 13 (6) 2365.
- [12] H. Derbal-Habak, C. Bergeret, J. Cousseau and J. Nunzi, *SPIE Sol. Ener. Tech. Intern. Soc. Opt. Phot.* (2010),. 77726 .77720P1.
- [13] R. Ratha, P.J. Goutam, P.K. Iyer and *Organ. Elec.* (2014), 15 (7) 1650.
- [14] V. Singh, S. Arora, M. Arora, V. Sharma and R.P. Tandon, *Phys. Lett. A*, (2014), 378 (41) 3046.
- [15] L. Ren, S. Wang, M. Holtz and J. Qiu, *Nanotech.* (2012), 23 (7) 075401.
- [16] M.-C. Wu, Y.-Y. Lin, S. Chen, H.-C. Liao, Y.-J. Wu, C.-W. Chen, Y.-F. Chen and W.-F. Su, *Chem. Phys. Lett.* (2009), 468 (1-3) 64.
- [17] A.T. Mallajosyula, S.S.K. Iyer and B. Mazhari, *J. Appl. Phys.* (2011), 109 (12) 124908.
- [18] V. Sadhu, N. Nismy, A. Adikaari, S.J. Henley, M. Shkunov and S.R.P. Silva, *Nanotech.* (2011), 22 (26) 265607.
- [19] X.C. Lau, Z. Wu and S. Mitra, *ACS appl. mater. inter.* (2014), 6 (3) 1640.
- [20] N.J. Alley, K.-S. Liao, E. Andreoli, S. Dias, E.P. Dillon, A.W. Orbaek, A.R. Barron, H.J. Byrne and S.A. Curran, *Synthetic Met.* (2012), 162 (1) 95.
- [21] S. Berson, R. de Bettignies, S. Bailly, S. Guillerez and B. Jousselme, *Adv. Fun. Mater.* (2007), 17 (16) 3363.
- [22] G. Keru, P.G. Ndungu and V.O. Nyamori, *J. Nanomater.* (2013)2013 (2) 1.
- [23] G. Keru, P.G. Ndungu, V.O. Nyamori, *Mater. Chem. Phys.* (2015), 153. 323.
- [24] Y. Zhong, A. Tada, S. Izawa, K. Hashimoto and K. Tajima, *Adv. Ener. Mater.* (2014),4 (1301331) 1.
- [25] J.M. Lee, B.H. Kwon, H.I. Park, H. Kim, M.G. Kim, J.S. Park, E.S. Kim, S. Yoo, D.Y. Jeon and S.O. Kim, *Adv. Mater.* (2013), 25 (14) 2011.
- [26] M. Terrones, N. Grobert and H. Terrones, *Carbon*, (2002), 40 (10) 1665.
- [27] L.M. Ombaka, P.G. Ndungu and V.O. Nyamori, *RSC Adv.* (2015), 5 (1) 109.

- [28] G. Bepete, Z.N. Tetana, S. Lindner, M.H. Rummeli, Z. Chiguvare and N.J. Coville, *Carbon*, (2013), 52, 316.
- [29] G.H. Jun, S.H. Jin, S.H. Park, S. Jeon and S.H. Hong, *Carbon*, (2012), 50 (1) 40.
- [30] C.M. Proctor, M. Kuik and T.-Q. Nguyen, *Prog. Poly. Sci.* (2013), 38 (12) 1941.



## Chapter Nine

### Conclusions and future work

The aim of this work was to incorporate doped CNTs (boron and nitrogen) in the photoactive layer of an OSC as charge extractors and transporters to the electrodes in a bulk heterojunction OSC composed of P3HT:PCBM photoactive layer.

#### 1. Summary

In this work a ferrocenyl derivative, (4-[[pyridin-4-yl)methylidene]amino]phenyl) ferrocene, was successfully synthesized. This was achieved by a solvent-free mechanochemical synthesis that involved grinding ferroceneaniline and 4-pyridinecarboxylaldehyde in a Pyrex tube. A 94% yield was obtained in a short reaction time of 30 minutes. Formation of the desired product was confirmed from its crystal structure and other standard characterization techniques. The solvent-free mechanochemical method of synthesis can be considered as a greener approach since no organic solvents were used during the actual synthesis. Thereafter, this compound was used as a catalyst for synthesis of N-CNTs.

N-CNTs were synthesized by use of (4-[[pyridin-4-yl)methylidene]amino]phenyl)-ferrocene as the catalyst. This ferrocenyl derivative acted as the nitrogen source and also as an extra source of carbon. Toluene or acetonitrile was the main carbon or for the latter additional nitrogen source in a CVD floating catalysis method. Three different temperatures were used, i.e. 800, 850 and 900 °C. N-CNTs were found to have bamboo compartments which were a preliminary indicator of nitrogen doping. The sizes of the bamboo compartments were found to be directly proportional to the amount of nitrogen-doped into the carbon nanotubes. In the case when smaller bamboo compartments were formed, it was an indication of more nitrogen being incorporated into the CNT framework. Nitrogen-doping was further confirmed by means of elemental analysis (CHNS) and XPS. In this thesis, acetonitrile at a temperature of 850 °C was found to be the best condition for a high yield of N-CNTs with a high nitrogen-doping content. Toluene as a carbon source formed a high percentage of impurities, either as amorphous carbon or carbon spheres. The amount of amorphous carbon and carbon spheres was dependent on the synthesis temperature. At a temperature of 800 °C, a high percent of

amorphous carbon was formed while at 900 °C a high percent of carbon spheres was achieved.

B-CNTs were successfully synthesised by the CVD floating catalysis method at 900 °C with ferrocene as the catalyst, triphenylborane as the boron source, and toluene as the main source of carbon. Both triphenylborane and ferrocene provided an extra source of carbon. The product obtained was found to be a mixture of B-CNTs with cone shaped structures and carbon nanofibres. The amount of boron incorporated, as determined by ICP-OES, revealed the percentage by weight of boron doped to be between 0.4–2.5% and this was dependent on the amount of boron-containing precursor used. From XPS, the types of boron incorporated were found to be oxidised species ( $\text{BC}_2\text{O}$ ,  $\text{BCO}_2$  and  $\text{B}_2\text{O}_3$ ) and very little substitutional boron such as  $\text{B}_4\text{C}$ .

Both B-CNTs and N-CNTs were fully characterised by using a range of instrumental techniques. TEM and SEM were used to study the structure and morphology. From the analysis, it was evident that doping changes the structure of CNTs by introducing either bamboo compartments for N-CNTs or cones structures for B-CNTs. N-CNTs were well aligned while B-CNTs had a spaghetti type of morphology. Other techniques used were EDX, BET, TGA, XPS and elemental analysis (CHNS) for N-CNTs. The XPS revealed the environment and species of nitrogen incorporated in the hexagonal carbon network in an increasing order of molecular-nitrogen, quaternary-nitrogen, pyridinic-nitrogen and eventually pyrrolic-nitrogen. Also, the EDX qualitatively revealed that nitrogen and boron were successfully doped. Additionally, TGA revealed that doping CNTs with heteroatoms (boron or nitrogen) reduces the thermal stability as compared to pristine CNTs. Likewise, BET results were able to show that the amount of nitrogen gas absorbed was dependent on the amount of impurities present. The BET results revealed that doped-CNTs with fewer impurities had the largest surface area and highest porosity. To further characterise B-CNTs, techniques such as VSM, IGC and electrical conductivity measurements were used. The ferromagnetic properties, dispersive component of surface energy and electrical conductivity of B-CNTs were found to increase with the amount of boron doped.

Apart from the synthesis and characterization of materials, the other main objective of the study was to incorporate B-CNTs and N-CNTs in the photoactive layer of OSCs. Thus, nanocomposites were synthesized with P3HT. Two methods were explored, i.e. firstly, *in situ* polymerization, where 3HT monomers were polymerized on the surface of the tubes, and, secondly, by direct solution mixing of P3HT and a dispersion of CNTs in a suitable solvent. The *in situ* polymerization approach was found to form a nanocomposite that gave a higher solar cell output compared with direct solution mixing. The morphology of the films was studied with SEM and AFM. This revealed that the doped-CNTs were well distributed in the polymer matrix for the nanocomposites synthesized by *in situ* polymerization as compared with the ones for direct solution mixing. Also, N-CNTs were found to quench excitons by  $\approx 50\%$  while B-CNTs did not. Both B-CNTs and N-CNTs improved the absorption maxima of P3HT by shifting it to longer wavelengths. This was a good indicator of increased conjugation length of the polymer due to a good organization of P3HT on the walls of CNTs.

The photovoltaic properties of the cell devices with either B-CNTs or N-CNTs in the photoactive layer of the OSCs revealed a similar behaviour despite the two types of doped-CNTs having different properties. B-CNTs and N-CNTs behaved as p-type and n-type semi-conductors, respectively, as determined by Hall Effect measurements. This was attributed to the metallic nature of the B-CNTs and N-CNTs used. This similarity was as a result of B-CNTs having a low concentration of substitutional boron while N-CNTs had a high atomic percent of pyridinic-nitrogen species. The length of the doped-CNTs (5-10 microns) was also found to influence the performance of the solar cell devices as they were cutting across the active layer which was  $\approx 250$  nm. N-CNTs in the photoactive layer were found to increase the number of photo-generated free charge carriers. However, this did not result in a good photovoltaic performance of these cell devices. In both cases (B- or N-CNTs in the photoactive layer), the photo-generated charge carriers were long-lived and revealed a bimolecular type of recombination of trapped separated charges. This was an indicator that there was a likelihood that B-CNTs and N-CNTs were acting as charge traps instead of charge carriers to the electrodes. Performance of the devices was improved by changing the position of B-CNTs and N-CNTs in the photoactive layer. A thin film of B-CNTs close to the hole

collecting electrode improved cell efficiency by 141% while, on the other hand, a thin film of N-CNTs close to the electron collecting electrode increased it by 38%.

This work has shown that inclusion of doped CNTs (boron or nitrogen) in the photoactive layer of an OSC and with a proper design of the device can greatly improve the performance.

## **2. Future work**

From the thesis findings, attempts should be made to synthesize B-CNTs and N-CNTs with controlled doping. This should not only be in terms of the amount of boron or nitrogen incorporated in the carbon network, but also the chemical environment of these heteroatoms. Also, defect-assisted substitution doping should be tried for boron to increase the amount of substitutional boron that is incorporated and, for N-CNTs, a small percentage by weight of oxygen atoms should be incorporated during the synthesis. This can reduce the atomic percentage of pyridinic-nitrogen which makes them metallic and enhances recombination.

It would also be interesting to investigate synthesis of doped-fullerenes with either boron or nitrogen as dopants. Thereafter, investigate their effect on incorporation in OSCs to replace doped-CNTs. Another area that would be of interest to investigate is the effects of addition of nanostructures such as carbon nanotubes in third generation OSCs using co-polymers such as PTB7. In short this research has a good scope of interesting ventures that one could investigate as future work.